DEVELOPMENT AND CHARACTERISATION OF METRONIDAZOLE-LOADED COLLAGEN-CHITOSAN SCAFFOLDS FOR PERIODONTAL BONE REGENERATION: *IN VITRO* AND *IN VIVO* STUDIES

BY

NORA AZIRAH BT MOHD ZAYI

A thesis submitted in fulfillment of the requirement for the degree of Doctor of Philosophy in Health Sciences

Kulliyyah of Allied Health Sciences
International Islamic University Malaysia

MAY 2025

ABSTRACT

Thousands of surgical procedures are performed daily to repair or replace tissue damaged by disease or trauma, with scaffolds playing a critical role in supporting bone regeneration. However, the clinical application of a scaffold remains challenging, particularly in the treatment of periodontal disease, where bone loss and microbial infection significantly impede the healing process. Tissue engineering aims to overcome these limitations by developing biodegradable scaffolds that not only support tissue regrowth but also deliver therapeutic agents to the defect site. These scaffolds act as temporary templates that guide regeneration while simultaneously preventing infection. Recent advances in nano-assisted drug delivery have enabled localised and sustained drug release, thereby reducing systemic side effects and minimising the risk of antibiotic resistance. This study aimed to develop a biodegradable collagen–chitosan scaffold loaded with metronidazole nanoparticles (CC-MNP) for periodontal bone regeneration. The scaffold was fabricated by blending chitosan and collagen at a 70:30 ratio, with MNP incorporated at various concentrations (0–40% w/v). Physical crosslinking was achieved using dehydrothermal treatment. Characterisation of the scaffolds was conducted using field emission scanning electron microscopy (FESEM) to assess morphology, pore structure, and pore size. *In vitro* studies were conducted to assess antibacterial activity, biocompatibility, and cell adhesion. Antibacterial efficacy was tested against *Porphyromonas gingivalis* and *Fusobacterium nucleatum* using the disc diffusion method. Biocompatibility was evaluated using the 3-(4,5-dimethylthiazol-2-yl)-2,5-diphenyltetrazolium bromide (MTT) assay with human gingival fibroblasts (HGF-1), and cell adhesion was visualised using FESEM. Based on the *in vitro* results, the scaffold exhibiting the optimal characteristic was selected for *in vivo* evaluation. The selected scaffold was implanted into critical-size calvarial bone defects in a rat model. Bone regeneration was assessed after a four-week healing period using histological staining and morphometric analysis. The findings revealed that the 30% w/v MNP-loaded scaffold exhibited desirable physical characteristics, including appropriate pore size and controlled biodegradability. It showed a significant inhibitory effect against the tested periodontal pathogens and promoted the proliferation, viability, and adhesion of HGF-1 cells. *In vivo* analysis demonstrated enhanced new bone formation at the defect site compared to controls, confirming the scaffold's regenerative potential. In conclusion, the CC scaffold loaded with 30% w/v MNP demonstrated promising results for periodontal bone regeneration. It offers a targeted, dual action approach by combining antimicrobial protection with structural support for tissue healing. This strategy provides an alternative to conventional systemic antibiotic therapies and contributes to the advancement of scaffold-based regenerative techniques in tissue engineering and dental medicine.

ملخص البحث

تُجرى الآف العمليات الجراحية يومياً لاستبدال الأنسجة المتضررة بسبب الأمراض أو الإصابات، حيث تلعب السقالات دوراً حيوياً في دعم تجديد العظام. ومع ذلك، لا تزال التطبيقات الإكلينيكية للسقالات تواجه تحديات، لا سيما في علاج أمراض اللثة، حيث تؤدي فقدان العظم والعدوى الميكروبية إلى إعاقة الشفاء بشكل كبير. تهدف هندسة الأنسجة إلى تجاوز هذه التحديات من خلال تطوير سقالات قابلة للتحلل الحيوي تدعم نمو الأنسجة وتعمل في الوقت نفسه على إيصال العوامل العلاجية مباشرة إلى موقع العيب. وتعمل هذه السقالات كقوالب مؤقتة توجه عملية التجديد مع منع العدوى في الوقت ذاته، مما يقلل من الآثار الجانبية الجهازية ويحد من خطر مقاومة المضادات الحيوية. وهدفت هذه الدراسة إلى تطوير سقالة محملة بميترونيدازول لعلاج عيوب العظام المرتبطة بعدوى اللثة. تم تحضير نانوجسيمات الميترونيدازول (MNP) وتحميلها ضمن سقالات الكولاجين والكيتوسان بنسبة 70:30، ثم دمج جسيمات الدواء مع السقالات وتجميدها باستخدام المعالجة الحرارية (Dehydrothermal treatment) لتثبيت البنية. وتم تحليل شكل السطح وحجم المسام باستخدام المجهر الإلكتروني الماسح (FESEM)، بينما تم تقييم الفعالية المضادة للبكتيريا ضد Porphyromonas gingivalis وFusobacterium nucleatum عن طريق اختبار الانتشار في الأقراص، وقياس التوافق الخلوي بناءً على النتائج .(HGF-1) على خلايا اللثة البشرية MTT باستخدام اختبار المخبرية، تم اختيار السقالات ذات الخصائص المثلى لإجراء اختبار حيواني باستخدام نموذج عيب الجمجمة في الفئران. بعد أربعة أسابيع من الزرع، أظهرت نتائج الأشعة السينية والتحليل النسيجي تحسناً كبيراً في تكوين العظام في المجموعة المعالجة بسقالات محملة بنسبة 30% من جسيمات الميترونيدازول مقارنة بالمجموعات الضابطة. وتوفر هذه السقالات نهجاً مزدوجاً يجمع بين الحماية المضادة للميكروبات والدعم البنيوي لشفاء العظم، وتعد هذه الاستراتيجية خطوة متقدمة نحو تحسين تقنيات التجديد المعتمدة على السقالات في مجال هندسة الأنسجة وطب الأسنان.

APPROVAL PAGE

The thesis of Nora Azirah Binti Mohd Zayi has been approved by the following:

Mohd Yusof Mohamad
Supervisor

Ahmad Fahmi Harun Ismail
Co-supervisor

Mohd Hafiz Arzmi
Co-supervisor

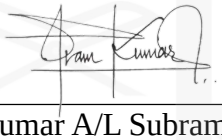

Pram Kumar A/L Subramaniam
Co-supervisor

Muhammad Salahuddin Haris
Internal Examiner

Nor Adinar Baharudin
External examiner

Azlini Binti Ismail
Chairman

DECLARATION

I hereby declare that this dissertation is the result of my investigations, except where otherwise stated. I also declare that it has not been previously or concurrently submitted as a whole for any other degrees at IIUM or other institutions.

Nora Azirah Bt Mohd Zayi

Signature…… Date…… 27/05/2025

INTERNATIONAL ISLAMIC UNIVERSITY MALAYSIA

DECLARATION OF COPYRIGHT AND AFFIRMATION OF FAIR USE OF UNPUBLISHED RESEARCH

EVALUATION OF FISH-DERIVED COLLAGEN-CHITOSAN SCAFFOLD LOADED WITH METRONIDAZOLE NANOPARTICLES FOR PERIODONTAL BONE RENEGERATION

I declare that the copyright holder of this thesis/dissertation are jointly owned by the student and IIUM.

No part of this unpublished research may be reproduced, stored in a retrieval system, or transmitted, in any form or by any means, electronic, mechanical, photocopying, recording or otherwise without prior written permission of the copyright holder except as provided below

1. Any material contained in or derived from this unpublished research may only be used by others in their writing with due acknowledgement.

2. IIUM or its library will have the right to make and transmit copies (print or electronic) for institutional and academic purpose.

3. The IIUM library will have the right to make, store in a retrieval system and supply copies of this unpublished research if requested by other universities and research libraries.

By signing this form, I acknowledged that I have read and understand the IIUM Intellectual Property Right and Commercialization policy.

Affirmed by Student Name

23/05/2025

…… ……..

Signature Date

This thesis is dedicated to my late father, Mohd Zayi Bin Yahya, who returned to the Almighty Allah on 5th Rajab 1427 / 30 July 2006. His memory continues to motivate and uplift me, reminding me of the strength and resilience he instilled in me. May Allah bless his soul, Ameen.

ACKNOWLEDGEMENTS

In the name of Allah, the Most Gracious, the Most Merciful. All praise be to Allah for His infinite blessings and guidance throughout my academic journey. His grace has been my strength in overcoming the challenges that came with completing this thesis.

I would like to extend my deepest gratitude and love to my husband, Muhammad Wasim Risma, and my son, Hadif Qasim Risma. Your unwavering support, patience, and love have been my pillars of strength. Not to forget, I am deeply thankful to my mother, Zainun Md Yusof, and my in-laws, Fauziah Ali and Rismayuddin Idris, whose prayers and encouragement have been invaluable throughout this journey. I am also grateful to my friends, siblings, and sister-in-law for their continuous support and companionship and for bringing joy and positivity into my life.

I am most indebted to my supervisor, Asst. Prof. Dr. Mohd Yusof Mohamad, for his exceptional guidance, kindness, insightful advice, and unwavering support. The encouragement, dedication, and moral support he extended to me were undoubtedly instrumental in helping me complete this research work. I am also grateful to my co- supervisors, Asst. Prof. Dr. Ahmad Fahmi Harun Ismail, Assoc. Prof. Dr. Mohd Hafiz Arzmi, and Dr. Pram Kumar A/L Subramaniam, for their valuable support and guidance, which contributed significantly to the success of this research.

My sincere thanks also go to the Kulliyyah of Allied Health Sciences, Kulliyyah of Pharmacy, Kulliyyah of Dentistry, Institute of Planetary Survival for Sustainable Well-being (PLANETIIUM), and the Cluster of Cancer Research Initiative IIUM (COCRI), as well as the Ministry of Higher Education, for the financial support provided under the grant (FRGS/1/2018/SKK11/UIAM/03/1), which was vital in bringing this research to fruition. Lastly, I once again praise Allah for His endless mercy and for granting me the strength and perseverance to complete this thesis. Alhamdulillah.

TABLE OF CONTENTS

LIST OF TABLES

LIST OF FIGURES

LIST OF SYMBOLS

RSD	Relative standard deviation
LOD	Limit of detection
S.D.	Standard deviation of the response
m	Slope
λmax	maximum absorbance
E	Young Modulus (MPA)
σ	Stress applied to the material (MPA)
ϵ	Strain
E	Sample size of animals

LIST OF SYMBOLS

3D	Three dimensional
3Rs	Replacement, reduction, and refinement
ATCC	American Type Culture Collection
BMP-2	Bone morphogenetic protein-2
CC-MNP	Collagen-Chitosan Scaffold Loaded with Metronidazole Nanoparticle
CMUIACUC	Institutional Animal Care and Use Committee of China Medical University
Co–Cr	Cobalt-chromium
CS	Chitosan
CSD	Critical-size defect
DHT	Dehydrothermal treatment
DMSO	Dimethyl sulfoxide
DNA	Deoxyribonucleic acid
ECM	Extracellular matrix
EDTA	Ethylenediaminetetraacetic acid
EE	Encapsulation efficiency
EVA	Ethylene vinyl acetate
FDA	Food and Drug Administration
FDI	FDI World Dental Federation
FESEM	Field Emission Scanning Electron Microscope
FT	Fibrous tissue

FTIR	Fourier Transform Infrared Spectroscopy
GBD	Global Burden Disease
GBR	Guided Bone Regeneration
GDP	Gross Domestic Product
GTR	Guided Tissue Regeneration
HA	Hydroxyapatite
HGF-1	Human Gingival Fibroblast cells
HPLC	High-performance liquid chromatography
H&E	Haematoxylin and eosin
IACUC	Institutional Animal Care and Use Committee
ICH Q2(R1)	International Conference on Harmonisation
KB	Kirby-Bauer
LDD	Local drug delivery
MIC	Minimal Inhibitory Concentration
Mg	Magnesium
MT	Metronidazole
MTT	3-(4,5-dimethylthiazol-2-yl)-2,5-diphenyltetrazolium bromide
NB	New bone
NCDs	Non-Communicable Diseases
OB	Old bone
OVAT	One-Variable-at-a-Time
PDI	Polydispersity
PE	Polypropylene
PEG	Polyethylene glycol
PGA	Polyglycolic acid

PHB	Poly(3-hydroxybutyrate)
PLA	Poly (lactic acid)
PLBW	Premature and Low Birthweight
PLGA	Poly (lactic-co-glycollic acid)
PLLA	Poly L-lactic acid
PMMA	Polymethyl Methacrylate
PMNs	Human Polymorphonuclear Neutrophils
PP	Polymethyl Methacrylate
PVP	Polyvinylpyrrolidone
rhBMP-2	Recombinant human BMP-2
ROI	Region of Interest
RSD	Relative standard deviation
SDGs	Sustainable Development Goals
SRP	Scaling and Root Planning
TPP	Tripolyphosphate
ULAM	University of Michigan's Unit for Laboratory Animal Medicine
UV-Vis	Ultraviolet visible spectroscopy
WHO	World Health Organisation

CHAPTER ONE

INTRODUCTION

1.1 RESEARCH BACKGROUND

Periodontal disease is recognised as a major global oral health burden in developed and developing countries. The Global Burden of Disease (GBD) study estimates that as of 2019, severe periodontal disease affected approximately 10.8% of the global population aged 15 years and older. This condition, which involves chronic inflammation of the tissues supporting the teeth, can lead to tooth loss and other serious health complications if not properly managed. According to the World Health Organization (WHO), this issue is a major concern, especially in noncommunicable diseases, requiring more attention and preventive measures (Chen et al., 2021). In Malaysia, periodontal disease continues to be a major public health concern. The Ministry of Health Malaysia (2020) reported that approximately 94.5% of Malaysian adults were affected by periodontal disease. The economic burden of managing periodontitis in Malaysia was estimated at around MYR 32.5 billion, representing 3.83% of the 2012 Gross Domestic Product (GDP). This total encompasses the costs of treating moderate and severe disease cases (Dom et al., 2016). Severe periodontal disease, also known as advanced periodontitis, is marked by extensive inflammation of the gums, significant loss of the supporting bone structure, deep periodontal pockets, and mobility of teeth. If not properly managed, it can lead to serious complications, including tooth loss (Kwon et al., 2021; Salvi et al., 2023). Guided bone regeneration (GBR) therapy has emerged as a promising approach in the treatment of periodontal disease (Wang et al., 2023). In the context of GBR therapy, scaffolds highlight a significant potential in periodontal regeneration, particularly with ongoing research advancement in biomaterial technology (Chen et al., 2024). Scaffolds are designed to mimic the natural extracellular matrix, promoting the growth and integration of new bone tissue while protecting the regenerating site from mechanical disruptions and bacterial invasion (Woo et al., 2021). By enhancing the regenerative capacity of the periodontal tissues, scaffolds improve clinical outcomes and contribute to the overall effectiveness of

periodontal treatment (Valamvanos et al., 2024). The use of animal-derived scaffolds, particularly from bovine and porcine sources in GBR for periodontal disease raises several concerns, including cultural and ethical issues related to religious restrictions and animal welfare, as well as risks associated with disease transmission and allergic reactions. These challenges highlight the need for alternative materials and approaches that address safety and patient acceptability (Nurilmala et al., 2022). Fish-derived scaffolds have been explored as a promising alternative to traditional animal-derived biomaterials due to their ethical and cultural acceptability, biocompatibility, and sustainability. These scaffolds, often made from fish scales or collagen, offer several advantages for tissue engineering applications while addressing some of the concerns associated with terrestrial animal sources (Yamada et al., 2014; Zain & Hamdan, 2021). Among the numerous biomaterials developed from different sources, the collagen-chitosan (CC) scaffold has gained significant attention in the field of tissue engineering and regenerative medicine due to its promising properties such as biocompatibility, biodegradability, and structural versatility, making it a suitable candidate for various biomedical applications (Irastorza et al., 2021; Martínez et al., 2015; Parenteau-Bareil et al., 2010). However, a major issue with current scaffolds is their susceptibility to infection due to their colonisation by pathogens in the periodontal pocket during the bone healing process, which decreases the amount of regenerated bone (Ma et al., 2016).

The use of scaffolds in GBR poses notable risks during the healing process, particularly due to their susceptibility to microbial contamination. The colonisation of scaffolds by periodontal pathogens such as *Porphyromonas gingivalis* and *Fusobacterium nucleatum* has been shown to compromise tissue integration and impair bone regeneration outcomes (Wang et al., 2023). While systemic antibiotic therapy is commonly used to manage infection, it often results in challenges such as bacterial resistance, gastrointestinal disturbances, and allergic reactions. Furthermore, achieving and maintaining effective drug concentrations at the targeted site remains difficult, leading to the development and preference for localised antibiotic delivery methods (Zucchelli et al., 1999). Several antibiotics have been explored for local delivery in periodontal regeneration, including tetracycline**,** minocycline**,** doxycycline**,** amoxicillin**,** clindamycin**,** and ciprofloxacin, each

selected based on their antimicrobial spectrum and compatibility with delivery systems (Al-Delayme, 2017; Jain et al., 2020; Sedghi et al., 2021). Among these, metronidazole (MT) has gained special interest due to its selective efficacy against obligate anaerobes such as *P. gingivalis* and *F. nucleatum*, which are key pathogens interfering with scaffold integration and bone healing (Dingsdag & Hunter, 2018; Nastri et al., 2019). These pathogens produce toxins and proteolytic enzymes that degrade extracellular matrix proteins and hinder the regenerative capacity of scaffolds, thereby contributing to GBR failure (Valamvanos et al., 2024). Although MT gel has been locally applied to reduce microbial loads in periodontal pockets, limitations such as rapid clearance and inadequate retention at the site have restricted its long-term efficacy. As a result, advanced strategies involving the encapsulation of MT into nanoparticulate drug delivery systems have been developed to enhance therapeutic outcomes. Embedding metronidazole-loaded nanoparticles (MNP) into biodegradable scaffolds offers dual benefits, sustained, localised release of the antibiotic and simultaneous support for cellular infiltration and new bone formation (Garg et al., 2018; Xue et al., 2014). These scaffolds not only act as physical barriers and regenerative matrices but also serve as reservoirs for controlled drug delivery, thereby improving infection control and regeneration efficiency (Chen et al., 2024). Therefore, this study aims to formulate MNP and incorporate them into a CC scaffold for enhanced periodontal bone and tissue regeneration. The experiment was divided into (1) the development and characterisation of metronidazole-loaded nanoparticles (MNP), (2) the assessment of CC scaffolds with and without MNP in terms of their physicochemical properties, (3) antimicrobial, (4) biocompatibility properties, and (5) pre-clinical *in vivo* bone regeneration capacity. This study focuses on the development of enhanced CC scaffolds with targeted drug delivery, which may contribute to future improvements in periodontal therapy. Moreover, the use of fish-derived collagen supports sustainability by utilising marine by-products, while contributing to innovation in biomaterials and localised drug delivery for periodontal regeneration.

1.2 PROBLEM STATEMENT

Periodontitis is a progressive and destructive inflammatory disease that compromises the soft tissue and alveolar bone supporting the teeth. If left untreated, it leads not only to tooth loss but also contributes to systemic complications, including diabetes mellitus and cardiovascular diseases (Chen et al., 2021). The persistence of periodontitis in the population places a substantial burden on both individual health and national healthcare systems. In Malaysia, this issue is especially severe. According to the National Oral Health Survey of Adults (NOHSA) 2020, 94.5% of Malaysian adults show signs of periodontal disease, with only 5.1% exhibiting a healthy periodontium (Ministry of Health Malaysia, 2020). The management of periodontitis was previously estimated to cost MYR 32.5 billion annually, representing 3.83% of Malaysia's Gross Domestic Product (GDP) and exceeding the Ministry of Health's 2012 annual budget by 60.6% (Dom et al., 2016). A more recent estimate showed that non-surgical periodontal treatments alone impose a financial burden of MYR 696 million annually in Malaysia's public and private sectors (Yusof et al., 2024). Without effective regenerative therapies, these costs are expected to rise due to increased disease prevalence and aging demographics. These statistics highlight a persistent public health challenge that urgently requires innovative and sustainable solutions. GBR represents a significant advancement in periodontal therapy, aiding bone healing by providing a physical barrier that supports cellular migration and tissue regeneration (Alavi et al., 2023). Traditional GBR materials, including non-resorbable scaffolds such as poly(lactic-co-glycolic acid) (PLGA), gelatin sponges, and bioactive ceramics, require secondary surgery for removal, increasing the risk of infection and patient discomfort (Shimauchi et al., 2013; Abtahi et al., 2023). This has led to growing interest in developing resorbable scaffold materials that eliminate the need for surgical retrieval while still supporting bone regeneration. Among various biomaterials, fish-derived collagen has attracted attention due to its excellent biocompatibility, availability, and reduced zoonotic risk. However, However, collagen alone has limitations, such as poor mechanical strength and rapid degradation. To overcome these issues, it has been cross-linked with CS, resulting in composite scaffolds with enhanced structural stability and regenerative potential (Zain & Hamdan, 2021). Despite these advancements, infection remains a critical challenge in

GBR, as microbial colonisation can compromise healing and reduce bone regeneration. Bacterial colonisation of scaffolds particularly by periodontal pathogens like *Porphyromonas gingivalis* and *Fusobacterium nucleateu*n can impair healing by producing proteolytic enzymes that degrade the extracellular matrix (Valamvanos et al., 2024). While systemic antibiotics are commonly used to combat these infections, they are often associated with systemic side effects, rising antimicrobial resistance, and limited drug availability at the targeted site (Zucchelli et al., 1999). As a result, several antibiotics including tetracycline, minocycline, doxycycline, amoxicillin, clindamycin, and ciprofloxacin have been investigated for local delivery in periodontal applications (Al-Delayme, 2017; Jain et al., 2020; Sedghi et al., 2021). Among these, MT has attracted considerable interest due to its selective efficacy against obligate anaerobic bacteria, minimal disturbance to beneficial oral flora, low systemic toxicity, and established clinical use. However, topical delivery of MT is limited by poor drug retention at the infection site, rapid salivary clearance, and insufficient sustained release (Garg et al., 2018; Xue et al., 2014). Among these, MT has attracted considerable interest due to its selective efficacy against obligate anaerobic bacteria, minimal disturbance to beneficial oral flora, low systemic toxicity, and established clinical use. However, topical delivery of MT is limited by poor drug retention at the infection site, rapid salivary clearance, and insufficient sustained release (Garg et al., 2018; Xue et al., 2014). To address these limitations, recent studies have explored the incorporation of MT into nanoparticulate drug delivery systems embedded within biodegradable scaffolds. This approach offers dual benefits, sustained, site-specific antibiotic release and structural support for tissue regeneration (Garg et al., 2018; Xue et al., 2014). These composite scaffolds act not only as regenerative matrices but also as antimicrobial reservoirs, significantly enhancing both infection control and bone healing (Chen et al., 2024). Therefore, the development and evaluation of a MT-loaded CC scaffold addresses a critical gap in current periodontal therapy by offering an integrated solution to control infection and promote periodontal bone regeneration.

1.3 SIGNIFICANT OF STUDY

The 11th Malaysian Plan highlights the importance of research, development, and commercialisation in enhancing both national and organisational competitiveness and sustainability. Within this framework, health-related innovation particularly in clinical interventions, dentistry, pharmacy, and epidemiology, is recognised as a key contributor to Malaysia's Gross Domestic Product (GDP) and the advancement of public healthcare. In line with these national priorities, this study presents a novel advancement in GBR technology through the development of a bioactive scaffold with antibacterial properties. Compared to traditional GBR scaffolds, the proposed biomaterial offers a more affordable and sustainable alternative by utilising the fish derived collagen crosslinked with CS. This highlights the potential use of underexploited marine by-products such as tilapia skin and scales as a future sustainable resource. These by-products, widely available through Malaysia's aquaculture and fish processing industries, could offer a local, low-cost alternative for collagen production in future scaffold manufacturing. This approach may help reduce reliance on imported biomaterials and contribute to domestic economic development and sustainability. Currently, many GBR materials in the market are derived from expensive or culturally sensitive sources. For example, AlloDerm (LifeCell, USA) is sourced from human cadaveric dermis, Lyoplant (B. Braun, Germany) is derived from bovine pericardium, and Bio-Gide (Geistlich Pharma, Switzerland) is produced from porcine collagen. These materials pose challenges not only in terms of cost and accessibility but also in terms of cultural and religious acceptance, particularly in multiethnic societies. In contrast, marine-based collagen represents a promising alternative that could address these issues while supporting local industry and resource circularity. Beyond economic and resource advantages, the scaffold developed in this study incorporates MNP, enabling sustained, site-specific antibiotic release. This dual functionality addresses a critical limitation in GBR applications, bacterial contamination during the healing process which often compromises the regenerative outcome. By enhancing both bone regeneration and localised infection control, the scaffold improves therapeutic effectiveness in clinical settings where pathogenic organisms such as *Porphyromonas gingivalis* and *Fusobacterium nucleatum* are prevalent. Given that periodontitis is a prevalent oral

condition with strong links to systemic diseases such as diabetes and cardiovascular disease, this study supports broader public health efforts to manage chronic disease through improved periodontal care. Moreover, the development of a locally relevant, cost-effective, and scalable scaffold has the potential to alleviate financial pressures on Malaysia's healthcare system by improving treatment outcomes and reducing long-term care needs. In summary, this study provides an innovative, practical, and culturally adaptable contribution to periodontal regenerative therapy. It not only advances clinical treatment strategies but also opens opportunities for future material sourcing from sustainable marine by-products. As such, it supports national goals in health innovation, economic resilience, and bioresource utilisation.

1.4 RESEARCH OBJECTIVE

1.4.1 General Objective

To develop and characterise CC-MNP scaffolds and evaluate their potential for periodontal bone regeneration through *in vitro* and *in vivo* studies.

1.4.1.1 Specific Objectives

The specific objectives of this study were outlined as follows:

For chapter 3: The objective of this chapter is to develop and validate a UV spectrophotometric method for quantifying MT in CS noncarrier, ensuring that it meets the standards set by the ICH Q2(R1) guidelines. The chapter also aims to formulate MT loaded onto CS nanocarrier using ionic gelation and to characterise their size, stability (zeta potential), morphology, and encapsulation efficiency to ensure their suitability for treating local periodontal disease.

For chapter 4: The objective of this chapter is to fabricate CC scaffolds incorporating MNP at various concentrations and to conduct an extensive evaluation of the scaffolds' properties, including pore size, swelling behaviour, biodegradation rate, and mechanical properties, to assess their suitability for periodontal therapy.

For chapter 5: The objective of this chapter is to evaluate the effectiveness of the CC-MNP scaffold in inhibiting the growth of *Porphyromonas gingivalis* (ATCC 3327) and *Fusobacterium nucleatum* (ATCC 25586) *in vitro*, characterise the *in vitro* drug release profile of MT over 14 days, and analyse the molecular interactions within the scaffold using FTIR measurements. Additionally, the study will assess the biocompatibility of the CC-MNP scaffold with human gingival fibroblast cells (HGF-1) to ensure support for cell viability and proliferation necessary for periodontal bone regeneration.

For chapter 6: The objective of this chapter is to conduct surgical procedures utilizing a rat skull defect model to mimic conditions with periodontal disease. The study aims to evaluate the effectiveness of the CC scaffold loaded with MNP nano-antibiotics in enhancing new bone formation within the skull defect compared to control groups. This evaluation will involve imaging techniques (X-rays) and histological analysis to assess the integration of the scaffold with the surrounding bone and the presence of new bone formation. The CC scaffolds loaded with MNP will effectively promote periodontal bone and tissue regeneration, leading to enhanced healing compared to scaffolds without MNP

1.5 RESEARCH HYPOTHESES

1.5.1 General Hypotesis

The CC scaffolds loaded with MNP will effectively promote periodontal bone and tissue regeneration, leading to enhanced healing compared to scaffolds without MNP

1.5.2 Specific Hypotheses

Hypotheses for Chapter 3 (Nanoparticle Formulation and Characterisation):

The development and validation of the UV spectrophotometric method will meet the ICH Q2(R1) guidelines for accurately and reliably quantifying MT in CS nanoparticle. MT-loaded CS nanoparticles formulated via ionic gelation will exhibit optimal size, stability, morphology, and efficiency for effective drug delivery in periodontal applications.

Hypotheses for Chapter 4 (Scaffold Fabrication and Characterisation):

CC scaffolds with incorporated MNP will exhibit favourable properties, such as adequate pore size, controlled swelling, appropriate biodegradation rates, and mechanical properties suitable for periodontal therapy.

Hypotheses for Chapter 5 (Antibacterial Activity, Drug Release, and Biocompatibility):

The CC-MNP scaffold will inhibit the growth of *P. gingivalis* and *F. nucleatum in vitro*. The MT released from the CC-MNP scaffold will follow a controlled release profile over 14 days, with an initial burst release followed by a sustained release phase. The CC-MNP scaffold will be biocompatible with human gingival fibroblast (HGF-1) cells, supporting cell viability and proliferation necessary for periodontal bone regeneration.

Hypotheses for Chapter 6 (Animal Model and *In Vivo* Assessment):

The CC scaffold loaded with MNP will promote new bone formation in the periodontal defect area compared to control groups, as evidenced by imaging and histological analysi

1.6 FLOWCHART OF RESEARCH STUDY

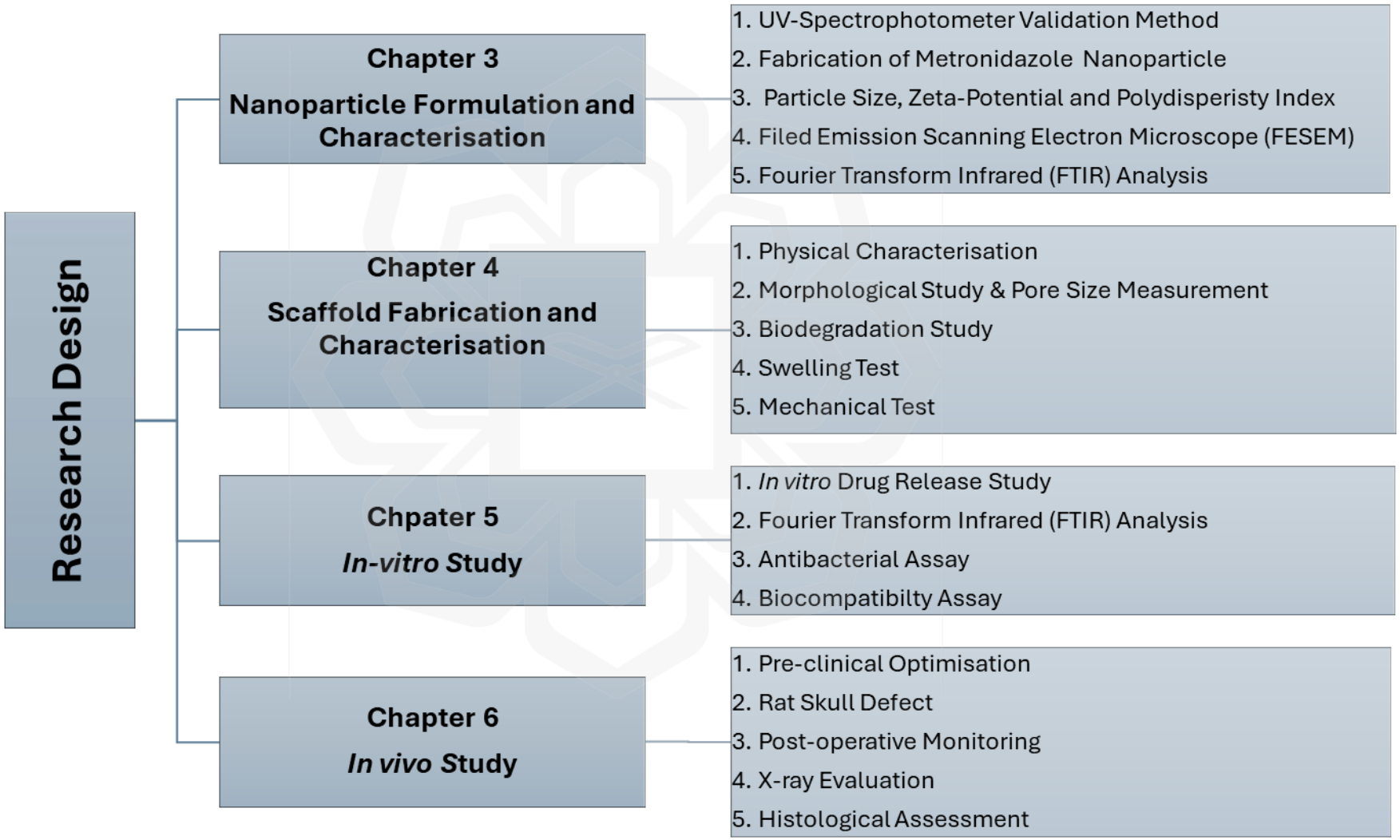

CHAPTER TWO

LITERATURE REVIEW

2.1 PERIODONTAL DISEASE

Periodontal disease encompasses a range of inflammatory conditions affecting the tissues surrounding the teeth and remains a significant global public health concern. It affects a large proportion of the adult population, with severe forms such as aggressive periodontitis causing rapid attachment loss and bone destruction, particularly in adolescents and young adults (Hung et al., 2023). The disease spectrum begins with gingivitis, which is a reversible condition characterised by red, swollen gums and bleeding on probing due to dental plaque accumulation (Pahuja, 2019). If left untreated, gingivitis may progress to periodontitis, an irreversible condition involving not only inflammation but also the degradation of the periodontal ligament and alveolar bone (Hajishengallis & Lamont, 2012; Salvi et al., 2023).

Periodontitis is marked by the formation of periodontal pockets where bacteria and inflammatory mediators accumulate, leading to progressive destruction of periodontal support structures (Armitage, 1999). The systemic impact of periodontitis is profound and multifaceted, as it contributes to chronic systemic inflammation and is associated with an increased risk of several non-communicable diseases, including cardiovascular disease, diabetes, and adverse pregnancy outcomes (Sanz et al., 2020). Additionally, research has drawn connections between periodontal disease and conditions such as rheumatoid arthritis, adverse pregnancy outcomes, and even certain cancers (Winning & Linden, 2017).

The underlying mechanisms involve the translocation of periodontal pathogens and their byproducts into the systemic circulation, which triggers inflammatory and immune responses in distant organs (Hajishengallis & Lamont, 2012; Preshaw et al., 2012). This is consistent with the focal infection theory first proposed by Miller in 1891, which suggested that oral infections could impact systemic health. Contemporary evidence supports this

theory, particularly in the context of preterm and low-birthweight (PLBW) deliveries, where infections are implicated in 30% to 50% of cases (Saini et al., 2010).

In this context, understanding the pathogenesis and systemic implications of periodontal disease highlights the urgent need for effective, targeted, and sustainable treatments. This underscores the importance of developing novel therapeutic strategies, such as localised drug delivery systems and bioactive scaffolds, which this study aims to explore. These approaches could significantly enhance clinical outcomes by addressing both microbial control and tissue regeneration on a single platform.

2.2 MANAGEMENT OF PERIODONTITIS

Periodontitis management is crucial for preventing tooth loss and reducing the risk of systemic complications associated with this chronic inflammatory disease. A comprehensive management strategy includes both surgical and non-surgical approaches, such as scaling and root planing, guided tissue regeneration (GTR), guided bone regeneration (GBR), and the adjunctive use of antibiotics like MT (Moskvin & Khadartsev, 2024; Graziani et al., 2018). Furthermore, emerging therapies such as light-activated antibacterial treatments and antimicrobial photodynamic therapy (aPDT) have shown promise in improving treatment outcomes in severe cases (Šidlauskienė et al., 2024; Kademani et al., 2024). These advances highlight the shift toward multimodal therapies that combine antimicrobial control and tissue regeneration. The integration of MT into a CC scaffold supports targeted antibacterial action while providing regenerative support, enhancing overall treatment efficacy and aligning with current innovations.

2.2.1 Guided Tissue Regeneration/ Bone Regeneration Therapy

Guided tissue regeneration (GTR) and guided bone regeneration (GBR) are advanced surgical techniques employed in periodontology and implant dentistry to restore periodontal tissues and alveolar bone, respectively. These techniques are crucial for

managing tissue deficiencies resulting from periodontal disease, trauma, or surgical interventions. In the 1980s, guided tissue regeneration (GTR) was introduced, proposing that regeneration of a specific tissue type could be achieved by allowing regenerative cells to populate the defect during the healing process. Similarly, Guided Bone Regeneration (GBR) was developed based on this principle but focused on bone regeneration. GBR aims to prevent unwanted soft tissue from invading the bone defect, allowing only bone-forming cells to repopulate the area (Nyman, 1991; Retzepi & Donos, 2010).

Tissue engineering and regenerative medicine have significantly advanced the treatment of bone loss caused by disease, trauma, or cancer. A key element in these techniques is the use of engineered scaffolds or barrier membranes, which can be either biodegradable or non-biodegradable. These scaffolds provide structural support and guide the regeneration process (McGovern et al., 2018). Biomimetic materials, such as collagen, are crucial in GTR and GBR. Collagen mimics the native extracellular matrix (ECM) and supports cell recruitment, adhesion, proliferation, differentiation, and neo-tissue formation (Ebert & Greenberg, 2008). Synthetic biomaterials like polylactic acid (PLA) and hydroxyapatite enhance scaffold performance. These materials offer benefits such as controlled degradation rates and mechanical stability, essential for successful regeneration (McGovern et al., 2018). Clinical studies have demonstrated that GTR and GBR effectively improve clinical outcomes. GTR techniques enhance clinical attachment levels and reduce probing depths in periodontal defects, improving overall periodontal health. GBR is successful in restoring bone volume and contour, which facilitates successful implant placement and improves aesthetic outcomes (Gottlow et al., 1986; Needleman et al., 2006). The incorporation of MT-loaded nanoparticles into CC scaffolds, as proposed in this study, aligns with current trends in enhancing scaffold performance. This approach enables site-specific antimicrobial delivery and creates a regenerative environment conducive to bone and tissue healing, addressing two critical challenges in periodontal therapy.

2.3 SCAFFOLD IN TISSUE ENGINEERING

Since the first term “tissue engineering” emerged in the late 1990s, biomaterial-based scaffolds have played a vital role in GBR by providing mechanical stability and creating a favourable environment for cellular activity, essentially replicating native tissue functions (Ebert & Greenberg, 2008). Scaffolds serve as three-dimensional structures that support cell adhesion, proliferation, and differentiation, ultimately forming new tissue. Scaffolds are three-dimensional structures that enable cell attachment, proliferation, and differentiation to form new tissue. Their core functions include mimicking the ECM, offering mechanical support, and guiding tissue formation. Ideally, these scaffolds degrade at a controlled rate, making way for newly regenerated tissue (O’Brien, 2011; Patterson et al., 2010). An ideal 3D tissue-engineered scaffold mimicks native tissue by providing a suitable environment for tissue repairs such as low toxicity, high porosity, biocompatibility, and suitable absorbability, allowing water vapour to pass through and promoting cell growth while protecting against infections (El-Shanshory et al., 2022). Secondly, an ideal scaffold for GBR must meet specific mechanical and structural requirements. It should provide adequate support to maintain the space for new bone formation while resisting collapse or deformation. Mechanical strength, porosity, and structural integrity are crucial factors that influence the scaffold’s effectiveness in guiding bone regeneration and supporting newly formed tissue (McGovern et al., 2018). These characteristics underscore the rationale for selecting CC as the base material in this study. Collagen offers biological compatibility, while CS contributes structural strength. The scaffold’s ability to stimulate natural ECM and degraded in parallel with new tissue formation makes it ideal for periodontal bone regeneration applications.

2.3.1 Types of Scaffolds

Scaffolds used in guided bone regeneration fall broadly into two categories, non-resorbable and resorbable. Non-resorbable scaffolds, such as metallic structures and certain synthetic polymers, offer durable support but may elicit foreign body responses or necessitate surgical removal. Common non-degradable materials include titanium, cobalt-chromium

alloys, and polymers like polyethylene and PMMA, which offer mechanical resilience but often lack bioactivity (Alavi et al., 2023; Maitz, 2015; Nikolova & Chavali, 2019).

Non-resorbable scaffolds are intended to remain permanently within the body, offering long-term structural support without being broken down or absorbed by the surrounding tissue (Alavi et al., 2023). Metallic 3D scaffolds, as first-generation bone substitute materials, are particularly favoured for load-bearing applications due to their high mechanical strength, fatigue resistance, and ease of manufacturing, with common materials including titanium, stainless steel, cobalt-chromium (Co–Cr) alloys, and magnesium (Mg). Synthetic polymer materials are also extensively used in tissue repair due to their advantageous properties, such as biocompatibility, consistent mechanical and physical characteristics, workability, and cost-effectiveness. Examples of these materials include polyethene (PE), polypropylene (PP), and polymethyl methacrylate (PMMA) (Maitz, 2015; Nikolova & Chavali, 2019). While non-resorbable scaffolds provide long-term support, they can pose challenges such as biomaterial stiffness. This may lead to soft tissue degradation and subsequent failure within the first three weeks after membrane implantation. This can expose the area to bacterial infection, chronic inflammation, and foreign body reactions and potentially necessitate a second surgical procedure for removal (Gentile et al., 2011).

In contrast, resorbable scaffolds degrade over time and are naturally replaced by regenerating tissue. Materials such as polylactic acid (PLA), polyglycolic acid (PGA), and collagen have shown promise in this regard (Ikada, 2006; Rezwan et al., 2006). Natural scaffolds like collagen, gelatin, and CS offer excellent biocompatibility and bioactivity, mimicking ECM and encouraging cellular processes. However, these natural biomaterials are sometimes limited by inconsistent source quality and rapid degradation rates (El-Shanshory et al., 2022). The present study's scaffold selection is grounded in the advantages of resorbable natural biomaterials. The collagen–chiotsan composite harnesses collagen's bioactivity and CS's durability, forming a synergistic platform capable of supporting bone regeneration while providing localised drug delivery. This alignment between material properties and therapeutic objectives reinforces the scaffold's potential as a next-generation GBR material.

2.3.2 Collagen-Based Scaffolds

In Collagen-based scaffolds are increasingly used in regenerative medicine due to their biocompatibility and structural similarity to the natural ECM. As the most abundant ECM protein, collagen supports cellular adhesion, proliferation, and differentiation, a key process in tissue repair (Zhao et al., 2023). Traditionally, collagen is sourced from mammalian tissues such as bovine and porcine origins. However, concerns over disease transmission, including bovine spongiform encephalopathy (BSE), and religious or cultural restrictions have spurred interest in alternative sources like marine collagen (Zhang et al., 2021). Marine-derived collagen, particularly from fish like tilapia, cod, salmon, and carp, has gained traction for its lower immunogenicity and eco-sustainable origin. For instance, collagen extracted from tilapia skin demonstrates promise for scaffold production with minimal waste and high acceptance across diverse populations (Gaikwad & Kim, 2024; Lim et al., 2019). Marine collagen, mainly derived from fish, has emerged as a promising alternative due to its biocompatibility, low immunogenicity, and environmental benefits. For instance, collagen extracted from tilapia skin has been identified as a viable biomaterial for scaffold production, aligning with environmental sustainability and religious requirements (Gaikwad & Kim, 2024; Lim et al., 2019). Moreover, the use of fish by-products for collagen extraction not only minimises waste but also enhances the financial value of fishery products (Zain & Hamdan, 2021). However, collagen scaffolds face challenges such as rapid degradation and poor mechanical strength, which limit their application in long-term tissue engineering (Yan et al., 2010). Despite these advantages, collagen scaffolds face challenges, notably rapid degradation and limited mechanical strength, which can hinder their application in long-term tissue engineering. To address these issues, researchers have explored various cross-linking techniques and the incorporation of other biomaterials. For example, combining collagen with CS has been shown to enhance the structural integrity and functionality of the scaffolds. This approach not only improves mechanical properties but also aligns sustainability goals and cultural considerations, supporting broader adoption of the developed scaffolds.

2.3.2.1 Collagen-chitosan (CC) Scaffolds

In recent years, research on collagen-based scaffolds has progressed significantly, focusing on improving mechanical strength, biocompatibility, and degradation behaviour through advanced cross-linking techniques and the integration of composite materials (Kaczmarek-Szczepańska et al., 2023). Among these, CC composite scaffolds have emerged as promising candidates due to their synergistic properties. Collagen facilitates biological recognition and cell adhesion, while CS contributes to mechanical reinforcement (Grabska-Zielińska et al., 2021; Przybyłek et al., 2023). Together, they form a bioactive and biodegradable matrix that closely mimics the ECM, making them highly suitable for applications in bone, cartilage, skin, and periodontal regeneration (Filippi et al., 2020).

Grabska-Zielińska et al. (2021) reported that the incorporation of dialdehyde chitosan (DAC) improves the physicochemical properties of collagen-based scaffolds without compromising cellular viability, reinforcing their potential in tissue regeneration. Furthermore, molecular simulations by Przybyłek et al. (2023) demonstrated that environmental pH and ionic concentrations significantly influence CC interactions, offering critical insights for optimising fabrication protocols. The high porosity and interconnected pore network of these scaffolds create a favourable environment for drug encapsulation and controlled release (Li et al., 2021). This dual functionality is particularly beneficial in periodontal and orthopaedic contexts, where simultaneous tissue regeneration and infection control are essential (Chacon et al., 2023).

Recent advancements in scaffold fabrication, including electrospinning and 3D bioprinting, have enabled the incorporation of growth factors, nanoparticles, and antibiotics into the CC matrix (Dasgupta et al., 2023). For instance, Liu et al. (2021) utilised 3D-printed CC scaffolds embedded with brain-derived neurotrophic factor (BDNF), demonstrating multifunctional therapeutic potential in spinal cord injury repair. The excellent biocompatibility and minimal immunogenicity of these scaffolds support their clinical translation, particularly when the degradation rate is synchronised with new tissue formation (Hidalgo-Vicelis et al., 2020). Additionally, sourcing collagen and CS from halal

and sustainable materials, such as fish skin and fungi, aligns with ethical, cultural, and environmental values, thereby enhancing public acceptance and global commercialisation prospects (Nurilmala et al., 2022; Coppola et al., 2020; Huq et al., 2022).

2.4 APPLICATION OF SCAFFOLD IN DRUG DELIVERY

Recent advancements in scaffold technology have led to the development of third-generation scaffolds designed to serve dual purposes such as barriers and drug delivery devices (Sam & Madhavan Pillai, 2014). These advanced scaffolds provide structural support and enable the controlled release of therapeutic agents, including antibiotics, anti-inflammatory drugs, growth factors, proteins, nucleic acids, and herbal extracts (Yang et al., 2019). For instance, asymmetric membranes loaded with nanoparticles have been engineered for targeted drug delivery, optimising drug release profiles to improve therapeutic outcomes (Da Silva et al., 2016).

Controlled drug delivery through scaffolds can be achieved by physically or chemically adsorbing drugs onto the scaffold's surface, encapsulating drugs within the scaffold, or incorporating drug delivery systems into the scaffold (Rambhia & Ma, 2015). Drugs attached to the scaffold surface via surface loading allow for rapid release, leaving little to no residual drug in the implanted materials after a set release period. This reduces the harmful effects of residual drugs on subsequent bone regeneration and is particularly useful for delivering high doses of drugs to control infections in the early stages of implantation (Wei et al., 2019). The surface attachment of antimicrobial agents on scaffolds can rapidly respond to bacterial contamination, thereby preventing infection and promoting healing (Liang et al., 2022; Sheehy et al., 2025). Drug release from scaffolds can occur through diffusion or via the degradation of the scaffold or encapsulating material (Rambhia & Ma, 2015). CC scaffolds have been explored as drug delivery systems for controlled release applications. Advances in scaffold design include incorporating stimuli-responsive elements and improved drug loading capacities, allowing drug release in response to specific stimuli such as changes in pH, temperature, or enzymatic activity (Schoeller et al.,

2021). CS-based scaffolds are especially effective in responsive release due to their pH-sensitive nature (Kumar et al., 2021). With its pH-sensitive properties, CS is well-suited for targeted drug delivery in slightly acidic environments, such as inflamed or infected tissues (Donos et al., 2015). For example, CC-MNP has shown the potential to promote bone regeneration by delivering antibiotics directly to the implantation site (Porgham Daryasari et al., 2019). Integrating drug-loaded scaffolds into tissue engineering strategies represents a significant advancement in the field, allowing for the simultaneous delivery of therapeutic agents and providing structural support for tissue regeneration.

Pre-clinical trials investigating scaffold-based drug delivery systems have demonstrated significant promise across various medical applications, particularly in wound healing and bone regeneration. In wound healing, scaffold-based systems have been employed to deliver growth factors, antibiotics, and anti-inflammatory agents, facilitating faster and more efficient tissue repair. For instance, the use of nanoparticles in a diabetic mouse model has shown potential for promoting wound healing, suggesting their utility as dressings for patients with diabetic foot ulcers (Losi et al., 2013). In bone regeneration, scaffold-based drug delivery systems have been notably successful in promoting the repair of bone defects and enhancing the integration of bone grafts. A prominent clinical trial examined the use of hydroxyapatite (HA) scaffold combined with bone morphogenetic protein-2 (BMP-2) for treating critical-sized bone defects. Results indicated that patients receiving the BMP-2-loaded scaffold exhibited significantly higher bone regeneration and graft integration rates than those treated with the scaffold alone (Deininger et al., 2022). This finding underscores the critical role of localised BMP-2 delivery in stimulating osteogenesis and accelerating the healing process. Further clinical trials have explored the incorporation of hydroxyapatite into collagen scaffolds, which has been shown to enhance the therapeutic efficacy of recombinant human BMP-2 (rhBMP-2). This combination has demonstrated superior bone healing and regeneration in weight-bearing femoral defect models compared to collagen-only scaffolds (Lackington et al., 2021). Integrating antibiotics and growth factors into scaffolds also shows promise for promoting new bone growth and supporting the healing process.

Overall, scaffold-based drug delivery systems significantly advance regenerative medicine and tissue engineering. By integrating drug delivery capabilities into scaffolds, these systems provide both structural support and controlled release of therapeutic agents, thereby enhancing the efficacy of treatments for tissue repair and regeneration (Sheehy et al., 2025).

2.5 ENCAPSULATION OF NANO ANTIBIOTIC SCAFFOLD

The encapsulation of nano-antibiotics into biodegradable scaffolds has emerged as a highly effective strategy for managing periodontal and bone infections. Systemic antibiotic therapy, although commonly prescribed, is associated with side effects such as gastrointestinal discomfort, hypersensitivity reactions, and an increasing threat of bacterial resistance (Shrestha et al., 2023). In contrast, local drug delivery systems (LDDS) offer notable advantages by enabling the targeted release of high concentrations of antibiotics directly at the infection site while minimising systemic toxicity (He et al., 2020). Incorporating antibiotics into scaffold matrices particularly based on collagen and CS able to facilitate sustained and localised release, thereby overcoming challenges such as biofilm formation and poor drug penetration into deep tissues (Alghofaily et al., 2024). This approach also offers the advantage of protecting antibiotics from enzymatic degradation and allows for better retention in the periodontal pocket, which is otherwise prone to rapid clearance (Jiang et al., 2020). For example, Lazarević et al. (2023) reported that a collagen membrane modified with CS and nano-hydroxyapatite showed enhanced antibacterial activity against periodontal pathogens and promoted osteogenic differentiation of dental stem cells, supporting its dual therapeutic role.

Nano-antibiotics with particle sizes below 500 nm have been demonstrated to effectively penetrate biofilms and infected tissues, thereby improving therapeutic efficacy while reducing the need for frequent dosing (Shrestha et al., 2021). Encapsulation also enhances drug stability and enables controlled release within dynamic microenvironments, such as those found in inflamed periodontal tissues. Various techniques including ionic

gelation, solvent evaporation, spray drying, and electrospinning are employed to integrate nano-antibiotics into scaffolds (Theodoridis et al., 2023). In more advanced applications, cell membrane-coated nanoparticles have been developed to enhance both targeting and immune evasion. For instance, Park et al. (2021) designed dexamethasone-loaded nanoparticles cloaked with genetically engineered cell membranes, allowing them to home to inflame tissues and suppress local inflammation effectively. This strategy reflects growing interest in scaffold systems that not only deliver antibiotics but also modulate immune responses to foster a conducive healing environment.The convergence of antimicrobial activity and tissue regeneration within a single biomaterial platform aligns well with the objectives of periodontal and orthopaedic therapy. Alghofaily et al. (2024) demonstrated that antibiotic-loaded CS–gelatin scaffolds exhibited both strong antibacterial effects and compatibility with dental stem cells. Similarly, Theodoridis et al. (2023) showed that 3D-printed polycaprolactone scaffolds loaded with tetracycline hydrochloride achieved effective antibacterial action and supported osteoblast proliferation, indicating suitability for alveolar bone regeneration.Thus, nano-antibiotic encapsulation within CC and composite scaffolds offers a promising dual-function approach by providing structural support for regeneration while ensuring sustained antimicrobial protection. This strategy has significant potential to overcome the limitations of conventional antibiotic therapy, improve clinical outcomes, and enhance patient compliance through localised, controlled delivery.

2.6 PERIODONTAL PATHOGENS

Periodontitis is a chronic inflammatory disease driven by dysbiotic oral microbiota and aberrant host responses, leading to destruction of periodontal tissues and alveolar bone (Lamont & Kuboniwa, 2024; Shi et al., 2023). Among the diverse subgingival microbiota, *Porphyromonas gingivalis* and *Fusobacterium nucleatum* have emerged as key contributors to periodontitis. *P. gingivalis* is a Gram-negative anaerobe traditionally classified in the “red complex” of periodontal pathogens and is strongly associated with disease development and progression (Hajishengallis & Diaz, 2020). *F. nucleatum*, a Gram-

negative fusiform anaerobe, is highly prevalent in the oral cavity of both healthy and diseased individuals but plays a pivotal role in the transition from health to disease by bridging and integrating the microbial community (Groeger et al., 2022).

P. gingivalis adheres to and invades host tissues using fimbriae and outer membrane vesicles (OMVs) that deliver virulence factors into host cells. It secretes gingipain, a cysteine protease that degrades extracellular matrix components and immune mediators leading to tissue destruction and evasion of immune responses (Hajishengallis & Diaz, 2020; Lamont & Kuboniwa, 2024). It also selectively dysregulates innate immunity and activates host receptors to incite the immune response, promoting chronic inflammation. *F. nucleatum* acts as a bridging organism in oral biofilms, physically linking early and late colonisers. Its adhesins, including Receptor Antigen D (RadD) and Fusobacterium adhesion A (FadA), facilitate co-aggregation with other bacteria and invasion of host cells (Groeger et al., 2022). It also induces matrix metalloproteinases and stimulates secretion of pro-inflammatory cytokines such including interleukin-6 (IL-6) and interleukin-8 (IL-8), thereby exacerbating tissue damage and sustaining the inflammatory milieu (Shi et al., 2023). Both pathogens disrupt host–microbe homeostasis. *P. gingivalis* functions as a keystone pathogen by promoting dysbiosis and chronic inflammation despite being a minor constituent of the microbiota. It manipulates Toll-like receptors and complement pathways to evade immune clearance while inducing cytokine release (Hajishengallis & Diaz, 2020). *F. nucleatum* flourishes in the resulting inflammatory environment, further amplifying immune activation and supporting the survival of other pathogens (Shi et al., 2023). Their interaction enhances pathogenicity. *F. nucleatum* facilitates the colonisation and invasion of *P. gingivalis*, and co-infection results in higher levels of inflammation and tissue destruction than either species alone. Co-culture studies have shown synergistic upregulation of IL-6 via TLR4 signalling in oral epithelial cells (Yáñez et al., 2024). *In vivo*, mixed infections lead to more severe bone loss and immune cell infiltration compared to monoinfections (Binder Gallimidi et al., 2015).

Clinically, both pathogens are markers of periodontal disease. *P. gingivalis* is rarely detected in health but commonly found in deep periodontal pockets and correlates with

disease severity (Suhaimi et al., 2025). Its detection is predictive of ongoing tissue destruction. *F. nucleatum*, while present in health, increases in abundance in severe periodontitis and enhances the pathogenic biofilm (Groeger et al., 2022). Monitoring and targeting these pathogens are crucial for accurate diagnosis, effective treatment, and preventing disease progression. The pathogenic roles and synergy of *P. gingivalis* and *F. nucleatum* in periodontitis highlights the necessity for designing targeted scaffolds for dual-pathogen control that could enhance the efficacy of antimicrobial delivery systems and promote more effective periodontal tissue regeneration.

2.7 THE RATIONALE OF ANTIBIOTIC THERAPY

The oral route is regarded as the most convenient means of drug administration due to its ease and non-invasiveness. However, systemic antibiotic therapy is frequently associated with undesirable side effects, most notably the development of antimicrobial resistance, which poses a significant challenge in the management of microbial infections (Mamikutty & Ng, 2022). Furthermore, oral drug delivery is often hindered by the first-pass effect, in which drug absorption through the gastrointestinal tract and liver leads to a substantial reduction in bioavailability due to pH variations and enzymatic degradation (Amato et al., 2023). These limitations have prompted growing interest in local drug delivery (LDD) systems. LDD allows the administration of antimicrobials directly into the periodontal pocket, resulting in higher concentrations of the therapeutic agent at the site of infection while requiring lower doses. This targeted approach not only enhances clinical efficacy but also minimises systemic toxicity and side effects (Amato et al., 2023). Additionally, LDDs are less likely to disrupt the oral microbial balance and may reduce the risk of bacterial resistance that arises from the prolonged or inappropriate use of systemic antibiotics. Given these advantages, LDD systems present a promising strategy for managing periodontal disease with greater safety and precision.

2.7.2 MT as an Effective Antibiotic

MT is a nitroimidazole antibiotic widely recognised for its efficacy against obligate anaerobic bacteria, which constitute many of the key pathogens in periodontitis. Mechanistically, MT acts as a prodrug that is activated by anaerobic microbial enzymes to produce cytotoxic free radicals, leading to DNA strand breakage and bacterial cell death (Gandhi et al., 2025). Since its initial discovery in the treatment of *Trichomonas vaginalis*, it has been increasingly employed in the management of various infections, including periodontitis, due to its broad-spectrum activity against obligate anaerobes such as *Porphyromonas gingivalis*, *Tannerella forsythia*, and *Treponema denticola* (Gandhi et al., 2025; Hagenfeld et al., 2020). Compared to other antibiotics like tetracyclines, MT exerts a lower impact on the host's normal microbiota and carries a reduced risk of promoting multi-drug resistance, making it a safer and more selective alternative. The bactericidal mechanism of MT involves the reduction of its 5-nitro group within the anaerobic cell, resulting in the production of cytotoxic free radicals that disrupt DNA synthesis and lead to cell death (Gandhi et al., 2025). Its efficacy has been demonstrated against a broad range of periodontal pathogens, including *Aggregatibacter actinomycetemcomitans*, *Prevotella intermedia*, *Fusobacterium nucleatum*, *Streptococcus sanguinis*, *Parvimonas micra*, and *Eikenella corrodens* (Mugri, 2022).

MT has been extensively employed in the treatment of periodontitis due to its potent activity against obligate anaerobic bacteria, particularly *Porphyromonas gingivalis* and *Fusobacterium nucleatum*, both of which play pivotal roles in the pathogenesis of periodontal disease. *In vitro* and *in vivo* studies have consistently demonstrated the susceptibility of these pathogens to MT, with minimal resistance. Numerous clinical studies support the use of MT, particularly in combination with mechanical debridement such as scaling and root planing, as this approach consistently yields greater reductions in periodontal pocket depth and improved clinical attachment levels compared to mechanical treatment alone (Gandhi et al., 2025; Mugri, 2022). Rams et al. (2020) showed that clinical isolates of *P. gingivalis* and *F. nucleatum* were completely inhibited by therapeutic concentrations of MT, indicating strong antimicrobial efficacy. Similarly, Werner et al.

(2025) found that systemic administration of MT significantly reduced the levels of these pathogens in periodontal pockets and improved clinical parameters when used alongside scaling and root planing. The antimicrobial mechanism of MT involves the intracellular reduction of its nitro group under anaerobic conditions, leading to the formation of free radicals that damage bacterial DNA and result in cell death (Gandhi et al., 2025). This mechanism ensures selective toxicity against anaerobic pathogens while sparing beneficial aerobic microbiota, thereby preserving microbial homeostasis. Clinical outcomes further support by Jepsen et al. (2021) observed that susceptibility of MT among subgingival isolates remained consistently high over several years of surveillance, with no significant emergence of resistance. Furthermore, longitudinal studies have confirmed that MT retains its efficacy against *P. gingivalis*, with resistance levels remaining below 1% in patient samples (Rams et al., 2023). Furthermore, it is capable of achieving effective concentrations in the gingival crevicular fluid, ensuring its local action at the site of infection while minimising systemic exposure and side effects (Mugri, 2022). MT delivery in gel or tablet form enables sufficient therapeutic concentrations within the gingival crevicular fluid, which enhances its local effectiveness while minimising systemic exposure (Mamikutty & Ng, 2022). Adverse effects are generally mild and transient, with gastrointestinal discomfort and metallic taste being the most frequently reported.The evidence strongly supports MT as a key adjunctive agent in the management of periodontitis, particularly against anaerobic pathogens associated with disease progression.

2..7.3 Topical Antibiotic in Managing Periodontitis

Antibiotic resistance remains a major global health concern, with the World Health Organisation projecting a sharp increase in antimicrobial-resistant infections if current prescribing trends continue. Systemic administration of MT has proven effective in reducing bacterial load in the oral cavity, however, it is frequently associated with undesirable side effects such as gastrointestinal discomfort, metallic taste, and in some cases, peripheral neuropathy. Moreover, its systemic use contributes to the growing concern of antimicrobial resistance, especially when administered broadly (Mehravani et al., 2024). To address these limitations, the local delivery of MT has gained increasing interest due to its ability to provide high concentrations of the drug directly to the

infection site, while reducing systemic exposure and adverse effects (Dental Update, 2021). The targeted application of MT via local delivery helps mitigate this risk by minimising the impact on the host's systemic microbiome, thus preserving the efficacy of existing antibiotics and reducing selective pressure for resistance (Gager and Götz, 2023).

LDD systems such as gels, films, and fibres have been developed to enhance the efficacy of MT. Recent advancements include the formulation of thermosensitive hydrogels incorporating polymers such as pluronic F127, methylcellulose, and silk fibroin. These hydrogels exhibit sol-gel transitions at body temperature, thereby facilitating sustained MT release over an extended period and ensuring drug stability within the periodontal pocket (Wang et al., 2021). Similarly, pectin-based films loaded with MT have demonstrated promising antimicrobial activity against key periodontal pathogens, offering a controlled release profile suitable for clinical application (Phaechamud and Mahadlek, 2018). Electrospun fibres made from polylactic acid (PLA) containing MT have also been developed to target periodontal infections. These fibres exhibit slow drug elution over a period of several days to weeks, which effectively reduces bacterial populations while maintaining biocompatibility with periodontal tissues (Budai-Szűcs et al., 2020). These emerging technologies highlight the critical role of biomaterials in targeted, sustained-release therapies. Building on these concepts, the current study introduces a novel biodegradable scaffold composed of marine-derived collagen and CS, which not only provides mechanical support for tissue regeneration but also acts as a smart carrier for nano-encapsulated MT. This scaffold-based delivery approach is designed to overcome the limitations of existing LDD systems by offering improved biocompatibility, structural integrity, and degradation kinetics tailored to the healing dynamics of periodontal tissues.

.

2.7.3.1 Potential Application of Local Metronidazole

Various carriers have been employed for the local delivery of MT, each demonstrating unique drug release profiles suitable for periodontal therapy. Advances in local drug delivery (LDD) technologies have facilitated the design of novel MT-based delivery systems, including hydrogels, films, fibres, and nanogels. These systems are designed to

provide sustained and controlled release of MT within the periodontal pocket, thereby enhancing therapeutic efficacy while minimising systemic side effects. Gels typically provide a rapid release within 1–7 days, whereas films and fibre mats offer extended-release durations ranging from 2 to 28 days. These carriers have demonstrated biocompatibility, mechanical stability, and non-toxic behaviour which are crucial characteristics for effective periodontal pocket treatment (Mirzaeei et al., 2021; Pham et al., 2021; Hasan et al., 2020). For example, thermosensitive hydrogels composed of Pluronic F127 and silk fibroin were able to sustain MT release for up to 10 days (Pham et al., 2021). Mucoadhesive films derived from low methoxyl pectin provided an initial burst release followed by a sustained seven-day delivery, ensuring effective contact with the periodontal site (Azadi Boroujeni et al., 2020). Meanwhile, electrospun polylactic acid (PLA) fibres extended MT release for up to 28 days, facilitating prolonged antimicrobial activity and bacterial inhibition (Mirzaeei et al., 2021). These delivery vehicles not only enhance the local therapeutic effects of MT but also reduce systemic exposure and the associated risk of antibiotic resistance. As illustrated in Figure 2.1, the variety of MT-loaded vehicles underscores the evolving strategies in periodontal therapy.

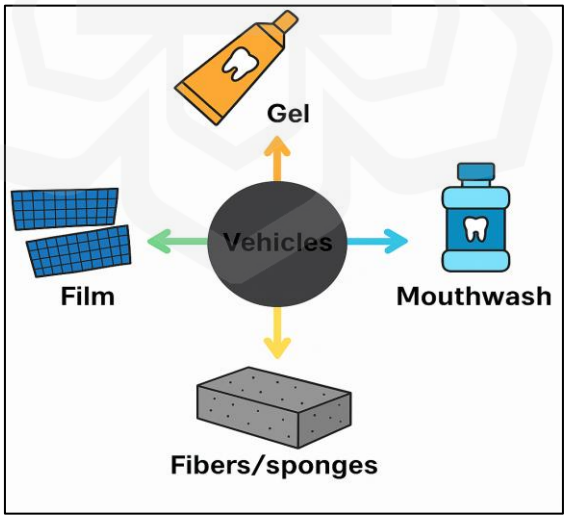

Figure 2.1 Vehicles used for local drug delivery of MT

Additionally, various MT-based LDD systems investigated globally over the past decade, highlighting their mechanisms, types, and therapeutic outcomes in periodontal treatment. Moreover, there is an increasing trend towards employing scaffolds as local drug delivery systems due to their ability to provide sustained and targeted release, improved biocompatibility, and enhanced therapeutic efficacy (Mirzaeei et al., 2021; Pham et al., 2021). Thus, scaffolds have gained increasing interest as promising carriers for delivering MT locally in periodontal therapy. Table 2.1 presents a summary of MT-based LDD applications reported worldwide over the last ten years, highlighting their formulation types, release profiles, and therapeutic implications.

Table 2.1 Summary of MT applications via LDD systems for periodontal therapy

Authors	Mechanism	Local drug delivery system	Findings
Mirzaeei et al., 2021	Electrospinning	Nanofiber	Controlled drug release over 7-10 days in animal models. Bio-compactible, non-toxic, and good mechanical properties.
Pham et al., 2021	Physical mixing	Thermosensitive hydrogel	The hydrogels sustained the release of MT for 10 days.
Dhedage et al., 2020	Modified solvent casting	Intrapacket film	An initial burst release followed by a continuous release of more than 11 days. Exhibited a biphasic drug release profile

Azadi Boroujeni et al., 2020	Casting	Mucoadhesive film	Releases the antibiotics up to 48 hours
Léber et al., 2019	Complex composition	Anhydrous lipid-based	Sustain drug release with swellable and degradable systems. Antimicrobial activity against six different strains of the pathogen that initiate periodontitis
Laurén et al., 2018	liquid moulding	Mucoadhesive films	Rapid drug release of MT observed in 30 minutes
Rivis et al., 2018	Lyophilisation of composite gels	Collagen/Strontium sponges	The degradable system within 24 hours Rapid release of drug at first 30- 60 minutes followed by gradual release over about 4 hours
Hasan et al., 2020	Clinical phase trial	Gel and mouthwash	Significant reduction of periodontitis within four weeks The gel is more effective than mouthwash in reducing clinical attachment loss and inflammatory biomarkers. No side effects reported

Rangabhatla et al., 2017	Thermoresponsive in-situ	Hydrogel	Mucoadhesive ability and biocompatible. Sustained the release of MT over 24 hours.
Mei et al., 2017	Inverse lyotropic liquid crystalline (LCC)	Solution–gel	The MIC of the drug is maintained for over 10 days in rabbits without a detectable drug in the blood. Intra-pocket LLC system for local treatment of chronic periodontitis.
Labib et al., 2014	Solvent casting	Films	The burst release rate of MT for the first two hours then decreased. Enhances the therapeutic effect of scaling and root planning (SRP) procedure than SRP alone
Peerapattana et al., 2015	Chemical mixing	Films	MT slowly released from the matrices over five days.
Reise et al., 2012	Electrospun	Polylactide fibres	MT is released up to the 28th day from fibre mats.

2.7.3.2 Metronidazole-Loaded onto Scaffold as Local Drug Delivery

GBR scaffolds are widely used in dental surgeries to facilitate bone healing. However, a significant challenge with these scaffolds is their susceptibility to infection due to pathogen

colonisation at wound sites, necessitating the use of antibiotics to mitigate infection risk during the healing process (Sánchez-Carreño López et al., 2025). The integration of MT into GBR scaffolds as a localised drug delivery system has emerged as a promising strategy to enhance the effectiveness of these scaffolds in preventing infections. Localised delivery of MT offers the advantage of maintaining high drug concentrations at the wound site, thereby reducing the risk of systemic side effects. Recent studies have advanced the development of MT-loaded scaffolds with enhanced antimicrobial and regenerative properties. For instance, multilayered scaffolds incorporating MT and ozone have demonstrated improved antimicrobial efficacy against resistant bacterial strains while supporting bone regeneration due to the presence of hydroxyapatite (Sánchez-Carreño López et al., 2025). Similarly, MT-loaded silk fibroin methacrylated (SilkMA) electrospun scaffolds have been developed for the localised treatment of periapical lesions, effectively managing infection and promoting bone healing (Chakraborty et al., 2025). Furthermore, Gandhi et al. (2025) highlighted the successful application of MT as a local drug delivery agent in periodontal therapy, demonstrating significant improvements in clinical parameters by targeting periodontal pathogens directly at the site of infection.These advancements underscore the potential of MT-loaded scaffolds in GBR applications, offering targeted antimicrobial therapy that not only mitigates infection risks but also supports the regenerative processes essential for successful bone healing. Despite these promising attributes, further research is needed to optimise scaffold composition, drug loading capacity, and release kinetics to meet the complex environment of periodontal pockets. Aditionally, comprehensive *in vitro* and *in vivo* investigations are required to validate the long-term efficacy, safety, and clinical performance of these scaffolds before routine clinical use.

2.7.3.3 Properties and Mechanism Action of Metronidazole

MT ($C_6H_9N_3O_3$) is a synthetic 5-nitroimidazole derivative widely used for its antimicrobial and antiparasitic properties. It exists as a white to pale-yellow crystalline powder with a molecular weight of 171.15 g/mol and a water solubility of approximately 10 mg/mL at

room temperature, moderately soluble in water (Chen et al., 2022). Its solubility can be significantly influenced by the pH of the medium and the presence of solubilising agents. According to the Japanese Pharmacopoeia, MT is freely soluble in acetic acid, highlighting its favourable solubility under acidic conditions (Japanese Pharmacopoeia, 2021). This property makes it particularly amenable to inclusion in acid-based solvent systems, eutectic solvents, and biodegradable scaffolds where pH-sensitive or sustained release is desired. Chemically MT is known as 2-(2-methyl-5-nitro-1H-imidazol-1-yl) ethanol. Its chemical structure is illustrated in Figure 2.2 (created with BioRender.com). It exhibits moderate lipophilicity (logP ≈ −0.02) and remains stable in solid form under controlled conditions (Chen et al., 2022).

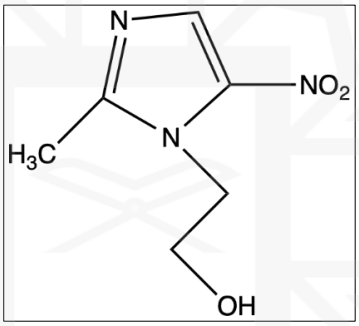

Figure 2.2 Structure of MT (Biorender.com)

Pharmacologically, MT acts as a prodrug that requires intracellular activation under anaerobic conditions. Upon diffusion into microbial cells, its 5-nitro group is reduced by redox enzymes such as ferredoxins and nitroreductases, producing cytotoxic intermediates like nitro radical anions and hydroxylamines (Olaitan et al., 2023). These reactive species bind to microbial DNA, causing strand breaks and inhibiting nucleic acid synthesis, ultimately resulting in cell death. This mechanism is selective for anaerobic and microaerophilic organisms because the presence of oxygen inhibits this activation by competing for electrons (Olaitan et al., 2023). In scaffold-based applications, MT's anaerobic selectivity is particularly advantageous for targeting infections in low-oxygen

environments, such as periodontal pockets. Its incorporation into localised drug delivery systems allows for sustained therapeutic concentrations directly at the site of infection, minimising systemic exposure. For instance, Mirzaeei et al. (2021) developed electrospun nanofibres made of poly(lactic-co-glycolic acid) (PLGA) and polycaprolactone (PCL) loaded with MT and amoxicillin, demonstrating prolonged release, excellent biocompatibility, and over 80% cell viability in periodontal therapy applications. Additional studies have used MT in thermosensitive hydrogels and bioadhesive films for localised treatment. Bastos et al. (2024) reported that MT-containing polymeric gels and films significantly improved clinical parameters such as probing depth and bleeding index when used as adjuncts to scaling and root planing in periodontitis patients. These findings support the clinical relevance of sustained-release scaffold systems incorporating MT. Moreover, Herold (2022) demonstrated the feasibility of custom 3D-printed silicone scaffolds impregnated with MT. These scaffolds showed controlled drug release profiles over 14 days and potential applicability in managing localised infections. Together, these technologies leverage the drug's physicochemical properties specifically, its moderate solubility and anaerobic targeting to enable effective and targeted antimicrobial delivery. The combination of MT's chemical stability, selective mechanism of action, and moderate solubility makes it a suitable candidate for scaffold-based drug delivery systems.

2.8 NANOPARTICLE IN SCAFFOLD SYSTEM

The incorporation of nanoparticles into three-dimensional (3D) scaffold systems has become a significant advancement in medical and dental regenerative applications. These nanoscale materials can be engineered to modulate scaffold properties by enhancing mechanical strength, mimicking ECM nanostructure, and serving as carriers for bioactive or antimicrobial agents (Farjaminejad, S., Farjaminejad, R., & Garcia-Godoy, 2024; Mansour et al., 2023). When encapsulated within scaffold matrices, these nanoparticles enable localised and sustained drug delivery to target sites, thereby improving treatment efficacy while minimising systemic exposure (Grierosu et al., 2023; Li et al., 2024). For example, incorporating nanoparticles such as silver or bioactive glass confers antimicrobial

and osteogenic properties, respectively, without compromising scaffold biocompatibility (Takallu et al., 2024). Additionally, scaffolds incorporating growth factors and anti-inflammatory agents, delivered through nanoparticle systems, have shown improved bone healing and reduced inflammation. For example, nanocarriers containing bone morphogenetic proteins (BMPs) and other regenerative factors can enhance scaffold performance by promoting osteogenesis and minimising inflammatory responses (Narayanan, 2025).

Porous scaffolds serve as biomimetic ECM substitutes, facilitating cell adhesion, proliferation, and differentiation. Ideal scaffolds exhibit high porosity (typically >80%) with interconnected pore networks that allow for adequate vascularisation, nutrient diffusion, and waste removal (Lutzweiler, Halili, & Vrana, 2020; Borges et al., 2023). Natural polymers such as collagen and CS are frequently employed due to their biocompatibility, biodegradability, and similarity to native tissue structures (Farjaminejad, S., Farjaminejad, R., & Garcia-Godoy, 2024; Piszko et al., 2024). Collagen provides a fibrillar framework essential for osteoblastic activity, whereas CS regulates degradation kinetics. The combination of these polymers results in scaffolds with optimal physical and biological characteristics. Furthermore, scaffold architecture, including pore size and distribution, is critical in regulating cell behaviour, with studies showing that pores between 50–150 μm are ideal for periodontal tissue engineering applications (Lutzweiler et al., 2020). Their high porosity with interconnected pores is critical in facilitating essential biological processes such as vascularisation, nutrient diffusion, and cellular infiltration. These structural characteristics are vital for supporting tissue regeneration, particularly in compromised or infected wound environments. In a recent study, Dorazilová et al. (2020) demonstrated that freeze-dried CC scaffolds formed a highly porous, three-dimensional matrix with interconnected pores that enabled efficient nutrient transport and created a favourable microenvironment for cellular activity. Furthermore, the study integrated selenium nanoparticles (SeNPs) into the scaffold without compromising its porosity. The resulting composite not only maintained structural integrity but also provided sustained antibacterial activity, effectively inhibiting common wound pathogens such as *Staphylococcus aureus*, MRSA, and *S. epidermidis*. Furthermore, the incorporation of nanoparticles into porous scaffolds has gained significant interest in regenerative medicine due to its capacity to substantially enhance their functional and mechanical properties. The process of incorporating nanoparticles within the scaffold matrix, commonly referred to as nano-crosslinking resulting in improved structural integrity. For instance, Asghar et al. (2021) reported that scaffolds doped with

zinc-doped hydroxyapatite (Zn-HAp) nanoparticles showed enhanced load-bearing strength and biocompatibility, highlighting their suitability for bone tissue regeneration. These enhancements are attributed to the nanoparticles' ability to interact with the scaffold's polymer network, improving mechanical stability while also influencing cell behaviour and promoting tissue integration.

In periodontal therapy, the incorporation of antibiotic-loaded nanoparticles into scaffolds is a promising strategy for enhancing treatment efficacy. Periodontitis is a chronic inflammatory disease primarily driven by anaerobic bacteria in the deep periodontal pockets (Mirzaeei et al., 2022). Conventional systemic delivery of antimicrobials often fails to maintain therapeutic concentrations in these sites, so localised delivery via scaffolds is desirable. Scaffolds can act as controlled-release drug delivery systems, releasing MT directly at the infection site and thus minimising the need for systemic administration and its associated side effects. Recent studies have explored MT-loaded nanoparticles in periodontal tissue engineering. Nanoformulations of MT have also been shown to improve drug penetration into biofilms and to sustain antimicrobial activity within periodontal pockets (Ho et al., 2022). For example, Chen et al. (2023) developed guided-tissue-regeneration membranes incorporating MT-loaded nanoparticles to improve drug permeation and support periodontal tissue recovery. These advances underscore the potential of nanoparticle-integrated scaffolds to deliver targeted antimicrobial therapy that mitigates infection and supports the regenerative processes essential for successful bone healing. By loading MT nanoparticles into a scaffold, a sustained, site-specific antimicrobial action can be achieved directly within periodontal defects, reducing reliance on systemic therapy and enhancing healing outcomes.

Figure 2.3 presents a schematic diagram of a 3D-printed porous scaffold with nanoparticles incorporated throughout (created using BioRender.com) and conceptually adapted from Yang et al., 2024; Toosi et al., 2022). The scaffold is illustrated as a cylindrical structure with visible interconnected pores, reflecting the characteristic architecture of tissue-engineered scaffolds. Such a porous environment is essential for mimicking the native tissue microenvironment, allowing for vascularisation, nutrient diffusion, and cellular infiltration critical processes for successful tissue regeneration (Yang

et al., 2024; Toosi et al., 2022). The nano-crosslinked scaffolds have shown the potential to serve as dual-function systems providing mechanical support for tissue in-growth while delivering bioactive compounds or antimicrobials at the site of interest (Piszko et al., 2024).These findings highlight the potential of nano-crosslinked scaffolds not only as structural templates for tissue growth but also as bioactive platforms for improved cellular responses and targeted therapeutic delivery. Despite these promising attributes, further research is needed to optimise scaffold design, drug loading capacity, and release kinetics to align with the dynamic conditions present in periodontal lesions. Extensive *in vitro* and *in vivo* studies are essential to assess long-term safety, efficacy, and translational potential before clinical application.

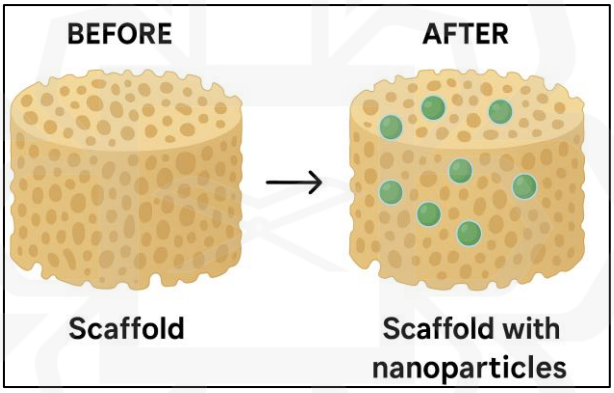

Figure 2.3: Schematic diagram of porous scaffolds before and after nanoparticle incorporation (created using Biorender.com)

2.8.1 Chitosan as Nanocarrier

Chitosan (CS), a cationic, biocompatible, and biodegradable polysaccharide derived from chitin, has been widely investigated as a nanocarrier in drug delivery applications. It is frequently employed in biomedical research, particularly as a coating material for nano-sized drug carriers, to improve their stability, bioavailability, and targeting efficiency (Jafernik et al., 2023).Additionally, CS has been approved for several medical applications

by regulatory agencies, including the U.S. Food and Drug Administration (FDA), reflecting its established safety profile in specific contexts such as wound care products (FDA, 2021; Pawar et al., 2023). The protonation of its amino groups under acidic condition promotes pH-responsive solubility and facilitate electrostatic interactions with negatively charged mucosal surfaces and biological membranes, thereby enhancing mucoadhesion and improving bioavailability (Pérez-Pacheco et al., 2025; Sangnim et al., 2023). This mucoadhesive nature allows CS noncarrier to adhere to mucosal tissues such as buccal, nasal, and gastrointestinal surfaces resulting in prolonged drug residence time and improved absorption (Sangnim et al., 2023). One of CS's most notable characteristics is its pH responsiveness. It swells in acidic conditions and remains stable in neutral environments, which is particularly beneficial for delivering drugs to inflamed or infected tissues with lower pH levels, such as periodontal pockets (Pérez-Pacheco et al., 2025). Additionally, CS nanocarrier provide controlled drug release via a biphasic mechanism with an initial burst release of surface-bound drug, followed by a slower, sustained diffusion phase (Cadinoiu et al., 2025). The properties of CS nanocarrier can be modulated by altering formulation parameters. For example, the chitosan- tripolyphoptate (CS-TPP) mass ratio influences the cross-linking density, particle size, and surface charge. The higher TPP levels tend to produce more compact particles, while excess CS can result in larger aggregates (Yanat & Schröen, 2021). Similarly, the concentration of CS affects viscosity and nanoparticle yield and significantly influence nanoparticle size and polydispersity (Gutiérrez-Ruíz et al., 2024). These variables offer tunable control over the drug-loading capacity, stability, and release profile of the nanoparticles. Due to its operational simplicity, lack of cytotoxic agents, and compatibility with biologically active compounds, ionic gelation remains the most practical and biocompatible technique for fabricating CS-based nanocarriers for therapeutic delivery

CS nanocarrier can be prepared by various methods. Traditional approaches include physical or chemical cross-linking. For example, covalent cross-linking in emulsions (e.g. using glutaraldehyde) and precipitation or desolvation methods. Such methods often require organic solvents, high shear or toxic reagents. For instance, early protocols used emulsification with glutaraldehyde as a cross-linker (Akdaşçi et al., 2025), but

glutaraldehyde's toxicity and drug compatibility issues have led to a decline in its use. In contrast, ionic gelation has emerged as the simplest and most biocompatible method for CS nanocarrier, avoiding harsh conditions and toxic crosslinkers. In contrast, ionic gelation has emerged as a widely preferred method for preparing CS nanocarrier due to its simplicity, biocompatibility, and avoidance of harsh solvents or reagents (Gutiérrez-Ruíz et al., 2024). This method involves electrostatic interaction between the protonated amino groups of CS and anionic multivalent cross-linkers such as TPP forming polyelectrolyte complexes in aqueous media. CS solution is prepared in diluted acetic acid to protonate the amino groups, and then an aqueous solution of TPP is added under gentle stirring, leading to the spontaneous formation of nanoparticles. The mechanism of ionic cross-linking between CS and TPP is illustrated in Figure 2.4 (created using BioRender.com) and adapted from Pacheco et al. (2024). This mild, room-temperature, solvent-free method is particularly well-suited for the encapsulation of sensitive bioactive compounds. This includes antibiotics such as ciprofloxacin, tetracycline, gentamycin and MT whose stability and therapeutic efficacy may be compromised under harsh processing conditions (Ibrahim et al. 2015; Kalyane et al. 2020). For instance, a study by Kalyane et al. (2020) successfully formulated MT loaded CS nanoparticles using the ionic gelation method. The resulting nanoparticles exhibited controlled release properties and maintained the antimicrobial efficacy of MT. The process relies on electrostatic interactions between the cationic amino groups of CS and polyanionic cross-linkers such as TPP, facilitating the formation of stable nanoparticles without the use of organic solvents or high temperatures. This technique has been widely used for the development of CS-based nanocarriers aimed at improving the controlled release and bioavailability of various antibiotics.

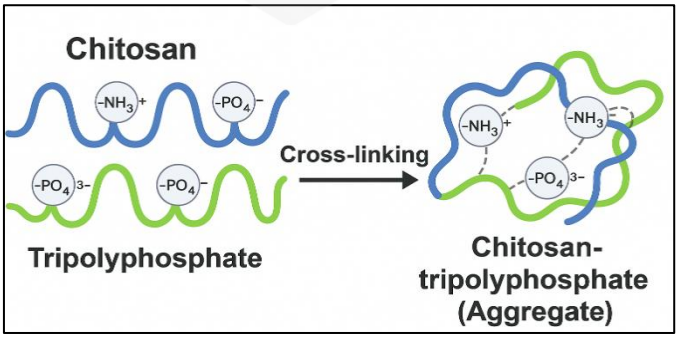

Figure 2.4: Schematic illustration of ionic cross-linking between chitosan (CS) and tripolyphospate (TPP) (created using BioRender)

In general, CS nanocarrier have been evaluated in biomedical applications for antimicrobial, anticancer, and anti-inflammatory therapies due to their ability to encapsulate both hydrophilic and hydrophobic drugs, cross epithelial barriers, and degrade into non-toxic by-products (Jafernik et al., 2023; Sangnim et al., 2023). In preclinical models, CS nanoparticles have demonstrated promising results across various administration routes including oral, nasal, buccal, and mucosal due to their adaptability, mucoadhesive properties, and ability to sustain drug release (Jha & Mayanovic, 2023). Their safety and effectiveness have also been confirmed for various mucosal applications, including oral and ocular delivery (Jafernik et al., 2023). In the context of periodontal therapy, CS nanocarrier have demonstrated considerable potential. Their small size allows penetration into periodontal pockets, and their mucoadhesive properties promote localisation at the site of infection (Sousa et al., 2024). This enhances drug retention and allows for sustained antimicrobial action. For instance, CS nanocarrier-loaded MT have shown prolonged release profiles and increased drug retention in gingival fluid compared to conventional formulations (Cadinoiu et al., 2025). Moreover, *in vivo* studies confirm their effectiveness in reducing periodontal inflammation and promoting tissue regeneration. Elangwe et al. (2022) demonstrated that curcumin-loaded CS nanocarrier improved periodontal healing and reduced inflammatory markers in hypertensive rat models of periodontitis. The combination of CS nanoparticles with scaffolds further enhances their therapeutic efficacy. Composite systems such as injectable CS–glycerophosphate hydrogels and CC membranes embedded with MT nanoparticles provide structural support and sustained drug delivery at the target site (Atia et al., 2022). These formulations have been found to be highly biocompatible with periodontal ligament fibroblasts and have successfully promoted bone regeneration in preclinical models (Atia et al., 2022; Sousa et al., 2024). Their biodegradability, mucoadhesion, and pH responsiveness make them ideal for controlled release applications, while ionic gelation provides a simple and efficient fabrication method. When integrated into scaffold systems, CS nanocarrier support localised drug action and tissue healing, thereby representing a promising strategy for advanced therapeutic interventions in periodontitis.

2.9 BONE REGENERATION SCAFFOLD IN ANIMAL MODEL

Preclinical animal models are essential in evaluating the safety, biocompatibility, osteoconductivity, and therapeutic efficacy of scaffolds used in bone regeneration prior to clinical application. The selection of an appropriate model must account for anatomical relevance, bone turnover rates, mechanical loading, cost, surgical complexity, and ethical considerations (McGovern & Hutmacher, 2018; Haff et al., 2022; Zhang & Li, 2021). Among the numerous animal models employed ranging from rodents to large animals such as rabbits, pigs, and sheep, the rat calvarial critical-size defect (CSD) model has become a widely accepted standard for early-stage scaffold evaluation. Compared to large animals, rats offer several practical advantages. These include low maintenance costs, well-established handling protocols, high reproducibility, and compatibility with advanced imaging and histological techniques. Importantly, rats exhibit consistent bone healing pathways such as intramembranous ossification, vascularisation, and inflammatory response similar to humans in early phases of regeneration, despite differences in skeletal structure (Wang et al., 2024).

The rat calvarial defect model involves the creation of a standardised, non-load-bearing bone defect in the parietal region of the skull, allowing researchers to isolate scaffold-related effects from mechanical stresses encountered in load-bearing bones (Chakka et al., 2021). The CSD typically ranging from 5 to 8 mm in diameter, is defined as the smallest intraosseous wound that does not heal spontaneously during the animal's lifetime. This model facilitates consistent comparison across studies and is suitable for evaluating scaffolds made from both synthetic and natural polymers, with or without cellular or drug loading (Hudieb et al., 2021; Uribe et al., 2022). In terms of methodology, the surgical procedure involves creating a circular bone defect using a trephine drill while preserving the underlying dura mater. The periosteum and skin are then sutured, and the healing response is monitored using micro-computed tomography (µCT), histological staining, and biomechanical testing (Hatakeyama, 2022).

A key advantage of the rat model is its suitability for antibiotic-loaded scaffolds, which are increasingly important in managing infected or compromised bone defects. For example, Li et al. (2021) demonstrated that a CS-based scaffold loaded with ciprofloxacin nanoparticles not only enhanced bone healing in rat calvarial defects but also prevented microbial colonisation. This underscores the model's effectiveness in assessing multifunctional biomaterials, such as the MT loaded CC scaffold developed in the present study. Other studies have also validated the use of the rat model in assessing bioactive and gene-activated scaffolds. Chakka et al. (2021) reported enhanced osteogenesis using a VEGF gene-activated polydopamine-coated scaffold in a rat CSD model, while Fazeli et al. (2023) confirmed rapid calvarial bone regeneration using a 3D-printed polycaprolactone scaffold coated with hydroxyapatite and bioglass. While larger animals such as sheep and pigs better replicate human bone size and mechanical loading, their use is more appropriate in later translational stages due to ethical, financial, and logistical limitations (Gómez-Cerezo et al., 2019). In contrast, the rat calvarial defect model remains ideal for early-phase testing, enabling rapid, ethical, and reproducible assessment of bone scaffolds before scaling up to more complex models. This highlights the rat model offers a balance between biological relevance and experimental feasibility, making it the most suitable animal model for evaluating the scaffold in this study. Its successful use in previous research further supports its selection as a validated platform for bone tissue engineering applications.

When generating bone defect models, the size of the induced defect, referred to as the CSD is crucial. Schmitz and Hollinger (1986) originally defined the CSD as the smallest intraosseous wound in a specific bone and species that will not heal spontaneously during the animal's lifetime, thereby necessitating external intervention to induce bone regeneration. This concept is particularly pivotal in the calvarial defect model, where the non-load-bearing nature of the cranial bone and ease of surgical access make it suitable for consistent and reproducible experimentation (Spicer et al., 2012). In rat models, calvarial defects ranging from 5 to 8 mm in diameter are widely accepted as critical, as they typically fail to undergo spontaneous healing and instead become filled with fibrous connective tissue (Hatakeyama et al., 2022). This inability to self-repair through mechanical fixation alone highlights the necessity for scaffold-based interventions or bone grafts to stimulate

osteogenesis (Fazeli et al., 2023; Zain & Hamdan, 2021). The CSD model, therefore, allows for the assessment of both the osteoconductive and osteoinductive properties of scaffolds without interference from the host's natural bone repair mechanisms (Amid et al., 2021).

Recent studies employing advanced biomaterials, including 3D-printed polycaprolactone-based scaffolds and composite matrices, have demonstrated the model's capacity to yield consistent and translational results (Elsayed, 2023). These models are essential in establishing "proof-of-principle" for emerging therapies prior to their transition into larger animal studies or clinical application. Moreover, a systematic review by Cao et al. (2023) emphasized the need for standardisation in defect dimensions and evaluation parameters to enhance the comparability of outcomes across studies. The reproducibility, simplicity, and anatomical relevance of the rat calvarial model make it widely accepted for preclinical evaluation. The procedure typically involves creating a sagittal incision, raising a flap to expose the calvarial bone, and using a trephine drill to generate a standardized circular defect, with careful removal of the bone disc to avoid damaging the dura mater. The periosteum and skin are then repositioned and sutured (Spicer et al., 2012). Recent studies have demonstrated the utility of the calvarial CSD model for testing advanced biomaterials. For example, highly pressed nano-hydroxyapatite/collagen (P-nHAP/COL) scaffolds promoted significant bone regeneration within four weeks (Hatakeyama et al., 2022). Similarly, 3D-printed polycaprolactone (PCL) scaffolds coated with hydroxyapatite and bioglass confirmed accelerated calvarial bone regeneration, with increased bone volume and trabecular thickness compared to unmodified PCL (Fazeli et al., 2023). Moreover, combinatorial strategies using photobiomodulation and adipose-derived stem cells (ADSCs) have shown synergistic effects in promoting osteogenesis within CSD, further demonstrating the versatility of this model for evaluating emerging therapies (Khosravipour et al., 2022). Collectively, CSD models remain the gold standard for early-stage assessment of bone regeneration strategies, offering a discriminative platform to validate the biological performance and therapeutic potential of novel interventions under well-controlled *in vivo* conditions (Bassi et al., 2021; Amid et al., 2021).

2.10 SAMPLE SIZE IN ANIMAL MODEL

Accurate determination of sample size in animal studies is crucial for balancing scientific rigour, ethical responsibility, and resource efficiency. In line with the 3Rs principle (Replacement, Reduction, and Refinement), researchers must minimise animal usage while ensuring statistically meaningful results (Russell & Burch, 1959; Tadich & Tarazona, 2022).

Among several statistical approaches available, the Resource Equation Method (REM) also known as the Resource Equation Approach (RSD)is one of the most widely adopted methods in exploratory biomedical research where variance and effect sizes are difficult to predict (Liang et al., 2022). This is especially relevant in tissue engineering studies involving novel scaffolds or drug-delivery systems, where data variability is often high and prior knowledge is limited. The REM evaluates sample size based on the error degrees of freedom (E) in an ANOVA framework, with an optimal range for E between 10 and 20. This range ensures that the study has sufficient power to detect meaningful differences without inflating animal numbers unnecessarily (Liang et al., 2022; Uribe et al., 2022). The formula used to determine (E) is shown in Equation (2.1):

$$E = \text{Total number of animals} - \text{Total number of groups} \quad (2.1)$$

For example, a study with 24 rats divided into 4 groups would yield E = 20, falling within the optimal range. This method is particularly advantageous in pilot studies or in cases where preliminary screening of scaffold efficacy is needed prior to scaling up to larger or more complex animal models (Ko & Lim, 2021). In rat calvarial bone defect models, which are commonly used in scaffold evaluation, published studies have reported consistent and statistically significant outcomes with 5–6 animals per group, especially when differences in bone volume, new tissue formation, or biomaterial degradation are the primary endpoints (Priya et al., 2021; Al Qabbani et al., 2023). Applying the REM in this context provides a rational framework that justifies sample size in the absence of precise power calculations. Moreover, the REM is supported by institutional ethical guidelines, IIUM Animal Care and Use Committee (IACUC), which emphasise careful planning of

sample size to minimise unnecessary animal use while ensuring scientific integrity. Surgical procedures such as creating CSD inherently carry a risk of post-operative complications. Hence, an attrition of approximately 20% is typically added to the calculated sample size to accommodate expected attrition and still retain sufficient statistical power for analysis (Uribe et al., 2022).

By adopting the REM, researchers can demonstrate compliance with ethical principles, satisfy regulatory expectations, and maintain methodological rigour. The method is particularly well-suited for bone regeneration studies involving scaffold evaluation in small animal models, where resource limitations and animal welfare are of heightened concern. Pakgohar and Mehrannia (2024) emphasise that the Resource Equation Method (REM) is particularly useful in situations where precise effect sizes are unknown, a common scenario in innovative biomaterial research. It helps minimise unnecessary animal use while maintaining statistical validity, especially in pilot studies or early-phase scaffold evaluations. Furthermore, documenting the rationale behind sample size using this method adds transparency and reproducibility to the research, both of which are critical in publishing and ethical review processes. In conclusion, the Resource Equation Method offers a robust, flexible, and ethically defensible approach to sample size determination in preclinical animal research. When combined with empirical evidence from prior studies and institutional recommendations, it ensures that scaffold evaluations are conducted with scientific integrity while upholding animal welfare standards.

CHAPTER THREE

PREPARATION AND CHARACTERISATION OF METRONIDAZOLE NANOPARTICLE (MNP)

3.1 INTRODUCTION

In conventional drug administration, a significant challenge lies in the inability of many drugs to reach their therapeutic target due to limitations such as large molecular size. For instance, MT with a molecular weight of 171.15 g/mol and moderate aqueous solubility, can face diffusion barriers, particularly in poorly vascularised or infected tissues (Li et al., 2021). These limitations often result in only a small proportion of the administered dose reaching the intended site, with most of the drug dispersing systemically. This widespread distribution not only reduces efficacy but also heightens the risk of systemic side effects. Therefore, designing a drug delivery system that enhances therapeutic efficiency while minimising toxicity is a critical focus in pharmaceutical research. One promising strategy is the utilisation of colloidal drug carriers, such as nanoparticles, which allow site-specific or targeted delivery along with controlled drug release. Nanoparticles can enhance the bioavailability of drugs like MT and improve clinical outcomes, particularly when localised treatment is desired as in the case of periodontal disease (Basudan, 2022).

Among various drug carriers, polymeric nanoparticles have shown notable potential due to their reproducibility, stability, and functional versatility. Nanoencapsulation encasing drugs within nanoparticles ranging from 1 to 1000 nm can effectively increase the concentration of MT at the site of infection while reducing systemic exposure (Sreeharsha et al., 2020). However, effective periodontal drug delivery, particle size, plays a crucial role. Studies have shown that nanoparticles must be smaller than 500 nm to effectively penetrate the junctional epithelium and localise within periodontal pockets (Aminu et al., 2018). Particles larger than this threshold may be less effective at reaching the subgingival target site and are more likely to be cleared or diluted in the oral cavity. Thus, nanoparticles below 500 nm not only facilitate epithelial permeation but also prolong retention time,

enabling sustained drug release and enhanced therapeutic effect. Additionally, a review by Chen et al. (2022) highlighted the challenges of nanoparticle permeability in periodontal pockets due to their complex and constricted structures. The study emphasised that many previously reported nanoparticles exhibited poor penetration and retention in periodontal sites, reinforcing the importance of optimizing nanoparticle size and surface properties for successful localised delivery. These findings collectively reinforce the strategy of formulating nanoparticles with sizes below 500 nm to enhance penetration through the junctional epithelium and improve localized treatment outcomes in periodontal disease.

CS a natural biopolymer, is especially suitable for this purpose due to its biocompatibility, biodegradability, mucoadhesive properties, and inherent antimicrobial activity. Despite its solubility constraints, CS remains widely employed in biomedical applications and is considered safe by regulatory agencies such as the FDA (Sreeharsha et al., 2020). In this study, CS nanoparticles were synthesised using ionic gelation, a process that leverages electrostatic interactions between the positively charged amino groups of CS and negatively charged polyanions such as TPP to form stable particles (Basudan, 2022). Such nanoparticles are particularly relevant for localised periodontal therapy, where prolonged retention and controlled release of MT at the diseased site are crucial for therapeutic success. Accurate quantification of MT encapsulated in CS nanoparticles is essential for evaluating the formulation's efficacy. In this regard, UV spectrophotometry offers a simple, cost-effective, and reproducible analytical approach suitable for routine quality control. Despite the higher sensitivity and specificity of high-performance liquid chromatography (HPLC), its cost, operational complexity, and resource requirements make UV spectrophotometry preferable for this study (Ganieva & Yunuskhodjaev, 2020). Furthermore, MT exhibits strong UV absorbance near 320 nm, making it amenable to this technique (Sánchez-Carreño López et al., 2025). The analytical parameters employed in this study were established in accordance with the International Council for Harmonisation (ICH) Q2(R1) guidelines, with method validation conducted through statistical analysis of the relative standard deviation (RSD) to ensure the reliability and reproducibility of the results (European Medicines Agency ICH, 2005). The objectives of this research are twofold, first, to develop and validate a UV spectrophotometric method for the quantitative

determination of MT in CS nanocarrier and second, to formulate and characterise MT-loaded CS nanocarrier with optimised properties for localised treatment of periodontal disease. By achieving these aims, this study intends to support more effective management of periodontitis through localised, sustained drug release, thereby enhancing therapeutic outcomes while reducing the risk of antibiotic resistance.

3.2 MATERIAL AND METHODS

3.2.1 Analytical Method Development and Validation

A simple, precise, and rapid UV spectrophotometric analytical method for post-fabrication of MNP was developed to confirm that the analytical procedure employed is suitable for identifying and quantifying substances of interest. Thus, this research develops and validates the spectrophotometric method according to International Conference on Harmonisation (ICH) Q2 (R1) guidelines. The guidelines provide all the detailed parameters to perform the analytical method and analysis, which included specificity, linearity, accuracy, precision (in the form of repeatability), the limit of detection (LOD) as well as the limit of quantification (LOQ), range, and robustness. The validation procedures consist of specific characteristic parameters that must meet a particular acceptance criterion to make the analytical method acceptable.

3.2.1.1 Preparation of Stock Solution of Metronidazole

A primary stock solution of MT was prepared by accurately weighing 10 mg of MT and dissolving it in 100 mL of distilled water, resulting in a final stock concentration of 100 µg/mL From this stock, serial dilutions were prepared using distilled water to obtain working standard solutions with concentrations of 2 µg/mL, 4 µg/mL, 6 µg/mL, 8 µg/mL, 10 µg/mL, and 12 µg/mL. This concentration range was selected to ensure that the

absorbance readings remained below 1.0, which is necessary for accurate and reliable measurements in accordance with the linearity range of the Beer–Lambert Law. Moreover, these values reflect the anticipated concentration of MT released from the scaffold during *in vitro* drug release studies, ensuring the calibration curve is both analytically valid and biologically relevant. Each concentration was prepared and analysed in triplicate (n = 3) to ensure accuracy, precision, and repeatability in method validation.

3.2.1.2 Specificity

The specificity of the UV spectrophotometric method was evaluated by analysing a standard solution of MT at a concentration of 8 µg/mL, prepared from the stock solution. The UV absorbance spectrum of the solution was recorded across the wavelength range of 200 nm to 400 nm using a UV-Vis spectrophotometer. The objective was to identify the maximum absorbance wavelength (λmax) specific to MT, ensuring no interference from excipients or other substances. This analysis was performed in triplicate (n = 3) to confirm the reproducibility of the λmax and the method's specificity.

3.2.1.3 Linearity and Calibration Curve

The aliquots of concentration, ranging from 2 µg/mL, 4 µg/mL, 6 µg/mL, 8 µg/mL, 10 µg/mL, and 12 µg/mL, were prepared in triplicate. The calibration curve concentration vs. absorbance was plotted and subjected to least squares regression analysis, yielding the equation y = mx + c, and the R2 was established. The analyte concentration was determined using the notations "x" and "y" as the absorbance values. The correlation coefficient R^2 value for all the standard curves constructed must not be less than 0.995 as one of the acceptance criteria.

3.2.1.4 Precision

There is a need to ascertain that the time variation does not influence MT concentration measurement. Thus, in this study, the precision of the assay method was assessed in terms of repeatability via intraday and interday measurements by subjecting three concentration levels of MT (8 µg/ml, 10 µg/mL, and 12 µg/mL) to the same wavelength. Intraday precisions were measured by analysing the three prepared samples at three different specific time points on the same day, and interday precisions were measured on three consecutive days, respectively. The precision was calculated using the percentage relative standard deviation (% RSD), as shown in Equation (3.1), with % RSV values required to be less than 2.0% to meet the acceptance criteria.

$$\% \text{ RSD} = \frac{\text{standard deviation of measurement}}{\text{mean value of measurement}} \times 100 \qquad (3.1)$$

Precision was identified by the repeatability of an analytical method under normal operation conditions; repeatability was done using method precision. Method precision was achieved by repeating the same solution preparation procedure six times, measuring the absorbance, and calculating the %RSD. This shows whether a method is giving constant results for a single batch. The precision of the assay was determined by repeatability (intraday) and intermediate precision (inter-day). In the intraday variation study, nine different solutions of concentration 8 µg/mL, 10 µg/mL, and 12 µg/mL were analysed three times a day, i.e. from the morning, afternoon, and evening, and the absorbances were noted. From the absorbance, the result means, standard deviation, and %RSD were calculated. In the inter-day variation studies, the solution of concentration 8-12 µg/mL was analysed three times for three consecutive days, and the absorbance result was observed. Mean, standard deviation and %RSD were calculated. The precision was determined by considering the deviation of the absorbance value obtained for each concentration. The percentage recovery should not be less than 98% and over 102%, with a %RSD value smaller than 2.0% to meet the acceptance criteria (Rajitha et al., 2011).

3.2.1.5 Accuracy (Recovery)

For accuracy, three different concentrations of MT (8 µg/ml, 10 µg/mL, and 12 µg/mL) were subjected to a wavelength of 320 nm, and the experimental concentrations, as well as the mean and standard deviation, were recorded in triplicate. The accuracy was calculated using the percentage recovery from the calibration curve. The percentage recovery was calculated using Equation (3.2), and was required to fall within the range of 98% to 102% to be deemed acceptable

$$\% \text{ Recovery } = \frac{\text{Amount found}}{\text{Amount added}} \text{ x } 100 \qquad (3.2)$$

3.2.1.6 Robustness

The robustness analysis was conducted to evaluate the reliability of the UV-Vis spectrophotometric method concerning deliberate variations in method parameters. In this study, robustness was tested by adjusting the set wavelength of 320 nm by ± 2 nm, measuring absorbance at 318 nm and 322 nm. An 8 µg/mL concentration of MT was prepared and measured in triplicate at these two different wavelength conditions. The absorbance values obtained were used to calculate the results, which are presented as % relative standard deviation (% RSD), as shown in Equation (3.1).

3.2.1.7 Ruggedness

The ruggedness was carried out using two different instruments (Secomam UVline 9400 and UV-1800, Shimadzu). The UV-spectrophotometer method was performed by analyzing seven samples of 8 µg/mL MT. The results are presented in % RSD, as shown in Equation (3.1).

3.2.1.8 Limit of Detection (LOD) and Limit of Quantification (LOQ)

The limit of quantification (LOQ) of an analytical procedure is the lowest amount of drug in a sample that can be quantitatively determined with suitable precision and accuracy. To determine the LOD and LOQ of MT, the solution was prepared in triplicate near the lower limit of the analytical curve and subjected to the same wavelength to quantify the samples. The limit of detection (LOD) and limit of quantification (LOQ) of MT were determined using the standard deviation of the response (σ), referring to the σ. of the sample and slope (S) obtained from the calibration curve constructed and calculated according to Equations (3.3) and (3.4) described below:

$$\text{LOD} = \frac{3.3\ X\ \sigma}{S} \quad (3.3)$$

$$\text{LOQ} = \frac{10\ X\ \sigma}{S} \quad (3.4)$$

3.2.2 Fabrication of Metronidazole Nanoparticle (MNP)

MT; 99% purity was sourced from Xi'an Henrikang Biotech, China; chitosan (CS) from Xi'an Ceres Biotech, China; and tripolyphosphate (TPP) and acetic acid from Evachem, Selangor, Malaysia. MT-loaded onto CS nanocarrier (CS-MNP) were synthesised via the ionic gelation method, following protocols previously described with slight modifications (Oliveira et al., 2021; Omar et al., 2015; Sukhbir et al., 2017). Initially, 300 mg of CS was dissolved in 100 mL of 2% (v/v) aqueous acetic acid under continuous stirring until a clear homogenous solution was obtained. Various concentrations of MT (150 mg, 300 mg, 450 mg, and 600 mg) were subsequently incorporated into the CS solution and homogenised to ensure uniform dispersion of the drug. A 0.1% (w/v) TPP solution was then added dropwise to the MT-CS mixture over a 60-minute period, under constant stirring at 800 rpm. The electrostatic interaction between the positively charged CS and negatively charged TPP induced ionic gelation, resulting in the formation of a turbid, white suspension indicating successful nanoparticle synthesis. The resultant dispersion was centrifuged at 1,500 rpm for 30 minutes to collect the nanoparticle-containing gel-like pellet, which was then freeze-dried at −80 °C for 24 hours to obtain dry MT-CS nanoparticle powder. Blank CS

nanoparticles were also prepared using the same method without the addition of MT. The overall preparation process is illustrated in Figure 3.1, adapted from Zhang et al. (2016), showing the step-by-step formation of MT-loaded onto CS nanoparticles via the ionic gelation technique.

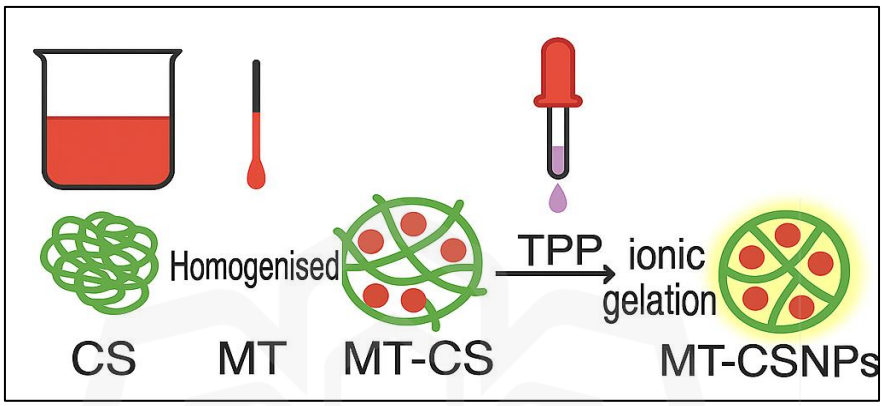

Figure 3.1 Preparation of MT-loaded CS nanoparticles via ionic gelation, where CS is mixed with MT and crosslinked with TPP for encapsulation (created using Biorender.com)

3.2.2.1 Particle size, PDI, and zeta potential

The average particle size and PDI were measured by the dynamic light scattering (DLS) technique using Nano S (Malvern Zetasizer, Malvern, United Kingdom). Zeta potentials were measured by laser Droppler microelectrophoresis using Nano Z (Malvern Zetasizer, Malvern, United Kingdom) (Ataide et al., 2021). All the samples were run in triplicate. The samples were sonicated for 5 min in a bath ultrasonicator (QSonica, Connecticut, USA) before being analysed and immediately used for measurements. All measurements were obtained in triplicate (n = 3) (Karimi et al., 2018; Katas et al., 2013).

3.2.2.2 Drug encapsulation efficiency (EE)

The encapsulation efficiency of the MT nanoparticle was determined by an indirect method. Briefly, the nanoparticle was centrifuged at 1,500 rpm for 30 minutes. The amount of MT

in nanoparticles was calculated as the difference between the total amount used to prepare the nanoparticles and the amount of MT present in the supernatant (non-encapsulated MT). The concentration of free MT was determined by UV-spectrophotometry, as shown in Figure 3.2. The encapsulation efficiency was calculated in triplicate using Equation (3.5), following the method described by Jackson et al. (2019) and Oliveira et al. (2021).

$$\% \text{ EE} = \frac{\text{drug concentration in the formulaion} - \text{drug concentration in supernatant}}{\text{drug concentration in the formulation}} \text{ x } 100 \quad (3.5)$$

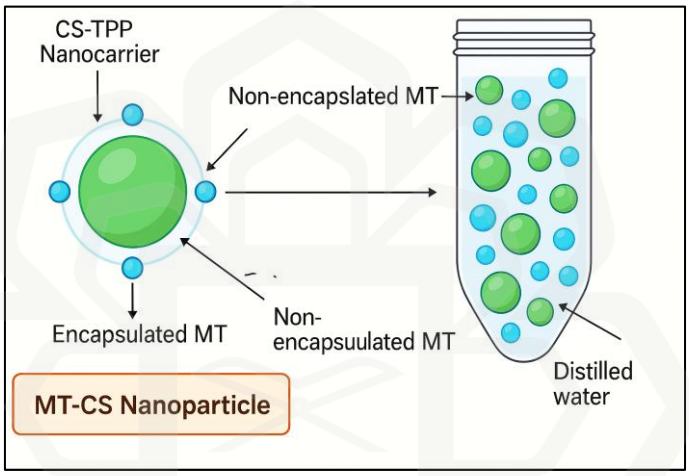

Figure 3.2 A schematic illustration of encapsulated and unencapsulated MT nanoparticles created using (BioRender.com)

3.2.2.3 Formulation selection of MNP

The development of MNP was guided by a one-variable-at-a-time (OVAT) optimisation strategy, which allows systematic investigation of each formulation parameter while maintaining others constant. This approach was selected to clearly understand the influence of individual variables on the physicochemical properties of the nanoparticles and to facilitate reproducible formulation development.

Key selection criteria were established based on widely accepted benchmarks in nanoparticle drug delivery systems. A polydispersity index (PDI) below 0.3 was targeted

to ensure a narrow particle size distribution, which is critical for achieving consistent drug release kinetics, enhanced cellular uptake, and batch-to-batch uniformity. Higher PDI values typically indicate heterogeneity, which may lead to aggregation or unpredictable drug behaviour in biological environments (BOC Sciences, 2024; Diversa Technologies, 2024; Inside Therapeutics; 2024). In a similar context, Ren et al. (2019) developed piperine-loaded nanoparticles using a nanoprecipitation method for epilepsy control and observed a PDI less than 0.3, demonstrating a relatively narrow distribution that contributed to enhanced oral bioavailability and dissolution. A zeta potential threshold of +20 mV or higher was adopted to promote colloidal stability. Nanoparticles with sufficient surface charge generate electrostatic repulsion, reducing the likelihood of aggregation during storage and application. A positive zeta potential is also favourable for interactions with negatively charged bacterial cell membranes and periodontal tissues, potentially enhancing mucoadhesion and therapeutic efficacy (Malvern, n.d.; Öztürk, & Calis, 2024). These criteria were applied throughout formulation screening to identify nanoparticle systems most suitable for further *in vitro* and *in vivo* evaluation. A positive zeta potential is also favourable for interactions with negatively charged bacterial membranes and mucosal surfaces, enhancing mucoadhesion and drug delivery performance (Le-Vinh et al., 2019). The concentration of MT varied from 0.15% to 0.60% (w/v), while maintaining a constant CS concentration of 0.3% (w/v), to explore the effect of drug loading on particle characteristics and encapsulation behaviour. The formulation compositions are listed in Table 3.1.

Table 3.1 Experimental design for the development of MNP.

Formulation	Concentrations	
	CS (% w/v)	MT (% w/v)
1	0.3	0.15
2	0.3	0.30
3	0.3	0.45
4	0.3	0.60

3.2.2.4 Field emission scanning electron microscope (FESEM)

The surface morphology of optimised MNP was analysed to observe the shape and aggregation phenomena. The nanoparticle was fixed on a glass plate and dried at room temperature. The dry nanoparticle was coated with gold under a vacuum and then analysed using field emission scanning electron microscopy (FESEM).

3.2.2.5 Fourier transform infrared spectroscopy (FTIR)

The functional groups present in empty MT and CS, as well as MNP and CS nanoparticles, were characterised using attenuated total reflectance Fourier transform infrared (ATR-FTIR) spectroscopy (Spectrum 100, Perkin Elmer, Massachusetts, USA). Approximately 5 mg of each sample was analysed. Spectra were acquired using 16 scans over the wavenumber range of 4000–600 cm^{-1} (Ruchika & Himanshi, 2019).

3.3 RESULT AND DISCUSSION

3.3.1 Analytical Method Development and Validation (UV-Spectrophotometer)

Validation of an analytical procedure refers to the process of verifying and documenting that an analytical method is suitable for its intended use. The validation process involves demonstrating that the analytical procedure is accurate, precise, specific, and robust for its intended application. It is an essential step in ensuring that the results obtained from the analytical method are reliable.

3.3.1.1 Specificity

The ultraviolet-visible (UV-Vis) absorption spectrum of MT reveals a single prominent absorption peak centred at 320 nm, which is characteristic of MT molecular structure. This observation confirms the specific absorbance profile of MT, aligning with previously reported findings (Mondal et al., 2007). The absorbance value, which remains below 1.0, lies within the optimal range for UV-Vis spectrophotometry, ensuring linearity and reliability of the measurements. Maintaining absorbance values under this threshold is crucial for accurate determination of λ_max and minimises potential deviations due to instrumental limitations or sample oversaturation. These results validate the use of 320 nm as the analytical wavelength for subsequent quantification and characterisation studies involving MT, particularly in drug encapsulation and release investigations, as illustrated in Figure 3.3.

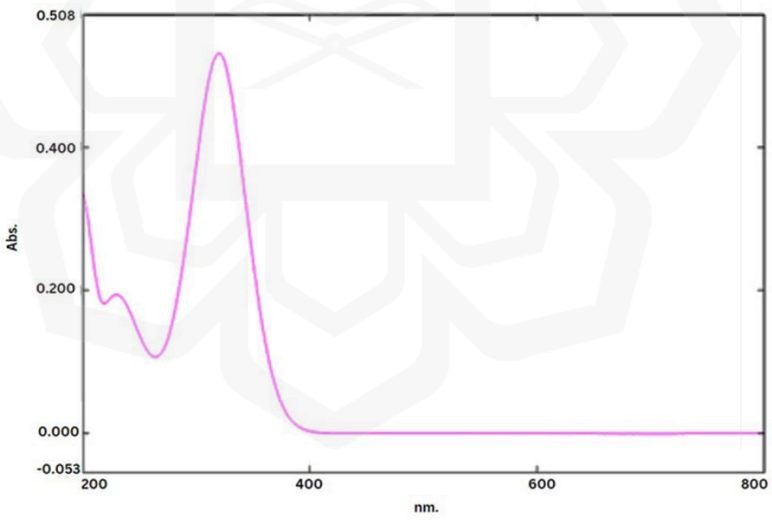

Figure 3.3 The λ max of MT using a spectrophotometer at 320 nm

As stated in a previous study, CS is water-insoluble due to strong intermolecular hydrogen bonds between polymer chains, and drug release from CS is

driven by swelling, drug diffusion, degradation, or a combination of both (Bashir et al., 2022; Herdiana et al., 2022). The CS nanocarrier that dissolves upon contact with the media causes an explosive effect on the drug trapped, which may fail the nanosystem. As a result, the insoluble nanocarrier is an essential feature for nanoparticle formulation because it can provide a slow release of encapsulated drugs.In this study, CS was used as the primary carrier in the nanosystems and was also shown to be insoluble in water. Because CS can only disperse in water, they effectively act as nanocarriers, preventing rapid drug release and promoting MT release via nanocarriers. As a result, long-term control of MT release at the site of action is possible. Furthermore, the interaction between two oppositely charged polymers, CS and TPP, leads to more hydrogen bond formation, causing the outer layer of nanocarrier CS-TPP to swell in the water system due to strong hydrogen bonds between polymers. As the pH rises, the CS-TPP swells, preventing the nanocarrier structure from breaking (Mohammed et al., 2017). However, a study found that the solubility of CS can be reduced due to entanglement with a polymeric matrix in an acidic medium (Sukhbir et al., 2017). Thus, CS-TPP was not included in the specificity because it is insoluble in water.

3.3.1.2 Linearity and Calibration Curve

The absorbance peaks of MT were analysed at a wavelength of 320 nm using a UV–visible spectrophotometer to determine the drug's linearity range and establish a standard calibration curve. A series of six MT standard solutions were prepared at concentrations ranging from 2 µg/mL to 12 µg/mL. The absorbance for each concentration was measured in triplicate to ensure consistency and reliability of the data. The results demonstrated a distinct and proportional increase in absorbance with rising MT concentrations, indicative of compliance with Beer's Law, which states that absorbance is directly proportional to concentration in a homogenous solution. This relationship is essential for ensuring accurate quantitative analysis.

The generated calibration curve plotted with precision and fitted using a linear regression analysis The regression equation obtained from the curve *was* y = 0.004628x + 0.04402, with a coefficient of determination *(*R^2) of 0.99902. This signifies the linear model demonstrates strong correlation between MT concentration and absorbance. According to Ismail et al. (2016), an R^2 value exceeding 0.995 is considered indicative of a robust and analytically reliable method. Thus, the findings in this study confirm the UV–Vis spectrophotometric method as precise and dependable for the quantification of MT within the tested concentration range. Figure 3.4 illustrates the calibration curve, which exhibits a clearly defined linear regression line.

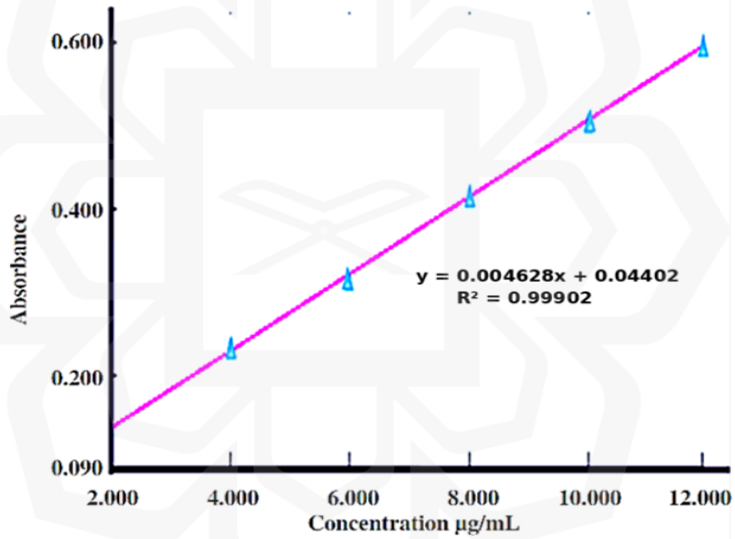

Figure 3.4 Calibration curve between absorbance vs concentration of MT

The mean absorbance values for each standard concentration, measured in triplicate (n = 3) and expressed as mean ± standard deviation (S.D.). These values reveal a progressive increase in absorbance with increasing MT concentration, with low standard deviations at each point, further supporting the method's precision. For instance, the absorbance for 2 µg/mL MT was recorded as 0.139 ± 0.006, while the highest concentration of 12 µg/mL yielded an absorbance of 0.606 ± 0.004. Notably,

the narrow range of standard deviations across all concentration levels (ranging from ±0.004 to ±0.015) reflects high measurement consistency and low intra-sample variation. The mean absorbance values corresponding to each concentration are summarised in Table 3.2**.**

Table 3.2 Means absorbance of MT (n = 3 ± S.D.).

MT (ug/mL)	Mean Absorbance (nm)
2	0.139±0.006
4	0.228±0.015
6	0.313±0.011
8	0.424±0.011
10	0.510±0.007
12	0.606±0.004

A calibration curve is a graphical representation of the relationship between the concentration of a substance and the corresponding signal response measured by an analytical instrument. Once established, this curve enables accurate determination of unknown sample concentrations by interpolating their absorbance values onto the curve. According to Beer's Lambert Law, absorbance is directly proportional to concentration, allowing the spectrophotometer to predict the concentration of an analyte based on its absorbance (Delgado, 2022). In this study, the calibration curve was constructed at the λ_max of 320 nm, with absorbance plotted against MT concentrations. The high linearity (R^2 = 0.999) further confirms the suitability of this method for accurately estimating the concentration of encapsulated MT in nanoparticle formulations. These findings support the use of this UV-Vis method in future quantification studies involving MT, especially where reliable estimation of drug loading and release is critical for evaluating formulation performance.

3.3.1.3 Precision

To evaluate the reliability and reproducibility of the UV-spectrophotometric method, both intraday and interday precision studies were conducted using MT concentrations of 8, 10, and 12 µg/mL. Precision was expressed as the percentage relative standard deviation (% RSD), calculated from the mean absorbance and standard deviation for three replicates (n = 3) at each time point. Table 3.3 shows the intraday precision results, with measurements taken at 9 a.m., 12 p.m., and 3 p.m. across the concentration range. The % RSD values remained consistently below 2.0, indicating good repeatability.

Table 3.3 Intraday - precision (n = 3 ± S. D.).

Time	Concentrations (µg/mL)	Mean absorbance (nm)	% RSD
9 am	8	0.456 ± 0.008	1.754
	10	0.525 ± 0.008	1.524
	12	0.627 ± 0.009	1.435
12 pm	8	0.458 ± 0.008	1.746
	10	0.518 ± 0.004	0.772
	12	0.615 ± 0.004	0.650
3 pm	8	0.460 ± 0.002	0.435
	10	0.534 ± 0.002	0.375
	12	0.627 ± 0.011	1.754

The interday precision study was conducted to evaluate the reproducibility of the UV-spectrophotometric method across three consecutive days using MT concentrations of 8, 10, and 12 µg/mL. The results consistently demonstrated percentage relative standard deviation (% RSD) values below the commonly accepted threshold of 2.0, indicating minimal variability between days. This confirms the method's high reproducibility, a critical factor in validating an analytical procedure for routine use. The ability of the method to yield stable results under varying temporal

conditions, which may include slight fluctuations in instrumentation or environmental factors, reflects its robustness and reliability. Such performance is essential for ensuring accurate drug quantification in longitudinal studies or quality control settings. These findings reinforce the method's validity for consistent application in the analysis of MT in nanoparticle formulations. The detailed interday absorbance values and associated % RSDs are presented in Table 3.4**.**

Table 3.4 Interday - precision (n=3± S.D.).

Day	Concentrations (µg/mL)	Mean absorbance (nm)	% RSD
1	8	0.438 ± 0.006	1.369
	10	0.516 ± 0.003	0.581
	12	0.610 ± 0.008	1.311
2	8	0.460 ± 0.002	0.435
	10	0.534 ± 0.002	0.375
	12	0.627 ± 0.011	1.754
3	8	0.438 ± 0.004	0.913
	10	0.516 ± 0.010	1.938
	12	0.593 ± 0.010	1.686

The precision of a measurement reflects the consistency and reproducibility of results under specified conditions and can be expressed either as standard deviation or the coefficient of variation (% RSD). A lower standard deviation or % RSD indicates higher precision. For an analytical method to be considered reliable, it must consistently produce reproducible results across multiple measurements. As highlighted by Mishra et al. (2014), precision contributes significantly to the overall accuracy of an analytical procedure. In this study, both intra- and interday precision analyses were conducted at three concentration levels (8, 10, and 12 µg/mL). The % RSD values for all measurements were less than 2.0, which falls within the accepted limits for analytical method validation. This demonstrates

the method's robustness and confirms its applicability for routine quantitative analysis of MT using UV spectrophotometry. These findings underscore the developed method's suitability for consistent performance across different time points and operational conditions, further supporting its use in nanoparticle formulation and drug release studies involving MT.

3.3.1.4 Accuracy

The accuracy of a measurement can be expressed as a percentage or an absolute value, such as the difference between the measured value and the true value. It is often evaluated by comparing the results obtained from the experiment to a known standard or reference material. The accuracy of an analytical method is an important parameter in chemical analysis, as it determines the reliability and validity of the results obtained. The accuracy of samples was assessed to evaluate the known impurity level following ICH Q2 (R1) guidelines. A minimum of nine determinations were conducted, consisting of three concentration levels and three replicates per sample. The result was expressed as a percent recovery and should be between 98% and 102% (Harun Ismail et al., 2015). The result showed that drug recoveries of 99.73–101.92% were obtained at concentrations of 8 µg/mL–12µg/mL. Based on the results, the developed UV method was found to be highly accurate, as the percentage recovery was within the standard range.

3.3.1.5 Robustness

The robustness of analytical methods measures the method's ability to remain unaffected when slight intentional changes in method parameters occur. In this study, the robustness of the UV spectrophotometer analytical method was established by reading the absorbance at a different wavelength. Change in wavelength did not affect the method's performance, as the %RSD values at 318 nm and 322 nm were found to be between 0.581 and 0.749, respectively, as shown in Table 3.5. The robustness of the proposed UV analytical method

was demonstrated by a value of % RSD less than two.

Table 3.5 Robustness.

Wavelength	Mean Absorbance (nm)	%RSD
318	0.516 ± 0.003	0.581
322	0.534 ± 0.004	0.749

3.3.1.6 Ruggedness

The ruggedness of an analytical method is the degree of reproducibility of test results obtained by analysing the same samples under different test conditions. This study used two different UV spectrophotometers in different laboratories and at different times to test the analytical method's ruggedness. The results obtained from lab-to-lab and time-to-time variation were reproducible, as the %RSD did not exceed 2%, as shown in Table 3.6.

Table 3.6 Ruggedness.

Instrument	Mean Absorbance (nm)	% RSD
UV line 9400, Secomam	0.626 ± 0.0077	1.230
UV-1800, SHIMADZU	0.617 ± 0.0049	0.794

3.3.1.7 Limit of Detection and Limit of Quantification

LOD, or limit of detection, is the lowest amount of analyte that can be reliably detected by an analytical method. This is typically defined as the concentration or amount of analyte. that produces a signal that is significantly different from the background noise of the method. In other words, the smallest substance can be detected with any certainty. LOQ, or

limit of quantification, is the lowest amount of analytes that can be accurately quantified or measured by an analytical method. This is typically defined as the concentration or amount of analyte that produces a signal that is reliably different from the background noise of the method and falls within an acceptable range of uncertainty. In other words, the smallest amount of a substance can be accurately measured with a specific degree of confidence. LOD and LOQ were calculated using standard calibration curves. LOD and LOQ were found to be 0.040 µg/mL and 0.120 µg/mL, respectively, indicating that the method was suitable for analysing samples containing even a small amount of MT.

Table 3.7 Summary of validation parameter of MT.

Parameter		Normal range	Result		
Linearity		0.999	0.999		
Accuracy		98-102	99.73 -101.92 %		
Precision	Max λ	-	320 nm		
	Repeatability	< 2%			
	Intraday		0.332- 1.790		
	Interday		0.332- 1.849		
LOD (µg/mL)		-	0.040µg/mL		
LOQ (µg/mL)		-	0.120µg/mL		
Robustness %RSD		<2%	318	320	322
			0.592	1.373	0.757
Ruggedness %RSD		<2%	1.314		

Table 3.7 shows the summary of validation parameter of MT. The validation study used UV-visible spectroscopy to check the concentration of MT over a wavelength range of 200-400 nm. The maximum absorbance was found at 320 nm. The method adhered to ICH Q2(R1) guidelines, ensuring that it met rigorous standards for analytical methods. The

calibration curve established with the equation y=0.4628x+0.4402 with r^2 value of 0.999 highlights the reliability and accuracy of the method. The relative standard deviations (%RSD) for precision, robustness, and ruggedness were consistently below 2%, confirming the method's reproducibility and reliability. The findings from the stability study, indicating that MT samples remained stable over a 24-hour period, confirmed that the method was effective for assessing drug concentration. This UV spectrophotometric approach is presented as a simple, fast, precise, and cost-effective method for quantifying MNP. This UV spectrophotometric approach was presented as a simple, fast, precise, and cost-effective method for quantifying MNP. The overall results from the validation parameters indicated that UV-visible spectroscopy was a suitable analytical method for measuring MT concentrations. The method's robustness, accuracy, and precision made it an excellent choice for determining the content of MNP, supporting its application in pharmaceutical analysis.

3.3.2 Development of metronidazole nanoparticles (MNP)

Initially, CS, soluble in acidic conditions, formed a clear solution. However, upon addition to the TPP solution, rapid gelation and precipitation occurred, turning the solution cloudy as a gel formed. This indicates that CS reacted with TPP and transformed into a solid-like structure. The reaction occurs because the positively charged amine groups on CS interact with the negatively charged phosphate groups in TPP. As the acid in the CS solution is neutralised, the pH increases, causing CS to become less soluble and initiate gel formation. The phosphate ions from TPP bind with CS, leading to its precipitation and the simultaneous entrapment of MT within the CS matrix. This process results in stable gel beads that can be used for drug delivery, as the MT remains encapsulated within the CS structure (Srinatha et al., 2008).

3.3.2.1 Particle Size, Polydispersity Index, and Zeta Potential

The synthesis of MT nanoparticles via ionic cross-linking between CS and TPP demonstrated that MT concentration significantly affected particle size, polydispersity index (PDI), and encapsulation efficiency (%EE). The particle sizes of the nanoparticle formulations ranged from 308.0 ± 9.18 nm to 746.9 ± 13.7 nm. A statistically significant increase in particle size was observed as the MT concentration increased from 0.15% w/v to 0.45% w/v ($p < 0.05$), indicating a direct correlation between drug concentration and nanoparticle size. This trend suggests that higher MT concentrations promote particle aggregation, likely due to increased molecular crowding. These findings are consistent with previous studies reporting that elevated drug loading can lead to larger particles as a result of aggregation phenomena (Ruchika & Himanshi, 2019). It is observed that formulation F1, which contained 0.15% w/v MT, exhibited the smallest particle size. This suggests an optimal balance between CS and TPP, achieving controlled gelation and efficient nanoparticle formation without excessive cross-linking. These observations highlight the importance of maintaining a critical balance between drug concentration and polymer-to-crosslinker ratio for desirable nanoparticle characteristics.

The PDI reflects the uniformity of particle size distribution, which is crucial for consistent drug release and bioavailability. In this study, PDI values ranged from 0.374 ± 0.625 to 0.625 ± 0.083, indicating increasing heterogeneity with higher MT concentrations. Formulation F1 (0.15% w/v MT) exhibited a PDI of 0.374, suggesting a moderately monodispersed system. In contrast, Formulation F4 (0.45% w/v MT) recorded the highest PDI (0.625), indicating a broader size distribution and reduced stability. While Formulations F1 and F2 (0.30% w/v MT) showed no statistically significant difference in PDI ($p = 0.0735$), In contrast, higher MT concentrations, as observed in F3 and F4, resulted in significantly elevated PDI values ($p < 0.05$), suggesting greater particle size heterogeneity and reduced stability This trend suggests that increasing MT concentration results in particle heterogeneity, likely due to the saturation of TPP and uneven crosslinking between CS and TPP, leading to the formation of particles with variable sizes (Oliveira et al., 2022). A PDI below 0.5 is generally considered acceptable for nanoparticle-based drug

delivery systems, as it denotes a narrow and uniform size distribution (Danaei et al., 2018). Values above 0.4 indicate moderate polydispersity, consistent with the findings of this study. A narrower distribution, as seen in F1, is desirable for enhanced nanoparticle stability and predictable drug release. As illustrated in Figure 3.5, Formulation F1 comprising 0.3% w/v CS and 0.15% w/v MT demonstrated a Z-average particle size of 308.0 nm with a PDI of 0.374. This indicates an optimal balance in the ionic gelation process, leading to the formation of uniform nanoparticles.

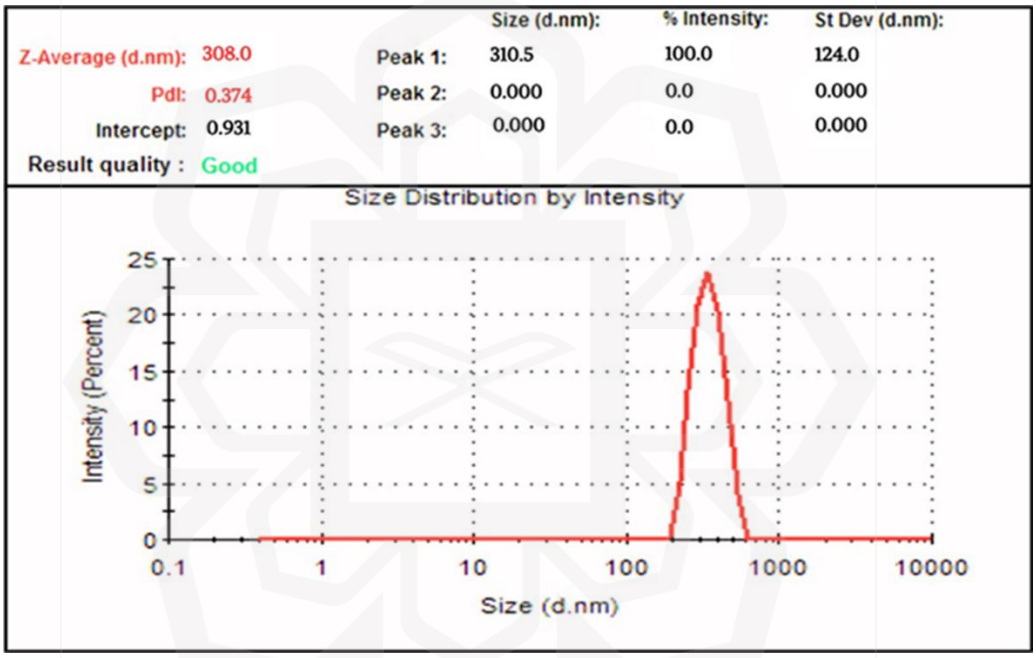

Figure 3.5 Z-average particle size and PDI of MT nanoparticles for Formulation F1

Another important parameter in evaluating nanoparticle performance, alongside particle size and PDI, is zeta potential. In this study, the zeta potential of the CS nanoparticles ranged from 26.6 ± 6.100 mV to 46.6 ± 0.231 mV, indicating positively charged surfaces that contribute to colloidal stability. Formulation F2 exhibited a significantly higher zeta potential compared to F1 and F3 ($p < 0.05$), which enhances electrostatic repulsion between particles, thereby minimising aggregation and improving dispersion stability. Notably, higher zeta potential values are generally associated with improved nanoparticle stability, owing to their ability to promote electrostatic repulsion

and prevent particle agglomeration (Honary & Zahir, 2013). The highest zeta potential recorded in this study was observed in Formulation F1, which comprised 0.3% w/v CS and 0.15% w/v MT, with a value of 46.6 ± 0.231 mV, as presented in Figure 3.6.

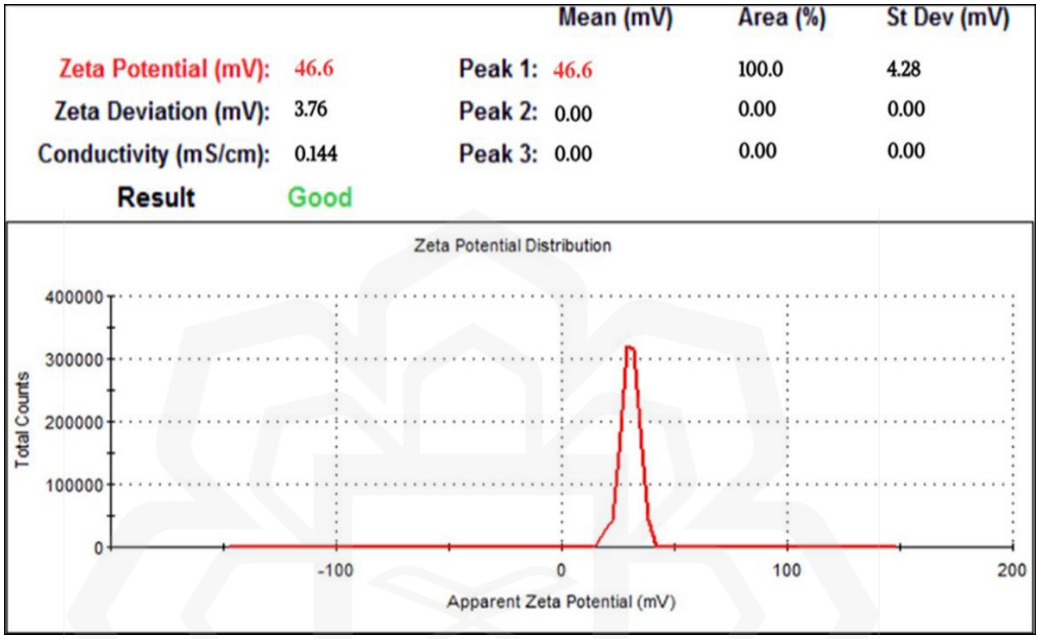

Figure 3.6 Zeta potential distribution

Nanoparticles prepared with CS are widely recognised for their significant role in drug delivery and tissue engineering, primarily due to their positive zeta potential. The positive zeta potential arises from the amino groups along the CS polymer backbone, which enhances stability and functionality in various applications (Mohammed et al., 2017). The charge facilitates electrostatic repulsion between nanoparticles, preventing aggregation and ensuring a stable dispersion in aqueous solutions (Honary & Zahir, 2013). Recent studies indicate that CS nanoparticle synthesised with TPP exhibits higher zeta potential and greater stability in suspension (Ribeiro et al., 2020). Positive zeta potential not only improves stability but also enhances cellular uptake by increasing interactions with negatively charged cell membranes. This leads to prolonged blood circulation time and reduces premature drug elimination (Mohammed et al., 2017).CS-based nanoparticles are

well recognised for their positive zeta potential, attributed to protonated amino groups along the polymer backbone. This positive surface charge facilitates electrostatic repulsion between particles, preventing aggregation and promoting colloidal stability (Honary & Zahir, 2013). Furthermore, nanoparticles crosslinked with TPP often exhibit improved zeta potential and enhanced stability (Ribeiro et al., 2020). The positive zeta potential also increases cellular uptake by enhancing interactions with negatively charged cell membranes, thereby prolonging circulation time and reducing premature drug elimination (Mohammed et al., 2017).

CS nanoparticles are crucial for drug delivery because their positive zeta potential improves cellular uptake and controls drug release. This has been observed with CS-capped gold nanoparticles, which exhibit higher zeta potentials and improved antibacterial activity due to better interaction with bacterial cell membranes (Fuster et al., 2020; Wang et al., 2017). Recent research has also highlighted the significant influence of zeta potential on bacterial adhesion. The antibacterial activity of CS-gold nanoparticles (Cs-AuNPs) is positively correlated with their zeta potential due to the electrostatic attraction between positively charged nanoparticles and negatively charged bacterial cell membranes (Wang et al., 2017). A higher zeta potential, around 50 mV, enhances this interaction, improving the nanoparticles' ability to disrupt bacterial growth and making them more effective against bacteria (Fuster et al., 2020). However, an increase in drug concentration, such MT, can reduce the zeta potential by neutralising positive surface charges, potentially impacting the stability and efficacy of the nanoparticles. This shift in surface charge dynamics can weaken electrostatic repulsion and affect the overall performance of the nanoparticles. The observed decrease in zeta potential with increasing MT concentration suggests that non-encapsulated MT may neutralise some of the positive charges, diminishing the nanoparticles' ability to maintain a high surface charge and potentially affecting dispersion stability (Kaur et al., 2017). Overall, an optimal physiochemicall properties of particle size, uniformity, and surface charge was achieved in Formulation F2 (0.3% w/v MT), identifying it as the most stable and suitable formulation for further investigation.

3.3.2.2 Encapsulation Efficiency (EE)

The encapsulation efficiency (EE) of MT within CS-based nanoparticles varied significantly, with values ranging from 26.42% to 87.95%. This variation highlights the influence of drug concentration on the entrapment capacity of the polymer matrix. At a fixed CS concentration of 0.3% w/v, an inverse relationship between MT concentration and EE was observed: increasing the MT concentration led to a notable decline in EE. The highest EE (87.95%), achieved at the lowest MT concentration (0.15% w/v, Formulation F1), reflects highly efficient encapsulation within the CS network. This suggests that at lower drug concentrations, the availability of cross-linking sites between CS and TPP is sufficient to retain most of the drug molecules within a stable nanoparticulate structure. In contrast, the lowest EE (26.42%), recorded at the highest MT concentration (0.6% w/v, Formulation F4), indicates that the saturation threshold of the polymer had been exceeded, leaving excess drug unencapsulated. This unentrapped drug could contribute to instability, undesired burst release, or reduced therapeutic efficiency. The EE values across formulations decreased with increasing MT concentration, reinforcing the critical role of polymer–drug ratio in nanoparticle design. The physicochemical characteristics of all tested formulations including particle size, PDI, zeta potential, and EE are summarised in Table 3.8, offering a comprehensive view of the formulation performance under varying MT concentrations.

Table 3.8. Physicochemical properties of nanoparticles (n = 3 ± S.D.)

No	Independent variable		Dependent variable			
	CS polymer (w/v%)	Drug (w/v%)	Size (nm)	PDI (nm)	Zeta Potential (mV)	EE%
F1	0.3	0.15	308.0 ± 9.18^{a}	0.374 ± 0.37^{a}	46.6 ± 0.23^{a}	87.95 ± 0.07^{a}
F2	0.3	0.30	594.2 ± 14.7^{b}	0.479 ± 0.04^{a}	35.6 ± 0.40^{b}	85.06 ± 0.08^{a}
F3	0.3	0.45	746.9 ± 13.7^{c}	0.581 ± 0.08^{b}	26.6 ± 6.10^{c}	35.79 ± 0.42^{b}
F4	0.3	0.6	600.5 ± 22.4^{b}	0.625 ± 0.08^{b}	32.9 ± 0.87^{b}	26.42 ± 1.35^{c}

The observed trend in encapsulation efficiency underscores the importance of maintaining an optimal balance between drug and polymer concentrations in nanoparticle formulations. As drug concentration increases, the polymer matrix eventually becomes saturated, limiting its ability to encapsulate additional drug molecules. This was evident in the current study, where increasing MT concentration from 0.15% to 0.6% w/v at a fixed 0.3% w/v CS led to a significant decline in EE from 87.95% to 26.42%. This aligns with findings from Sujathan and Sharma (2021), who emphasised that EE decreases when the drug load exceeds the polymer's entrapment capacity unless the polymer concentration is adjusted proportionally. This phenomenon reflects a trade-off commonly reported in nanoparticle systems: although higher drug concentrations increase the loading capacity, they often result in a lower percentage of drug being effectively encapsulated (Kandav et al., 2019; Sreeharsha et al., 2020). At a constant CS concentration, the polymer network reaches a threshold beyond which drug molecules remain unentrapped, reducing overall efficiency. This has been corroborated by studies showing that increasing CS concentration can improve EE by strengthening the polymeric network and enhancing drug retention (Garud & Garud, 2010; Sreeharsha et al., 2020). Moreover, Yang et al. (2009) reported that denser CS matrices formed at higher polymer concentrations provide better entrapment conditions and reduce early drug leakage. In the context of this study, 0.3% w/v CS appeared optimal for encapsulating lower concentrations of MT, achieving efficient loading with minimal loss. Formulation F1, containing the lowest drug concentration, achieved superior EE and stability, while higher drug loads (F4) resulted in reduced entrapment and poorer nanoparticle characteristics. These results suggest that for effective drug encapsulation, the drug-to-polymer ratio was carefully optimised based on the saturation threshold of the polymer system.

3.3.2.3 Selection of MNP

The capacity of CS to adhere to mucosal surfaces has gained significant attention over the past few decades. Its ability to provide longer residence times at the application site, harmonise release kinetics, and enhance mucoadhesive properties was a key reason for the

utilisation of CS in this study. The particle size was one of the key variables that needed to be controlled at the nanoscale (1–1,000 nm) to be recognised as a nanoparticle and suitable for application in the treatment of periodontal disease. Delivering a therapeutic agent across the gingival sulcus to the underlying connective tissue should be a key desirable property for any ideal drug delivery system intended for the localised treatment of periodontal disease. According to a previous study, particles larger than 500 nm in diameter may not permeate through the junctional epithelium to deliver the drug at the site of action (Aminu et al., 2018). Thus, this study chose the optimal nanoparticle formulations based on particle sizes less than 500 nm. Secondly, the PDI value reflects the nanoparticle size distribution, where samples with a wider range of particle sizes have higher PDI values, while samples consisting of an evenly distributed particle size distribution have lower PDI values (Masarudin et al., 2015). Our studies observed a lower PDI value of 0.374 ± 0.374, indicating monodisperse CS nanoparticle. Meanwhile, all of the formulated materials have a zeta potential greater than +20 mV, and the highest encapsulation efficiency in this study is 87.95 ± 0.07%.

Research has shown that varying the CS–TPP concentration can significantly influence nanoparticle characteristics, particularly particle size, polydispersity index (PDI), and zeta potential. These parameters are further affected when active pharmaceutical ingredients, such as MT are introduced, with particle size often displaying the most predictable change due to drug entrapment (Simpson & Lowry, 2024). To systematically assess these effects, the OVAT approach was adopted, as described by Sukhbir et al. (2017). In this study, OVAT was employed to examine the effect of varying MT concentrations, while the CS and TPP concentrations were maintained at 0.3% w/v and 0.1 w/v%, respectively. This approach enabled direct attribution of observed changes in nanoparticle characteristics such as particle size, PDI, zeta potential, and encapsulation efficiency to the concentration of MT. Statistical validation was carried out using one-way ANOVA followed by appropriate post hoc analyses, which revealed significant differences ($p < 0.05$) in all measured characteristics across formulations. Among the tested formulations, F1 significantly improved nanoparticle characteristics, with the smallest particle size (308.0 ± 9.18 nm), lowest PDI (0.374 ± 0.01), and highest encapsulation efficiency (87.95 ± 0.07%)

($p < 0.05$), indicating a strong influence of MT concentration on nanoparticle optimisation, as visualised in Figure 3.7.

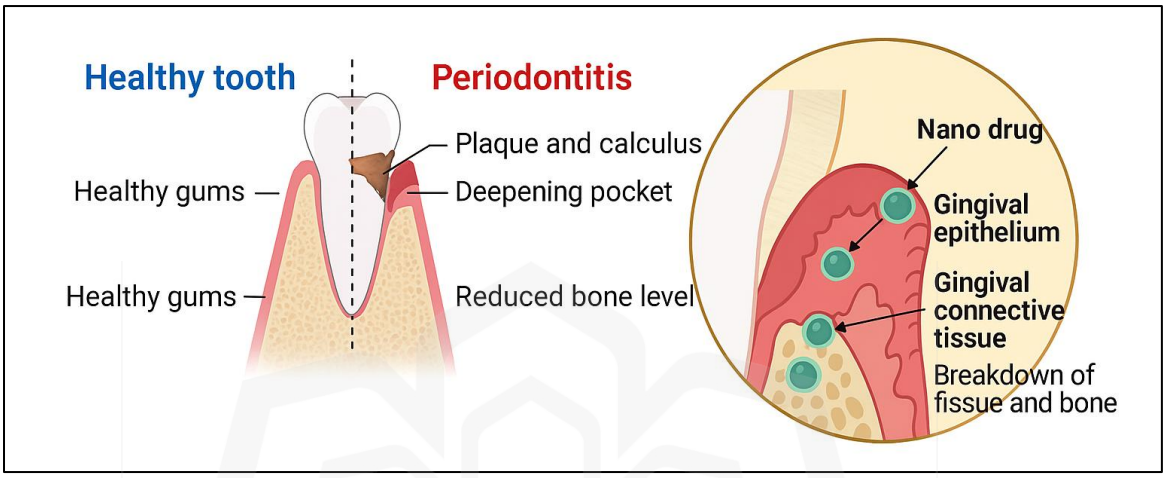

Figure 3.7 Visualisation of nanoparticle flow in periodontal disease treatment (created using Biorender.com

This mucoadhesion not only improved drug delivery by increasing the surface area but also enhanced bioavailability by protecting the drug from degradation. The adhesive properties of CS were particularly valuable for pharmaceutical applications, as mucosal drug delivery significantly improved drug absorption and bioavailability through mucosal membranes (Eliyahu & Bianco, 2018). This increased adhesion to mucosal surfaces enhanced the contact time for drug penetration, thereby facilitating better therapeutic outcomes (Mikušová & Mikuš, 2021). Previous research primarily focused on MNP aimed at selective delivery to the colon through the oral route (Ruchika & Himanshi, 2019; Sreeharsha et al., 2020). However, this study was the first to explore the potential of MNP for local drug delivery in periodontal applications. Figure 3.7 depicts a process similar to the flow of the nanoparticle drug at the affected site in periodontal disease, demonstrating the interaction of nanoparticles with inflamed bone tissue facilitates targeted drug delivery and enhances therapeutic action.

Although advanced experimental designs such as factorial design, response surface methodology (RSM), or Design of Experiments (DoE) enable simultaneous investigation of multiple variables and their interactions, OVAT was chosen for its straightforward and practical application in this initial formulation study. OVAT is particularly advantageous during preliminary research stages, where understanding the individual impact of each variable is critical (Matawo et al., 2020). Despite its inability to detect interactions between variables, OVAT continues to be widely accepted for initial screening and provides a strong foundation for future optimisation (Yousefi et al., 2023). These findings confirm the reliability of the OVAT approach and validate the robustness of the experimental setup. Previous literature supports these findings. For example, Omar et al. (2015) demonstrated that nanoparticles formulated with 0.3% w/v CS and 0.1% w/v TPP exhibited a high zeta potential, with particle size increasing only at higher CS concentrations without significantly altering zeta potential. This further justifies the selection of these concentrations in the present study and affirms that the observed trends are consistent with established scientific principles. Thus, F1 was identified as the optimal formulation, offering the most favourable nanoparticle properties for MT delivery in periodontal applications.

3.3.2.4 FESEM analysis

Figure 3.8 shows the morphology of pure CS as captured by a Field Emission Scanning Electron Microscope (FESEM). The images illustrate that CS appears to have an irregular shape and flake-like structure, with a wide size distribution consistent with the previous findings (Kim et al., 2020). Similar morphology was found in this study, where the selected MNP exhibited a uniform distribution and spherical-like structure in large clumps, which indicated that the MNP were successfully formulated.

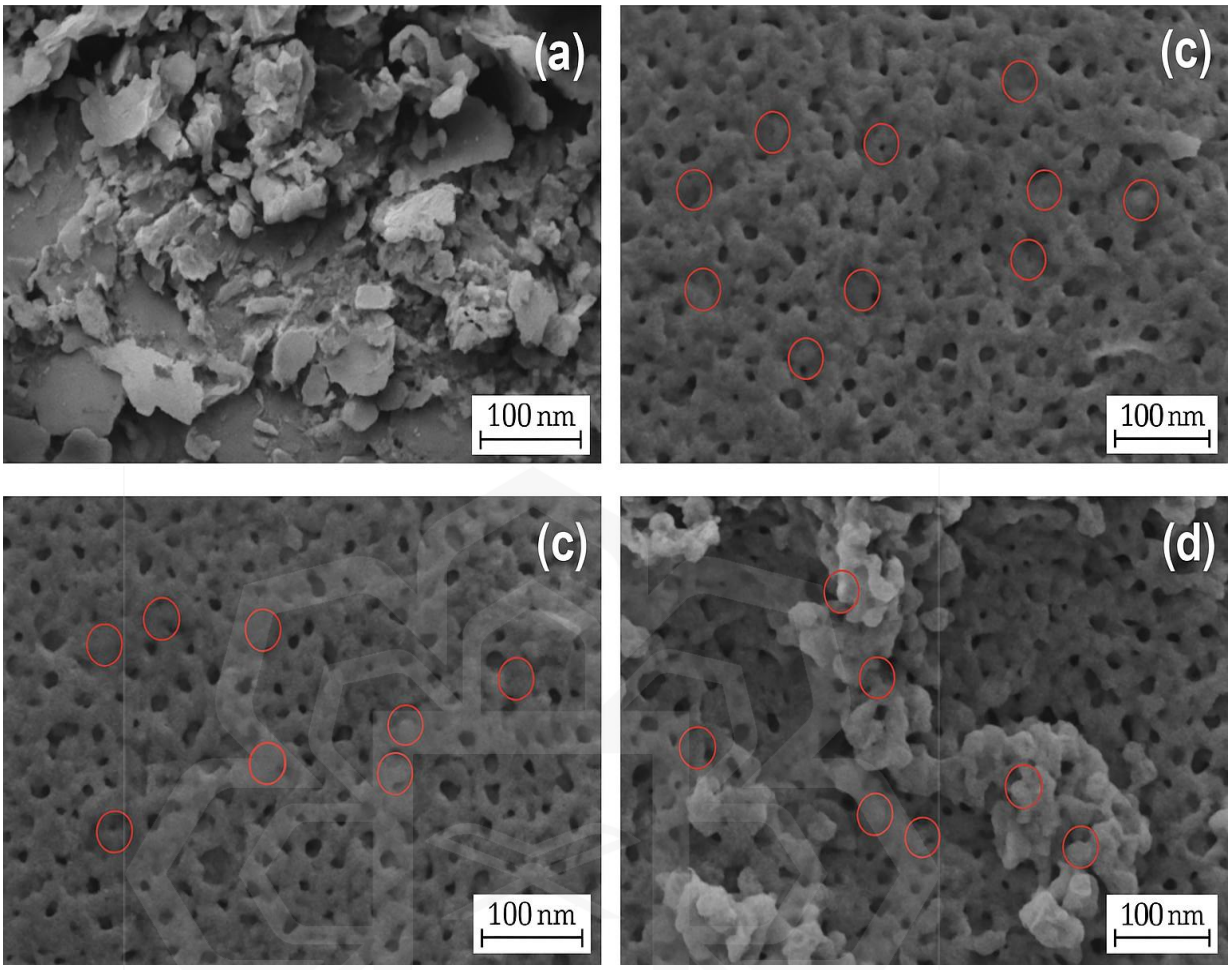

Figure 3.8 Images of CS (a) and MNP (b-c).

This observation aligns with previous studies, which also reported that CS in its native form exhibits a flaky appearance, whereas CS nanoparticle tend to exhibit a rounded shape (Vaezifar et al., 2013). In many studies, CS nanoparticles loaded with drug MT have been observed to have a spherical shape with a solid surface and a porous structure (Adlin & Anton, 2013; Oliveira et al., 2022; Sukhbir et al., 2017). SEM images of an empty CS nanoparticle also showed the spherical-like structure in the agglomerated state (Oh et al., 2019). The matrix structure observed in the nanoparticles is due to the electrostatic attraction between anionic and cationic groups of CS (Sukhbir et al., 2017). Freeze-drying, or lyophilisation, is another technique used to enhance the stability of CS nanoparticle by removing water and preserving particle properties (Ataide et al., 2021). However, the

agglomeration of MNP observed in the dry state is attributed to freeze-drying. This common drying method can cause particles to aggregate as water is removed, leading to close contact and subsequent agglomeration of the particles (Ataide et al., 2021; Oh et al., 2019). When particles are drying, the introduction of air-water interfaces (as water evaporates) can cause the particles to stick together due to capillary forces. This leads to the formation of clusters or agglomerates. During the drying process, the introduction of air-water interfaces as water evaporates can cause particles to stick together due to capillary forces. This leads to the formation of clusters or agglomerates. As the suspension dries and the concentration of ions and particles increases, the tendency for particles to clump together also increases. In high ion concentration suspensions, the usual repulsive forces that keep particles apart are neutralised, making attractive forces (such as London–Van der Waals and ion-ion correlation forces) more significant. This phenomenon, resulting in significant agglomeration in the dry state (Vertanessian et al., 2003), is confirmed by observations.

3.3.2.5 ATR-FTIR Analysis

Fourier-transform infrared spectroscopy (FTIR) analysis provides valuable insights into the molecular structure of both MT and the components of CS-based nanoparticles. In this study, the FTIR spectrum of MT offers a detailed characterisation of its molecular structure through specific vibrational peaks. The peak observed at 1185 cm^{-1}, assigned to C-O stretching vibrations, confirms the presence of ether or hydroxyl functionalities within the molecular structure of MT. This peak falls within the range of 1275–1096 cm^{-1}, as reported in previous literature (Trivedi et al., 2015). The principal absorption peaks at 1534 and 1367 cm^{-1} correspond to N=O asymmetric stretching, which typically falls within the range of 1550–1350 cm^{-1}, confirming the presence of the nitro group in the MT molecule. These peaks are essential for confirming the presence of the nitro group, which is critical for MT's biological activity (Kumar & Awasthi, 2015; Sukhbir et al., 2017). Furthermore, the peak at 3097 cm^{-1}, corresponding to C-H stretching vibrations of the aromatic rings, is consistent with expected stretching vibrations for aromatic C-H bonds in the nitroimidazole structure

of MT. This observation aligns with previously reported values of 3000–3100 cm^{-1}, providing additional confirmation of the integrity of the aromatic ring structure in the molecule (Kumar & Awasthi, 2015).

In pure CS, the region between 3600 and 3200 cm^{-1} is assigned to O–H stretching vibrations (Helen et al., 2020), with a peak maximum at 3343 cm^{-1}, indicating hydrogen bonding involving hydroxyl (–OH) and amine ($–NH_2$) groups. This broad absorption band results from extensive intramolecular hydrogen bonding (Szymańska-Chargot et al., 2019). The N-H bending vibration at 1591 cm^{-1}, associated with the amine group (Amide II), is also prominent in pure CS. After cross-linking with TPP, this peak shifts to 3199 cm^{-1}, reflecting a reduction in hydrogen bonding due to interactions between CS's functional groups and TPP's phosphate groups. The shift to a lower wavenumber indicates the formation of ionic bonds or complexation between protonated amine groups ($–NH_3^+$) and the phosphate groups of TPP (Ruchika & Himanshi, 2019). When MT is loaded into the CS-TPP complex, the peak shifts further to 3100 cm^{-1}, suggesting additional modifications in hydrogen bonding due to drug interactions.

The peak at 1591 cm^{-1} for pure CS, associated with the N-H bending vibration (Amide II band), decreases to 1533 cm^{-1} in CS nanoparticles. This shift indicates reduced hydrogen bonding or ionic interactions due to cross-linking. The consistent peak at 1533 cm^{-1} in MT-loaded CS nanoparticles suggests that drug incorporation does not significantly alter the N-H bending or C-N stretching vibrations of the amine group, reflecting effective drug loading while maintaining the structural integrity of the CS network (Ahmad et al., 2023; Lustriane et al., 2018). Another important feature is the C-O stretching vibration, which occurs at 1025 cm^{-1} in pure CS (Queiroz et al., 2015). This peak shifts to 1066 cm^{-1} after nanoparticle formation due to interactions between CS and the crosslinker. After MT loading, this peak shifts slightly to 1063 cm^{-1}, indicating that drug loading does not cause major structural changes in the nanoparticles, as demonstrated in Figure 3.9 (Alasas et al., 2024; Kumar et al., 2021).

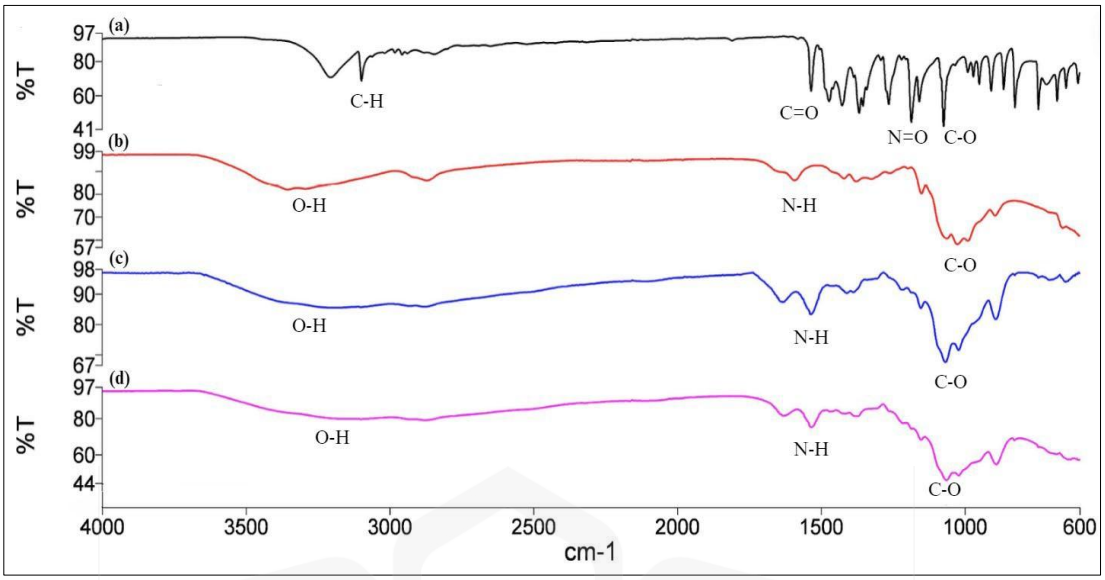

Figure 3.9: ATR-FTIR images of MT (a), CS (b), CS nanoparticle (c), and MNP nanoparticle (d).

The FTIR spectra of MT-loaded onto CS nanocarrier exhibited the absence of distinct drug-specific peaks, suggesting that MT exists in an amorphous state within the polymer matrix. This observation is attributed to a reduction in the crystallinity of the drug, likely caused by its physical entrapment within the CS-TPP network. Similar findings have been reported in previous studies, where drug-loaded nanoparticles frequently display diminished or absent sharp FTIR peaks, reflecting a loss of crystallinity upon integration into amorphous polymer matrices (Thamilselvan et al., 2023). For instance, Hamdi et al. (2021) documented a significant reduction in characteristic peaks in ascorbic acid-loaded PLGA nanoparticles, reinforcing the concept that encapsulated drugs undergo physical state transitions. In general, drug incorporation into nanoparticle systems leads to peak broadening or disappearance in FTIR spectra, attributed to molecular dispersion and reduced intermolecular order (Sakhi et al., 2022; Singh et al., 2018). Furthermore, the stability of the nanoparticle formulation in this study is corroborated by the retention of key spectral features and the absence of substantial changes in surface charge following drug loading (Oliveira et al., 2022). The FTIR spectra of CS-TPP loaded MNP closely resembled those of the unloaded formulation, with no emergence of new peaks. The preservation of

principal CS-TPP bands and the absence of MT-specific signals strongly suggest that MT is physically encapsulated rather than chemically bonded. The CC-MNP closely resembles that of pure CS nanoparticles, with observed shifts in wavenumbers attributed to crosslinking with TPP and no new peaks emerging. This similarity indicates that drug loading does not interfere with the CS-TPP bonds, thereby maintaining the stability of the nanoparticles. These findings underscore the potential of the CS-TPP nanocarrier system for efficient drug delivery, particularly for encapsulating hydrophilic drugs like MT.

These findings imply that no covalent bonding occurs between MT and the polymer matrix. Instead, recent studies have confirmed that drug encapsulation in CT-based or supramolecular polymer nanoparticles typically involves non-covalent interactions such as hydrogen bonding, van der Waals forces, and electrostatic attractions which facilitate stable yet reversible drug–polymer associations (Zhang et al., 2025; Buaksuntear et al., 2022). These interactions are particularly advantageous in controlled-release systems, as they allow for sustained release without compromising the structural integrity of either the carrier or the drug. In conclusion, the FTIR analysis confirms that MT does not chemically crosslink with the CS matrix but is successfully entrapped via non-covalent interactions within the CS-TPP nanoparticles. This encapsulation results in reduced drug crystallinity and stable incorporation, supporting the suitability of this nanoparticulate system for controlled-release drug delivery applications.

3.3 CONCLUSION

The quantification method for MT content in CS nanocarriers was developed and rigorously validated using UV spectrophotometry. This method met all the acceptance criteria outlined by ICH Q2 (R1) guidelines, showcasing its precision, linearity, specificity, accuracy, robustness, and ruggedness. The analysis identified a maximum absorbance wavelength of 320 nm and demonstrated a linear relationship ($R^2 = 0.999$) within the range of 2-12 µg/mL, confirming the method's reliability for quantifying MT in nanosized formulations.

Following successful validation of the UV spectrophotometry method, MNP was fabricated using an ionic gelation technique. The resulting nanoparticles exhibited desirable properties for local drug delivery, including a particle size of 308.0 ± 9.18 nm, a polydispersity index (PDI) of 0.374 ± 0.37, a zeta potential of 46.6 ± 0.23 mV, and an encapsulation efficiency of 87.95 ± 0.07%. These characteristics suggest that nanoparticles are well-suited for targeted, sustained-release applications, particularly in treating periodontal disease. Among the various formulations evaluated, formulation number one (F1) proved to be the most optimal, with a CS concentration of 0.3% w/v and a MT concentration of 0.15 w/v%. This formulation achieved the smallest particle size, the lowest PDI, the highest zeta potential, and the highest encapsulation efficiency, making it the most promising for further development.

The validated UV spectrophotometry method, coupled with the successful fabrication of MNP, lays a strong foundation for developing effective local antibacterial agents for periodontal therapy. Although the nanoparticles show significant promise, further *in vitro* and *in vivo* studies are required to assess their efficacy and safety. Future research will also focus on integrating MNP into guided bone regeneration (GBR) scaffolds to evaluate their impact on bone regeneration and infection prevention. In summary, the combination of precise UV quantification and effective nanoparticle fabrication highlights the potential of these mt-loaded CS nanocarriers for targeted, sustained, and controlled drug delivery in periodontal treatment.

CHAPTER FOUR

FABRICATION OF COLLAGEN-CHITOSAN SCAFFOLD LOADED WITH METRONIDAZOLE NANOPARTICLES (CC-MNP)

4.1 INTRODUCTION

Periodontal disease remains a significant global oral health challenge, impacting approximately 14.5% of the global population, as reported by the 2019 Global Burden of Disease Study (Arigbede et al., 2012). This chronic inflammatory condition affects the supporting tissues of the teeth and can lead to severe complications, including tooth loss, if inadequately managed. The Global Burden of Disease Study further indicates that severe periodontal disease affected approximately 10.8% of the population aged 15 years and older in 2019 (Chen et al., 2021). Early manifestations of periodontal disease include gum inflammation, swelling, discomfort, and bad breath, with advanced stages potentially resulting in tooth mobility and loss due to the degradation of the supporting alveolar bone (Arigbede et al., 2012).

Guided Bone Regeneration (GBR) therapy has become a pivotal intervention to halt the progression of periodontal disease and facilitate the restoration of lost tissue through scaffold utilisation. In tissue engineering, scaffolds are designed to replicate the extracellular matrix (ECM), providing a supportive framework for cellular activities essential for tissue repair and regeneration (Mao et al., 2003; Sahai et al., 2018). Collagen has been extensively utilised in scaffold fabrication due to its inherent biocompatibility and biodegradability. However, traditional collagen sources from mammals, such as porcine and bovine, raise concerns about halal compliance and disease transmission risks, such as bovine spongiform encephalopathy (Zain & Hamdan, 2021). As a result, fish-derived collagen has emerged as a promising alternative, offering a halal-compliant and safer source of collagen (Nurilmala et al., 2022). CS, a biopolymer derived from chitin, is commonly blended with collagen to enhance scaffold properties. The ionic interactions

between CS and collagen improve the mechanical strength and stability of the scaffold, addressing the rapid biodegradation and limited mechanical strength challenges faced by non-crosslinked collagen scaffolds (Eun et al., 2004; Ullah et al., 2017). Incorporating MNP into these scaffolds provides localised antibacterial effects, which are advantageous in periodontal therapy where systemic antibiotic use can lead to adverse side effects and bacterial resistance (Khabeer et al., 2021; Soares et al., 2012; Walker, 1996).

The fabrication process involves blending collagen and CS, incorporating MNP, and cross-linking the mixture to form a porous 3D scaffold. This approach optimises key scaffold characteristics, such as pore size, swelling behaviour, and biodegradation rate, which are essential for ensuring scaffold functionality. Recent advancements in tissue engineering and nanotechnology have focused on designing scaffolds with specific properties to support tissue regeneration and drug delivery (O'Brien, 2011). These scaffolds are designed as 3D biomaterials for host cells, guiding their attachment, growth, differentiation, proliferation, phenotype, and migration to facilitate new tissue development. Despite these advancements, achieving well-defined drug-loaded scaffolds with precise properties remains challenging due to the complexity of biological tissues. The scaffolds must meet various requirements, including appropriate pore size, swelling ability, biodegradability, and morphological and structural characteristics that promote cellular adhesion, integration, and interaction with the biological environment (Tipa et al., 2022). The scaffold should exhibit structural consistency, a suitable pore size, and the capacity to absorb and retain water while maintaining its 3D structure, thereby creating a favourable environment for essential biological interactions, such as nutrient and oxygen exchange crucial for cell proliferation, adhesion, differentiation, and tissue formation (Thang et al., 2023). Additionally, the degradation rate of scaffolds is critical, as it affects tissue viability and is influenced by factors such as physical loading, scaffold environment, structure, and surface and chemical modifications (Echeverria Molina et al., 2021). The ability of the scaffold to modulate biodegradation while ensuring controlled drug release is a crucial property that enhances its potential as a vehicle for drug delivery. This capability is crucial for advancing therapeutic and regenerative strategies. Key characteristics such as pore size, swelling behaviour, and biodegradation rate play significant roles in scaffold functionality.

Specifically, pore size influences cellular infiltration and tissue regeneration, while swelling behaviour affects moisture retention and cellular support. The biodegradation rate is essential for controlling the release of MT and maintaining scaffold integrity (Fernandes et al., 2011; Loh & Choong, 2013; Tipa et al., 2022). This study aims to develop and characterise CC scaffolds loaded with MT, focusing on the impact of varying MT nanoparticle concentrations (10, 20, 30, and 40 w/v%) on key properties of the scaffold. These properties include pore size, swelling behaviour, and biodegradation rate. By evaluating these factors, the study seeks to optimise the scaffold's performance in terms of cellular infiltration, moisture retention, and controlled drug release, ultimately enhancing its efficacy for periodontal disease treatment.

4.2 METHODOLOGY

4.2.1 Fabrication of CC-MNP

The fish collagen, derived from a *Tilapia mossambica* source, was purchased from Eva Chemicals in Kuala Lumpur, Malaysia. The CC blend was prepared by mixing 30 mL of collagen solution (3 w/v%) with 70 mL of CS solution (3 w/v%). The ratio of collagen to CS was maintained at 30:70. Glycerin (0.9% v/v) was added to the blend, which was continuously stirred until homogeneous. To neutralise the CC blend, sodium bicarbonate ($NaHCO_3$) solution was gradually added while stirring. The mixture was then transferred into 96-well plates as moulds, and MNP ranging from 10 mg, 20 mg, 30 mg, and 40 mg were uniformly dispersed into different wells. To achieve the desired structural characteristics, CC scaffolds were cross-linked by combining hydrothermal treatment. The samples were frozen at temperatures of -20°C, -40°C, and -70°C for 24 hours before undergoing lyophilisation (freeze-drying) under vacuum pressure (<100 mTorr) at a condenser temperature of -40°C for 24 hours. The resulting lyophilised samples were subsequently subjected to dehydrothermal treatment (DHT) at a temperature of 105°C for 48 hours. This process facilitated the removal of moisture and the generation of a dry,

porous structure. For comparative analysis, CS-collagen blends without the incorporation of MNP were fabricated using the same methodology. (Oliveira et al., 2021; Ullah et al., 2017).

4.2.2 Physical Characterisation of Scaffolds

The scaffold's thickness was measured with a micrometre screw gauge, which was used to measure by assessing three randomly selected scaffolds from each group. For the assessment of weight variation, each group was individually weighed using an analytical balance, and the average weight was then calculated (n = 3) (Khan et al., 2016).

4.2.3 Pore Size and Morphology of CC-MNP

The scaffold's morphology was characterised using scanning electron microscopy (SEM) (Fei Quanta 450 EDX, Oxford), and its pore size was measured randomly (n = 6). Before observation, the surface of the scaffold was coated with a thin layer of gold-coated and examined under the microscope at a voltage of 5 kV (Khan et al., 2016).

4.2.4 Swelling Ratio of CC-MNP

The swelling ratio was calculated by immersing the scaffold in phosphate buffer saline (PBS) with a pH of 7.4 at 37°C. After a 24-hour immersion period, the scaffold was gently dried on filter paper and weighed using an analytical balance. The swelling ratio was then calculated using the provided equation (4.1) (Grabska-Zielińska et al., 2020).

$$\text{Swelling ratio (\%)} = [(W_w - W_d) / W_d] \times 100 \qquad (4.1)$$

Where Wd is the dry weight of the scaffold, Ww is the weight of the scaffold after swelling (n = 3).

4.2.5 Biodegradation Study of CC-MNP

To assess the scaffold's biodegradation properties, it was immersed in 5 mL of PBS with a pH of 7.4, maintained at 37 °C, and maintained at 37 °C for 28 days. At specific time intervals of 7, 14, 21, and 28 days, the scaffold was removed from the degradation medium and allowed to air-dry. The degradation rate was then quantified as a percentage using equation (4.2) (Ullah et al., 2017).

$$\text{Degradation rate (\%)}: [(W_b - W_a)/W_b]x\ 100 \quad (4.2)$$

Where Wb represents the initial weight of the scaffold before degradation, and Wa represents the weight of the scaffold after degradation (n = 3).

4.2.6 Mechanical Analysis of CC-MNP

The mechanical properties of the scaffolds were determined using a texture analyser (Brookfield, UK) based on previous studies (Sangsen et al., 2011). Each sample was accurately placed on a plate under the punch of the instrument. Measurement The upper punch of the apparatus was compressed to half of the original height of the scaffold at a test speed of 0.5 mm/s, followed by the removal of the probe. The recovery was assessed by compressing the scaffold twice, and the stress was measured against time. The elastic modulus (*E*) of scaffolds can be calculated using the following equation, which involves measuring stress and strain (Zhang et al., 2019).

$$EE = \sigma/\epsilon \quad (4.4)$$

Where σ is the stress applied to the material (MPa), ϵ is the strain experienced by the material (dimensionless).

4.2.7 Statistical Analysis

A one-way analysis of variance (ANOVA) was conducted using GraphPad Prism (Version 9.01) to determine the significance of differences among the means. ANOVA was followed by post-hoc analysis using Tukey's Honest Significant Difference (HSD) test to determine the exact p-values for each comparison and verify statistical significance.

4.3 RESULT AND DISCUSSION

4.3.1 Fabrication of CC-MNP scaffold

4.3.1.1 Physical characteristics of the CC-MNP scaffold

In the initial phase of preparation, CC was neutralised using a sodium hydroxide solution, followed by the addition of MNP to the CC blend. As highlighted in Chapter 4, nanoparticles, particularly MNP, tend to precipitate or agglomerate in aqueous media due to their insolubility in neutral pH, posing a risk of potential precipitation. This emphasises the need for careful consideration when integrating nanoparticles into aqueous mediums, as achieving uniform dispersion of nanoparticles within the CC matrix can be challenging. Despite these challenges, prior research has shown that collagen-gelatin blends synthesised with different nanoparticles can serve as a stabilising agent for nanoparticles, preventing their agglomeration (Sethi et al., 2022). In our study, a CC blend with a specific ratio (30:70) exhibited increased viscosity compared to an aqueous medium. This is attributed to CS, a robust viscosity-building agent. The amino groups in CS can interact with water molecules through hydrogen bonding, resulting in the thickening or gelling of the solution (Rodríguez-Vázquez et al., 2015). This property makes CS an effective viscosity-building agent in mediums, allowing for control over fluidity and the ability to form a stable scaffold. This improved viscosity contributed to the homogeneous distribution of nanoparticles in

the blend and hindered the precipitation of the nanoparticles. The CC blend not only prevented the MNP from settling down but also facilitated their uniform dispersion in the blend without clumping. Our findings indicate that the viscosity of the (30:70) blend played a crucial role in achieving an even dispersion of nanoparticles, distinguishing it from blends with ratios (70:30) and (50:50), as mentioned in a previous study, the colloidal dispersion (opalescent) instead of white precipitate achieved at the bottom of the vial indicates the stabilisation of the nanoparticle (Smith et al., 2019). This observation suggests that the MNP was effectively stabilised, as evidenced by the absence of precipitation in the blend. Therefore, we chose the (30:70) ratio for incorporating the MNP.

CC scaffolds typically exhibited an off-white or beige colour due to the natural colour of the collagen and CS materials. This observation was supported by a previous study in which CC scaffolds loaded with L-glutamic acid displayed an off-white scaffold colour (Kumar et al., 2022). Furthermore, CC-hydroxyapatite scaffolds for bone repair in ovariectomised rats were also noted to exhibit similar white three-dimensional structures (Chacon et al., 2023). Consistent with previous findings, both the drug-free scaffold and scaffold containing different concentrations of MNP (10 - 40 w/v%) in this study appeared beige in colour with no noticeable physical appearance. In this study, the scaffold without the MNP (0 w/v%) served as a blank scaffold, while the CC scaffold with the drug (ranging from 10 - 40 w/v%) was also examined. The thickness and weight variation of the scaffold were directly associated with mass uniformity and dosing accuracy (Khan et al., 2016). The average thickness of all prepared scaffolds ranged from 5.003 ± 0.004 mm to 5.017 ± 0.012 mm in length, 6.037 ± 0.010 mm to 6.072 ± 0.007 mm in width, showing a consistent three-dimensional structure of similar size. The weight variation values increased as the concentration of MNP increased, ranging from 5.96 ± 0.07 mg to 6.31 ± 0.08 mg. However, each group exhibited uniform weight, indicating that the drug was uniformly distributed. The consistent thickness and weight values obtained in this study depicted the scaffold's uniformity in their physical appearance. These dimensions were specifically designed to comply with established CSD models in rat calvarial and mandibular bones, where 5 mm defect diameters are widely recognised as non-healing thresholds (Schmitz & Hollinger, 1986; Spicer et al., 2012; Hatakeyama et al., 2022). The scaffold dimensions therefore fall

within suitable parameters for use in preclinical CSD models aimed at evaluating bone regeneration. Their dimensional consistency supports reliable assessment of regenerative efficacy without the risk of spontaneous healing.

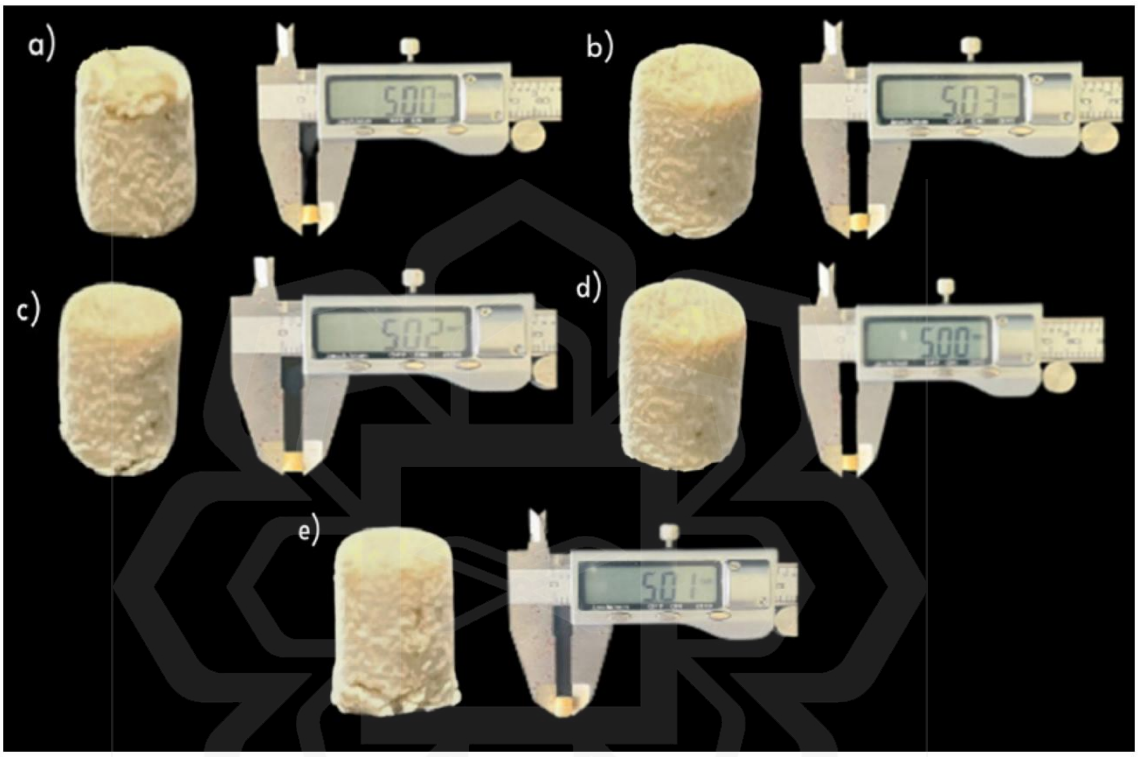

Figure 4.1 The photograph of a scaffold containing different amounts of MNP (a) 0% w/v, (b) 10% w/v, (c) 20% w/v, (d) 30% w/v, (e) 40% w/v.

Figure 4.1 visually demonstrates the macroscopic appearance of CC scaffolds containing increasing MNP concentrations (0–40 w/v%), reinforcing the physical uniformity and colour consistency described above. The beige colour, consistent thickness, and weight uniformity across formulations confirm the reproducibility of the fabrication process. The observed absence of nanoparticle precipitation in the selected (30:70) blend further validates the role of CS in stabilising MNP within the scaffold matrix. The combination of favourable handling properties and standardised dimensions suitable for

critical-sized defect models positions this scaffold formulation as a strong candidate for subsequent *in vivo* evaluation.

4.3.1.2 Morphological Properties of Scaffold

The 3D porous structures of scaffolds play a crucial role in supporting cell nutrition, proliferation, and migration, aiding tissue vascularisation and tissue formation. The SEM micrographs of both the prepared drug-free scaffold and the scaffold containing different concentrations of MNP in the range of 10–40% w/v showed an open porous structure with a uniformly interconnected network, as illustrated in Figure 4.2.

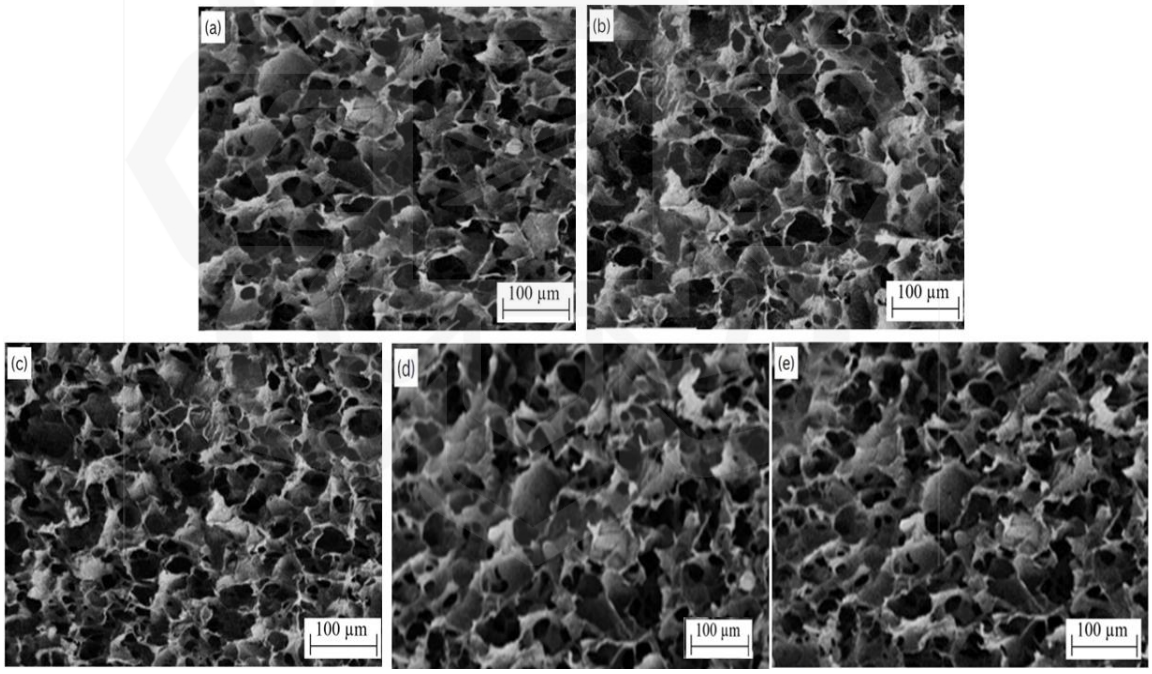

Figure 4.2 The SEM micrographs of a scaffold containing different amounts of MNP (a) 0% w/v, (b) 10% w/v, (c) 20% w/v, (d) 30% w/v, (e) 40% w/v.

This structural characteristic is predominantly achieved through a combination of freeze-drying and subsequent hydrothermal crosslinking treatment, forming a

porous scaffold (Xu et al., 2012). It was also noted in a previous study that lyophilisation produces an interconnected porous structure through the elimination of ice crystals from the frozen solution (Irastorza et al., 2021), an essential parameter for exchanging gas, waste, and nutrients for cells inside the scaffolds (Felfel et al., 2019). Instead of the pore network structure that guides and promotes the development of new tissue, the porous surface also facilitates mechanical interlocking, thereby enhancing the implant's stability (Loh & Choong, 2013). Following the crosslinking process, the samples underwent DHT for 24 hours under static vacuum conditions. This crucial step produces an interconnected porous structure, enhancing the scaffolds' stability and long-term integrity. The DHT process played a vital role in removing excess water content from the scaffolds, further improving their stability and resistance to degradation. This is supported by a previous study wherein CC blend samples, after undergoing cross-linking and DHT treatment, demonstrated enhanced stability when exposed to an aqueous medium (Oliveira et al., 2021). As a result, the scaffold became better equipped to withstand the various physiological conditions within the body. Furthermore, scaffold morphology can be noticed in elongated or round shapes (Felfel et al., 2019). In this study, an empty scaffold (Figure 4.2a) and drug-loaded scaffolds (Figure 4.2b–e) exhibited a similar structure and geometry of the surface of the scaffold with similar rounded pores. Thus, the drug-loaded scaffold did not influence the structure and geometry of the surface of the scaffold.

4.3.1.3 Pore Size of Scaffold

In this study, the mean values of pore size displayed a gradual decline as the MNP concentration incorporated into the scaffold increased, as shown in Figure 4.3**.** The control group exhibited the highest mean value pore size of 110.9 ± 5.8 μm, followed by the MNP-loaded scaffolds (105.2 ± 3.2 μm, 104.8 ± 4.8 μm, 101.9 **±** 5.2 μm, and 101.5 ± 4.8 μm for 10% w/v, 20% w/v, 30% w/v, and 40% w/v groups, respectively). Thus, the pore size of both the empty scaffold and the drug-loaded scaffold met the minimum requirement of pore size for 3D bone regeneration.

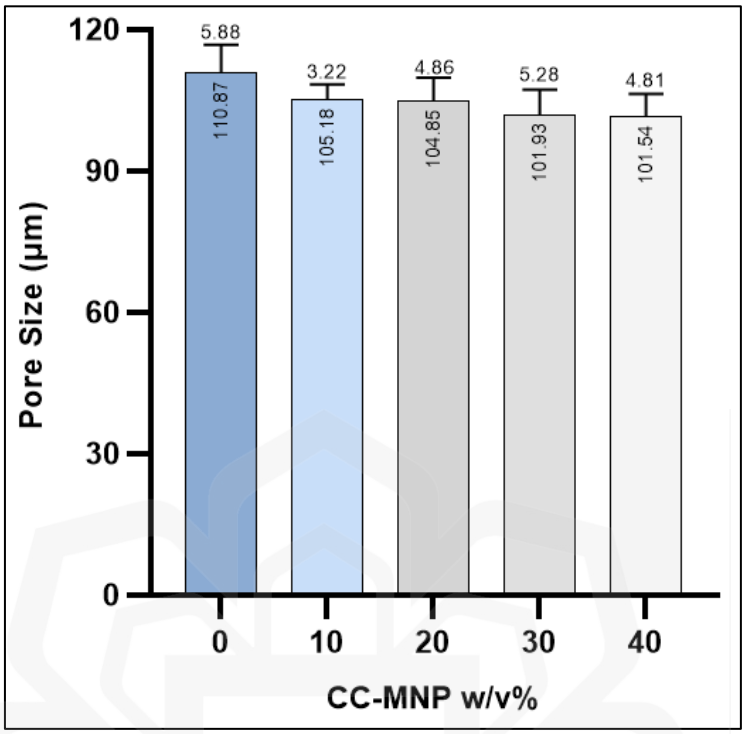

Figure 4.3 The average pore size of scaffolds at different concentrations of MNP (0 -40% w/v). Error bars indicate the mean ± S.D. (n = 6). No statistically significant differences were observed among the groups ($p > 0.05$)

In the field of bone tissue engineering, the ideal pore size for engineered scaffolds remains a topic of debate. This is because the average pore size of a scaffold plays a critical role in influencing cell penetration and proliferation within the structure (Nokoorani et al., 2021). Additionally, it is essential for cell adhesion and attachment to the pore surface of scaffolds (Bružauskaitė et al., 2016). The range of pore sizes offers diverse advantages for various applications. Generally, scaffold pores in the range of 20 to 1500 µm have been used (Loh & Choong, 2013), with larger pore sizes being advantageous for promoting cell attachment (Felfel et al., 2019). However, it has been reported that the best cell attachment is on 3D scaffolds with 100 µm pores (Bružauskaitė et al., 2016), and the minimum recommended pore size for a scaffold is 100 µm to ensure adequate vascularisation of the repaired tissue or organ (Qasim et al., 2015). This is because the scaffold's macropore size

is crucial for cell seeding, distribution, migration, and further neovascularisation *in vivo* (Bružauskaitė et al., 2016; Qasim et al., 2015). Further analysis of variance (ANOVA) was conducted to compare the means of the pore sizes between the scaffold without the drug (control) and the scaffold with the drug. However, the highest concentrations of the drug did not show any significant difference in the pore size compared to the empty scaffold, and the pore size falls within the range mentioned in the previous study of 50 to 300 μm achieved through freeze-drying techniques (Bružauskaitė et al., 2016). This indicates the effectiveness of the physical crosslinking technique employed in the fabrication of the scaffold.

The scaffold's pores can be broken down into nanosize (100 nm), micropore size (100 nm – 100 μm), and macro-roughness (100 μm–millimetres) (Felfel et al., 2019). This suggests that the 100 μm pore size of the scaffold will not hinder the release of the drug, making it suitable for the efficient release of MNP in nanometre dimensions. This can be supported by previous studies where melatonin in the range of 110–200 nm could sustain the release of the drug from the scaffold for 21 days (Rao et al., 2020). Another study revealed that nanoparticles were homogeneously dispersed on a porous collagen scaffold, forming an interconnected porous structure with a pore size ranging from 150 to 200 μm, irrespective of the amount of nanoparticles, and the porosity of scaffolds kept almost unchanged with the increment of the nanoparticles (Xu et al., 2012). Thus, the pore size of the scaffold is suitable not only to facilitate tissue growth and regeneration but also to release nanoparticle drugs, providing a sustained and localised drug delivery system.

4.3.1.4 Swelling ratio of CC-MNP

Previous research has demonstrated that silk fibroin, collagen, and CS can be crosslinked and lyophilised to make a 3D scaffold that swells up to 3000% after 1 hour of immersion. This characteristic makes them well-suited for tissue engineering applications (Grabska-Zielińska et al., 2020b). The swelling ratio of the CC-MNP scaffold was evaluated across varying MNP concentrations. The highest swelling ratio was observed in the scaffold

without incorporating MNP at 0% w/v. At 10% w/v, the swelling ratio reduced to 77.51% ± 0.63. This trend continued with increasing MNP concentration: at 20% w/v, the swelling ratio dropped to 51.86% ± 0.60, while at 30% w/v and 40% w/v, it further reduced to 43.42% ± 0.45 and 42.26% ± 1.06, respectively. This reduction correlates with the influence of nanoparticles on the water transport pathways within the scaffold matrix.

Table 4.1 Swelling ratio of CC-MNP scaffold.

CC-MNP (% w/v)	Swelling Ratio (x100%) ± SD
0	85.17 ± 3.26
10	82.97 ± 2.17
20	77.42 ± 0.30
30	75.90 ± 0.30
40	70.75 ± 2.55

The swelling ability is a crucial factor in tissue engineering scaffold applications, impacting critical parameters like pore size, interconnection conditions, and scaffold volume. Additionally, swelling contributes to an increase in pore size and total porosity, thereby maximising the internal surface area of the scaffolds. This optimisation of the internal surface area is essential for facilitating the infiltration of cells into scaffolds during both *in vitro* and *in vivo* tissue formation. Scaffolds with a heightened degree of swelling exhibit a greater surface area-to-volume ratio, thus allowing the samples to have the maximum probability of cell infusion into the 3D scaffold and better attachment and cell growth to the scaffold surface (Azhar et al., 2014). The swelling capability of the scaffold is crucial as it enables the absorption and retention of a significant amount of water or biological fluids and facilitates biological interaction (Thang et al., 2023). However, while the swelling of scaffolds would promote cell adhesion, it could inversely affect the mechanical properties of the scaffold. To determine the swelling properties, the scaffolds were subjected to the swelling test as described in the previous study (Grabska-Zielińska et al.,

2020). In this study, the swelling ratio is expressed as a percentage of the original scaffold size, as shown in Figure 4.4**.**

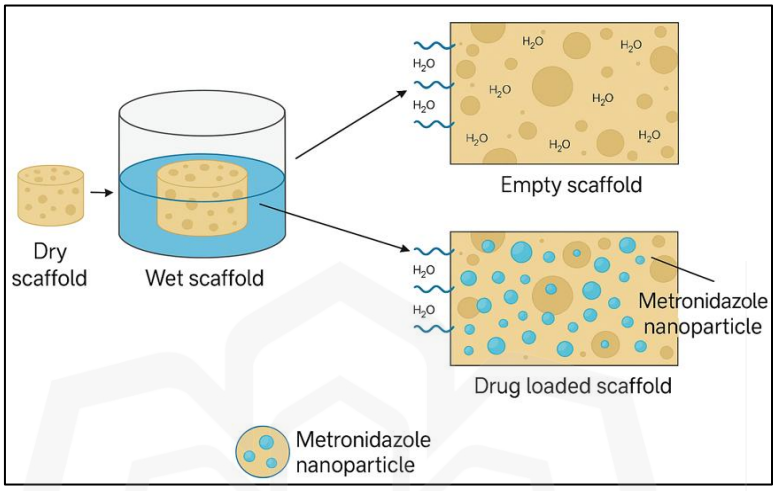

Figure 4.4 Illustration of swelling behaviour of the scaffold (created using BioRender.com)

As shown in Figure 4.4, water molecules diffuse into the scaffold, causing swelling until it reaches equilibrium (Namazi et al., 2019). However, the presence of nanoparticles might decrease the available holes within the scaffold, leading to less water diffusion into the drug-loaded scaffold and a subsequent decrease in swelling compared to the empty scaffold (Tipa et al., 2022). This observation aligns with prior research involving CS-collagen scaffolds with zinc oxide nanoparticles, where reduced swelling was noted due to nanoparticle-restricted water penetration (Ullah et al., 2017).

Another phenomenon can be noticed in a previous study where ZnO nanoparticles were added to swollen oxidised starch hydrogel, and there was a decrease in the swelling ratio due to ZnO nanoparticles as crosslinking (Namazi et al., 2019). Furthermore, MNP exhibits poor solubility in water at pH 7.4 (Celebioglu & Uyar, 2019), reducing the scaffold's water retention capability. This is similar to a previous study where incorporating ibuprofen in scaffolds may reduce water retention capability because ibuprofen is non-polar

and insoluble in water (Sangsen et al., 2011). Despite these considerations, water retention is well-suited for sustained drug delivery over an extended period, allowing for the control of the swelling behaviour of scaffolds and aiding in filling specific tissue defects for stable implantation (Kumar et al., 2019). This efficiency in delivering bioactive molecules, such as drugs or growth factors, also enables targeted drug delivery at the site of action, indirectly minimising systemic side effects and maximising therapeutic efficiency (Thang et al., 2023). However, both the scaffolds with different MNP concentrations (10–40% w/v) and the MNP-free scaffold (0% w/v) displayed significant swelling capability, exceeding 3000%. As previously noted in a different study, a swelling score surpassing 3000% indicates the scaffold's excellent swellability. Additionally, it was observed in a prior investigation that the CC scaffold reached equilibrium after being immersed in a PBS solution overnight. Consequently, all scaffolds displayed excellent swelling abilities when submerged in a PBS solution for 24 hours. This can be attributed to the highly hydrophilic nature of collagen and CS polymers, which exhibit a notable capacity to absorb and retain water while maintaining their 3D structure (Tripathi et al., 2021). This highlights its suitability for tissue engineering applications, aligning with the swelling behaviour indicated in prior studies (Priya et al., 2021; Thang et al., 2023).

4.3.1.5 Biodegradation Study of CC-MNP

The biodegradation profiles of CC-MNP scaffolds with varying concentrations of MNP (0–40% w/v) exhibited degradation rates of 69%, 68%, 60%, and 57%, respectively, after one week of immersion in phosphate-buffered saline (PBS). Notably, scaffolds containing 0% w/v and 10% w/v MNP degraded more rapidly, reaching 92% and 90% degradation within two weeks. In contrast, scaffolds loaded with higher MNP concentrations (20–40% w/v) showed a slower and more gradual degradation trend over the four-week period. By week two, the degradation rates for scaffolds with 20%, 30%, and 40% w/v MNP were 78%, 75%, and 73%, respectively. These values increased to 88%, 88%, and 87% by the end of week four. Table 4.2 presents the scaffold’s biodegradation rate (%) at different concentrations of MNP **(**0–40% w/v**).**

Table 4.2 Biodegradation percentage of CC-MNP scaffold.

Weeks	Concentration MNP (% w/v)				
	0	10	20	30	40
Week 1	68.80 ± 1.51	67.83 ± 2.48	60.19 ± 0.80	57.03 ± 1.71	53.68 ± 0.87
Week 2	92.33 ± 2.08	89.95 ± 0.42	78.4 ± 1.36	74.77 ± 2.55	72.89 ± 2.54
Week 3	92.47 ± 2.25	90.38 ± 0.50	88.19 ± 0.49	87.77 ± 1.05	82.33 ± 0.47
Week 4	94.00 ± 1.00	90.69 ± 0.36	87.80 ± 0.33	87.47 ± 0.69	87.36 ± 1.05

*Not*e. The values are expressed as mean ± standard deviation (n=3)

The immersion medium employed in this study was PBS at pH 7.4, a standard buffer system widely used in biomaterials research to simulate physiological conditions for *in vitro* degradation and drug release studies. PBS at this pH closely mimics the ionic composition and osmolarity of extracellular fluids, providing a stable and reproducible environment for scaffold evaluation (Mndlovu et al., 2024). Although PBS is slightly more alkaline than the typical pH of the oral cavity during active periodontal disease, it is a widely accepted medium for standardised degradation testing due to its physiochemical stability and ease of reproducibility (Mndlovu, & Choonara, 2024). In the oral cavity, pH levels are dynamic, fluctuating in response to salivary composition, dietary intake, and microbial metabolism. Under healthy conditions, salivary pH generally ranges from 6.2 to 7.6, but may decrease significantly during inflammation, bacterial activity, or pathological changes due to periodontitis (Amtha et al., 2024; Choi et al., 2017; Schwerdt & Gekle, 2025). While PBS at pH 7.4 does not precisely mimic these acidic conditions, it serves as a reliable and controlled environment for comparative scaffold degradation profiling and initial drug release modelling.

The observed slower degradation with increasing MNP concentration is attributed to reduced water infiltration and the low aqueous solubility of MNP at pH 7.4 (Celebioglu & Uyar, 2019; Ullah et al., 2017). Nevertheless, all scaffold groups demonstrated excellent biodegradability, with degradation percentages exceeding 80% by week four. Importantly, the presence of MNP did not hinder the scaffold's breakdown but instead facilitated a more controlled and sustained degradation profile.This gradual degradation is advantageous in the context of local drug delivery, as the release of the active compound is regulated by both diffusion and scaffold matrix degradation (Egorikhina et al., 2021; Potrč et al., 2015; Rambhia & Ma, 2015). The structural stability of the scaffolds over four weeks correlates well with the early phases of bone regeneration observed *in vivo* (Ma et al., 2016). Previous studies have reported that 3D CC scaffolds treated with DHT crosslinking retained their architecture for over 45 days, which supports the current findings. In the present study, drug-loaded CC scaffolds with varying MNP concentrations successfully maintained their three-dimensional porous structure and demonstrated delayed degradation over four weeks. These findings indicate that scaffolds possess both biodegradability and biostability, making them promising candidates for use in tissue engineering and regenerative applications, particularly in periodontal defect repair.

4.3.1.6 Mechanical Analysis

The mechanical properties of scaffolds loaded with varying concentrations of MNP. The control scaffold (0 mg MNP) had Young's modulus of 9.40 ± 1.19 MPa, serving as a baseline for comparison. Incorporating 10 mg of MNP increased the modulus to 11.38 ± 1.48 MPa, indicating enhanced stiffness. However, at 20 mg and 30 mg MNP, Young's modulus decreased to 7.94 ± 0.44 MPa and 7.65 ± 0.29 MPa, respectively, suggesting a reduction in stiffness with increasing MNP concentrations. The scaffold containing 40 mg MNP exhibited the lowest Young's modulus of 4.68 ± 0.12 MPa, representing a significant reduction compared to the control and other concentrations. While the differences between the control and scaffolds with 10–30% w/v MNP were not statistically significant ($p > 0.05$),

a significant difference was observed between the control and the scaffold containing 40 mg MNP ($p = 0.013$). This indicates that an excessive concentration of MNP compromises the mechanical strength of the scaffold. Table 4.3 shows Table 4.3 Mechanical properties of scaffold-loaded MNP at varying concentrations (0- 40 mg MNP)

Table 4.3 Mechanical properties of CC-MNP scaffold.

Scaffold + MNP (% w/v)	Strain (ϵ) ± S.D.	Stress ($\sigma\sigma$) (N/mm²)	(E) (MPa)
0	0.24 ± 0.04	2.22 ± 0.10	9.40 ± 1.19
10	0.27 ± 0.04	3.02 ± 0.08	11.38 ± 1.48
20	0.43 ± 0.02	3.37 ± 0.15	7.94 ± 0.44
30	0.49 ± 0.02	3.57 ± 0.14	7.65 ± 0.29
40	0.95 ± 0.05	4.43 ± 0.10	4.68 ± 0.12

Note: The values areexpressed as mean ± standard deviation (n=3)

Previous research shows that adding nanoparticles can improve the mechanical properties of scaffolds, such as stiffness, strength, and load-bearing capacity. For instance, incorporating bioactive glass (BG) nanoparticles into poly(ε-caprolactone) (PCL) scaffolds enhance their tensile strength and modulus, making them suited for bone regeneration. Increasing the nanoparticle concentration to 15% w/v improves stiffness due to the reinforcing effect of BG. However, adding more than 15% w/v up to 20% w/v reduces strength and increases brittleness, indicating a threshold limit where further additions cause clumping and weaken the material (Ielo et al., 2022). Similar observations have been observed in studies involving electrospun nanohybrids. The incorporation of 5% hydroxyapatite (HA) nanoparticles into a poly(3-hydroxybutyrate) (PHB) matrix yielded the highest mechanical strength and elastic modulus. However, exceeding 10% HA nanoparticles led to a decline in mechanical strength, indicating an optimal concentration range for nanoparticle inclusion (Kouhi et al., 2013). Similarly, adding zirconia to polymer

scaffolds improved tensile modulus at low concentrations. However, it reduced mechanical performance at higher concentrations due to disrupted fibre interactions and fibre continuity loss (Martin et al., 2015).

Scaffolds utilised in tissue engineering and regenerative medicine are subjected to various mechanical loads once implanted into the human or animal body. These loads include compression, tension, and shear, with compression being the most prevalent *in vivo*. Due to their critical role in maintaining structural integrity and functionality, the mechanical properties of scaffold are crucial for ensuring successful tissue integration and load-bearing capacity. One of the most important properties is the elastic modulus, which determines a scaffold's ability to resist deformation under applied stress. This property is typically assessed in tensile and compressive modes to ensure the scaffold can effectively support the required load (Zhang et al., 2019). The mechanical behaviour of scaffolds is highly dependent on their composition and structural design. For example, scaffolds intended for hard tissues, such as bone, must exhibit high stiffness and strength, while scaffolds for soft tissues, like skin or nerves, require more flexibility (Suamte et al., 2023). A key mechanical parameter, Young's modulus (denoted by E), represents the ratio between stress and strain, quantifying the stiffness or rigidity of a material. It is also often referred to as rigidity, elasticity, or tissue modulus, that is, its resistance against deformation when subjected to a given stress (Akhmanova et al., 2015). In this study, the focus is on evaluating the impact of MNP on the mechanical properties of scaffolds, explicitly examining how MNP influences scaffold stiffness as measured by Young's modulus.

In this study, the addition of MNP initially enhanced scaffold stiffness, but higher concentrations (40% w/v) negatively impacted stiffness, as observed in other nanoparticle studies. This may be due to the high surface area-to-volume ratio of nanoparticles, which promotes aggregation. Aggregation reduces the potential enhancement of mechanical properties, as clumping forms stress concentration points that weaken the material (Zare et al., 2017). Nanoparticle aggregation disrupts their uniform distribution, resulting in uneven load transfer and diminished scaffold performance under mechanical stress. This alters the mechanical behaviour of the nanocomposite and reduces its structural integrity (Ashraf et al., 2018). Similar findings have been reported in earlier studies, where low nanoparticle

concentrations enhanced scaffold strength, but excessive loading caused brittleness due to reduced matrix flexibility (Zainol et al., 2022). This aggregation behaviour is shown in Figure 4.5 and is consistent with the morphology reported by Ashraf et al. (2018).

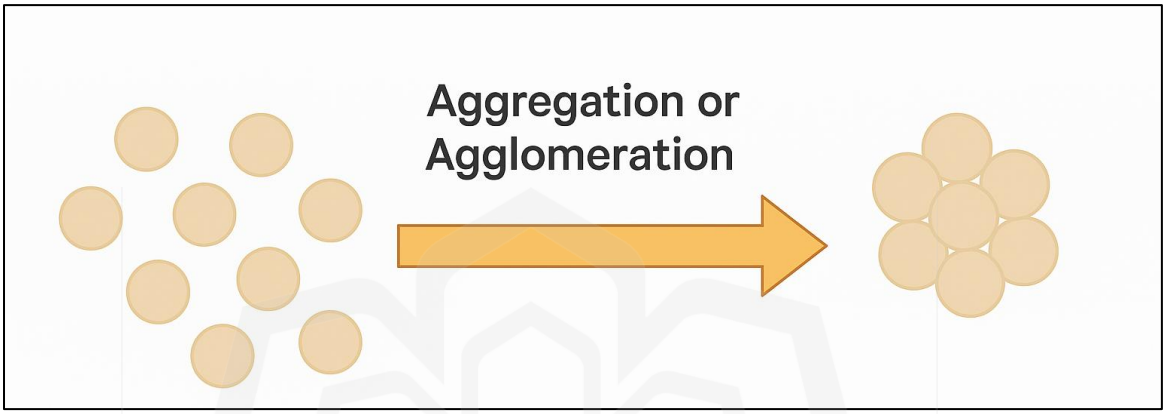

Figure 4.5 Illustration of nanoparticle aggregation within the scaffold matrix (created using BioRender.com)

Based on a comprehensive analysis of physical characteristics, morphological features, swelling behaviour, biodegradation, and mechanical properties, the scaffold containing 30% w/v MNP was selected as the optimal formulation for further application in bone tissue engineering. The 30% w/v MNP scaffold demonstrated consistent thickness and uniform weight distribution, indicating reliable fabrication and homogeneous drug loading, which are critical for dosing accuracy and reproducibility (Khan et al., 2016). The pore size of approximately 101.9 ± 5.2 µm falls within the ideal range for bone regeneration (50–300 µm), facilitating effective cell infiltration, vascularisation, and nutrient exchange, while also supporting sustained, localised drug release (Bružauskaitė et al., 2016; Rao et al., 2020). Additionally, the swelling ratio of 30% w/v MT-scaffold (75.90%) provided a balanced hydration state, avoiding excessive swelling that could compromise scaffold integrity and mechanical stability *in vivo* (Oliveira et al., 2021). The biodegradation profile demonstrated controlled and gradual degradation, with approximately 75% mass loss by week two and 88% by week four, aligning well with the typical bone healing timeline,

thereby ensuring sufficient mechanical support during early regeneration phases whilst allowing gradual load transfer to newly formed tissue (Spicer et al., 2012). Furthermore, mechanical testing showed that the 30% w/v MNP scaffold exhibited enhanced stiffness and Young's modulus compared to lower concentrations, without the brittleness associated with higher nanoparticle loading, which can cause aggregation and reduced structural integrity (Zainol et al., 2022; Zare et al., 2017). This balance of mechanical strength and biodegradability is essential for scaffolds intended for load-bearing applications such as bone repair (Akhmanova et al., 2015). Collectively, these characteristics demonstrate that the 30% w/v MNP scaffold offers an optimal combination of structural, functional, and biological properties, making it the most suitable candidate to promote effective bone regeneration and localised antimicrobial therapy.

4.4 CONCLUSION

In conclusion, this study successfully fabricated and characterised a CC scaffold loaded with MNP, demonstrating its potential for tissue engineering, particularly in periodontal therapy. The scaffold's fabrication process resulted in a well-structured three-dimensional porous matrix incorporating MNP, further enhancing its functionality. Key characteristics of the scaffold include its optimal pore size, which is crucial for cell adhesion, proliferation, and differentiation, thereby supporting effective tissue regeneration. Key characteristics of the scaffold include optimal pore size, which is essential for cell adhesion, proliferation, and differentiation and support effective tissue regeneration. The scaffold's excellent swelling ability also promotes cellular activity and nutrient exchange. Scanning electron microscopy (SEM) analysis confirmed that the scaffold maintained its intended three-dimensional porous structure, which is essential for providing reliable tissue support and regeneration framework.

A pivotal finding of this study is the impact of MNP incorporation on the scaffold's biodegradation rate. Scaffolds without MNP exhibited rapid degradation, which can be suitable for applications requiring fast tissue regeneration. However, adding MNP slowed

the degradation process, creating a controlled release system for metronidazole. This slower degradation rate is important for therapeutic applications requiring prolonged drug delivery and tissue regeneration, such as bone and periodontal repair. The controlled, sustained release of MT aligns with the body's natural bone formation process *in vivo*. This can help the scaffold serve as an effective delivery system for localised, long-term antibiotic therapy. While MNP can reinforce the scaffold at lower concentrations, excessive amounts lead to nanoparticle aggregation, compromising the scaffold's structural integrity. Therefore, an optimal MNP concentration range between 10 – 30 mg provides mechanical stability and is suitable for further analysis. This finding highlights the importance of balancing nanoparticle concentration to maintain scaffold performance. Furthermore, successfully integrating fish collagen with the CS scaffold introduces a novel, ethical, and sustainable material with potential applications in various medical fields, mainly where halal compliance is a critical consideration. The scaffold demonstrated excellent tissue regeneration properties, with optimal pore sizes and robust structural integrity, particularly when incorporating 10–30% (w/v) of MNP. The inclusion of MNP may provide effective localised drug delivery, which can help reduce the need for systemic treatment. This design ensures halal compliance while potentially enhancing healing and minimising side effects, making the scaffold a promising solution for future biomedical application

CHAPTER FIVE

IN VITRO STUDY OF COLLAGEN CHITOSAN SCAFFOLD INCORPORATED WITH METRONIDAZOLE NANOPARTICLE (CC-MNP)

5.1 INTRODUCTION

Periodontal disease arises from multifactorial inflammation primarily triggered by the accumulation of bacterial pathogens within the periodontal tissues, often leading to damage to the supporting structure of the teeth, such as tissue and bone, eventually resulting in tooth loss (Atia et al., 2022). In the field of dental tissue engineering, various strategies have been implemented to address periodontal diseases, with one promising approach involving the use of biomaterials to facilitate the regeneration of local tissues. Among the numerous biomaterials developed from different sources, the collagen-CC scaffold has gained significant attention in the field of tissue engineering and regenerative medicine due to its promising properties such as biocompatibility, biodegradability, and structural versatility, making it a suitable candidate for various biomedical applications. However, a major issue with current scaffolds is their susceptibility to infection due to their colonisation by pathogens in the periodontal pocket during the bone healing process, decreasing the regenerated bone (Ma et al., 2016a). Thus, incorporating antibiotics into biomaterials has become an important strategy for preventing or treating infections at the implantation site.

Previous studies have shown that antibacterial agents such as metronidazole, chlorhexidine, tetracycline, amoxicillin, and minocycline effectively treat periodontal disease. Among these antibiotics, MT is particularly effective for treating patients with periodontal disease by inhibiting *Porphyromonas gingivalis*, an anaerobic pathogen primarily responsible for periodontal disorders. Although previous studies have successfully fabricated CC scaffolds loaded with MNP (Zayi et al., 2023), the examination mainly focused on fabrication and characterisation. Further *in vitro*

investigations are necessary before advancing to *in vivo* and clinical implementation. *In vitro* studies play a crucial role in evaluating biomaterials' effectiveness and potential applications for various medical purposes.

Thus, this study aims to investigate the potential of CC scaffold incorporated with metronidazole nanoparticles (CC-MNP) *in vitro*. The study's first goal was to determine if the CC-MNP effectively inhibits *Porphyromonas gingivalis* (ATCC 3327) and *Fusobacterium nucleatum* (ATCC 25586) bacteria. Additionally, the *in vitro* drug release profile of MT from the scaffolds was evaluated over 14 days, involving the assessment of the initial burst release followed by a sustained release phase. This release profile was crucial for maintaining effective antibiotic levels in tissues, aiding in infection control, and promoting wound healing. Furthermore, FTIR measurements were conducted to analyse the molecular interactions within the scaffold before and after loading with MNP. The CC-MNP, which exhibited a prominent zone of inhibition, was also selected for further evaluation of its biocompatibility with human gingival fibroblast cells (HGF-1), which play a vital role in periodontal bone regeneration. These preliminary studies are essential to ensure the safety and efficacy of the CC-MNP before implementation in *in vivo* studies, significantly contributing to the development of an effective scaffold for treating periodontal disease.

5.2 METHODOLOGY

5.2.1 Disc Diffusion Method

The study aimed to assess the antibacterial effects of scaffolds loaded with different concentrations of MNP on *P. gingivalis* and *F. nucleatum* using disk diffusion. The test followed the methodology described by the Kirby-Bauer Disc Diffusion Susceptibility Test Protocol. The Brain Heart Infusion agar surface was inoculated with *P. gingivalis* and *F. nucleatum* at a density of 0.5 McFarland. After a 5-minute drying period, scaffolds at

different concentrations of MNP (0%, 10%, 20%, and 30%) were placed on the agar plates. The scaffolds used in this assay exhibited consistent dimensions, with an average length of 5.010 ± 0.010 mm and an average width of 6.055 ± 0.010 mm. The uniformity in scaffold size was maintained to ensure experimental consistency across all test groups. All plates were incubated anaerobically at 37 °C for 24 hours. Following the incubation period, the diameter of the zone of inhibition surrounding each scaffold was measured using a digital calliper to evaluate antibacterial efficacy. MT antibiotic discs were used as positive controls, while scaffolds without MNP (0%) served as negative controls to confirm that any antibacterial activity observed was due to the presence of MNP. The minimum inhibitory concentration (MIC) for each concentration of composite scaffold (CC-MNP) was determined through visual inspection, defined as the lowest concentration at which no visible bacterial growth occurred (Ibrahim et al., 2023). All experiments were performed in triplicate, and data were subjected to one-way ANOVA to assess statistically significant differences ($p < 0.05$) among scaffold concentrations and controls.

5.2.2 *In-vitro* release of MT nanoparticles from Nanocarrier and CC-MNP

In vitro drug release of Mt from nanocarrier and scaffold was evaluated in phosphate buffer solution, PBS (pH 7.4 at 37 °C). At each time interval, the supernatant was collected, and ultraviolet spectrophotometry (BioSpectrometer, Eppendorf, Germany) was used to measure the amount of MT released at 320 nm (n = 3). Sampling was at specified time intervals, and an equal amount of fresh PBS was added. Each drug release experiment was tested in triplicate *in vitro*. The concentrations of MTwere calculated through comparisons with a standard curve.

5.2.3 Fourier Transform Infrared Analysis

The chemical composition of the CC-MNP scaffold was analysed to verify any chemical interactions between the MNP and the CC matrix. ATR-FTIR was performed using a

Spectrum 100 instrument (Perkin Elmer, Massachusetts, USA. An average of 20 spectra was recorded for each sample over a wavenumber range of 4000–400 cm^{-1}, with a resolution of 1 cm^{-1} (Khan et al., 2016).

5.2.4 Biocompatibility Analysis of CC-MNP Scaffold

5.2.4.1 Standard Curve

To establish a linear relationship for estimating cell counts based on absorbance readings, a standard curve was generated using Human Gingival Fibroblast cells with concentrations ranging from 5.0×10^3 to $\times10^4$ cells/mL, which were seeded into a 96-well plate containing complete medium, Dulbecco's modified Eagle's medium (DMEM, GIBCO), supplemented with 10% foetal bovine serum (FBS) and 1% penicillin/streptomycin,. Each concentration had three replicates on the same plate. After a 4-hour incubation period, the MTT assay was performed, and absorbance was measured at 570 nm using a microplate reader. The linear regression equation derived from the standard curve facilitated the estimation of cell counts in the experimental samples based on their absorbance values. A calibration curve was constructed by plotting optical density (Y-axis) against cell concentration (X-axis), enabling accurate estimation of cell numbers in the samples (Singh et al., 2015).

5.4.2.2. MTT (3-(4,5-dimethylthiazol-2-yl)-2,5-diphenyltetrazolium bromide) assay

The scaffold was sterilised by UV irradiation on both sides for 15 min and via ethanol (70%), followed by a PBS washing treatment. After sterilisation, the scaffold was placed into 96 well plates and pre-wetted with culture medium before being seeded with Human Gingival Fibroblast Cells at a density of 2×10^4 cells/mL. The 3D culture plates were incubated at 37 ºC in an incubator with 5% CO_2. After every 48 hours, the culture media, Dulbecco's modified Eagle's medium (DMEM, GIBCO), containing 10% foetal bovine

serum (FBS) and 1% penicillin/streptomycin, were changed. The cell proliferation of the 3D culture was evaluated on days 1, 3, and 7 post-culturing via an MTT assay kit. The plates were incubated with MTT formazan at 37 °C for 4 hours and measured at 570 nm via microplate spectrophotometer (Power Wave XS, Biotek) (Ullah et al., 2017).

5.2.4.3 Cellular attachment morphology on CC-MNP

For FESEM preparation, the CC-MNP was fixed with 4% glutaraldehyde (Sigma Aldrich, UK) overnight, then washed with phosphate buffer saline (PBS) and dehydrated using a series of graded ethanol. Finally, dried cells were coated with a thin layer of gold, and the morphology of cells on the CC-MNP was observed using FESEM imaging (Ullah et al., 2017).

5.3 RESULT AND DISCUSSION

5.3.1 Antibacterial Assay

Previous research has identified an effective concentration of metronidazole, particularly for oral applications. For example, 25% MT incorporated into a gel (Elyzol®) has been shown to eliminate certain periodontal pathogens in clinical settings (Bottino et al., 2014). Another study involving CS hydrogel-based MT (0.12 – 3% CS hydrogel) demonstrated enhanced cell viability and non-cytotoxicity in 3T3 fibroblast cells (Rasni et al., 2018). Furthermore, an electrospun biodegradable PCL nanofiber membrane loaded with 30% MT was found to be an optimal option for localised drug delivery through GTR/GBR membranes, effectively preventing implant-associated infections and treating periodontal disease (Xue et al., 2014). As demonstrated in the mechanical analysis in Chapter 4, scaffold stability was found to be optimal at 10 – 30 % MT concentrations. Based on these findings, we conducted disk diffusion tests using scaffolds containing MT concentrations

ranging from 0% to 30% w/v. The inoculum was prepared from microbial cultures with a density of 0.5 McFarland standard. The samples' antimicrobial activity was tested using the disc diffusion method, as described in the Kirby–Bauer Disc Diffusion Susceptibility Test Protocol.

BHI agar plates were inoculated with an overnight culture of each bacterial suspension, containing approximately 1.0 x10^8 cells, which were evenly spread using sterile cotton swabs. The diameters of the clear zones around the scaffolds were measured from one edge of the clear zone to the opposite edge, passing through the scaffold. The characteristic black pigmentation of *P. gingivalis* colonies, when cultured on horse blood agar, is due to the accumulation of haemin, which is the oxidised form of heme, on the bacterial cell surface during its growth as shown in Figure 5.1 (How et al., 2016). In contrast, *Fusobacterium nucleatum*, another key Gram-negative bacterium involved in periodontal disease, forms whitish colonies on blood agar, visually distinct from *P. gingivalis*.

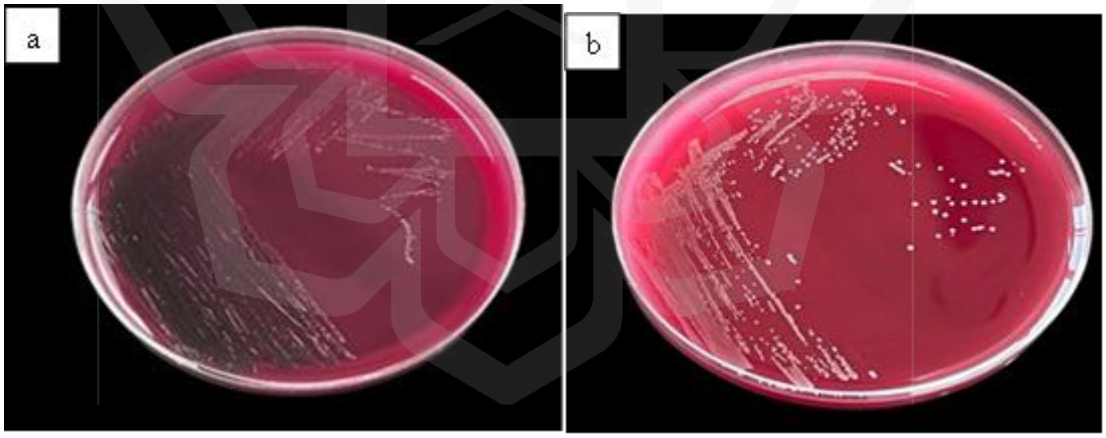

Figure 5.1 *P. gingivaliIs* (a) and *F.bacterium* (b) on blood agar

P. gingivalis is a Gram-negative, short, rod-shaped bacterium. Its ability to form biofilms and contribute to the pathogenesis of periodontal disease establishes it as a significant oral pathogen, particularly in the advanced stages of periodontitis. Both *P. gingivalis* and *F. nucleatum* are notable as a significant contributor to the pathogenesis of

periodontal disorders. Their ability to form biofilms and evade host immune responses poses significant treatment challenges. Under light microscopy at ×100 magnification, *P. gingivalis* exhibits its characteristic short rod shape, as depicted in Figure 5.2(a), consistent with observations reported by Gamboa et al. (2014). In contrast, *F. nucleatum* exhibits a fusiform rod morphology that varies in length. These rods may appear either short with rounded ends or long and slender with pointed ends, both of which are morphological features of *F. nucleatum*, as shown in Figure 5.2(b), consistent with previous observation by Brennan & Garrett (2019), Garrett & Onderdonk (2017), and Rahbari et al (2017).

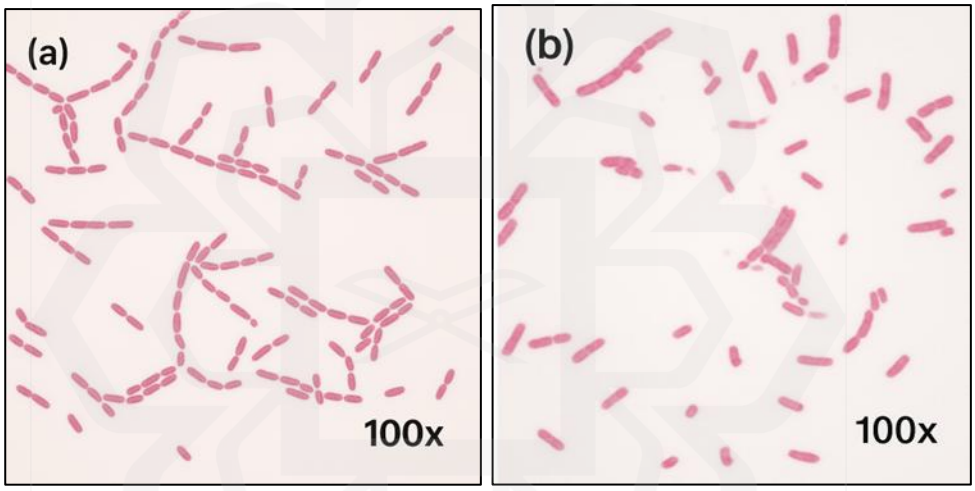

Figure 5.2 Gram-Positive Staining of the Rod-Shaped P. gingivalis (a) and F. bacterium (b) at 100x magnification.

Based on the Kirby–Bauer (KB) test from the American Society of Microbiology, the size of the inhibition zone is used to determine the sensitivity or resistance of a pathogen to varying concentrations of the same antimicrobial agent. This antimicrobial susceptibility testing (AST) was performed using the disc diffusion method with scaffolds containing MNP ranging from 0% to 30% w/v. Classification of inhibition zones was based on established standards. For *P. gingivalis*, diameters less than 16 mm were classified as resistant, 16–20 mm as intermediate, and ≥21 mm as susceptible (Andrei et al., 2022; Xia et al., 1994). For *F. nucleatum*, diameters ≥17 mm indicated susceptibility, while ≤15 mm

indicated resistance (Hazim et al., 2020). Prior studies reported an inhibition zone of 26.65 mm ± 0.52 for *P. gingivalis* and 24.5 mm ± 0.1 for *F. nucleatum*, using standard MT treatments (Justesen et al., 2023). In this study, the blank CC scaffold (0% MNP) showed no inhibition zone for either bacterial strain. At 10% MNP, inhibition zones were minimal for both *P. gingivalis* (16.67 ± 1.53 mm) and *F. nucleatum* (11.33 ± 0.58 mm), indicating resistance. At 20% MNP, a significant increase was observed for *P. gingivalis* (25.83 ± 1.61 mm, susceptible), while *F. nucleatum* remained intermediate (15.67 ± 1.58 mm). The 30% MNP scaffold demonstrated the highest inhibition for both strains: *P. gingivalis* (26.17 ± 0.76 mm) and *F. nucleatum* (25.33 ± 1.26 mm), both within the susceptible category. The MT control disc confirmed expected activity with comparable zones.

Table 5.1 Inhibition zones of CC-MNP scaffolds against *P. gingivalis* and *F. nucleatum.*

Scaffold + MNP (% w/v)	*P. gingivalis* (mm)	Classification (*P. gingivalis*)	*F. nucleatum* (mm)	Classification (*F. nucleatum*)
Blank CC	0.00 ± 0.00	-	0.00 ± 0.0	-
10	16.67 ± 1.53	Resistance	11.33 ± 0.58	Resistance
20	25.83 ± 1.61	Susceptibility	15.67 ± 1.58	Moderate
30	26.17 ± 0.76	Susceptibility	25.33 ± 1.26	Susceptibility
MT disc	25.67 ± 1.16	Susceptibility	25.17 ± 0.76	Susceptibility

Note. The values areexpressed as mean ± standard deviation (n=3)

The antibacterial activity of scaffolds loaded with varying concentrations of MNP (0–30% w/v) was evaluated against *P. gingivalis* and *F. nucleatum* using the agar diffusion method. As shown in Figure 5.3a and Figure 5.4a, inhibition zones were observed around scaffolds containing MNP, with increasing diameters corresponding to higher MNP

concentrations. The positive control exhibited a clear inhibition zone, while no inhibition was observed for the negative control, as illustrated in Figure 5.3b and Figure 5.4b. These results confirm the antibacterial efficacy of CC-MNP scaffold against both pathogens.

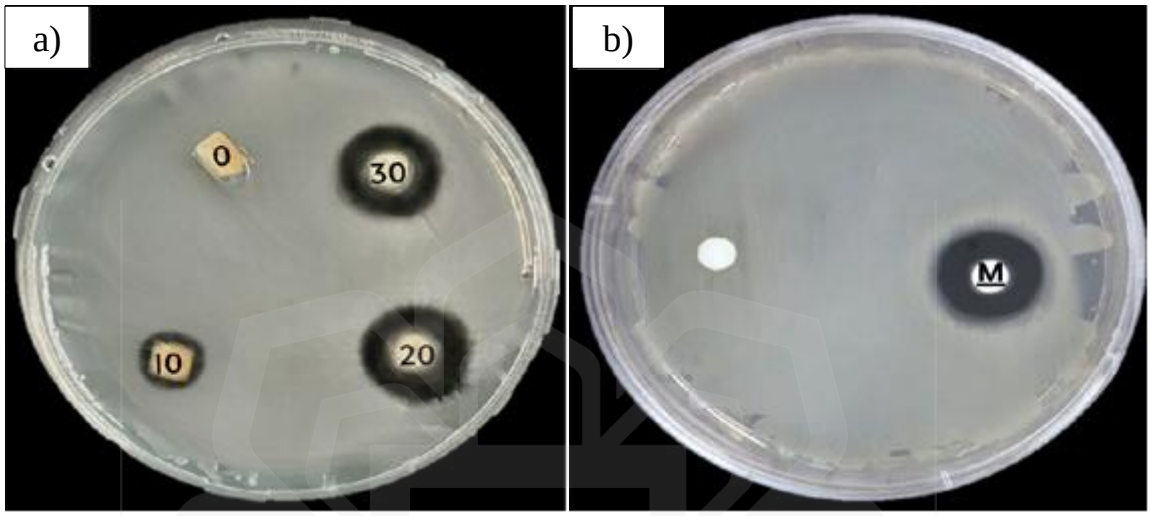

Figure 5.3 Inhibition zone of scaffold loaded with MNP (0 -30% w/v) (a), positive and negative control (b) against *P. gingivalis*

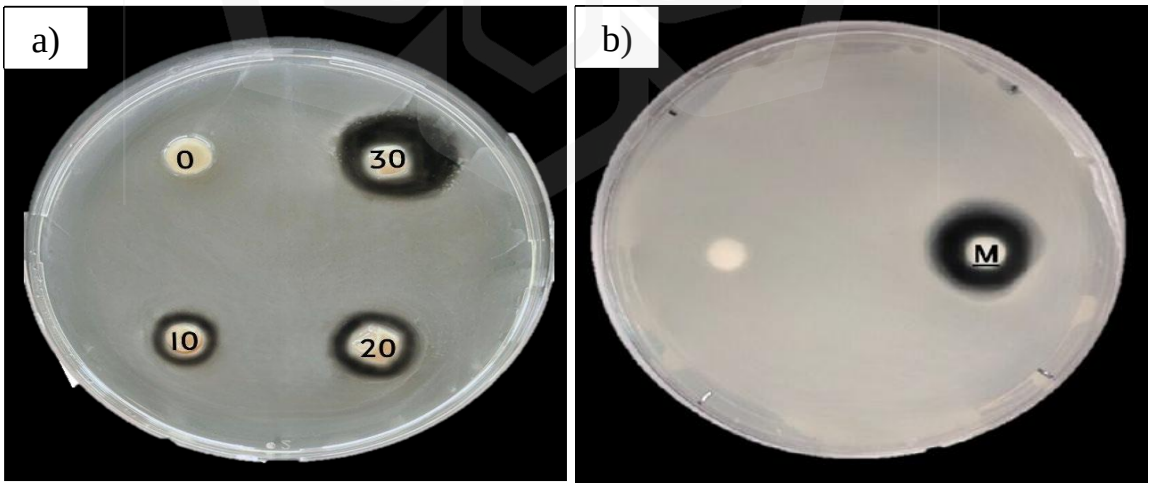

Figure 5.4 Inhibition zone of scaffold loaded with MNP (0 -30% w/v) (a), positive and negative control (b) against *F. nucleatum*

The inhibition zones of CC-MNP against *P. gingivalis* and *F. nucleatum* are illustrated in Figures 5.4 and 5.5. The blank scaffold (0% MNP) demonstrated no inhibition against either bacterium, confirming that MT was the active agent. The least inhibition was observed at 10% MNP, and a concentration-dependent increase in activity was noted up to 30%. There was no statistically significant difference ($p > 0.05$) between the inhibition zones of the 20% and 30% MNP scaffolds against *P. gingivalis*, both exceeding the susceptibility threshold. However, *F. nucleatum* showed a more distinct concentration response, transitioning from resistance at 10% to susceptibility at 30%. At 30% MNP, the scaffold showed strong inhibitory effects against both pathogens, comparable to the standard MT disc ($p = 0.6495$). These findings indicate that MNP was successfully incorporated and released from the scaffold. This release mechanism is particularly important for addressing the initial high bacterial burden in periodontal pockets (Khan et al., 2016; Zamani et al., 2010). Overall, the 30% MT-loaded scaffold exhibited optimal antimicrobial performance and is considered a promising candidate for localised periodontal drug delivery.

5.3.2 *In vitro* Drug Release

The release profile of MT from both the CS nanocarrier and scaffolds exhibited a clearly defined biphasic pattern, reflecting two distinct kinetic behaviours. During the initial phase, spanning the first 2–3 days, a rapid burst release was observed. This was more pronounced in the empty MNP group, which released a greater proportion of its drug content early on compared to the CC-MNP scaffold. On day 2, approximately 49.55% of the drug was released from the empty scaffold, while 38.82% was released from the MNP-loaded scaffold. This rapid diffusion of MT molecules is likely due to drug located near the scaffold surface escaping quickly into the surrounding medium.

From days 3 to 7, the release became more gradual and controlled. The cumulative release during this phase was 64.60% for the empty scaffold and 55.95% for the MNP-loaded scaffold. By day 14, total release reached 83.56% and 79.81%, respectively. This

slower, sustained release in the MNP-loaded scaffold reflects the influence of the nanoparticle matrix in moderating drug diffusion, supporting its potential for prolonged therapeutic action, as illustrated in Figure 5.6.

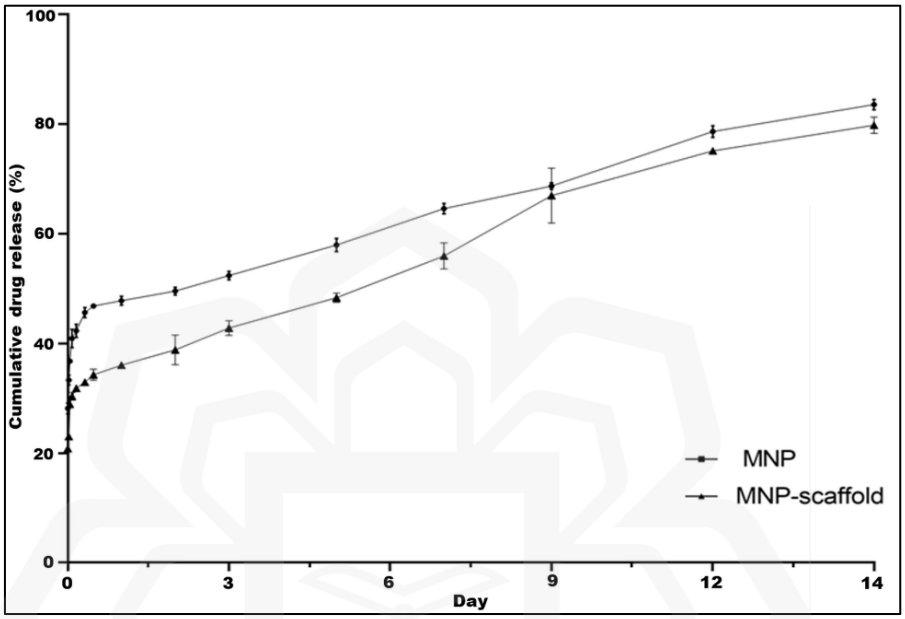

Figure 5.6 Drug release profile of MNP encapsulated in nanocarriers and scaffold system

This biphasic release behaviour is a defining feature of drug delivery systems based on hydrophilic biopolymers like CS. In the early phase, water rapidly penetrates the outer regions of the polymeric matrix, leading to immediate swelling and the fast release of drug molecules loosely bound to or located near the surface. As hydration continues, polymer chains expand and form a gel-like network, allowing the encapsulated drug to gradually diffuse outward through this hydrated matrix. This controlled swelling not only facilitates a sustained and prolonged release profile but also protects the drug from rapid degradation or clearance. Such a mechanism ensures extended therapeutic availability, making it particularly beneficial for localised treatments requiring prolonged drug action, such as in periodontal therapy. The stepwise diffusion enabled by this polymer swelling mechanism is visually represented in Figure 5.7.

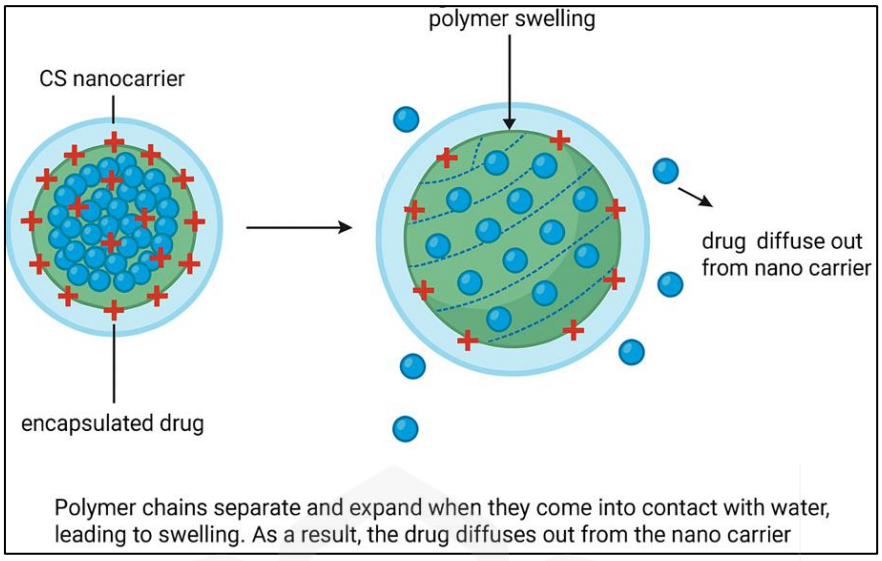

Figure 5.7 Water-induced swelling in polymer matrices for controlled drug release (created using Biorender.com)

Similar biphasic behaviours have been reported in other studies. For example, drug delivery systems encapsulating paclitaxel exhibited a significant burst release within the first three days, releasing over 60% of the total drug, followed by a slower release up to day 13 (Li et al., 2009). Muhsin et al. (2016) reported that CS nanoparticles released 16 ± 0.32% initially, reaching 23 ± 0.31% by day 8 and 52 ± 1.55% by day 16. This dual-phase release is advantageous for achieving immediate therapeutic effects and sustaining drug availability, which is particularly useful in wound healing (Cam et al., 2020; Setterstrom et al., 2000).

The sustained release observed in the scaffold loaded MNP likely results from the combination of scaffold swelling and diffusion barriers provided by the nanoparticles. The scaffold acts as an additional matrix, hindering drug mobility and enabling prolonged release. This mechanism is supported by evidence that bioactive agents can be physically adsorbed or chemically bound to scaffolds to allow for gradual release (Mo et al., 2023). Similarly, electrospun and electrosprayed scaffolds have demonstrated slowed and stabilised release profiles compared to systems without such modifications (Kass & Nguyen, 2022; Abudula et al., 2020; Jiang et al., 2023).

Clinical application of such release profiles is particularly relevant in periodontal therapy. Antibiotic therapy typically spans 6 to 14 days, targeting infection control and healing support. Devices such as EVA fibres and acrylic strips exemplify systems that release drugs over this duration (Nair & Anoop, 2012). This aligns with current findings where the sustained release observed in the CC-MNP scaffold supports a 14-day therapeutic window, as required for post-surgical treatment (Salgado-Peralvo et al., 2022; Alassy et al., 2021). Thus, incorporating MNP into the scaffold effectively modulated release kinetics, achieving a balance between initial therapeutic concentration and prolonged delivery.

5.3.3 FTIR measurement

The FTIR spectrum of the empty CC scaffold reveals important molecular interactions between collagen and CS, as shown in Figure 5.8. Key peaks are identified in the O-H/N-H stretching, amide I, II, III, and C-H bending regions reflecting the scaffold's intermolecular interactions. This aligns with previous findings that highlight the importance of these bands in evaluating the structural integrity and intermolecular interactions within the scaffold (Fernandes et al., 2011). In the FTIR analysis, the peak at 3311.43 cm^{-1} corresponds to the O-H and N-H stretching vibrations. It is characteristic of the hydrogen bonding interactions within the collagen and CS empty scaffold (Rodrigues et al., 2023). After loading the scaffold with MNP encapsulated in CS nanocarriers, this peak shifts to 3363.59 cm^{-1}. The shift to a higher wavenumber suggests the formation of stronger hydrogen bonds due to the collagen, CS, and drug-loaded nanoparticles, which could enhance the scaffold's structural properties.

The amide I peak, associated with C=O stretching and primarily indicates the structural integrity of collagen, appears at 1636.08 cm^{-1} in the empty scaffold and was shifted slightly to 1637.15 cm^{-1} upon loading with MNP. This minimal shift suggests that the triple helix structure of collagen remained largely intact, in agreement with studies indicating that amide I changes reflect only subtle alterations in molecular conformation

(Ramli et al., 2016). The amide II peak, located at 1557.53 cm^{-1} in the empty scaffold, remained relatively unchanged, appearing at 1556.09 cm^{-1} in the loaded scaffold, indicating that the core structure of the collagen remained intact after the addition of the drug. There were no significant changes in the amide II band after incorporating therapeutic agents into collagen-based scaffolds. The amide III band, observed at 1407.94 cm^{-1}, corresponds to N-H stretching and C-H bending. After adding metronidazole-loaded nanoparticles, this peak shifted slightly to 1411.33 cm^{-1}, indicating a slight modification in molecular interactions but not significantly altering the molecular interactions within the scaffold. Similarly, the peaks at 1076.84 cm^{-1} and 1032 cm^{-1}, corresponding to C-O stretching and C-N bonds, also demonstrated minor shifts upon nanoparticle incorporation. The slight shifts suggest that the hydrogen bonding network within the scaffold remained largely unaffected. The preservation of this network indicates that the scaffold's molecular architecture is stable, even after the introduction of drug-loaded nanoparticles, further supporting the conclusion that the collagen matrix maintained its triple helix integrity (Rodrigues et al., 2023).

The peaks at 1076.84 cm^{-1} and 1032 cm^{-1} indicate the presence of C-O stretching and C-N bonds associated with the interactions between collagen and CS (Rodrigues et al., 2023). These peaks suggest a stable hydrogen bonding network within the scaffold matrix. The peak at 1077 cm^{-1} indicates a slight increase in wavenumber, while the incorporation of MNP into the scaffold slightly shifts the peak at 1031 cm^{-1}, showing a corresponding decrease. The peak at 1032 cm^{-1} in the empty scaffold shifts to 1031 cm^{-1} in the loaded scaffold. This slight reduction suggests that the incorporation of MNP encapsulated in CS nanocarriers has a minor effect on the molecular interactions while preserving the overall integrity of the collagen and CS matrix. Moreover, the absence of any significant shift in the acetic acid band at 1700-1725 cm^{-1} suggests that no free acetic acid remained in the sample, further confirming the scaffold’s chemical stability after the freeze-drying process (Fernandes et al., 2011).

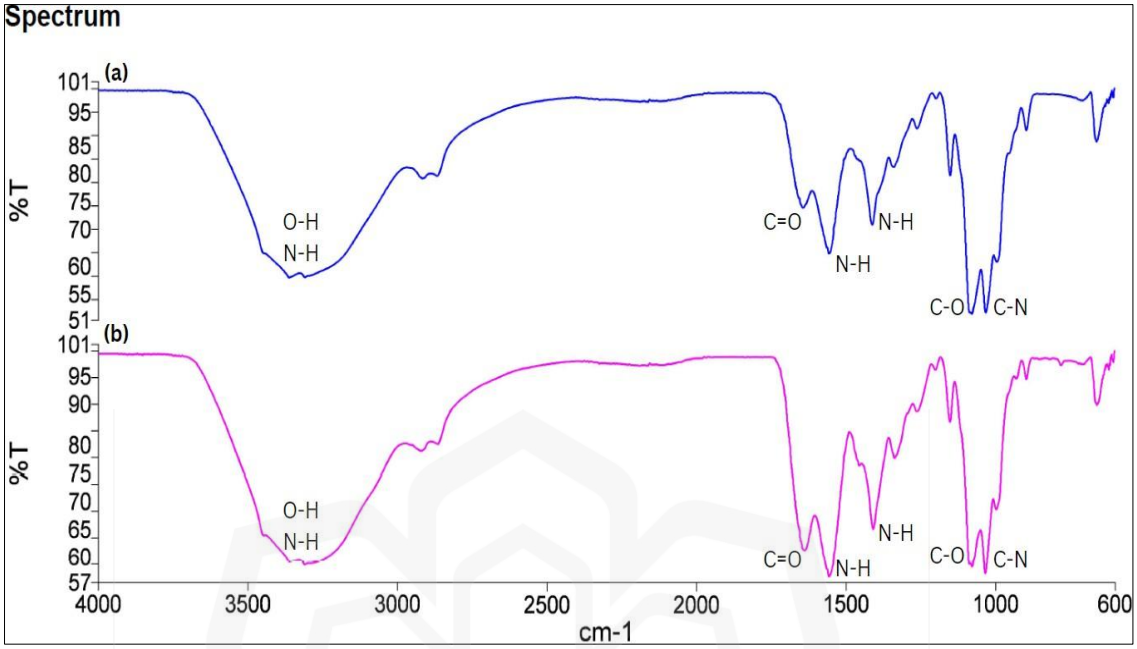

Figure 5.8 FTIR spectra of (a) CS nanocarrier and (b) MT-loaded onto CS nanocarrier

5.3.4 Biocompatibility Analysis of CC-MNP Scaffold

5.3.4.1 Standard curve

Prior to establishing the standard curve, the morphology of human gingival fibroblast cells (HGF-1) was assessed using an inverted optical microscope to verify cellular health and suitability for subsequent cytocompatibility studies. Blue dye staining was employed to differentiate viable cells, enabling clearer visualisation of cellular morphology and arrangement. The HGF-1 cells displayed characteristic fibroblastic features, including elongated, spindle-shaped bodies and the tendency to align in parallel arrays or small clustered formations. These observations align with previous reports by Guo et al. (2011), Marconi et al. (2021), and Saczko et al. (2008), which described similar fibroblast characteristics under optimal culture conditions. The presence of such features supports the

absence of cytotoxic stress and affirms the suitability of these cells for further MTT-based assays, including scaffold seeding to evaluate biocompatibility. The illustrated cellular morphology is shown in Figure 5.9.

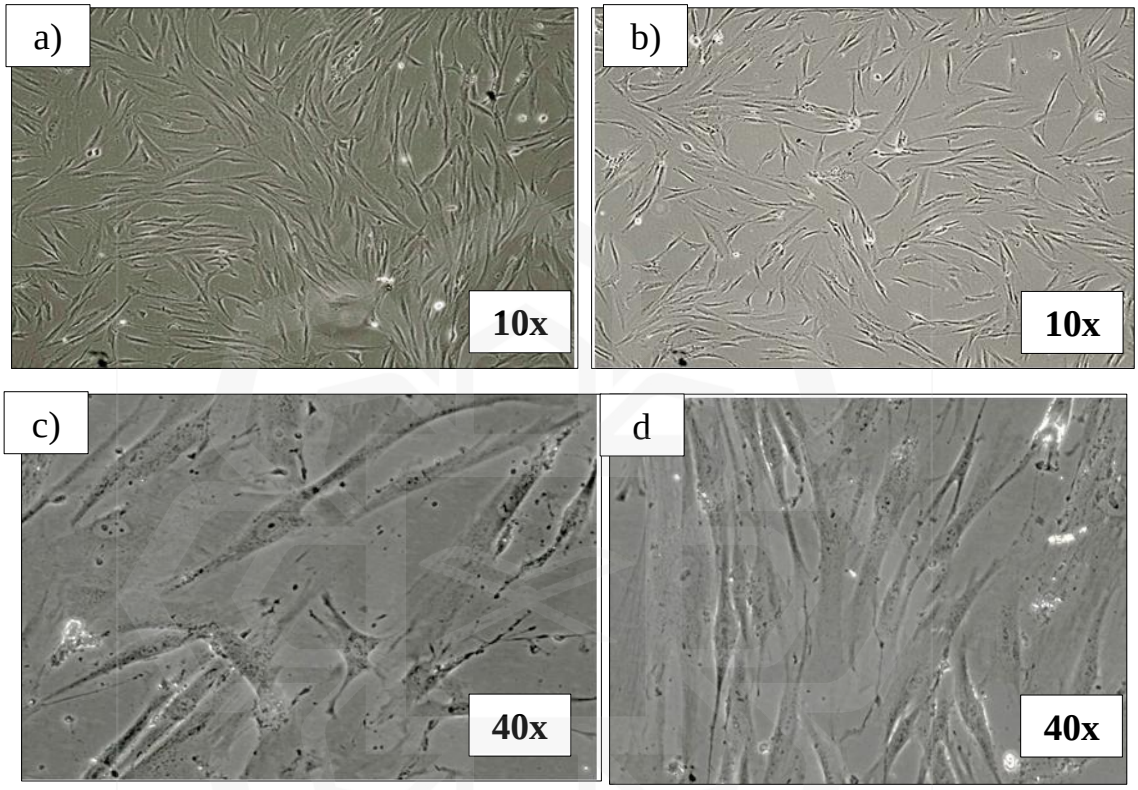

Figure 5.9 Morphology of HGF-1 cells at 10× (a–b) and 40× (c–d) magnification

To quantify cell viability and proliferation, the MTT assay was employed. This colorimetric assay measures the enzymatic reduction of MTT to insoluble formazan crystals by metabolically active mitochondria. MTT solution was added to each well and incubated for four hours. Subsequently, dimethyl sulfoxide (DMSO) was used to solubilise the formazan, and the absorbance was measured at 570 nm using a microplate reader (Yildiz et al., 2023). The standard curve generated from the linear regression analysis demonstrated a robust linear relationship between absorbance and cell concentration, with the equation $y = 6\times10^{6}x + 0.2741y$ as and an R^2 value of 0.9605, as shown in Figure 5.10.

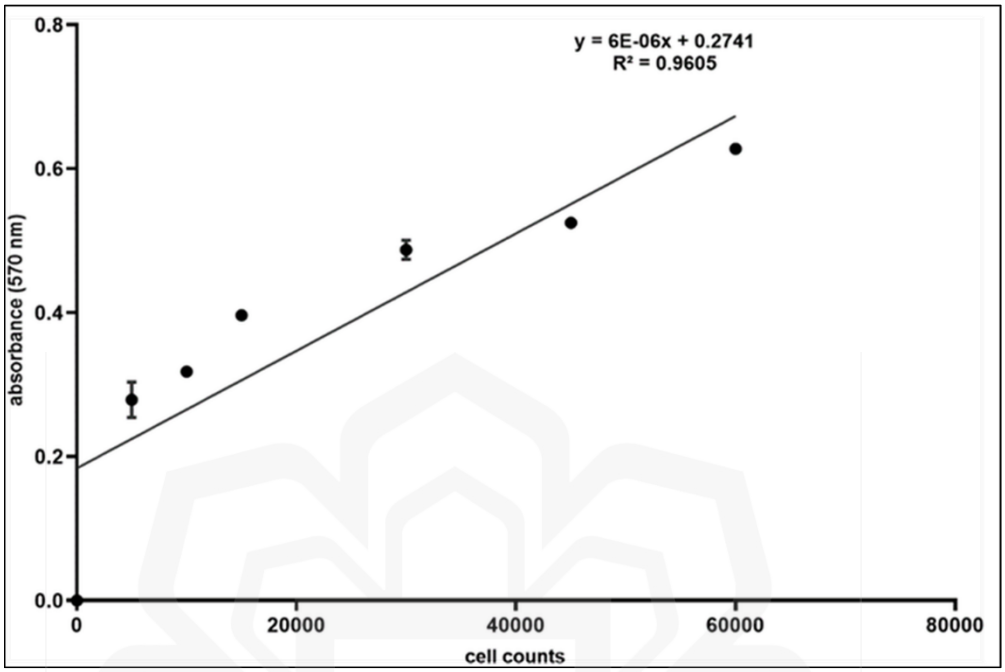

Figure 5.10 Standard calibration curve of HGF-1 using the MTT assay

While the linear regression model offers statistical accuracy for estimating cell numbers within a defined range, *in vitro* cell proliferation generally follows a sigmoidal growth pattern consisting of three phases: lag, exponential, and plateau (Sigma-Aldrich, n.d.; AAT Bioquest, 2020). In the lag phase, cells are metabolically active but not dividing as they adapt to the culture environment. The exponential phase is characterized by rapid cell division, while the plateau phase results from nutrient depletion and waste accumulation, leading to reduced proliferation (Sigma-Aldrich, n.d.; AAT Bioquest, 2020).

The linear relationship observed in the current MTT assay likely reflects the exponential growth phase, particularly given the early points assessed (Days 1, 3, and 7), during which cells were actively proliferating without confluent or nutrient constraints (Abcam, n.d.). This correlation aligns with typical short-term assays under optimal seeding densities, where cell growth is relatively uninhibited. In this context, the MTT assay

provided a practical and reliable approach for quantifying relative cell viability through absorbance measurements. The strong linear correlation between absorbance and viable cell concentration confirms the assay's utility in evaluating the initial biological performance of scaffold formulations. This method is especially valuable for comparing the cytocompatibility of biomaterials, such as CC and CC-MNP scaffolds, and for assessing their influence on early cellular proliferation dynamics (Salis et al., 2021).

5.3.4.2 MTT Assay

The MTT assay, a widely used colourimetric assay, measures cell viability and proliferation by quantifying the reduction of MTT (a yellow tetrazole) to formazan crystals by metabolically active cells. The amount of formazan produced is proportional to the number of viable cells, making this assay a reliable indicator of cell proliferation. The absorbance values obtained from the MTT assay show a direct correlation with cell proliferation, enabling accurate estimation of cell counts at various time points. Thus, the MTT assay is essential in demonstrating the biocompatibility of biomaterials intended for *in vivo* application (Subramanian & Sekaran, 2024). In this study, the MTT assay was employed to evaluate the biocompatibility of CC and CC-MNP scaffolds by measuring absorbance values. The results, presented in Table 5.2, show an increasing trend in absorbance values from Day 1 to Day 7, reflecting cell growth and viability in both the scaffold loaded with MNP and scaffold empty" conditions. On Day 1, the scaffold loaded with MNP showed an absorbance of 0.2933 ± 0.0050, corresponding to approximately 3.20×10^3 cells/mL, while the scaffold empty group had an absorbance of 0.2900 ± 0.0030, corresponding to approximately 2.6 5× 10^3 c cells/mL. The relatively low cell numbers observed on day 1 in all groups might be due to oxygen and nutrients not fully penetrating and distributing on the scaffold, limiting cell proliferation and leading to lower absorbance, as stated by a previous study (Edmondson et al., 2014; Magliaro et al., 2019). As shown in Table 1, the results demonstrate an increasing trend in absorbance values from Day 1 to Day 7, indicating cell growth and viability on both the "scaffold loaded with MNP" and "scaffold empty" conditions.

Table 5.2 MTT assay of HGF-1 on CC scaffolds with and without MNP at 1, 3, and 7 Days.

Time (Days)	Day 1	Day 3	Day 7
Scaffold Loaded with MNP	0.2933 ± 0.0050^{a}	0.3877 ± 0.0065^{a}	0.9912 ± 0.455^{a}
Scaffold Empty (No Drug)	0.2900 ± 0.0050^{a}	0.3607 ± 0.0070^{a}	0.9450 ± 0.0373^{a}

Note. The table displays the mean and standard deviation values (n=3).

On Day 1, the scaffold loaded with the MNP group showed an absorbance of 0.2933 ± 0.0050, corresponding to a cell count of approximately 3.20×10^3 cells/mL. In contrast, the "scaffold empty" group had an absorbance of 0.2900 ± 0.00300, corresponding to approximately 2.65×10^3 cells/mL. This lower initial proliferation might be due to insufficient oxygen and nutrient distribution within the 3D scaffold structure, limiting cell proliferation and leading to lower absorbance, as stated by a previous study (Edmondson et al., 2014; Magliaro et al., 2019). By Day 3, a significant increase in cell proliferation was observed in both groups. The scaffold loaded with MNP exhibited an absorbance of 0.3877 ± 0.0065, corresponding to 1.89×10^4 cells/mL, while the scaffold empty had an absorbance of 0.3607 ± 0.0070, approximately 1.44×10^4 cells/mL. These findings were aligned with previous findings, where 3D-printed scaffolds demonstrated lower cell proliferation on Day 1, followed by significant increases on Days 3 and 7 (Zhang et al., 2019). On Day 7, both groups showed a marked increase in absorbance. The scaffold loaded with MNP had an absorbance of 0.9912 ± 0.4550, correlating to approximately 1.20×10^5 cells/mL, while the scaffold empty showed an absorbance of 0.9450 ± 0.0373, corresponding to 1.12×10^5 cells/mL. Although the difference in cell numbers between the two groups was not statistically significant, the trend suggests that the presence of magnetic nanoparticles (MNP) may enhance cell proliferation.

The hydrophilic nature of the CS-based scaffold likely contributed to favourable conditions for cell attachment and growth, as supported by previous studies demonstrating the role of surface hydrophilicity and biocompatibility in enhancing cell adhesion and proliferation on hydrophilic polymeric scaffolds (Dong et al., 2020). Moreover, adding collagen further enhanced the scaffold's hydrophilic properties, improving its ability to support cell adhesion, such as collagen, the primary ECM protein inherently promotes cell anchorage (Sousa et al., 2014). The positive effect of nanoparticles, especially in promoting cellular proliferation without inducing cytotoxicity, is well documented. These findings are vital for the development of tissue engineering materials, as the enhanced cell proliferation observed in the scaffold loaded with the MNP group highlights the scaffold's potential as a smart carrier for bioactive molecules, accelerating tissue regeneration. This is particularly important for applications such as periodontal disease treatment, where rapid and efficient healing is critical. Previous research has also supported the role of hydrophilic nanoparticles in improving cell viability, attachment, and proliferation on scaffolds. Studies have shown that the hydrophilic nature of CS nanocarriers promotes favourable conditions for cell attachment (Wang et al., 2017), while hydrophilic poly (L-lactic acid) (PLLA) nanoparticles were found to increase cell numbers (Xu et al., 2012). The bioactivity was enhanced in the presence of nanoparticles in scaffolds, revealed by greater cell adhesion and cell spreading, which was mainly attributed to increased hydrophilicity (Dasari et al., 2022). In short, the hydrophilic nature of collagen scaffolds plays a crucial role in supporting cell growth. The incorporation of hydrophilic nanoparticles further enhances this property, improving the scaffold's ability to facilitate cell attachment, proliferation, and overall tissue regeneration.

5.3.4.3 Morphology of HGF-1 cell on CC-MNP

The adhesion and spreading of anchorage-dependent cells, such as HGF-1 fibroblasts, are essential for cell viability and proliferation on scaffolds (Bashur et al., 2006). Figure 5.11 illustrates the morphology of HGF-1 fibroblasts cultured on the CC-MNP scaffold. The FESEM images reveal several distinct cell morphologies indicating different stages of cell

adhesion and interaction with the scaffold. In Figure 5.11 (a), fibroblast cells appeared spheroid, typical during early attachment phases (Rabie et al., 2022). Figure 5.11 (b) shows elongated cells with filopodia, signifying that the cells are exploring their microenvironment and establishing contact points with the scaffold surface. In Figure 5.11 (c), cells are seen in direct contact with the scaffold, further confirming scaffold compatibility. Figure 5.11 (d) presents flattened fibroblasts with extensive filopodia, suggesting strong adhesion and active remodelling activity. This morphological behaviour implies good biocompatibility and scaffold performance in supporting cellular activities such as migration, proliferation, and ECM interaction (Szewczyk et al., 2019; Kyykallio et al., 2020).

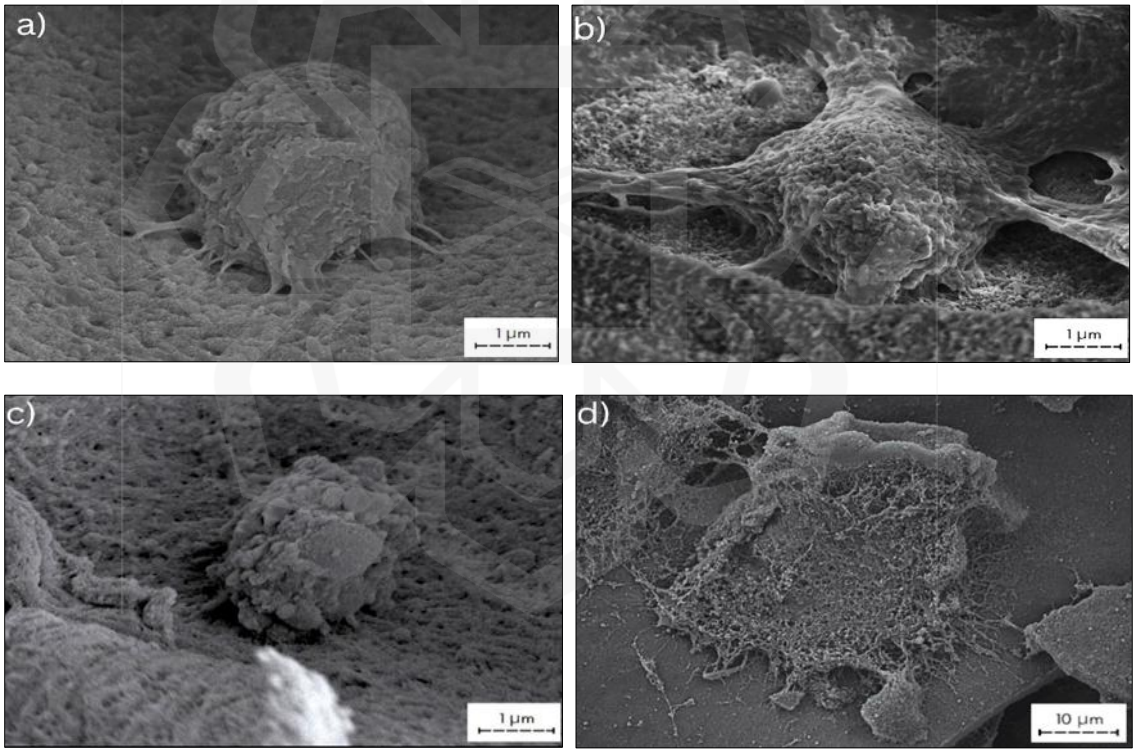

Figure 5.11 Morphology of fibroblasts on CC-MNP scaffolds showing spheroid cells (a), elongated cells with filopodia (b), cells in contact with scaffold (c), and flattened cells (d).

Figure 5.12 demonstrates the morphology of HGF-1 fibroblasts on the empty CC scaffold. Similar to the CC-MNP scaffold, cells displayed spheroid shapes in the early stages of attachment (Figure 5.12 (a)). Figure 5.12 (b) shows elongated fibroblasts with filopodia, indicating scaffold interaction and early-stage spreading, a key marker of scaffold compatibility. In Figure 5.12 (c), the cells are observed in contact with the scaffold structure, and in Figure 5.12 (d), the fibroblasts appear flattened and well-spread across the scaffold surface. These cell morphologies support the scaffold's potential in promoting cell adhesion and viability, although the structural features of the empty CC scaffold may result in slightly less interaction intensity compared to the CC-MNP scaffold.

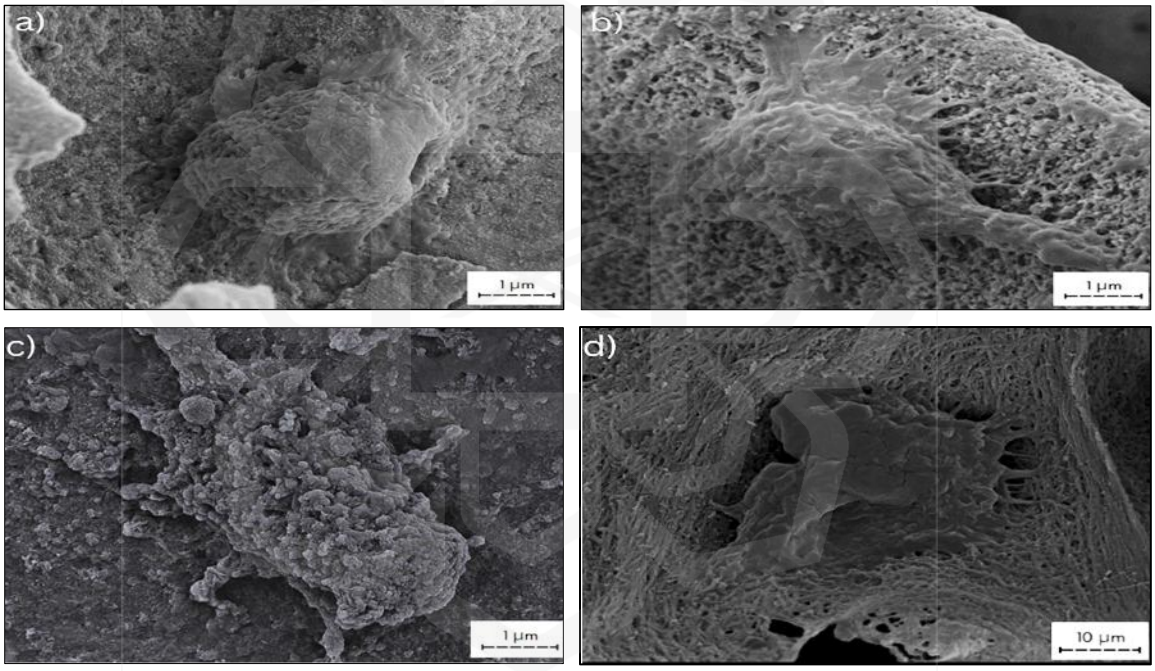

Figure 5.12: Morphology of fibroblasts on empty CC scaffolds showing spheroid cells (a), elongated cells with filopodia (b), cells in contact with scaffold (c), and flattened cells spread on the scaffold (d).

As described in previous studies, HGF-1 cells initially exhibit spheroid morphology, transitioning to elongated and spread forms with filopodia as they adhere and

proliferate on scaffolds (Rabie et al., 2022; Sun et al., 2021; Wood & Martin, 2002). The presence of filopodia in both scaffolds reflects active cellular exploration, vital for ECM interaction, scaffold remodelling, and tissue regeneration (Kyykallio et al., 2020). The **CC**-MNP scaffold, however, demonstrated more extensive filopodia networks and cell spreading compared to the empty CC scaffold, indicating superior biocompatibility and enhanced support for cellular functions. This can be attributed to the synergistic properties introduced by the magnetic nanoparticles, which may improve surface characteristics and cell-material interactions (Liu et al., 2020). Both scaffolds supported fibroblast adhesion and proliferation, but the CC-MNP scaffold exhibited more robust cellular interaction, making it a more promising candidate for tissue engineering applications.

5.4 CONCLUSION

This study underscores the promising potential of a novel CC scaffold loaded with MNP in treating periodontal diseases. Periodontal conditions present significant challenges to oral health, often necessitating advanced therapeutic interventions that can effectively combat the underlying bacterial infections while promoting tissue regeneration. Traditional approaches, while beneficial, have been limited by inflammatory responses and suboptimal antibacterial efficacy. Therefore, the development of innovative antibacterial scaffolds has become increasingly important in the field of dental tissue engineering. Our findings reveal that CC-MNP exhibits significant antibacterial activity against key periodontal pathogens, specifically *Porphyromonas gingivalis* and *Fusobacterium nucleatum*. Notably, the CC-MNP formulation containing 30% MT demonstrated a marked inhibitory effect, with a minimum inhibitory concentration (MIC) established to inhibit these pathogens effectively. This highlights the scaffold's potential to deliver therapeutic agents and maintain a favourable pharmacological profile. The Fourier transform infrared spectroscopy (FTIR) analysis further supports the successful incorporation of MTinto the CC matrix. The characteristic peaks observed in the FTIR spectra confirm the interactions between the drug and the scaffold materials, indicating the effective loading and stability of the drug within the scaffold structure. This chemical characterisation is crucial as it ensures the preservation

of the drug's efficacy while embedded in the scaffold. The Fourier-transform infrared spectroscopy (FTIR) analysis confirmed the successful incorporation of MT into the CC scaffold. The analysis indicated that the structural integrity of the CC matrix was preserved after drug loading. These findings suggest that the CC-MNP scaffold retains its molecular structure, which is essential for its application in periodontal therapy. The stability and compatibility demonstrated through FTIR analysis support the potential of CC-MNP as an effective drug delivery system for managing periodontal diseases.

In addition, this study highlights the biocompatibility of CC-MNP. The *in vitro* release profile of MT from scaffolds showed a slower and more sustained release compared to the unloaded scaffold, aligning with the objective of achieving controlled drug delivery in periodontal treatment. By day 14, approximately 80% of the drug had been released, indicating the potential of this system for extended drug delivery applications. Furthermore, cytocompatibility assessments using Human Gingival Fibroblast (HGF-1) cells showed that CC-MNP did not negatively impact cell morphology, viability, or proliferation, which may support integration with host tissues and aid healing. Overall, the dual functionality of CC-MNP as a drug delivery system and tissue engineering scaffold suggests its potential applicability in periodontal therapy. The capability to address bacterial infection while supporting cellular activity may contribute to improved treatment outcomes in periodontal disease management. Future research should focus on evaluating the *in vivo* performance and long-term effects of CC-MNP in periodontal health to support its clinical translation.

CHAPTER SIX

IN VIVO ASSESSMENT CC-MNP FOR BONE REGENERATION IN RAT SKULL DEFECTS

6.0 INTRODUCTION

Bone loss resulting from periodontal disease, trauma, or anatomical factors poses a common therapeutic problem in the field of periodontology (Donos et al., 2015). In order to promote bone regeneration in various types of bone defects under different systemic conditions, various bone grafts and bone substitutes, biomaterials, or combined regenerative procedures have been employed. However, current research has primarily focused on investigating GBR scaffolds in the treatment of periodontal disease. This scaffold provides a three-dimensional (3D) structure for cell attachment, growth, and tissue regeneration (Lim et al., 2019). However, one of the common issues in GBR applications is the biodegradation of non-biodegradable scaffolds. Non-biodegradable scaffolds do not degrade naturally over time within the body. Therefore, a second surgical procedure is often required to remove the scaffold once bone regeneration is complete. After the scaffold removal, the site becomes exposed, creating a favourable environment for bacterial colonisation and an increased risk of infection at the surgical site. This bacterial colonisation infection can hinder the natural bone regeneration process by causing inflammation and tissue damage, necessitating additional treatments such as antibiotics, which can further increase systemic side effects such as antibiotic resistance, compromising the success of the GBR procedure. By utilising a biodegradable scaffold with antibacterial properties, we aimed to overcome the limitations associated with a non-resorbable scaffold, reducing the risk of infection, thus promoting a favourable environment for bone regeneration and improving the outcomes of GBR treatments. Before assessing the biomaterial's *in vivo* biocompatibility and potential toxicity, *in vitro* testing was employed as an initial step. In this study, firstly, we developed a CC scaffold loaded with MT nanoantibiotic and determined the suitability and effectiveness of the CC scaffold loaded with MNP for its intended application in periodontal regeneration.

The scaffold successfully fulfilled the required criteria for mechanical properties, biocompatibility, controlled drug release, stability degradation, and antibacterial assay. It exhibited significant antibacterial activity against *Porphyromonas gingivalis* (ATCC No. 33277) and *Fusobacterium nucleatum* (ATCC No. 10953), which are the predominant pathogenic bacteria involved in periodontitis. Another critical aspect of the GBR scaffold is ensuring the released drugs do not interfere with cellular activity. In our experiment, the prepared scaffold demonstrated satisfactory biocompatibility, as human gingival fibroblast cells (HGF-1 cells) successfully attached to and proliferated on the scaffold. Given the positive results obtained from the *in vitro* analysis, the CC scaffold loaded with MNP shows excellent promise as a therapeutic option for periodontal regeneration. It is now well-suited for further evaluation through *in vivo* studies to assess its biocompatibility, effectiveness in promoting tissue regeneration, and overall performance in a living organism. These *in vivo* studies provided valuable insights into the scaffold's performance and suitability for clinical applications in the treatment of periodontal diseases. Therefore, the specific objective of this study was to assess the effectiveness of the scaffold in promoting new bone formation within the rat skull defect and to evaluate the scaffold's capability to prevent inflammation in the affected area.

6.1.1 Rationale for Animal Use

Preclinical animal models played a critical role in the research and development process by providing proof-of-concept efficacy in a short interval, as well as preliminary safety and effectiveness of newly fabricated scaffolds before their implementation in human subjects. The Sprague-Dawley rat was chosen as an animal model based on several factors, including its economic feasibility, logistical convenience, ease of handling and maintenance, and suitability for verifying basic biological principles. Moreover, the Sprague-Dawley rat model allowed for the efficient generation of bone defects within a relatively short timeframe, which enhanced its practicality for studying the effectiveness of the newly fabricated scaffold in promoting bone regeneration. In this study, we used 18 animals divided into three groups, with six rats per group. Applying the Resource Equation Method,

the calculated sample size 'E' was 12. This sample size fell within the recommended range of 10-20 animals for preclinical studies, indicating that our chosen sample size was adequate for this study.

6.2 METHODOLOGY

6.2.1 Animal Requirements

Table 6.1 outlines the specific requirements for the animal subjects used in the rat skull defect study. All procedures involving animals were conducted in compliance with the guidelines approved by the Institutional Animal Care and Use Committee (I-ACUC), under ethical approval number IACUC 2023-013 with supporting documentation provided in Appendix I.

Table 6.1 Animal requirement for rat skull defect study

Parameter	Details
Species	Wistar rats
Strain	*Sprague-Dawley*
Genus	*Rattus norvegicus*
Age	8 weeks old
Weight	250–300 g
Sex	Male
Number of Animals Used	18
Source	A Sapphire Enterprise

6.2.2 Source and Transportation

The vendor, A Sapphire Enterprise, Selangor, Malaysia handled the transportation of animals, which were delivered to the primary housing location at PLANETIIUM, Jalan Penjara Kuantan Pahang.

6.2.3 Acclimatisation Period

Prior to the surgical procedure, the animals were subjected to a seven-day acclimatisation period to facilitate physiological, psychological, and nutritional stabilisation in their new environment. This period is essential to mitigate the stress associated with transportation and environmental changes (Munk et al., 2024; Rinwa et al., 2024). Rats were housed under controlled conditions (20–26°C, 40–60% humidity, 12-hour light/12-hour dark cycle) with free access to food and water, in accordance with standard laboratory animal care guidelines (Marin et al., 2023). The acclimatisation period also serves to allow animals' physiological parameters, such as blood glucose and stress hormone levels, to return to baseline following transport (Marin et al., 2023). Throughout this duration, the animals were monitored daily for signs of stress, abnormal behaviour, or any indication of illness to confirm their suitability and optimal health status for inclusion in the experimental procedures (Munk et al., 2024).

6.2.4 Biological Material Use for Animals

The primary biological material used in this study was CC scaffolds integrated with MNP specifically developed for *in vivo* applications. This composite scaffold was designed as a dual-function therapeutic platform intended to support bone tissue regeneration while simultaneously delivering a localised antimicrobial effect. The rationale behind this design is grounded in the need to prevent post-surgical infections, which frequently occur in the context of bone defects and can significantly compromise the healing process.

The CC scaffold was synthesised and subsequently loaded with MNP using a freeze-drying (lyophilisation) technique to enable localised drug delivery. As the scaffold was not commercially available, it was formulated and characterised through laboratory protocols tailored to the requirements of this study. Each scaffold was shaped to match the dimensions of the critical-sized bone defect in the rat model, ensuring precise and minimally invasive implantation. By contrast, an empty scaffold (containing no MNP) was prepared and served as a control to evaluate the specific impact of the antibiotic-loaded system on bone healing. Figure 6.1 illustrates the final scaffold employed in this study.

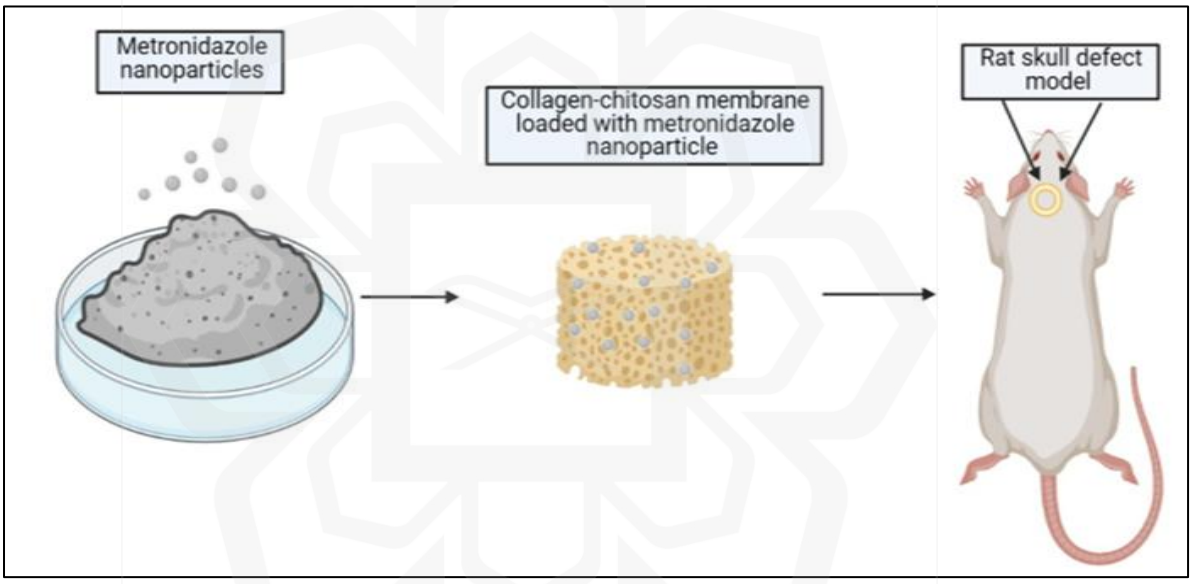

Figure 6.1 Schematic illustration of the preparation and application of CC-MNP scaffold in a rat skull defect model (created using Biorender.com)

6.2.5 Experimental Design and Procedure

6.2.5.1 Sample Size

This study utilised the Sprague-Dawley rat critical-sized calvarial defect model to evaluate

bone regeneration capacity. The sample size was determined using the Resource Equation Method as outlined by Charan and Kantharia (2013). According to this method, the value of E (error degrees of freedom) between 10 and 20 is considered adequate for detecting statistically significant differences. The value ‘E’ was calculated using the formula shown in Equation (6.1):

$$E = \text{Total number of animals} - \text{Total number of groups} \quad (6.1)$$

In this study, the sample size 'E' was determined by subtracting the total number of groups from the total number of animals. The total number of animals refers to the number of individual animals available for the study, and the total number of groups refers to the number of experimental groups being compared. A total of 15 animals were included across 3 groups. Therefore:

$$E = 15 - 3 = 12$$

This value of E = 12 falls within the acceptable range, confirming that the sample size is statistically appropriate. Thus, based on the Resource Equation Method, the calculated sample size ‘E’ is 12, which falls within the 10–20 range and is considered adequate (Charan & Kantharia, 2013). The calculated sample size of 15 represents the minimum number required to meet the predefined study parameters. To adjust for potential attrition, the sample size was increased by 20%, using the following formula:

Adjusted sample size (E): sample size + (20% of sample size)

: 15 + (20% x 15)

E: 18 rats

Although the calculated sample size was 15, it was increased to 18 animals to accommodate possible attrition, in compliance with the Institutional Animal Care and Use Committee (IACUC-IIUM) recommendation for high-risk surgical procedures (Zhang & Hartmann, 2023). This adjustment ensures data robustness while adhering to the ethical

principle of the 3Rs (Replacement, Reduction, Refinement) for animal research (Liang et al., 2022). Dropouts or attrition during the study period are common in animal research involving surgery (Zhang & Hartmann, 2023). For instance, in previous studies where sample size software recommended 10 animals per group, an additional 10% was added, resulting in 11 animals per group accounting for expected attrition (Charan & Kantharia, 2013). Similarly, the IACUC-IIUM recommends accounting for a 20% attrition rate in high-risk procedures. Therefore, the sample size in this study was adjusted accordingly. Male Male Sprague-Dawley rats, aged approximately eight weeks and weighing between 250–300 g, were randomly divided into three main groups and sacrificed on day 28 (week 4) post-surgery, as detailed in Table 6.2.

Table 6.2 Study design

Groups	A	B	C
(n = 6)	Rats' skull defect without any scaffold implantation 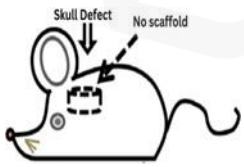	Rats' skull defect implanted with CC scaffold 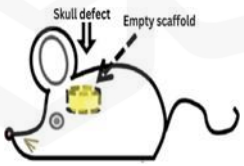	Rats' skull defect implanted with CC-MNP Scaffold 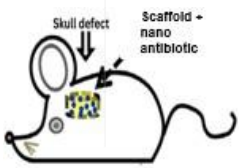

In this study, a proof-of-concept study was carried out in rats using a relatively minimum number of animals, in line with the 3Rs (replacement, reduction, and refinement) principles for animal testing (Liang et al., 2022). A total of six rats were sacrificed in each group at the end of the study. This approach is consistent with previous studies using similar models. For example, in studies on titanium membranes in a rat calvarial defect mode,

critical-size defects (8 mm) were surgically created in calvaria, and biopsies were collected at week 4 (n = 6 per group) for micro-computed tomography and histomorphometry analysis (Jang et al., 2019). In another study, 8 mm critical-size defects were created in the skulls and treated with PCL-GO-CQ-hUCMSCs scaffolds, using five animals per group for radiographic and micro-CT analysis (Kashte et al., 2021). Another study focused on comparing the efficacy of rhBMP-2 combined with different materials for bone regeneration in critical-sized rat calvarial defects. The study followed the ethical principles outlined by Russell and Burch's 3Rs and aimed to use the minimum number of animals necessary (n = 5 per group) to detect significant differences (Uribe et al., 2022). Additionally, another study that implanted C3CA scaffolds in a rat model also used five animals per group for analysis, demonstrating potential applications in bone tissue engineering (Priya et al., 2021). Therefore, based on the calculated sample size, anticipated attrition rate, and precedent from previous studies, the final sample size of 18 rats comprising 6 animals per group is deemed adequate to fulfil the experimental parameters of this study.

6.2.5.2 Anaesthesia

In several previous studies involving bone regeneration in rat calvarial defect models, anaesthesia was consistently administered using a combination of ketamine and xylazine (Chang et al., 2023; De Santana et al., 2010; Mohan et al., 2022; Uribe et al., 2022). For instance, in a study where Sprague Dawley rats were used to create defects and inject collagen hydrogel, anaesthesia was achieved via intraperitoneal injection of ketamine (30 mg/kg body weight) and xylazine hydrochloride (10 mg/kg body weight), as approved by the Institutional Animal Care and Use Committee of China Medical University (CMUIACUC-2020-125) (Chang et al., 2023). Similarly, in a biomaterials study by Uribe et al. (2022), rats were anaesthetised using ketamine (80 mg/kg) and xylazine (10 mg/kg) to provide a longer anaesthetic duration appropriate for surgical procedures.

Accordingly, in this study, anaesthesia was administered via intraperitoneal injection of ketamine hydrochloride (80 mg/kg) and xylazine (10 mg/kg), following the protocol

described by Uribe et al. (2022). This dosage was chosen to ensure an extended duration of anaesthesia suitable for calvarial surgery. The anaesthetic combination is also aligned with recommendations outlined by various institutions, as summarised in Table 6.3.

Table 6.3 Recommended anaesthesia agents based on different sources

Source	Dosage	Duration of anesthesia
IACUC- The University of lowa (University of IOWA, 2020)	Ketamine 40 - 100mg/kg IP, Xylazine 5 - 13mg/kg IP	60 - 80 min
IACUC - Pennsylvania State University (Drugs & Anesthesia, n.d.)	Ketamine 80 - 100mg/kg IP, Xylazine 5 - 10mg/kg IP	20 - 50 min

Initially, Zoletil was considered as an anaesthetic agent. However, it was not used in this study due to limited availability and concerns about possible side effects, such as increased salivation. Instead, ketamine and xylazine were selected for their proven efficacy and minimal impact on salivation, as well as their compatibility with the ethical and procedural guidelines set by IACUC-IIUM. Anaesthesia was administered via intraperitoneal injection. Each rat was briefly restrained using a clean towel to minimise handling stress. A sterile 1 mL syringe fitted with a 26G needle was used for the injection. The injection site was located in the lower right quadrant of the abdomen, a region that reduces the risk of puncturing vital internal organs such as the bladder and intestines. The skin was gently lifted to form a tent, and the needle was inserted at a shallow angle of approximately 30–45° to ensure proper entry into the peritoneal cavity. The anaesthetic solution was injected slowly and steadily to minimise the risk of reflux and tissue irritation. Following the injection, each rat was returned to its individual cage and monitored closely until surgical anaesthesia was achieved.

The depth of anaesthesia was confirmed by the absence of pedal withdrawal reflexes in the hind and forelimbs, as well as the absence of the corneal reflex. Normal, non-laboured breathing was maintained throughout the surgical procedure, indicating a stable and adequate depth of anaesthesia (Wang et al., 2022). Xylazine was chosen not only for its sedative properties but also for its muscle relaxant and analgesic effects, which synergistically enhanced the anaesthetic efficacy of ketamine (Lemke, 2004). As outlined above, this anaesthetic protocol was reviewed and approved by the Institutional Animal Care and Use Committee of the International Islamic University Malaysia (IACUC-IIUM), ensuring compliance with ethical and scientific standards.

6.2.5.3 Surgical Procedure

All surgical procedures were conducted under aseptic conditions following ethical approval from the Institutional Animal Care and Use Committee (IACUC-IIUM). Eighteen healthy male Sprague Dawley rats, aged 8–10 weeks and weighing approximately 250–300 g, were used in this study. The surgical site, located at the frontoparietal region of the calvaria, was shaved and disinfected using a 10% polyvinylpyrrolidone-iodine (PVP-I) solution. A 4 cm sagittal linear incision was made along the midline of the scalp using a sterile scalpel blade. The skin and periosteum were carefully retracted using blunt dissection with a retractor to fully expose the calvarial bone without causing damage to the underlying structures.

A standardised critical-size defect, 5 mm in diameter, was created at the centre of the exposed skull using a sterile trephine bur attached to a slow-speed handpiece. Once the bur reached the internal cortex, the bone disc was gently removed using a dentin curette and scalpel blade. The surgical site was irrigated with sterile saline to remove bone debris. Subsequently, prepared according to the experimental group allocations were gently placed over the defect to ensure complete coverage and contact with the defect margins. Following placement of the scaffold, the skin incision was closed using absorbable sutures in an interrupted pattern, ensuring proper alignment and closure of the wound edges to minimise post-operative complications. The surgical area was disinfected again using iodine solution.

Following surgery, each rat was housed individually under controlled environmental conditions, with unrestricted access to food and water. The surgical procedure is visually summarised in Figure 6.2.

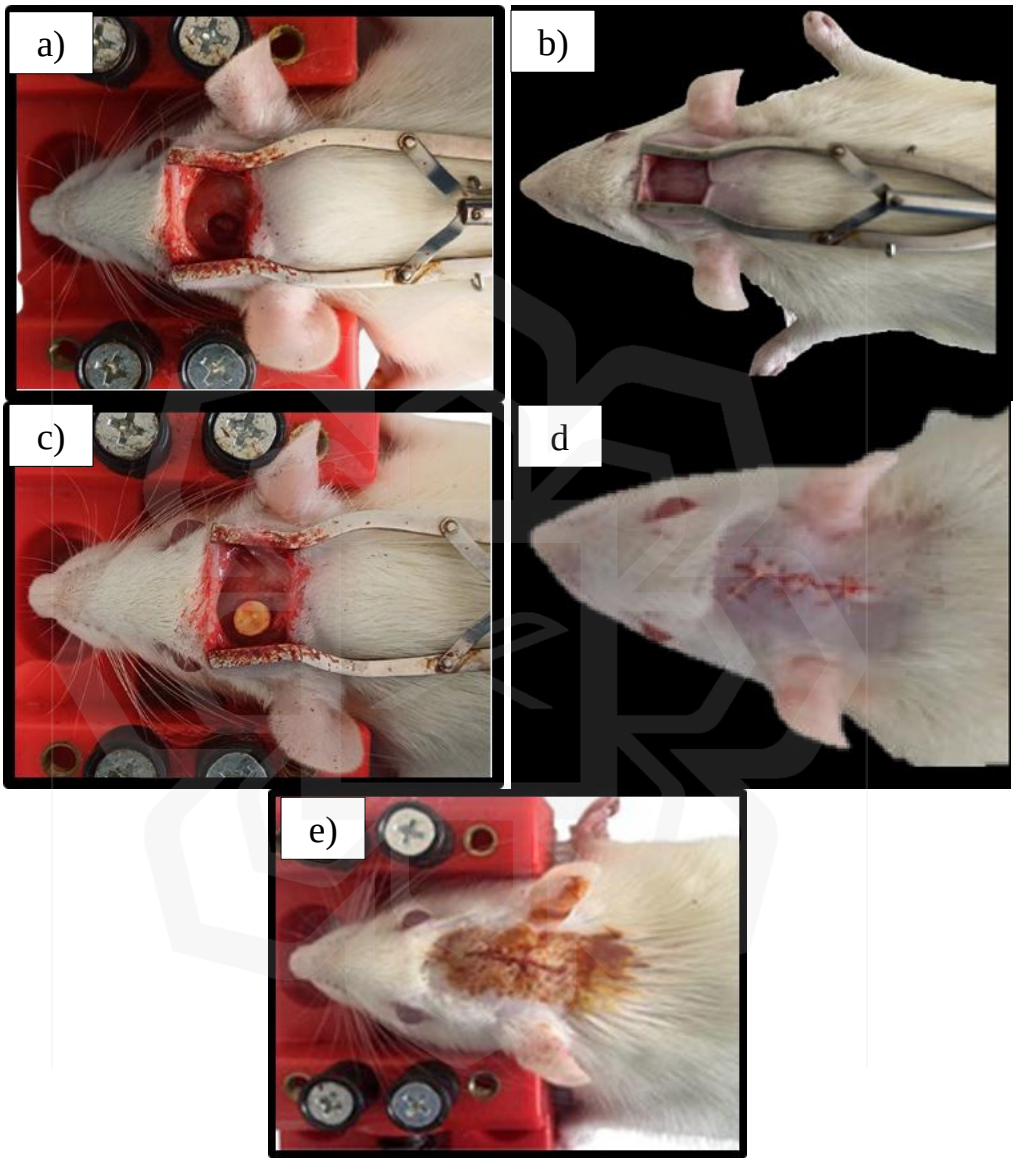

Figure 6.2 Photograph of surgical procedure. (a) Separation of skin and periosteum using a retractor, (b) Creation of the calvarial defect using a trephine bur, (c) Placement of the hydrated scaffold in the defect area, (d) Suturing of the incision with absorbable sutures, (e) Disinfection of the closed surgical site using iodine solution.

6.2.5.4 Post-operative Observation

In order to monitor pain, the rats were inspected every 12 hours for the first 48 hours following skull defect surgery and then every other day thereafter. Pain assessments were conducted using the *Pain Assessment in Rats* guidelines from the University of Michigan's Unit for Laboratory Animal Medicine (ULAM,2015) following the IACUC-IIUM Code of Practice for the Care and Use of Animals. Observations focused on specific indicators of pain, such as lack of grooming, changes in appetite (eating and drinking), aggressive or abnormal behaviour, unusual stances or movements, abnormal sounds, rough coat, and porphyrin staining around the eyes. Key signs of pain included cat-like back arching, writhing, twitching, and aggressive behaviours, which were monitored to evaluate postoperative pain.

6.2.5.4.1 External changes

The surgical incision wound on each rat was visually examined for signs of infection, focusing on indicators such as haemorrhage, ulceration, scab formation, suture loss, discharge (abscess), swelling, and any opening of the incision (Grant, 2009; Lansdown & Rowe, 2001).

6.2.5.5 Experiment Endpoint

The euthanasia process for the 18 rats was conducted as follows:

The euthanasia chamber was prepared, and the required amount of CO_2 gas was calculated based on the chamber size and the number of rats. The chamber was pre-filled with 20 - 30% CO_2 concentration, and then the rats were gently placed inside (Moody et al., 2014). Gradually, the CO_2 concentration increased to around 70 - 100%. The rats were monitored closely to ensure they became unconscious. After the procedure, rat mortality was

confirmed by checking for the absence of vital signs. After the animals were euthanised, the skullcap was removed, and the specimens were fixed in 10% formalin. Subsequently, the specimens were undergoing processing for microscopic analysis. The primary objective of this study is to evaluate the *in vivo* performance of scaffolds, with a particular focus on assessing their material integrity over 4 weeks. Consequently, all rats in each group were sacrificed at the end of post-surgery to examine and analyse the scaffold's performance and material integrity.

6.2.5.6 In vivo X-ray

At the end of the 4^{th} week, all rats were euthanised and subjected to X-ray techniques to assess the ability of the scaffold to promote critical-size defect healing. The X-ray machine parameters were set for small animal imaging (X-ray source, mFX-1000 (FUJIFILM, Tokyo, Japan). The rat was aligned with the X-ray beam, with images focusing on the calvarial defect area. Comparisons of variables during the observation period (baseline) were performed using a paired-sample t-test (Chalikias et al., 2021). For the evaluation of bone regeneration, the percentage of bone regeneration was measured with Image J software determined by ROI area (Image J, JAVA-based free software) and expressed in percentage to the total defect area (Chen et al., 2013; Ono et al., 2014).

$$\%\ Bone\ Regeneration\ = \frac{Iniaitla\ ROI\ area - Final\ ROI\ area}{Initial\ ROI\ area}\ x\ 100 \qquad (6.1)$$

6.2.5.7 Histological Analysis

After the CT scan, the sample was further processed for histological analysis. The rats were sacrificed, and tissue samples were taken from the rat skull defect fixed with 10% formalin. The calvarial tissue specimens were decalcified in 17% EDTA solution. Subsequently, the specimens were dehydrated using a series of alcohol solutions and embedded in paraffin. A thin section (around 5μm) was stained with haematoxylin and eosin (H&E) staining. The

sections underwent microscopic examination using a light microscope (BX51, Olympus, Japan) (Carlos et al., 2020; Ma et al., 2016).

6.3 RESULT AND DISCUSSION

6.3.1 Post-operative observation

Throughout the observation period, no significant behavioural differences were observed between the experimental and control groups, from the first 48 hours following surgery to day 28. All animals exhibited normal grooming, feeding, and locomotor activity, and no mortality or distress was noted. The absence of behavioural changes suggests that the surgical procedure and subsequent post-operative care were effective in minimising discomfort and maintaining the animals' overall well-being.

At the end of the study, clinical examination revealed no signs of inflammation across all groups. Specifically, there was no swelling, pus formation, distress, or reduced activity. By the second week, gross observations revealed noticeable differences in wound healing among the groups. In the control group, which did not receive a scaffold, visible redness and swelling were present at or near the implantation sites. In contrast, the treatment groups that received scaffolds loaded with nanoantibiotics exhibited improved healing, characterised by wound closure with no signs of redness or swelling. These differences are illustrated in Figure 6.3.

By week four, redness had subsided across all groups. The rats demonstrated normal fur regrowth at the implantation sites. The presence of fur regrowth, observed in all groups and depicted in Figure 6.3, was considered a key indicator of skin regeneration and successful wound healing.

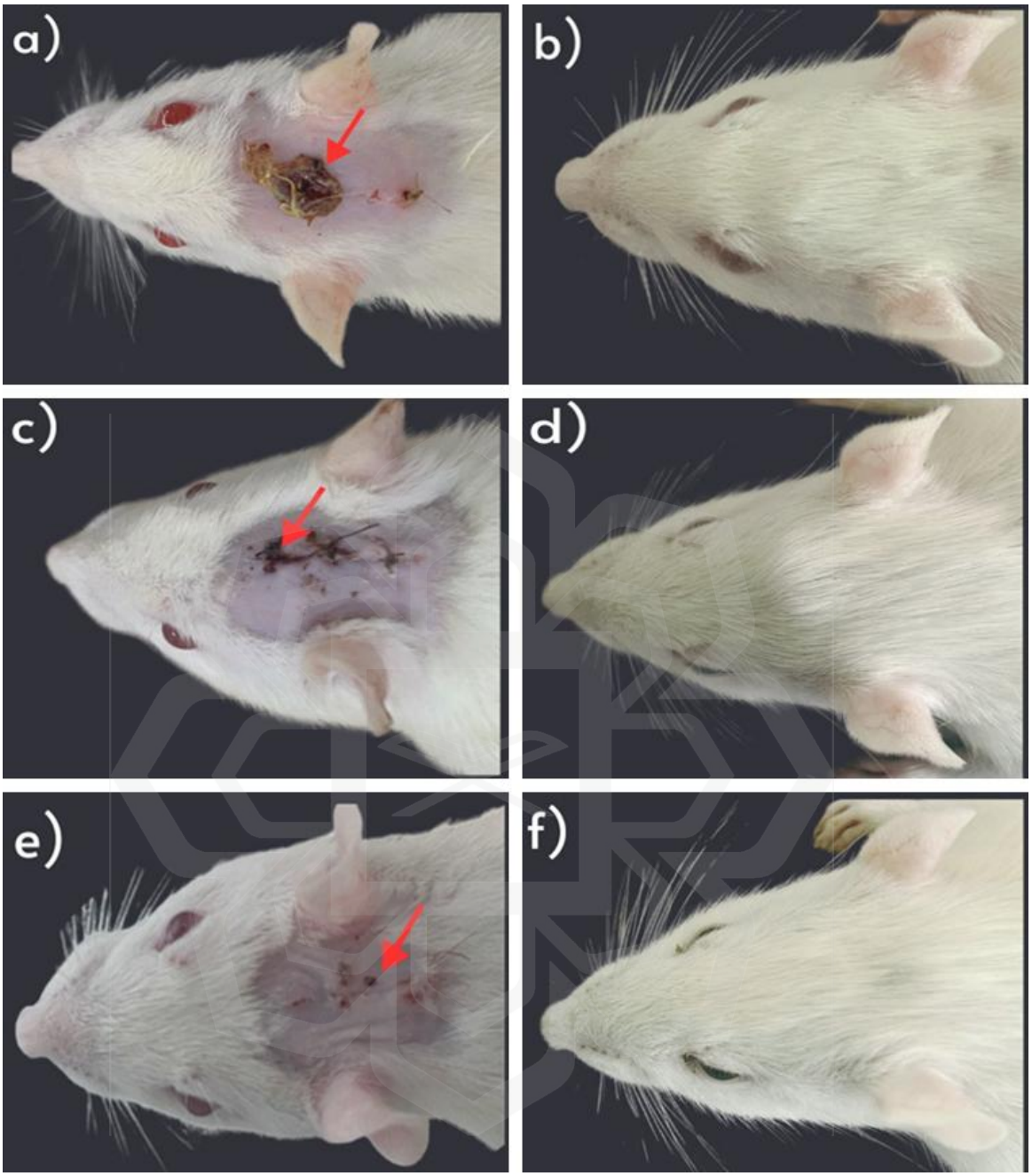

Figure 6.3 Wound area photographs of non-implanted (a–b), empty scaffold-implanted (c–d), and MNP-loaded scaffold-implanted groups (e–f) at days 14 and 28

Figure 6.3 illustrates the visual progression of wound healing in all experimental groups at the 14th and 28th postoperative days, including the non-implanted group (a–b), the group implanted with an empty scaffold (c–d), and the group implanted with

the scaffold containing MNP (e–f). These sequential images reveal observable differences in wound closure, inflammation, and tissue regeneration across the groups. A more detailed comparison of these findings including the presence of scab formation, signs of infection, and degree of wound contraction is systematically presented in Table 6.4**,** providing quantitative and qualitative support for the visual observations depicted in the figure.

Table 6.4 Analysis of wound area in experimental groups at days 14 and 28.

Groups	Day 14	Day 28
Non-implanted	- Large scab covering wound (red arrow) - Visible inflammation and tissue damage - Slow/incomplete healing	- Wound mostly healed - No scab visible - Fur regrowth observed in the wound area
Implanted with an empty scaffold	- Partial wound closure - Smaller scab than non-implanted - - No inflammation	- Complete wound closure - Minimal signs of wound - Fur regrowth observed
Implanted with scaffold + MNP	- Wound nearly healed - No scab and inflammation - Accelerated healing compared to other groups	- Complete wound closure - No scab or inflammation - Fur regrowth observed, suggesting full recovery

Wound healing is a complex, sequential process triggered by tissue injury. It begins with haemostasis, which occurs within minutes of surgery and involves the formation of a clot composed of fibrin mesh, white blood cells, platelets, and nutrients that collect in the wound space to form a scab (Choudhary et al., 2024; Cross, 2003). In rats, this is typically

marked by crusting and scab formation along the suture line, lasting about five days. In this study, wound debris and scabs were more extensive in the control group and persisted for at least seven days post-surgery. By this time, many sutures had externalised and been lost, although the suture insertion points remained visible for at least 10 days (Lansdown et al., 2001).

Scab formation is a crucial part of the wound healing process. It denotes the onset of skin regeneration and plays a protective role by sealing the wound from external contaminants. The scab forms from the denaturation of proteins in the coagulation zone and typically presents as a hard, dry, brownish crust (Chhabra et al., 2017). This crust serves to maintain wound cleanliness, shield regenerating tissue, prevent oxidative damage, and inhibit infection by blocking microbial invasion (Desmiaty et al., 2024). The scab remains until the underlying tissue has sufficiently healed. Once the granulation tissue and epithelium regenerate beneath it, the scab loosens and naturally detaches. This final stage, the proliferative phase, spans approximately days 4 to 14 and is marked by the development of fibroblasts, collagen, and extracellular matrix components essential for epidermal regeneration (Desmiaty et al., 2024). In this study, these biological events were accelerated in groups treated with CC scaffolds, particularly those loaded with MNP. The wounds in these groups exhibited early scab detachment and smoother healing surfaces, consistent with scaffold-facilitated support for angiogenesis, granulation, and re-epithelialisation.

The observation of fur regrowth across all groups indicated substantial healing. The CC scaffold loaded MNP group demonstrated the most favourable outcomes at day 14, with scabs already detached and wound surfaces appearing smoother, reflecting near-complete healing. This was attributed to the antimicrobial effect of MT, which likely reduced microbial colonisation and inflammation while creating an optimal environment for tissue regeneration. These findings are in line with those of El-Shanshory et al. (2022), who reported enhanced wound healing using metronidazole-immobilised nanofibrous scaffolds. By comparison, the non-implanted control group exhibited thicker scabs and more persistent wound debris, indicative of slower healing. The yellowish crust observed is a classic sign of the early inflammatory stage, which was prolonged in the absence of scaffold

support (Choudhary et al., 2024). Without structural or antimicrobial assistance, the wound environment may have lacked the conditions necessary for efficient epithelial migration and angiogenesis, delaying tissue regeneration (Cross, 2003).

Scaffolds contributed significantly to wound healing by mimicking the extracellular matrix, regulating moisture levels, absorbing wound exudate, and providing sustained release of antimicrobial agents. These functions are crucial in maintaining hydration, limiting infection, and promoting collagen synthesis and vascularisation within the granulation tissue (Negut et al., 2020; Jiang et al., 2023). The resulting environment not only facilitated effective wound healing but also accelerated the overall recovery timeline. By the end of the study, all rats had survived, with scabs and sutures having loosened and naturally fallen off. Hair regrowth was evident, and there were no lingering signs of inflammation, infection, or animal distress. These outcomes affirm that the surgical procedure and post-operative protocol were effective and further validate the CC scaffold system particularly when loaded with MNP as a promising therapeutic approach for enhancing tissue regeneration.

6.3.3 Radiological Observation

6.3.3.1 X-ray Evaluation of Bone Defects

Radiographic imaging was employed to evaluate bone regeneration in cranial defects under different treatment conditions. As shown in Figure 6.4, distinct differences in healing outcomes were observed among the experimental groups. In the baseline image (Figure 6.4a), a well-defined, circular radiolucent void is clearly visible at the centre of the skull, representing the surgically created critical-size defect. The sharp margins and dark centre confirm the absence of mineralised tissue prior to treatment. In the non-implanted control group (Figure 6.4b), the defect remains evident with only minimal peripheral radiopacity, indicating limited bone regeneration. The persistence of the central void is consistent with the poor healing capacity of untreated critical-size defects.

In contrast, the groups treated with CC scaffolds, both with and without MNP (Figure 6.4c and 6.4d), exhibit substantial bone regeneration. The defect sites are scarcely distinguishable from the surrounding bone, and the radiographs reveal uniform radiopacity, indicative of mature and continuous mineralised tissue formation. These findings suggest that the scaffolds provided not only mechanical support but also enhanced osteogenesis and tissue integration. Overall, the X-ray images validate the enhanced regenerative potential of MNP-functionalised scaffolds, supporting their efficacy in promoting complete and uniform bone healing in critical-sized cranial defects.

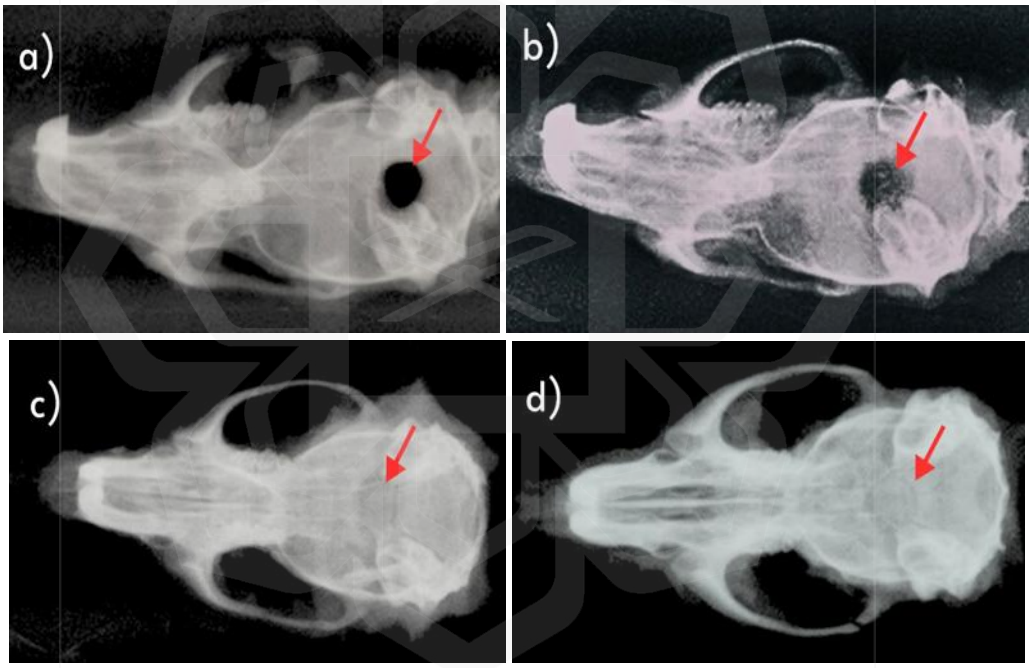

Figure 6.4 Radiographic comparison of bone healing in rats. The defect area is marked with arrows (→), and error bars indicate variation in radiographic bone density. Baseline defect, (b) no scaffold implantation, (c) empty CC scaffold, and (d) CC scaffold loaded with MNP.

6.3.3.2 Analysis of Region of Interest (ROI)

To complement the X-ray findings, a region of interest (ROI) analysis using ImageJ was conducted to visualise and quantify defect closure. In the baseline image (Figure 6.5a), a clearly defined circular void is observed, representing the unmineralised cranial defect prior to treatment. In the non-implanted control group (Figure 6.5b), the void remains largely visible, indicating minimal spontaneous bone regeneration. Some peripheral activity is evident, but the central defect remains unhealed. The empty scaffold group (Figure 6.5c) shows a noticeable reduction in void size, suggesting scaffold-assisted bone formation progressing from the margins inward. The CC scaffold-loaded MNP group (Figure 656d) demonstrates complete void closure, with uniform darkening across the defect area, indicating full mineralisation. These results confirm that the MNP-functionalised scaffold significantly enhanced osteogenesis and defect bridging.

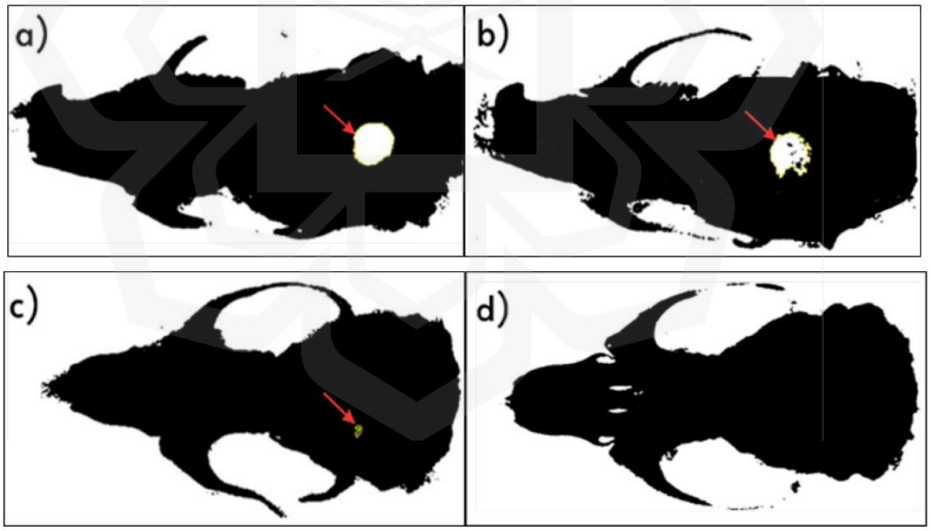

Figure 6.5 ROI images of the defect area analyzed using ImageJ. Error bars (→) indicate variation in grayscale intensity measurements. (a) Baseline defect, (b) no scaffold implantation, (c) empty CC scaffold, and (d) CC scaffold loaded with MNP.

6.3.3.2 Quantitative Assessment of Bone Regeneration

The control group, which received no implantation, exhibited minimal bone regeneration (16.79 ± 2.99%). The empty defect remained largely unhealed, indicating that natural bone healing was insufficient to repair the critical-size cranial defect. In contrast, rats implanted with scaffolds demonstrated significantly improved bone regeneration. The group treated with an empty scaffold showed nearly complete defect closure (97.45 ± 0.51%), confirming the osteoconductive role of the scaffold in supporting natural healing. The group treated with scaffolds loaded with magnetic nanoparticles (MNP) exhibited the highest bone regeneration rate (99.08 ± 0.76%), indicating enhanced healing compared to all other groups, as shown in Figure 6.6.

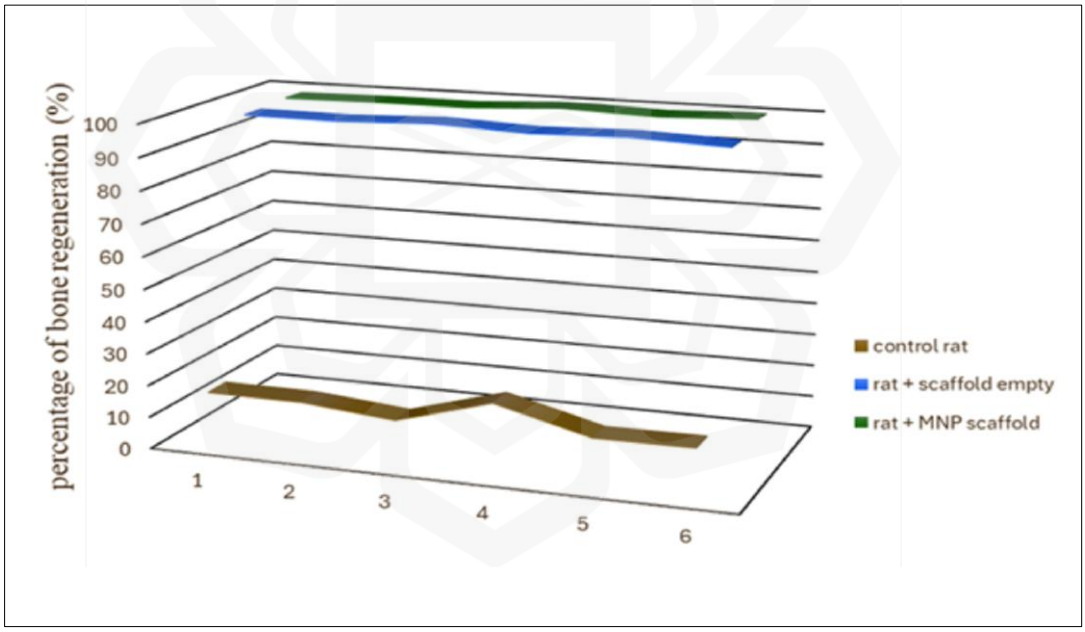

Figure 6.6 Percentage of bone regeneration in rat calvarial defects among the control group (no scaffold implantation), the group implanted with empty CC scaffold, and the group implanted with a CC scaffold loaded with MNP

The radiological data clearly demonstrated that bone regeneration in critical-sized cranial defects was significantly enhanced by scaffold implantation, with further

improvement observed when CC scaffolds were loaded with MNP. The minimal bone regeneration in the control group (16.79 ± 2.99%) is consistent with previous findings, which reported that spontaneous healing of large bone defects is limited due to insufficient endogenous repair mechanisms (Suvarnapathaki et al., 2022; Togari et al., 2012). Although some bone deposition was evident, the defect remained largely open, highlighting the need for external scaffolding to stimulate effective healing. The nearly complete bone regeneration observed in the empty scaffold group (97.45 ± 0.51%) validated the role of CC scaffolds as a supportive matrix that promotes cellular infiltration, vascularisation, and new tissue formation. Previous studies have similarly shown that even non-functionalised biodegradable scaffolds can facilitate bone healing by providing structural support and guiding new bone growth (Suvarnapathaki et al., 2022).

The group treated with CC scaffolds loaded with MNP achieved the highest regeneration rate (99.08 ± 0.76%). The X-ray and ROI images confirmed full defect closure, with dense bone tissue occupying the entire defect site. These findings strongly suggest that the incorporation of MNP not only enhances scaffold performance but also promotes osteogenic activity. Nanoparticles may improve bone formation by stimulating cell proliferation, differentiation, and migration, while also offering potential for controlled therapeutic delivery (Daei-Farshbaf et al., 2014; Hatakeyama et al., 2013; Kashte et al., 2021). The ROI images further supported these findings by visually confirming the extent of bone coverage in each group. In particular, the CC scaffold loaded MNP group exhibited no remaining void, indicating complete tissue restoration. This underscores the value of MNP integration in improving scaffold efficacy for cranial bone regeneration. Overall, these findings demonstrate that scaffolds particularly those loaded with bioactive nanoparticles, MNP represent a promising approach for enhancing bone regeneration in large defects. This outcome is consistent with existing literature on scaffold-based regenerative strategies and reinforces the potential of nanoparticle-enhanced biomaterials for future clinical applications in bone tissue engineering.

6.3.4 Histological analysis

Histological analysis using haematoxylin and eosin (H&E) staining was conducted to evaluate the progression of bone regeneration in the experimental groups. The comparison across baseline, control, empty scaffold, and CC-MNP groups highlighted the influence of scaffold architecture and bioactive agents on tissue regeneration. At baseline (Figure 6.7a), the defect area appeared as a wide, unfilled gap between the old bone (OB) margins, with no evidence of tissue organisation or early bone formation. The surrounding OB was clearly demarcated, and the central defect zone was devoid of fibrous or mineralised tissue, reflecting the immediate post-surgical condition before any regenerative response.

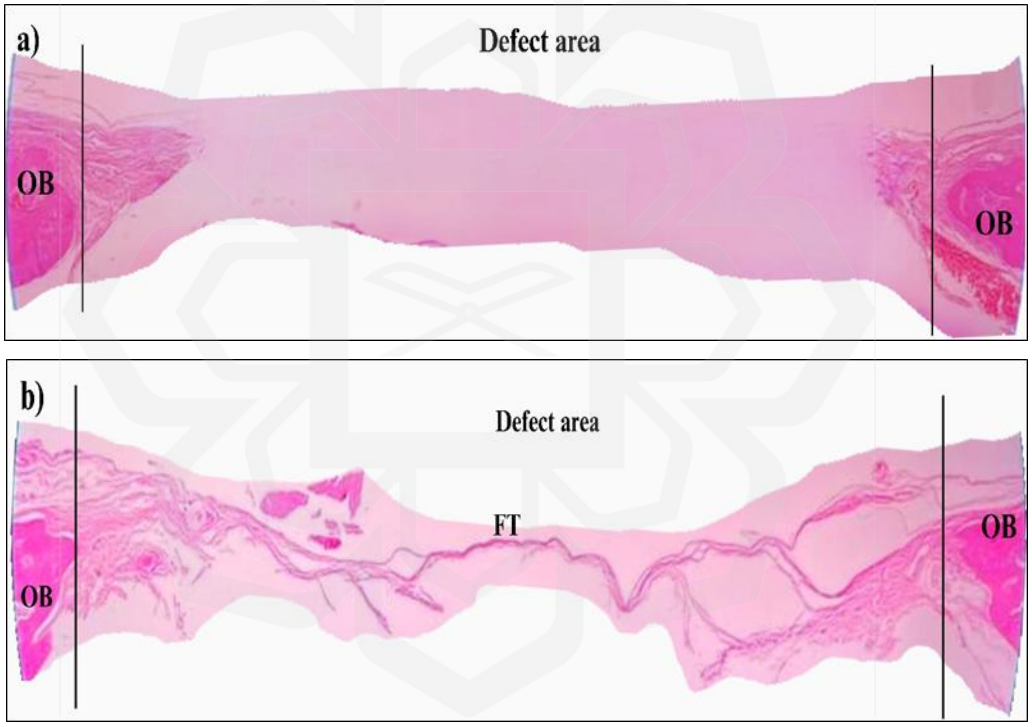

Figure 6.7 Histological images of rats in the control group. (a) At 0 weeks (baseline), (b) at 4 weeks, showing OB (old bone area) and FT (fibrous tissue) (4x magnification)

To further assess the early healing response, the non-implanted control group was examined at four weeks post-operation (Figure 6.7b). In this group, the defect remained unmineralised and was predominantly occupied by fibrous tissue (FT). The fibrous matrix extended across the defect zone, but there were no signs of trabecular bone or mineralised matrix formation. This fibrous filling indicates a typical soft-tissue repair response in the

absence of osteoconductive support. The OB margins showed minimal integration with the intervening tissue, suggesting poor regenerative progression. These findings are consistent with previous reports that untreated critical-size defects predominantly heal through connective tissue infiltration due to the absence of osteogenic stimuli and structural scaffolding (Ono et al., 2014; Sun et al., 2018; Chen et al., 2013; Zhou & Lee, 2016). The absence of new bone formation and the continued presence of fibrous tissue in the defect centre underscore the limited capacity for spontaneous bone regeneration in large cranial defects without scaffold support.

In contrast to the control group, animals implanted with empty scaffolds exhibited clear signs of new bone (NB) formation (Figure 6.8a). Although the newly formed trabeculae exhibited irregularity and a less organised structure characteristic of immature bone, the new bone (NB) extended across a substantial portion of the defect. This suggests that even in the absence of bioactive additives, the scaffold provided a physical framework the scaffold provided a physical framework that supported cellular infiltration and early bone matrix formation. These findings align with previous reports highlighting the osteoconductive role of biodegradable scaffolds in guiding early-stage bone regeneration (Sato et al., 2020). By comparison, rats implanted with MNP-loaded scaffolds demonstrated the most organised regenerative response (Figure 6.8b). The defect area was densely filled with NB, characterised by a uniform matrix structure and high cellularity. The integration between newly formed and old bone (OB) was well-integrated, indicating ongoing remodelling and scaffold-supported tissue maturation. This enhanced outcome suggests that the inclusion of MNP not only promoted osteogenesis but also contributed to a more stable and biologically active healing environment. These outcomes underscore the effectiveness of scaffold-based strategies in supporting bone healing and highlight the additional regenerative benefit conferred by bioactive agents, as visually confirmed in Figure 6.8.

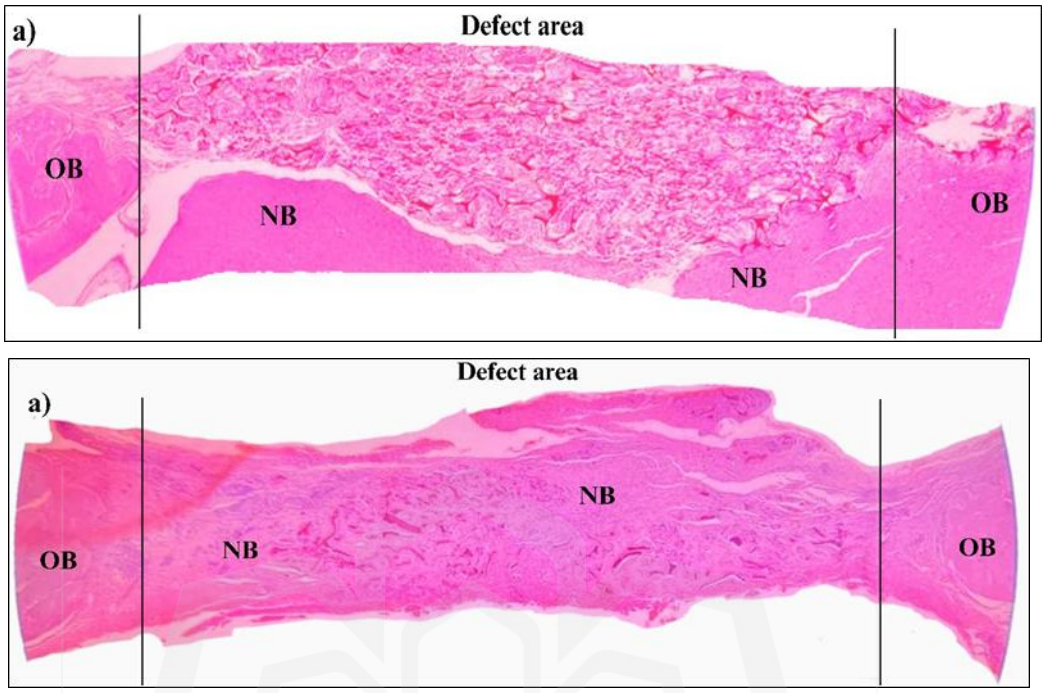

Figure 6.8 Histological images of rats implanted with scaffolds at 4 weeks. (a) Rats implanted with an empty scaffold, (b) rats implanted with an MNP-loaded scaffold, showing OB (old bone area) and NB (new bone) in the defect area (4x magnification)

At higher magnification, the H&E-stained sections in Figure 6.9 provide a detailed view of cellular activity and bone matrix development within the defect area at four weeks post-implantation. The presence of osteocytes, identified by dark-staining nuclei within lacunae (highlighted by arrows), confirms active bone regeneration. Osteocytes are terminally differentiated osteoblasts that have become embedded within the mineralised matrix and are essential for maintaining bone homeostasis and coordinating bone remodelling (Bonewald, 2011). In the empty scaffold group (Figures 6.9a and 6.9b), osteocytes were visible but appeared fewer in number and more scattered within a loosely arranged, immature bone matrix. The trabeculae were thin, and the overall organisation of the bone tissue remained incompletely organised. This suggests that while the empty scaffold was sufficient to initiate osteogenesis, the absence of additional bioactive components limited the extent and maturity of bone formation at this time point. These features are indicative

of early-phase bone regeneration and are consistent with prior studies that reported modest osteogenic activity in plain scaffold systems (Kashte et al., 2021).

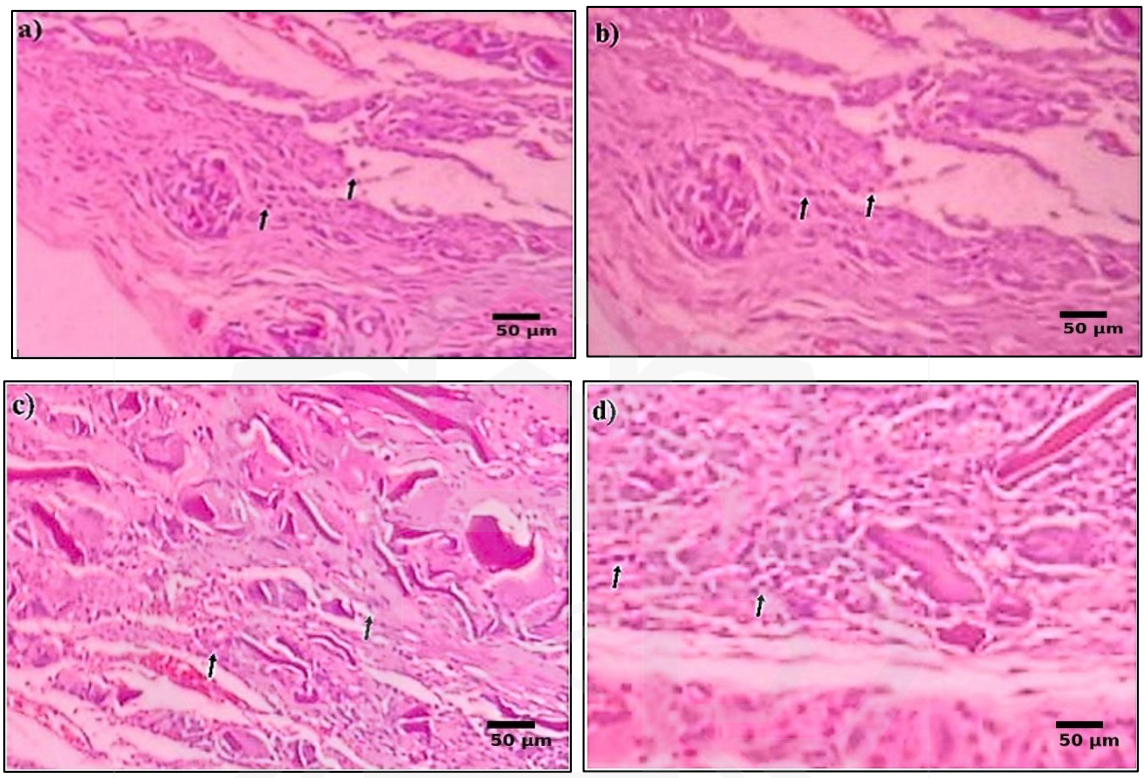

Figure 6.9 Histological images of rats implanted with scaffolds at 4 weeks. (a-b) Rats implanted with an empty scaffold; (c-d) rats implanted with an CC scaffold loaded MNP. The arrows indicate osteocytes distributed within the bone matrix (100x magnification)

In contrast, the MNP-loaded scaffold group (Figures 6.9c and 6.9d) exhibited numerous osteocytes that were more uniformly distributed throughout a denser and better-organised bone matrix. The trabecular architecture appeared thicker and more continuous, suggesting a higher level of bone maturity and mineralisation. This observation reflects an advanced stage of healing and is supported by previous research indicating that magnetic nanoparticles enhance cellular recruitment, promote osteoblast differentiation, and improve scaffold integration (Dasari et al., 2022; Farazin & Mahjoubi, 2024). The distribution and morphology of osteocytes also suggest the presence of active bone remodelling as these

cells play a critical regulatory role in mechanotransduction and in directing osteoclast and osteoblast activity during tissue turnover. The improved matrix quality and higher osteocyte density in the MNP group align with reports of enhanced angiogenesis, osteoinduction, and scaffold degradation mediated by nanoparticle incorporation (Hatakeyama et al., 2013). The histological findings provide strong evidence that while both scaffold types supported osteocyte development and early bone regeneration, the inclusion of MNP significantly enhanced bone matrix maturation and cellular activity, indicating a superior regenerative outcome. These regenerative effects are likely driven by the coordinated mechanism of scaffold degradation and therapeutic release. In the early phase, the CC acts as a structural matrix enabling drug release and cell infiltration. CC-MNP are gradually released from the scaffold, establishing a localised antimicrobial environment that also encourages the recruitment of osteogenic cells. This early-stage interaction is visually represented in Figure 6.10, which summarises the multi-phase regeneration process facilitated by the scaffold.

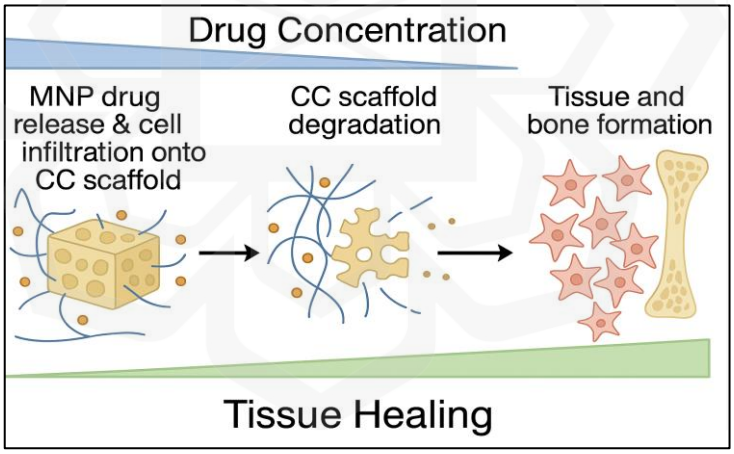

6.10 Schematic Diagram of the sequential release of MNP, biodegradation of the CC scaffold, and subsequent tissue and bone regeneration over time (Created using BioRender.com)

This initial stage plays a critical role in preventing infection and initiating regeneration, as supported by previous findings (Farazin & Mahjoubi, 2024). As healing progresses, the scaffold undergoes controlled degradation, breaking down into smaller components that are resorbed or assimilated into the surrounding tissue. This degradation coincides with a gradual reduction in drug concentration and enhanced cellular activity. The scaffold's resorbability is essential, as it eliminates the need for surgical removal while supporting dynamic tissue interactions (Johnson & García, 2015). In the final phase, the coordinated release of bioactive agents, scaffold degradation, and cellular infiltration contribute to tissue and bone formation. Osteoblasts and other reparative cells proliferate within the scaffold voids, laying down a mineralised matrix that progressively restores the defect site. This multi-phase process is depicted in Figure 6.10, highlighting the coordinated progression of scaffold resorption, drug delivery, and new tissue formation.

The histological findings confirm that scaffold-based interventions significantly improve bone regeneration in critical-sized cranial defects. The control group demonstrated fibrous tissue infiltration but lacked new bone formation, consistent with earlier studies showing that untreated defects heal poorly due to a lack of structural and biochemical support (Chen et al., 2013; Zhou & Lee, 2016). The empty scaffold group supported partial bone formation, highlighting the importance of structural scaffolds in guiding tissue growth and cellular migration (Sato et al., 2020). However, the bone tissue appeared immature and less organised. The CC-MNP group showed the most advanced regeneration, with well-organised new bone (NB), seamless integration between old bone (OB) and NB, and osteocyte-rich matrices. These outcomes align with previous reports that nano-antibiotics and magnetic nanoparticles can accelerate bone healing by reducing infection risk and enhancing osteogenic cell recruitment (Farazin & Mahjoubi, 2024; Dasari et al., 2022). The antimicrobial effect also prevents chronic inflammation, which would otherwise impair healing. Bioactive scaffolds degrade in synchrony with tissue growth, releasing therapeutic agents that enhance cell proliferation and scaffold integration (Johnson & García, 2015). This is further validated by the presence of osteocytes, indicating that the remodelling cycle mediated by osteoblasts and osteoclasts was actively restoring the defect site. Similar findings were observed in previous scaffold systems involving PLLA-hydroxyapatite-

gelatin composites (Kashte et al., 2021). Overall, the data support the conclusion that CC-MNP creates a conducive microenvironment for osteogenesis and remodelling, contributing to superior healing outcomes in large bone defects.

6.4 CONCLUSION

The findings of this study provide valuable insights into the regenerative potential of scaffold-based interventions for critical-sized bone defects. Although X-ray imaging did not reveal substantial differences between the empty scaffold and CC-MNP groups in terms of overall bone volume, histological analysis offered a more discerning view. Scaffolds loaded with MNP supported the formation of denser, more structurally organised bone tissue compared to empty scaffolds. This highlights the added benefit of incorporating bioactive agents such as MNP, which not only enhance the scaffold's biological performance but also contribute to a more conducive microenvironment for osteogenesis at the cellular level. The MNP-loaded scaffolds demonstrated improved tissue density and matrix organisation, suggesting enhanced cellular recruitment, osteoblastic activity, and matrix mineralisation. These improvements underline the pivotal role of MNP in accelerating and refining bone healing, beyond the structural support offered by the scaffold alone. The presence of uniformly distributed osteocytes within the new bone further indicates active remodelling, validating the long-term functional integration of regenerated tissue.

In contrast, the non-implanted control group exhibited minimal bone regeneration, characterised predominantly by fibrous tissue formation and poor integration with surrounding bones. This emphasises the fundamental necessity of scaffolds in providing mechanical support and a permissive biological niche for healing, especially in large or critical-sized defects where spontaneous regeneration is insufficient. These results futher underscore the importance of scaffold functionalisation with bioactive materials such as MNP to optimise the regenerative process. The synergistic effect achieved through the combination of structural support and enhanced cellular activity positions thw CC scaffold

loaded MNP as a promising platform for future advancements in bone tissue engineering. Their superior performance in promoting bone quality, tissue organisation, and healing kinetics supports their potential translation into clinical applications. In summary, this study confirms that scaffolds enhanced with MNP offer a more effective strategy for addressing large bone defects. Their dual mechanism in improving bone architecture and expediting the healing processes makes them a valuable tool for next-generation regenerative therapies.

CHAPTER SEVEN

CONCLUSION

7.1 CONCLUSION

Recognising the limitations of current periodontal treatments, this research developed and characterised a CC-MNP, designed to offer dual functionality through localised antimicrobial delivery and enhanced bone regeneration. The study successfully synthesised CC-MNP with high encapsulation efficiency and optimal particle size, which were incorporated into biodegradable scaffolds aimed at delivering a single-stage therapeutic solution. These scaffolds were engineered to provide both structural support and sustain antimicrobial activity while facilitating tissue integration. *In vitro* characterisation confirmed the scaffold's suitability for tissue engineering applications, demonstrating appropriate porosity, biodegradability, and fluid absorption capacity to support effective drug release and cellular activity. Antibacterial testing revealed strong inhibition against periodontal pathogens such as *Porphyromonas gingivalis* and *Fusobacterium nucleatum*, and biocompatibility assays indicated enhanced cellular adhesion and proliferation. *In vivo* experiments using a rat calvarial defect model further validated the scaffold's regenerative potential. Radiographic and histological assessments showed significantly improved bone formation and integration, particularly in the CC-MNP group, compared to non-loaded scaffolds and control groups. These outcomes directly align with the research objectives and support the conclusion that CC-MNP scaffolds offer a promising strategy for periodontal bone regeneration by combining infection control with osteoconductive support. The dual action of antimicrobial delivery and structural reinforcement minimises the need for systemic antibiotics and holds the potential to reduce treatment time and improve patient outcomes.

Nonetheless, the study has notable limitations. While the small animal model provided critical insights into scaffold performance, the findings may not fully reflect human clinical outcomes. This rat cranial defect model was selected due to its non-load-

bearing nature, making it suitable for assessing bone regeneration in a controlled environment. However, it does not replicate the complex anatomical structures and biomechanical environment of periodontal tissues, which include components such as cementum and the periodontal ligament and are subjected to dynamic mechanical forces. Despite this, the inclusion of MNP, a potent antibiotic effective against periodontal pathogens, reinforces the scaffold's relevance for periodontal therapy and supports its potential for future application in dental regenerative strategies.

Beyond the model-specific constraints, the study was also limited by a short evaluation period, lack of immune response profiling, and absence of comparative testing with current clinical treatments. Additionally, the lack of long-term data and absence of comparison with conventional clinical treatments restricts conclusions about scaffold durability and integration in real-world conditions. To address these gaps, future studies should incorporate long-term evaluations in larger, more anatomically relevant animal models that simulate periodontal environments. Inclusion of immune response analyses and comparative studies against standard treatments will provide a more robust understanding of clinical utility. Investigating the performance of scaffolds under inflammatory or compromised healing conditions, as well as testing multi-drug delivery strategies, would further enhance the translational potential of the system. Despite these constraints, this work contributes meaningfully to the field of scaffold-mediated bone regeneration. The incorporation of MNP into biodegradable CC scaffolds produced superior regenerative outcomes, suggesting strong clinical potential for treating periodontal and other bone-related conditions. These findings lay a solid foundation for further preclinical development and future clinical translation. In summary, this study successfully fulfilled its research objectives to evaluate the effectiveness of a CC-MNP in promoting periodontal bone and tissue regeneration. The conclusions and recommendations are consistent with the study's aims and offer practical guidance for ongoing research and development. By addressing both biological and mechanical demands of bone repair, CC-MNP scaffolds present a promising platform for next-generation regenerative therapies in both dental and orthopaedic contexts.

7.2 FUTURE PLAN

Future directions may include conducting comprehensive studies in larger, load bearing animal models to further validate the efficacy, safety, and mechanical resilience of metronidazole-loaded scaffolds under clinically relevant conditions. These efforts may lay the groundwork for initiating well-designed clinical trials to evaluate scaffold performance in human subjects, focusing on both short-term and long-term outcomes related to bone regeneration and infection control. To advance this research toward commercialisation, the next phase may involve the optimisation of scaffold manufacturing processes, including scale-up strategies, quality control measures, and regulatory compliance aligned with Good Manufacturing Practices (GMP). Partnerships with biotechnology firms and regulatory bodies may be essential for ensuring product standardisation and clinical trial approval. Currently, scaffold packaging methods include lyophilised or pre-hydrated formats, often vacuum-sealed in sterile blisters or medical-grade pouches to preserve integrity and shelf life. To improve clinical usability and market readiness, future developments may focus on refining packaging by integrating features such as easy-peel sterile barriers, dual-compartment packaging for hydrated components, and form-fit kits that streamline surgical handling. Incorporating temperature-stable designs for distribution in varying climates may also enhance global accessibility. Further innovations may include incorporating patient-specific delivery models using 3D printing technologies to enhance clinical outcomes. Intellectual property protection through patent filing is also a priority to secure commercial viability. Targeted market introduction may initially focus on dental specialists and maxillofacial surgeons, with phased expansion into orthopaedic and trauma care sectors. By integrating preclinical success, regulatory planning, and industrial collaboration, the CC-MNP scaffold platform may be positioned for real-world application, ultimately improving patient outcomes while offering a scalable and commercially viable solution to bone regeneration and infection management.

7.3 LIMITATION OF STUDY

This study provides valuable insights into scaffold-mediated bone regeneration; however, it also possessed several limitations. The rat cranial defect model, selected for its experimental consistency and practical advantages, does not accurately replicate the anatomical structure, mechanical loading conditions, or microbial environment characteristic of human periodontal tissues. Consequently, the extrapolation of these findings to clinical settings particularly in load bearing or dynamically active regions remains limited for further validation. Moreover, this investigation focused on early-phase bone regeneration and did not extend to long-term assessments of scaffold integration, degradation kinetics, or host immune responses. These parameters are critical for evaluating the scaffold's durability, biocompatibility, and overall therapeutic performance in a clinical context. Additionally, the scaffold fabrication process was confined to a laboratory scale, which may pose challenges in terms of scalability, sterility assurance, structural consistency, and compliance with regulatory standards. These limitations underscore the need for further preclinical studies incorporating extended observation periods, larger and periodontally relevant animal models, and comprehensive immunobiological evaluations. Although these constraints were, in part, influenced by the timeframe of the current research, addressing them in future work will be essential to support the clinical translation and commercial feasibility of the CC-MNP scaffold system.

REFERENCES

AAT Bioquest. (2020, July 22). *What are the growth phases of culture cells?* Retrieved from https://www.aatbio.com/resources/faq-frequently-asked-questions/What-are-the-growth-phases-of-culture-cells

Abcam. (n.d.). *MTT assay protocol*. Retrieved from https://www.abcam.com/protocol/mtt-assay-protocol

Abtahi, S., Chen, X., Shahabi, S., & Nasiri, N. (2023). Resorbable membranes for guided bone regeneration: Critical features, potentials, and limitations. *ACS Materials Au*, *3*(5), 394–417. https://doi.org/10.1021/acsmaterialsau.3c00013

Abudula, T., Gauthaman, K., Mostafavi, A., Alshahrie, A., Salah, N., Morganti, P., Chianese, A., Tamayol, A., & Memic, A. (2020). Sustainable drug release from polycaprolactone coated chitin-lignin gel fibrous scaffolds. *Scientific Reports*, *10*(1), 1–12. https://doi.org/10.1038/s41598-020-76971-w

Adlin Jino Nesalin, J., & Anton Smith, A. (2013). Preparation and evaluation of stavudine-loaded chitosan nanoparticles. *Journal of Pharmacy Research*, *6*(2), 268–274. https://doi.org/10.1016/j.jopr.2013.02.004

Ahmad, N., Khan, M. R., Palanisamy, S., & Mohandoss, S. (2023). Anticancer Drug-Loaded Chitosan Nanoparticles for *In Vitro* Release, Promoting Antibacterial and Anticancer Activities. *Polymers*, *15*(19). https://doi.org/10.3390/polym15193925

Akhmanova, M., Osidak, E., Domogatsky, S., Rodin, S., & Domogatskaya, A. (2015). Physical, spatial, and molecular aspects of extracellular matrix of *in vivo* niches and artificial scaffolds relevant to stem cells research. *Stem Cells International*, *2015*, Article 167025. https://doi.org/10.1155/2015/167025

Alasas, A. B., Mohtar, N., & Gazzali, A. M. (2024). Preparation, characterization and *in vitro* drug release evaluation of chitosan nanoparticles for Atovaquone. *Malaysian Journal of Medicine and Health Sciences*, *20*(13), 75–84.

Alassy, H., Pizarek, J. A., Kormas, I., Pedercini, A., & Wolff, L. F. (2021). Antimicrobial adjuncts in the management of periodontal and peri-implant diseases and conditions: a narrative review. *Frontiers of Oral and Maxillofacial Medicine*, *3*(April). https://doi.org/10.21037/fomm-20-84

Alavi, S. E., Gholami, M., Shahmabadi, H. E., & Reher, P. (2023). Resorbable GBR

scaffolds in oral and maxillofacial tissue engineering: Design, fabrication, and applications. *Journal of ClinicalMedicine*, *12*(22). https://doi.org/10.3390/jcm12226962

Al-Delayme, R. A. (2017). Local delivery of antibiotics in periodontal therapy: A review. *Journal of Dental Research and Review*, *4*(4), 83–87. https://doi.org/10.4103/jdrr.jdrr_30_17

Alghofaily, M., Almana, A., Alrayes, J., Lambarte, R., Weir, M. D., & Alsalleeh, F. (2024). Chitosan–gelatin scaffolds loaded with different antibiotic formulations for regenerative endodontic procedures promote biocompatibility and antibacterial activity. *Journal of Functional Biomaterials*, *15*(7), 186. https://doi.org/10.3390/jfb15070186

Al-Nemrawi, N. K., Alsharif, S. S. M., & Dave, R. H. (2018). Preparation of chitosan-top nanoparticles: The influence of chitosan polymeric properties and formulation variables. *International Journal of Applied Pharmaceutics*, *10*(5), 60–65. https://doi.org/10.22159/ijap.2018v10i5.26375

Al Qabbani, A., Rani, K. G. A., AlKawas, S., Sheikh Abdul Hamid, S., Yap Abdullah, A., Samsudin, A. R., et al. (2023). Evaluation of the osteogenic potential of demineralized and decellularized bovine bone granules following implantation in rat calvaria critical-size defect model. *PLOS ONE*, *18*(12), e0294291. https://doi.org/10.1371/journal.pone.0294291

Amato, M., Santonocito, S., Polizzi, A., Tartaglia, G. M., Ronsivalle, V., Viglianisi, G., & Isola, G. (2023). Local delivery and controlled release drug systems: A new approach for the clinical treatment of periodontitis therapy. *Pharmaceutics, 15*(4), 1312. https://doi.org/10.3390/pharmaceutics15041312

Amid, R., Nanduri, A., Salazar, C., & Zhang, W. (2021). Evaluating the effectiveness of novel bone

grafts using the critical-sized defect model: A preclinical perspective. *Frontiers in Bioengineering and Biotechnology*, *9*, 734919. https://doi.org/10.3389/fbioe.2021.734919

Aminu, N., Chan, S. Y., & Toh, S. M. (2018). Formulation design and optimization of triclosan loaded nanoparticles for enhanced drug delivery across gingival sulcus by

Resolution IV modeling of Design-Expert®. *Journal of Biomedical and Clinical Sciences*, *3*(1), 83–90.

Andrei, V., Fiț, N. I., Matei, I., Barabás, R., Bizo, L. A., Cadar, O., Boșca, B. A., Farkas, N. I., Marincaș, L., Muntean, D. M., Dinte, E., & Ilea, A. (2022). *In Vitro* Antimicrobial effect of novel electrospun polylactic acid/hydroxyapatite nanofibres loaded with doxycycline. *Materials*, *15*(18), 1–11. https://doi.org/10.3390/ma15186225

Arigbede, A. O., Babatope, B. O., & Bamidele, M. K. (2012). Periodontitis and systemic diseases: A literature review. *Journal of Indian Society of Periodontology*, *16*(4), 487–491. https://doi.org/10.4103/0972-124X.106878

Armitage, G. C. (1999). Development of a classification system for periodontal diseases and conditions. *Annals of Periodontology / the American Academy of Periodontology*, *4*(1), 1–6. https://doi.org/10.1902/annals.1999.4.1.1

Asghar, M. S., Li, J., Ahmed, I., Ghazanfar, U., Irshad, M. S., Idrees, M., Haq, Z., Rizwan, M., Sheikh, F., & Yasmeen, F. (2021). Antioxidant and enhanced flexible nanoporous scaffolds for bone tissue engineering applications. *Nano Select*, *2*(1), e000261. https://doi.org/10.1002/nano.202000261

Ashraf, M. A., Peng, W., Zare, Y., & Rhee, K. Y. (2018). Effects of size and aggregation/agglomeration of nanoparticles on the interfacial/interphase properties and tensile strength of polymer nanocomposites. *Nanoscale Research Letters*, *13*. https://doi.org/10.1186/s11671-018-2624-0

Ataide, J. A., Geraldes, D. C., Gérios, E. F., Bissaco, F. M., Cefali, L. C., Oliveira-Nascimento, L., & Mazzola, P. G. (2021). Freeze-dried chitosan nanoparticles to stabilize and deliver bromelain. *Journal of Drug Delivery Science and Technology*, *61*(August). https://doi.org/10.1016/j.jddst.2020.102225

Atia, G. A. N., Shalaby, H. K., Zehravi, M., Ghobashy, M. M., Attia, H. A. N., Ahmad, Z., Khan, F. S., Dey, A., Mukerjee, N., Alexiou, A., Rahman, Md. H., Klepacka, J., & Najda, A. (2022). Drug-loaded chitosan scaffolds for periodontal tissue regeneration. *Polymers*, *14*(15), 3192. https://doi.org/10.3390/polym14153192

Azadi Boroujeni, A., Talebi Ardakani, M., Houshmand, B., & Moscowchi, A. (2020). Designing a novel chitosan-based periofilm containing metronidazole–

ciprofloxacin. *SN Applied Sciences*, *2*(4), 1–8. https://doi.org/10.1007/s42452-020-2362-7

Azhar, F. F., Olad, A., & Salehi, R. (2014). Fabrication and characterization of chitosan-gelatin/nanohydroxyapatite- polyaniline composite with potential application in tissue engineering scaffolds. *Designed Monomers and Polymers*, *17*(7), 654–667. https://doi.org/10.1080/15685551.2014.907621

Bashir, S. M., Ahmed Rather, G., Patrício, A., Haq, Z., Sheikh, A. A., Shah, M. Z. ul H., Singh, H., Khan, A. A., Imtiyaz, S., Ahmad, S. B., Nabi, S., Rakhshan, R., Hassan, S., & Fonte, P. (2022). Chitosan Nanoparticles: A Versatile platform for biomedical applications. *Materials*, *15*(19), 1–28. https://doi.org/10.3390/ma1519-6521

Bashur, C. A., Dahlgren, L. A., & Goldstein, A. S. (2006). Effect of fiber diameter and orientation on fibroblast morphology and proliferation on electrospun poly(d,l-lactic co-glycolic acid) meshes. *Biomaterials*, *27*(33), 5681–5688. https://doi.org/10.1016/j.biomaterials.2006.07.005

Bassi, A. P. F., Bizelli, V. F., Francatti, T. M., Rezende de Moares Ferreira, A. C., Carvalho Pereira, J., Al-Sharani, H. M., ... & Faverani, L. P. (2021). Bone regeneration assessment of polycaprolactone membrane on critical-size defects in rat calvaria. *Membranes*, *11*(2), 124. https://doi.org/10.3390/membranes11020124

Bastos, M. D. R., Dotta, T. C., Kubata, B. R., do Nascimento, C., de Oliveira, C. S., Figueiredo, F. A. T., Rocha, M. M., & Pedrazzi, V. (2024). Metronidazole modified-release therapy using two different polymeric systems (gels or films): Clinical study for the treatment of periodontitis. *Pharmaceutics*, *16*(9), 1108. https://doi.org/10.3390/pharmaceutics16091108

Basudan, A. M. (2022). Nanoparticle-based periodontal drug delivery – A review on current trends and future perspectives. *Saudi Dental Journal*, *34*(8), 669–680. https://doi.org/10.1016/j.sdentj.2022.09.006

BOC Sciences. (2024). *Polydispersity Index (PDI) Analysis*. Retrieved from https://liposomes.bocsci.com/solution/polydispersity-index-pdi-analysis.html

Bonewald, L. F. (2011). The amazing osteocyte. *Journal of Bone and Mineral Research*, *26*(2), 229–238. https://doi.org/10.1002/jbmr.320

Borges, J. R. M. A., Silva, E. C., Pires, F. S., et al. (2023). *In vivo evaluation of collagen and chitosan scaffold, associated or not with stem cells, in bone repair*. *Journal of Functional Biomaterials, 14*(7), 357. https://doi.org/10.3390/jfb14070357

Bottino, M. C., Arthur, R. A., Waeiss, R. A., Kamocki, K., Gregson, K. S., & Gregory, R. L. (2014). Biodegradable nanofibrous drug delivery systems: effects of metronidazole and ciprofloxacin on periodontopathogens and commensal oral bacteria. Clinical oral investigations, *18*, 2151-2158.

Brennan, C. A., & Garrett, W. S. (2019). Fusobacterium nucleatum — symbiont, opportunist and oncobacterium. *Nature Reviews Microbiology*, *17*(3), 156–166. https://doi.org/10.1038/s41579-018-0129-6

Bružauskaitė, I., Bironaitė, D., Bagdonas, E., & Bernotienė, E. (2016). Scaffolds and cells for tissue regeneration: different scaffold pore sizes—different cell effects. *Cytotechnology*, *68*(3), 355–369. https://doi.org/10.1007/s10616-015-9895-4

Buaksuntear, K., Limarun, P., Suethao, S., & Smitthipong, W. (2022). Non-covalent interaction on the self-healing of mechanical properties in supramolecular polymers. *International Journal of Molecular Sciences, 23*(13), 6902. https://doi.org/10.3390/ijms23136902

Budai-Szűcs, M., Léber, A., Cui, L., Józó, M., Vályi, P., Burián, K., Kirschweng, B., Csányi, E., & Pukánszky, B. (2020). Electrospun PLA fibers containing metronidazole for periodontal disease. *Drug Design, Development and Therapy*, 14, 233–242. https://doi.org/10.2147/DDDT.S231748

Cadinoiu, A. N., Rata, D. M., Daraba, O. M., Atanase, L. I., Horhogea, C. E., Chailan, J.-F., Popa, M., & Carauleanu, A. (2025). Metronidazole-loaded chitosan nanoparticles with antimicrobial activity against *Clostridium perfringens*. *Pharmaceutics, 17*(3), 294. https://doi.org/10.3390/pharmaceutics17030294

Cam, M. E., Yildiz, S., Alenezi, H., Cesur, S., Ozcan, G. S., Erdemir, G., Edirisinghe, U., Akakin, D., Kuruca, D. S., Kabasakal, L., Gunduz, O., & Edirisinghe, M. (2020). Evaluation of burst release and sustained release of pioglitazone-loaded fibrous mats on diabetic wound healing: An *in vitro* and *in vivo* comparison study. *Journal of the Royal Society Interface*, *17*(162). https://doi.org/10.1098/rsif.2019.0712

Carlos, C. R., Astarita, C., D'Aquino, R., & Pelegrine, A. A. (2020). Evaluation of bone

regeneration in rat calvaria using bone autologous micrografts and xenografts: Histological and histomorphometric analysis. *Materials*, *13*(19), 1–15. https://doi.org/10.3390/MA13194284

Celebioglu, A., & Uyar, T. (2019). Metronidazole/Hydroxypropyl-β-Cyclodextrin inclusion complex nanofibrous webs as fast-dissolving oral drug delivery system. *International Journal of Pharmaceutics*, *572*, 118828. https://doi.org/10.1016/j.-ijpha rm.2019.118828

Chacon, E. L., Bertolo, M. R. V., de Guzzi Plepis, A. M., da Conceição Amaro Martins, V., dos Santos, G. R., Pinto, C. A. L., Pelegrine, A. A., Teixeira, M. L., Buchaim, D. V., Nazari, F. M., Buchaim, R. L., Sugano, G. T., & da Cunha, M. R. (2023). Collagen- chitosan-hydroxyapatite composite scaffolds for bone repair in ovariectomized rats. *Scientific Reports*, *13*(1), 1–12. https://doi.org/10.1038/s41598-022-24424-x

Chakka, J. L., et al. (2021). Polydopamine functionalized VEGF gene-activated 3D printed scaffolds for bone regeneration. *RSC Advances*, *11*(21), 13282–13291. https://doi.org/10.1039/D1RA01193F

Chakraborty, A., Mishra, S., Das, S., Basu, D., & Patra, R. (2025). Metronidazole-laden silk fibroin methacrylated scaffolds for managing periapical lesions: Antimicrobial and regenerative potential. *Journal of Biomedical Materials Research Part B: Applied Biomaterials*. https://www.springermedicine.com/ metronidazole/apicectomy/metronidazolelade n-silk-fibroin-methacrylated scaffolds-for-man/50196182

Chalikias, S., Papaioannou, N., Koundis, G., Pappa, E., Galanos, A., Anastassopoulos, G., Sarris, I. N., Panteliou, S., Chronopoulos, E., & Dontas, I. A. (2021). Evaluation of femoral bone fracture healing in rats by the modal damping factor and its correlation with peripheral quantitative computed tomography. *Cureus*, *13*(2). https://doi.org/10.7759/cureus.13342

Chang, Y.-T., Lai, C.-C., & Lin, D.-J. (2023). Collagen scaffolds laden with human periodontal ligament fibroblasts promote periodontal regeneration in SD rat model. *Polymers*, *15*(12), 2649. https://doi.org/10.3390/polym15122649

Charan, J., & Kantharia, N. (2013). How to calculate sample size in animal studies? *Journal of Pharmacology and Pharmacotherapeutics*, *4*(4), 303–306. https://doi.org/10.41-

03/0976-500X.119726

Chen, H., Song, G., Xu, T., Meng, C., Zhang, Y., Xin, T., Yu, T., & Lin, Y. (2024). *Biomaterial scaffolds for periodontal tissue engineering.* Journal of Functional Biomaterials, 15(8), 233. https://doi.org/10.3390/jfb15080233

Chen, H., Zhang, Y., Yu, T., Song, G., Xu, T., Xin, T., Lin, Y., & Han, B. (2022). Nano-Based Drug Delivery Systems for Periodontal Tissue Regeneration. *Pharmaceutics*, 14(10), 2250. https://doi.org/10.3390/pharmaceutics14102250

Chen, K., Hao, J., Noritake, K., Yamashita, Y., Kuroda, S., & Kasugai, S. (2013). Effects of low intensity pulsed ultrasound stimulation on bone regeneration in rat parietal bone defect model. *Open Journal of Regenerative Medicine*, *2*(1), 8–14. https://doi.org/10.4236/ojrm.2013.21002

Chen, M.-L., Xu, H.-X., Yuan, W.-F., Zhao, S.-H., Li, X., Zhu, L.-X., Shen, Z.-Y., Liu, Y.-J., Wang, M.-J., Ma, A., Hoogmartens, J., & Adams, E. (2022). Identification of the major photodegradant in metronidazole by LC-PDA-MS and its reveal in compendial methods.

Chen, S., & Huang, X. (2022). Nanomaterials in scaffolds for periodontal tissue engineering: Frontiers and prospects. *Bioengineering*, 9(9), 431. https://doi.org/10.-3390/bioengineering9090431

Chen, Y., Wu, H., Lu, G., Zhu, Y., Ban, J., & Li, X. (2023). Membranes containing nanoparticles incorporated with metronidazole for improved permeability to promote periodontal tissue recovery. *Current Nanoscience, 21*(2), 319–332. https://doi.org/10.2174/0115734137276083231128082103

Chhabra, S., Chhabra, N., Kaur, A., & Gupta, N. (2017). Wound healing concepts in clinical practice of OMFS. *Journal of Maxillofacial and Oral Surgery*, *16*(4), 403–423. https://doi.org/10.1007/s12663-016-0880-z

Choi, J. E., Lyons, K. M., Kieser, J. A., & Waddell, N. J. (2017). Diurnal variation of intraoral pH and temperature. *BDJ Open*, 3(1), 1–6. https://doi.org/10.1038/bdjope-n.2017.15

Choudhary, V., Choudhary, M., & Bollag, W. B. (2024). Exploring skin wound healing models and the impact of natural lipids on the healing process. *International Journal of Molecular Sciences*, *25*(7). https://doi.org/10.3390/ijms25073790

Coppola, D., Oliviero, M., Vitale, G. A., Lauritano, C., D'Ambra, I., Iannace, S., & de Pascale, D. (2020). Marine collagen from alternative and sustainable sources: Extraction, processing and applications. *Marine Drugs, 18*(4), 214. https://doi.org/-10.3390/md18040214

Cross, H. (2003). *Wound Care For People Affected by Leprosy: A Guide for Low Resource Situations*.143.http://www.ilep.org.uk/fileadmin/uploads/Documents/Infolep_Documents/Self_care/ Wound_Care.pdf

Da Silva, M. A. C., Oliveira, R. N., Mendonça, R. H., Lourenço, T. G. B., Colombo, A. P. V., Tanaka, M. N., Tude, E. M. O., Da Costa, M. F., & Thiré, R. M. S. M. (2016). Evaluation of metronidazole-loaded poly(3-hydroxybutyrate) membranes to potential application in periodontitis treatment. *Journal of Biomedical Materials Research - Part B Applied Biomaterials*, *104*(1), 106–115. https://doi.org/10.1002/jbm.b.33357

Daei-farshbaf, N., Ardeshirylajimi, A., Seyedjafari, E., Piryaei, A., Fadaei Fathabady, F., Hedayati, M., Salehi, M., Soleimani, M., Nazarian, H., Moradi, S. L., & Norouzian, M. (2014). Bioceramic-collagen scaffolds loaded with human adipose-tissue derived stem cells for bone tissue engineering. *Molecular Biology Reports*, *41*(2), 741–749. https://doi.org/10.1007/s11033-013-2913-8

Dasgupta, S., Majumder, D., Ghosh, S., & Chatterjee, B. (2023). Chitosan–collagen–fibrinogen scaffolds possessing skin regeneration and vascularization potential. *Journal of Biomedical Materials Research Part A*, *111*(5), 725–739. https://doi.org/10.1002/jbm.a.37488

Danaei, M., Dehghankhold, M., Ataei, S., Hasanzadeh Davarani, F., Javanmard, R., Dokhani, A., Khorasani, S., & Mozafari, M. R. (2018). Impact of particle size and polydispersity index on the clinical applications of lipidic nanocarrier systems. *Pharmaceutics*, *10*(2), 1–21. https://doi.org/10.3390/pharmaceutics10020057

Dasari, A., Xue, J., & Deb, S. (2022). Magnetic nanoparticles in bone tissue engineering. *Nanomaterials*, *12*(5), 757. https://doi.org/10.3390/nano12050757

Dental Update. (2021). Local drug delivery in the management of periodontal diseases part 2: specific agents. *Dental Update*. https://www.dental-update.co.uk/content/periodontology/local-drug-delivery-in-the-management-of-periodontal-diseases-part-2-

specific-agents

De Santana, R. B., de Mattos, C. M. L., Francischone, C. E., & Van Dyke, T. (2010). Superficial topography and porosity of an absorbable barrier membrane impacts soft tissue response in guided bone regeneration. *Journal of Periodontology*, *81*(6), 926–933. https://doi.org/10.1902/jop.2010.090592

Deininger, C., Wagner, A., Heimel, P., Salzer, E., Vila, X. M., Weißenbacher, N., Grillari, J., Redl, H., Wichlas, F., Freude, T., Tempfer, H., Teuschl-Woller, A. H., & Traweger, A. (2022). Enhanced bmp-2-mediated bone repair using an anisotropic silk fibroin scaffold coated with bone-like apatite. *International Journal of Molecular Sciences*, *23*(1). https://doi.org/10.3390/ijms23010283

Delgado, R. (2022). Misuse of Beer-Lambert Law and other calibration curves. *Royal Society Open Science*, *9*(2). https://doi.org/10.1098/rsos.211103

Desmiaty, Y., Fahleni, F., Griselda, A., & Apriliana, A. Z. (2024). Enhanced ability of agarwood leaves (*Aquilaria malaccensis* Lam.) ointment as wound healing to heal second-degree burns in rats. *Sciences of Pharmacy*.

Dhedage, N., Khan, G., Ajmal, G., Kumar, M., Jha, A., & Mishra, B. (2020). Metronidazole loaded polycaprolactone-carbopol blends based biodegradable intrapocket dental film for local treatment of periodontitis. *Drug Delivery Letters*, *11*(1), 3443. https://doi.org/10.2174/2210303110999200910104334

Dingsdag, S. A., & Hunter, N. (2018). Metronidazole: An update on metabolism, structure-cytotoxicity and resistance mechanisms. *Journal of Antimicrobial Chemotherapy*, *73*(2), 265–279. https://doi.org/10.1093/jac/dkx351

Diversa Technologies. (2024). *A Deep Dive into Lipid Nanoparticle Size Distribution*. Retrieved from https://www.diversatechnologies.com/lipid-nanoparticle-size-distribution/

Dom, T. N. M., Ayob, R., Abd Muttalib, K., & Aljunid, S. M. (2016). National economic burden associated with management of periodontitis in Malaysia. *International Journal of Dentistry*, *2016*(1). https://doi.org/10.1155/2016/1891074

Dong, X., Cheng, Q., Long, Y., Xu, C., Fang, H., Chen, Y., & Dai, H. (2020). A chitosan based scaffold with enhanced mechanical and biocompatible performance for biomedical applications. *Polymer Degradation and Stability*, *181*, 109322.

https://doi.org/10.1016/j.polymdegradstab.2020.109322

Donos, N., Dereka, X., & Mardas, N. (2015). Experimental models for guided bone regeneration in healthy and medically compromised conditions. *Periodontology 2000*, *68*(1), 99–121. https://doi.org/10.1111/prd.12077

Dorazilová, J., Muchová, J., Šmerková, K., Kočiová, S., Diviš, P., Kopel, P., Veselý, R., Pavliňáková, V., Adam, V., & Vojtová, L. (2020). Synergistic effect of chitosan and selenium nanoparticles on biodegradation and antibacterial properties of collagenous scaffolds designed for infected burn wounds. *Nanomaterials, 10*(10), 1971. https://doi.org/10.3390/nano10101971

Drugs, C., Monitoring, A., Temperature, B., & Anesthesia, I. (n.d.). *Anesthesia in experimental animals: Controlled drugs, anesthetic monitoring, prevention of fluid loss, preparation and use of injectable anesthetic drugs* (pp. 2–3).

Ebert, D., & Greenberg, M. E. (2008). Biomimetic materials for tissue engineering. *Advance Drug Delivery Reviews, 60(5), 4353–4364.* https://doi.org/10.1016/j.addr.-2007.08.041.Biomimetic

Eliyahu, S., Aharon, A., & Bianco-Peled, H. (2018). Acrylated chitosan nanoparticles with enhanced mucoadhesion. *Polymers*, *10*(2), 106.

Echeverria Molina, M. I., Malollari, K. G., & Komvopoulos, K. (2021). Design challenges in polymeric scaffolds for tissue engineering. *Frontiers in Bioengineering and Biotechnology*, *9*(June), 1–29. https://doi.org/10.3389/fbioe.2021.617141

Edmondson, R., Broglie, J. J., Adcock, A. F., & Yang, L. (2014). Three-dimensional cell culture systems and their applications in drug discovery and cell-based biosensors. *Assay and Drug Development Technologies*, *12*(4), 207–218. https://doi.org/10.108-9dt.2014.573

Egorikhina, M. N., Bronnikova, I. I., Rubtsova, Y. P., Charykova, I. N., Bugrova, M. L., Linkova, D. D., & Aleynik, D. Ya. (2021). Aspects of *in vitro* biodegradation of hybrid fibrin–collagen scaffolds. *Polymers*, *13*(20), 3470. https://doi.org10.3/390/polym13203470

Eke, P. I., Dye, B. A., Wei, L., Thornton-Evans, G. O., & Genco, R. J. (2012). Prevalence of periodontitis in adults in the united states: 2009 and 2010. *Journal of Dental Research*, *91*(10), 914–920. https://doi.org/10.1177/0022034512457373

Elsayed, S. (2023). *Preclinical evaluation of 3D printed biomaterials for repairing critical-size bone defects* (Doctoral dissertation). University of Cambridge.

El-Shanshory, A. A., Agwa, M. M., Abd-Elhamid, A. I., Soliman, H. M. A., Mo, X., & Kenawy, E. R. (2022). Metronidazole topically immobilized electrospun nanofibrous scaffold: Novel secondary intention wound healing accelerator. *Polymers*, *14*(3). https://doi.org/10.3390/polym14030454

Eun, J., Eun, K., Chan, I., Jeong, H., Lee, S., Cho, H., Joong, H., Chul, S., & Chul, M. (2004). Effects of the controlled-released TGF-β1 from chitosan microspheres on chondrocytes cultured in a collagen/chitosan/glycosaminoglycan scaffold. *Biomaterials, 25*(25), 4163–4173. https://doi.org/10.1016/j.biomaterials.2003.10.-057

European Medicines Agency ICH. (2005). Q2 (R1): Validation of analytical procedures: text and methodology. *International Conference on Harmonization*, 1– 15.

Farazin, A., & Mahjoubi, S. (2024). Dual-functional hydroxyapatite scaffolds for bone regeneration and precision drug delivery. *Journal of the Mechanical Behavior of Biomedical Materials*, 157(September), 1–7. https://doi.org/10.1016/j.jmbbm.2024.-106661

Farjaminejad, S., Farjaminejad, R., & Garcia-Godoy, F. (2024). *Nanoparticles in bone regeneration: A narrative review of current advances and future directions in tissue engineering*. *Journal of Functional Biomaterials, 15*(9), 241. https://doi.org/10.33-90/jfb15090241

Fazeli, N., Arefian, E., Irani, S., & Seyedjafari, E. (2023). Accelerated reconstruction of rat calvaria bone defect using 3D-printed scaffolds coated with hydroxyapatite/bioglass. *Scientific Reports*, *13*, 38146. https://doi.org/10.1038/s41-598-023-38146-1

FDA. (2021). *510(k) Premarket Notification: Maxiocel Chitosan Wound Dressing (K212766)*. U.S. Food and Drug Administration. https://www.accessdata.fda.gov/cdrh_docs/pdf21/K212766.pdf

Felfel, R. M., Gideon-Adeniyi, M. J., Zakir Hossain, K. M., Roberts, G. A. F., & Grant, D. M. (2019). Structural, mechanical and swelling characteristics of 3D scaffolds from chitosan-agarose blends. *Carbohydrate Polymers*, *204*, 59–67. https://doi.org/10.1-

016/j.carbpol.2018.10.002

Fernandes, L. L., Resende, C. X., Tavares, D. S., Soares, G. A., Castro, L. O., & Granjeiro, J. M. (2011). Cytocompatibility of chitosan and collagen-chitosan scaffolds for tissue engineering. *Polimeros*, *21*(1), 1–6. https://doi.org/10.1590/S0104-14282011005000008

Filippi, M., Born, G., Chaaban, M., & Scherberich, A. (2020). Natural polymeric scaffolds in bone regeneration: A review. *Frontiers in Bioengineering and Biotechnology*, *8*, 474. https://doi.org/10.3389/fbioe.2020.00474

Fuster, M. G., Montalbán, M. G., Carissimi, G., Lima, B., Feresin, G. E., Cano, M., Giner-Casares, J. J., López-Cascales, J. J., Enriz, R. D., & Víllora, G. (2020). Antibacterial effect of chitosan–gold nanoparticles and computational modeling of the interaction between chitosan and a lipid bilayer model. *Nanomaterials*, *10*(12), 1–18. https://doi.org/10.3390/nano10122340

Gaikwad, S., & Kim, M. J. (2024). Fish by-product collagen extraction using different methods and their application. *Marine Drugs*, *22*(2), 1–20. https://doi.org/10.3390-/md22020060

Gager, M. and Götz, F. (2023). Antibiotic resistance genes in the subgingival mirobiome and implications for periodontitis therapy. *Journal of Periodontology*, 94(1), 1–10. https://doi.org/10.1002/JPER.22-0696

Gamboa, F., Acosta, A., García, D. A., Velosa, J., Araya, N., & Ledergerber, R. (2014). Occurrence of *porphyromonas gingivalis* and its antibacterial susceptibility to metronidazole and tetracycline in patients with chronic periodontitis. *Acta Odontologica Latinoamericana: AOL*, *27*(3), 137–144. https://doi.org/10.1590/-S1852-48342014000300007

Gandhi, U. H., Vyas, S. D., Mane, V., Patel, S. N., Patadiya, H. H., Kumar, S., & Haque, M. (2025). The effectiveness of metronidazole as a localized drug delivery system in the treatment of periodontal diseases: A narrative review. *Cureus*, 17(3), e80547. https://doi.org/10.7759/cureus.80547

Garg, U., Chauhan, S., Nagaich, U., & Neha Jain. (2019). Current advances in chitosan nanoparticles based drug delivery and targeting. *Advanced Pharmaceutical Bulletin*, *9*(2). https://doi.org/10.15171/jcvtr.2015.24

Garg, V., Chawla, K., & Pawar, S. K. (2018). Nanotechnology controlled local drug delivery system for the treatment of periodontitis. *Journal of Advances in Medicine and Medical Research*, *26*(6), 1–17. https://doi.org/10.9734/JAMMR/2018/40828

Garrett, W. S., & Onderdonk, A. B. (2017). Bacteroides, Prevotella, Porphyromonas, and Fusobacterium species (and other medically important anaerobic gram-negative bacilli) (pp. 1–5). Oncohemakey. Retrieved from https://oncohemakey.com/bacteroides-prevotella-porphyromonas-and-fusobacterium-species-and-other-medically-important-anaerobic-gram-negative-bacilli/

Garud, A., & Garud, N. (2010). Preparation and evaluation of chitosan microcapsules of metronidazole using tripolyphosphate cross-linking method. *Dhaka University Journal of Pharmaceutical Sciences*, *9*(2), 125–130. https://doi.org/10.3329/dujp.v9i2.7897

Gentile, P., Chiono, V., Tonda-Turo, C., Ferreira, A. M., & Ciardelli, G. (2011). Polymeric membranes for guided bone regeneration. *Biotechnology Journal*, *6*(10), 1187–1197. https://doi.org/10.1002/biot.201100294

Gómez-Cerezo, N., Casarrubios, L., Saiz-Pardo, M., Ortega, L., de Pablo, D., Díaz-Güemes, I., Fernández-Tomé, B., Enciso, S., Sánchez-Margallo, F. M., Portolés, M. T., Arcos, D., & Vallet-Regí, M. (2019). Mesoporous bioactive glass/ε-polycaprolactone scaffolds promote bone regeneration in osteoporotic sheep. *Acta Biomaterialia*, *89*, 386–398. https://doi.org/10.1016/j.actbio.2019.04.019

Gottlow, J., Nyman, S., Lindhe, J., Karring, T., & Wennström, J. (1986). New attachment formation in the human periodontium by guided tissue regeneration Case reports. *Journal of Clinical Periodontology*, *13*(6), 604–616. https://doi.org https://doi.org-/10.1111/j.1600- 051X.1986.tb00854.x

Grabska-Zielińska, S., Sionkowska, A., Carvalho, Â., & Monteiro, F. J. (2021). Biomaterials with potential use in bone tissue regeneration—Collagen/chitosan/silk fibroin scaffolds cross-linked by EDC/NHS. *Materials*, *14*(5), 1105. https://doi.org/10.3390/ma14051105

Grabska-Zielińska, S., Sionkowska, A., Coelho, C. C., & Monteiro, F. J. (2020). Silk fibroin/collagen/chitosan scaffolds cross-linked by a glyoxal solution as biomaterials toward bone tissue regeneration. *Materials*, *13*(15), 1–20. https://doi.

org/10.3390/ma13153433

Grant, K. (2009). Wounds. Rat guide: A guide to health, medication use, breeding, and care of rats. Rat Guide. Retrieved October 12, 2023, from https://ratguide.com/health/ trau ma/wounds.php

Graziani, F., Karapetsa, D., Mardas, N., Leow, N., & Donos, N. (2018). Surgical treatment of the residual periodontal pocket. *Periodontology 2000, 76*(1), 150–163. https://doi.org/10.1111/prd.12156

Grierosu, C., Calin, G., Damir, D., et al. (2023). *Development and functionalization of a novel chitosan-based nanosystem for enhanced drug delivery*. *Journal of Functional Biomaterials, 14*(11), 538. https://doi.org/10.3390/jfb14110538

Guo, D. (2017). New Developments in Long-Acting Injectable Nanoformulations. *Global Journal of Pharmacy & Pharmaceutical Sciences*, *4*(2). https://doi.org/10.19080/gj-pps.2017.04.555633

Guo, F., Carter, D. E., Mukhopadhyay, A., & Leask, A. (2011). Gingival fibroblasts display reduced adhesion and spreading on extracellular matrix: A possible basis for scarless tissue repair? *PLoS ONE*, *6*(11), 1–9. https://doi.org/10.1371/journal.pone. 0027097

Gutiérrez-Ruíz, S. C., Cortes, H., González-Torres, M., Almarhoon, Z. M., Gürer, E. S., Sharifi-Rad, J., & Leyva-Gómez, G. (2024). Optimize the parameters for the synthesis by the ionic gelation technique, purification, and freeze-drying of chitosan-sodium tripolyphosphate nanoparticles for biomedical purposes. *Journal of Biological Engineering, 18*(1), 12. https://doi.org/10.1186/s13036-024-00403-w

Hajishengallis, G., & Lamont, R. J. (2012). Beyond the red complex and into more complexity: The polymicrobial synergy and dysbiosis (PSD) model of periodontal disease etiology. *Molecular Oral Microbiology*, *27*(6), 409–419. https://doi.org/10. 1111/j.2041-1014.2012.00663.x

Hagenfeld, D., Matern, J., Prior, K., Harks, I., Eickholz, P., Lorenz, K., Kim, T.-S., Kocher, T., Meyle, J., Kaner, D., Schlagenhauf, U., Harmsen, D., & Ehmke, B. (2020). Significant short-term shifts in the microbiomes of smokers with periodontitis after periodontal therapy with amoxicillin and metronidazole as revealed by 16S rDNA amplicon sequencing. *Frontiers in Cellular and Infection Microbiology*, 10, 167.

https://doi.org/10.3389/fcimb.2020.00167

Hamdi, N. A. M., Haris, M. S., & Ismail, A. F. H. (2021). The positive impact of Vitamin C (Ascorbic Acid) utilisation in cancer treatment: A scoping review of published articles from the perspective of the *in vitro* studies. *Malaysian Journal of Medicine and Health Sciences, 17*(4), 275–284.

Harun Ismail, A. F., Doolaanea, A. A., Mohamed, F., Mansor, N. I., Mohd Shafri, M. A., & Yusof, F. A. (2015). Method development and validation using UV spectrophotometry for Nigella sativa oil microparticles quantification. *Journal of Applied Pharmaceutical Science, 5*(9), 082–088. https://doi.org/10.7324/JAPS.2015-.50915

Hasan, F., Ikram, R., Abbas, A., & Asadullah, K. (2020). Effectiveness of local drug delivery system using 1% metronidazole gel and mouthwash in treating periodontal diseases. *Pakistan Journal of Pharmaceutical Sciences, 33*(5), 2053–2058. https://doi.org/10.36721/PJPS.2020.33.5.REG.2053-2058.1

Hatakeyama, W., Taira, M., Takafuji, K., Kihara, H., & Kondo, H. (2013). Bone-regeneration trial of rat critical-size calvarial defects using nano-apatite/collagen composites. *Nano Biomedicine*, *5*(2), 98–103.

Hatakeyama, W., Taira, M., Sawada, T., Hoshi, M., Hachinohe, Y., Sato, H., Takafuji, K., Kihara, H., Takemoto, S., & Kondo, H. (2022). Bone regeneration of critical-size calvarial defects in rats using highly pressed nano-apatite/collagen composites. *Materials*, *15*(9), 3376. https://doi.org/10.3390/ma15093376

Hatt, L. P., Thompson, K., Helms, J. A., Stoddart, M. J., & Armiento, A. R. (2022). Clinically relevant preclinical animal models for testing novel cranio-maxillofacial bone 3D-printed biomaterials. *Clinical and translational medicine*, *12*(2), e690.

Hazim, F. A. B. U., Fasih, F., Asif, M., Iqbal, S. N., & Shaukat, L. (2020). Metronidazole susceptibility and resistance pattern anaerobes causing periodontitis in tertiary care unit. *Pakistan Journal of Pharmaceutical Sciences, 14*(4), 983–986.

He, Y., Jin, Y., Ying, X., Wu, Q., Yao, S., Li, Y., Liu, H., Ma, G., & Wang, X. (2020). Development of an antimicrobial peptide-loaded mineralised collagen bone scaffold for infective bone defect repair. *Regenerative Biomaterials, 7*(5), 515–525. https://doi.org/10.1093/rb/rbaa015

Helen, P. A., Perumal, P., Sivaraj, P., Diana, M. I., & Selvin, P. C. (2020). Mg-ion conducting electrolytes based on chitosan biopolymer host for the rechargeable Mg batteries. *Materials Today: Proceedings*, *50*, 2668–2670. https://doi.org/10.1016/j.matpr.2020.07.606

Herdiana, Y., Wathoni, N., Shamsuddin, S., & Muchtaridi, M. (2022). Drug release study of the chitosan-based nanoparticles. *Heliyon*, *8*(1), e08674. https://doi.org/10.1016-/j.heliyon. 2021.e08674

Herold, Sydney E., "Release kinetics of metronidazole from 3D printed silicone scaffolds." (2022). *Electronic Theses and Dissertations.* Paper 3921. https://doi.org/10.18297-/etd/3921

Herrera, D., Sanz, M., Jepsen, S., Needleman, I., & Roldán, S. (2002). A systematic review on the effect of systemic antimicrobials as an adjunct to scaling and root planing in periodontitis patients. *Journal of Clinical Periodontology*, *29*(s3), 136–159. https://doi.org/10.1034/j.1600-051x.29.s3.8.x

Hidalgo-Vicelis, R. et al. (2022). *Biocompatibility and degradation of collagen–chitosan scaffolds for tissue engineering applications*. Materials Science and Engineering: C, 138, 112286. https://doi.org/10.1016/j.msec.2022.112286

Ho, H. N., Le, H. H., Le, T. G., Duong, T. H. A., Ngo, V. Q. T., Dang, C. T., Nguyen, V. M., Tran, T. H., & Nguyen, C. N. (2022). Formulation and characterization of hydroxyethyl cellulose-based gel containing metronidazole-loaded solid lipid nanoparticles for buccal mucosal drug delivery. *International Journal of Biological Macromolecules, 194*, 1010–1018. https://doi.org/10.1016/j.ijbiomac.2021.11.161

Homayun, B., Lin, X., & Choi, H. J. (2019). Challenges and recent progress in oral drug delivery systems for biopharmaceuticals. *Pharmaceutics, 11*(3), 129. https://doi.org/10.3390/pharmaceutics11030129

Honary, S., & Zahir, F. (2013). Effect of zeta potential on the properties of nano-drug delivery systems - A review (Part 1). *Tropical Journal of Pharmaceutical Research, 12*(2), 255–264. https://doi.org/10.4314/tjpr.v12i2.21

Hou, D., Gui, R., Hu, S., Huang, Y., Feng, Z., & Ping, Q. (2015). Preparation and characterization of novel drug-inserted-montmorillonite chitosan carriers for ocular drug delivery. *Advances in nanoparticles*, *4*(03), 70-84.

How, K. Y., Song, K. P., & Chan, K. G. (2016). *Porphyromonas gingivalis*: An overview of periodontopathic pathogen below the gum line. *Frontiers in Microbiology*, *7*(FEB), 1–14. https://doi.org/10.3389/fmicb.2016.00053

Hung, M., Kelly, R., Mohajeri, A., Reese, L., Badawi, S., Frost, C., Sevathas, T., & Lipsky, M. S. (2023). Factors associated with periodontitis in younger individuals: A scoping review. *Journal of Clinical Medicine*, *12*(20). https://doi.org/10.3390/jcm-12206442

Hudieb, M., Haddad, A., Bakeer, M., Alkhazaaleh, A., AlKhader, M., Taani, D., & Kasugai, S. (2021). Influence of age on calvarial critical size defect dimensions: A radiographic and histological study. *Journal of Craniofacial Surgery*, 32(8), 2896–2900. https://doi.org/10.1097/SCS.0000000000007690

Huq, T. F., Khan, A., Khan, R. A., & Chowdhury, S. (2022). Sources, production and commercial applications of fungal chitosan: A review. *Journal of Bioresources and Bioproducts, 7*(2), 85–98. https://doi.org/10.1016/j.jobab.2022.01.002

Ibrahim, H. M., El-Bisi, M. K., Taha, G. M., & El-Alfy, E. A. (2015). Chitosan nanoparticles loaded

antibiotics as drug delivery biomaterial. *Journal of Applied Pharmaceutical Science*, 5(10), 85–90. https://doi.org/10.7324/JAPS.2015.501015

Ibrahim, S. M., Al-Mizraqchi, A. S., & Haider, J. (2023). Synergistic antimicrobial and antibiofilm activity of panax ginseng, symphytum officinale, and metronidazole against *P. gingivalis*. *Antibiotics*, 12(8), 1234. https://doi.org/10.20944/preprints20-2308.1409.v1

Ielo, I., Calabrese, G., De Luca, G., & Conoci, S. (2022). Recent Advances in Hydroxyapatite-Based Biocomposites for Bone Tissue Regeneration in Orthopedics. *International Journal of Molecular Sciences*, *23*(17). https://doi-.org/10.3390/ijms23179721

Ikada, Y. (2006). Challenges in tissue engineering. *Journal of the Royal Society Interface*, *3*(10), 589–601. https://doi.org/10.1098/rsif.2006.0124

Inside Therapeutics. (2024). *LNP and liposomes characterization guidelines*. Retrieved from https://insidetx.com/review/lnp-and-liposomes-characterization-guidelines/

Irastorza, A., Zarandona, I., Andonegi, M., Guerrero, P., & de la Caba, K. (2021). The

versatility of collagen and chitosan: From food to biomedical applications. *Food Hydrocolloids*, *116*, 106633. https://doi.org/10.1016/j.foodhyd.2021.106633

Ismail, A. F. H., Mohamed, F., Rosli, L. M. M., Shafri, M. A. M., Haris, M. S., & Adina, A. B. (2016). Spectrophotometric determination of dentamicin loaded PLGA microparticles and method validation via ninhydrin-gentamicin complex as a rapid quantification approach. *Journal of Applied Pharmaceutical Science*, *6*(1), 007–014. https://doi.org/10.7324/JAPS.2016.600102

Jackson, T. C., Agboke, A. A., Udofa, E. J., Ucheokoro, A. S., Udo, B. E., & Ifekpolugo, N. L. (2019). Characterization and release kinetics of metronidazole loaded silver nanoparticles prepared from carica papaya leaf extract. *Advances in Nanoparticles*, *8*(03), 47–54. https://doi.org/10.4236/anp.2019.83004

Jafernik, K., Ładniak, A., Blicharska, E., Czarnek, K., Ekiert, H., Wiącek, A. E., & Szopa, A. (2023). Chitosan-based nanoparticles as effective drug delivery systems—a review. *Molecules*, *28*(4), 1963. https://doi.org/10.3390/molecules28041963

Jain, N., Jain, G. K., & Ahmad, F. J. (2020). Antibiotic-loaded biopolymeric scaffolds for periodontal regeneration: A review. *Expert Opinion on Drug Delivery*, *17*(3), 329–345. https://doi.org/10.1080/17425247.2020.1723889

Jang, Y. S., Moon, S. H., Nguyen, T. D. T., Lee, M. H., Oh, T. J., Han, A. L., & Bae, T. S. (2019). *In vivo* bone regeneration by differently designed titanium membrane with or without surface treatment: A study in rat calvarial defects. *Journal of Tissue Engineering*, *10*. https://doi.org/10.1177/2041731419831466

Japanese Pharmacopoeia. (2021). *Metronidazole monograph (JP XVII)*. Retrieved from https://jpdb.nihs.go.jp/jp14e/14data/Part-I/Metronidazole.pdf

Jepsen, K., Falk, W., Brune, F., Mutters, R., & Jepsen, S. (2021). Prevalence and antibiotic susceptibility trends of periodontal pathogens in the subgingival microbiota of German periodontitis patients: A retrospective surveillance study. *Journal of Clinical Periodontology*, *48*(9), 1216–1227. https://doi.org/10.1111/jcpe.13499

Jha, R., & Mayanovic, R. A. (2023). A review of the preparation, characterization, and applications of chitosan nanoparticles in nanomedicine. *Nanomaterials*, *13*(8), 1302. https://doi.org/10.3390/nano13081302

Jiang, Y., Huang, J., Wu, X., Ren, Y., Li, Z., & Ren, J. (2020). Controlled release of silver

ions from AgNP-loaded konjac glucomannan–chitosan hydrogel for infected wound healing. *International Journal of Biological Macromolecules, 149*, 148–157. https://doi.org/10.1016/j.ijbiomac.2020.01.221

Jiang, Z., Zheng, Z., Yu, S., Gao, Y., Ma, J., Huang, L., & Yang, L. (2023). Nanofiber scaffolds as drug delivery systems promoting wound healing. In *Pharmaceutics 15*(7). https://doi.org/10.3390/pharmaceutics15071829

Johnson, C. T., & García, A. J. (2015). Scaffold-based anti-infection strategies in bone repair. *Annals of Biomedical Engineering*, *43*(3), 515–528.https://doi,org/10.1007/s10439-014-1205-3

Justesen, U. S., Åhman, J., Matuschek, E., & Kahlmeter, G. (2023). Assessing the quality of the anaerobic environment — a method developed to support EUCAST disk diffusion of anaerobic bacteria. *European Journal of Clinical Microbiology and Infectious Diseases*, *42*(7), 895–898. https://doi.org/10.1007/s10096-023-04622-9

Kaczmarek-Szczepańska, B., Polkowska, I., Paździor-Czapula, K., Nowicka, B., Gierszewska, M., Michalska-Sionkowska, M., & Otrocka-Domagała, I. (2023). Chitosan/phenolic compounds scaffolds for connective tissue regeneration. *Journal of Functional Biomaterials, 14*(2), 69. https://doi.org/10.3390/jfb14020069

Kademani, B. S., Singh, G., & Verma, S. (2024). Emerging therapies in periodontitis: Role of photodynamic treatment. *British Dental Journal*, 236(5), 205–209. https://doi.org/10.1038/s41415-024-8205-y

Kalyane, D., Raval, N., Maheshwari, R., Tambe, V., & Tekade, R. K. (2020). Development of metronidazole-loaded chitosan nanoparticles using QbD approach: A novel and potential antibacterial formulation. *ResearchGate Preprint*. https://www.researchgate.net/publication/344385393

Karimi, M., Avci, P., Ahi, M., Gazori, T., Hamblin, M., & Naderi-Manesh, H. (2018). Evaluation of chitosan-tripolyphosphate nanoparticles as a p-shRNA delivery vector: Formulation, optimization and cellular uptake study. *Physiology & Behavior*, *176*(5), 139–148. https://doi.org/10.4049/jimmunol.1801473

Kashte, S., Dhumal, R., Chaudhary, P., Sharma, R. K., Dighe, V., & Kadam, S. (2021). Bone regeneration in critical-size calvarial defect using functional biocompatible osteoinductive herbal scaffolds and human umbilical cord Wharton's Jelly-derived

mesenchymal stem cells. *Materials Today Communications*, *26*, 102049. https://doi.org/10.1016/j.mtcomm.2021.102049

Kass, L. E., & Nguyen, J. (2022). Nanocarrier-hydrogel composite delivery systems for precision drug release. *Wiley Interdisciplinary Reviews: Nanomedicine and Nanobiotechnology*, *14*(2). https://doi.org/10.1002/wnan.1756

Katas, H., Raja, M. A. G., & Lam, K. L. (2013). Development of chitosan nanoparticles as a stable drug delivery system for protein/siRNA. *International Journal of Biomaterials*, *2013*. https://doi.org/10.1155/2013/146320

Kaur, S., Narang, R. K., & Aggarwal, G. (2017). Formulation and development of colon-targeted mucopenetrating metronidazole nanoparticles. *Tropical Journal of Pharmaceutical Research*, *16*(5), 967–973. https://doi.org/10.4314/tjpr.v16i5.1

Kyykallio, H., Oikari, S., Álvez, M. B., Dodd, C. J. G., Capra, J., & Rilla, K. (2020). The density and length of filopodia associate with the activity of hyaluronan synthesis in tumor cells. *Cancers*, *12*(7), 1–14. https://doi.org/10.3390/cancers12071908

Khabeer, A., Alam, B. F., Noreen, S., Faridi, M. A., & Ali, S. (2021a). Systemic and local delivery of antibiotics in managing periodontal diseases: An update. *Journal of Medical Sciences (Peshawar)*, *29*(3), 120125. https://doi.org/10.52764/JMS.12.29.3.13

Khan, G., Yadav, S. K., Patel, R. R., Nath, G., Bansal, M., & Mishra, B. (2016). Development and evaluation of biodegradable chitosan films of metronidazole and levofloxacin for the management of periodontitis. *AAPS PharmSciTech*, *17*(6), 1312–1325. https://doi.org/10.1208/s12249-015-0466-y

Kida, D., & Szulc, M. (2019). Metronidazole-loaded porous matrices for local periodontitis treatment: In vitro evaluation and *in vivo* pilot study. *Applied Sciences*, *9*(21), 4545. https://doi.org/10.3390/app9214545

Kim, H. S., Lee, S. H., Eun, C. J., Yoo, J., & Seo, Y. S. (2020). Dispersion of chitosan nanoparticles stable over a wide pH range by adsorption of polyglycerol monostearate. *Nanomaterials and Nanotechnology*, *10*, 1–9. https://doi.org/10.1177/1847980420917260

Kouhi, M., Morshed, M., Varshosaz, J., & Fathi, M. H. (2013). Poly (ε-caprolactone) incorporated bioactive glass nanoparticles and simvastatin nanocomposite

nanofibers: Preparation, characterization and *in vitro* drug release for bone regeneration applications. *Chemical Engineering Journal 228*, 1057-1065. https://doi.org/10.1016/j .cej.2013.05.091

Kumar, G., Chaudhary, K., Mogha, N. K., Kant, A., & Masram, D. T. (2021). Extended release of metronidazole drug using chitosan/graphene oxide bionanocomposite beads as the drug carrier. *ACS Omega, 6*(31), 20433–20444. https://doi.org/10.1021 /acsomega.1c02422

Kumar, M., & Awasthi, R. (2015). Development of metronidazole-loaded colon-targeted microparticulate drug delivery system. *Polimery w Medycynie, 45*(2), 57–65. https:/ /doi.org/10.17219/pim/60583

Kumar, P., Dehiya, B. S., & Sindhu, A. (2019). Ibuprofen-loaded CTS/nHA/nBG scaffolds for the applications of hard tissue engineering. *Iranian Biomedical Journal*, *23*(3), 190–199. https://doi.org/10.29252/.23.3.190

Kumar Reddy Sanapalli, B., Tyagi, R., Shaik, A. B., Pelluri, R., Bhandare, R. R., Annadurai, S., & Venkata Satyanarayana Reddy Karri, V. (2022). L-Glutamic acid loaded collagen chitosan composite scaffold as regenerative medicine for the accelerated healing of diabetic wounds. *Arabian Journal of Chemistry*, *15*(6), 103841. https://doi.org/10.1016/j.arabjc.2022.103841

Kwon, T. H., Lamster, I. B., & Levin, L. (2021). Current concepts in the management of periodontitis. International Dental Journal, 71(6), 462–476. https://doi.org/10.111 1/idj.12630

Kyykallio, H., Oikari, S., Álvez, M. B., Dodd, C. J. G., Capra, J., & Rilla, K. (2020). The density and length of filopodia associate with the activity of hyaluronan synthesis in tumor cells. *Cancers*, *12*(7), 1–14. https://doi.org/10.3390/cancers12071908

Labib, G. S., Aldawsari, H. M., & Badr-Eldin, S. M. (2014). Correction to: Metronidazole and pentoxifylline films for the local treatment of chronic periodontal pockets: Preparation, *in vitro* evaluation and clinical assessment. *Expert Opinion on Drug Delivery*, *11*(12), 1981. https://doi.org/10.1517/17425247.2014.986034

Lackington, W. A., Gehweiler, D., Zderic, I., Nehrbass, D., Zeiter, S., González-Vázquez, A., O'Brien, F. J., Stoddart, M. J., & Thompson, K. (2021). Incorporation of hydroxyapatite into collagen scaffolds enhances the therapeutic efficacy of rhBMP-

2 in a weight-bearing femoral defect model. *Materials Today Communications*, *29*(January 2022). https://doi.org/10.1016/j.mtcomm.2021.102933

Lansdown, A. B. G., Sampson, B., & Rowe, A. (2001). Experimental observations in the rat on the influence of cadmium on skin wound repair. *International Journal of Experimental Pathology*, *82*(1), 35–41. https://doi.org/10.1046/j.1365-2613.2001.008 0.x

Laurén, P., Paukkonen, H., Lipiäinen, T., Dong, Y., Oksanen, T., Räikkönen, H., Ehlers, H., Laaksonen, P., Yliperttula, M., & Laaksonen, T. (2018). Pectin and mucin enhance the bioadhesion of drug-loaded nanofibrillated cellulose films. *Pharmaceutical Research*, *35*(7). https://doi.org/10.1007/s11095-018-2428-z

Lazarević, M., Petrović, S., Pierfelice, T. V., Ignjatović, N., Piattelli, A., Tovilović, T. V., & Radunović, M. (2023). Antimicrobial and osteogenic effects of collagen membrane decorated with chitosan–nano-hydroxyapatite. *Biomolecules*, *13*(4), 579. https://doi.org/10.3390/biom13040579

Léber, A., Szücs, M. B., Urbán, E., Vályi, P., Gácsi, A., Berkó, S., Kovács, A., & Csányi, E. (2019). Combination of zinc hyaluronate and metronidazole in a lipid-based drug delivery system for the treatment of periodontitis. *Pharmaceutics*, *11*(3). https://doi.org/10.3390/pharmaceutics11030142

Lemke, K. A. (2004). Perioperative use of selective alpha-2 agonists and antagonists in small animals. *Canadian Veterinary Journal*, *45*(6), 475–480.

Le-Vinh, B., Le, N. M. N., Nazir, I., Matuszczak, B., & Bernkop-Schnürch, A. (2019). Chitosan based micelle with zeta potential changing property for effective mucosal drug delivery. *International Journal of Biological Macromolecules*, *133*, 647–655. https://doi.org/10.1016/j.ijbiomac.2019.04.115

Li, F., Li, J., Wen, X., Zhou, S., Tong, X., Su, P., Li, H., & Shi, D. (2009). Anti-tumor activity of paclitaxel-loaded chitosan nanoparticles: An *in vitro* study. *Materials Science and Engineering C*, *29*(8), 2392–2397. https://doi.org/10.1016/j/msec.2009.07.001

Li, J., Hao, X., Wang, C., Liu, H., Liu, L., He, X., & Sun, C. C. (2021). Improving the solubility, dissolution, and bioavailability of metronidazole via cocrystallisation with ethyl gallate. *Pharmaceutics*, *13*(4), 546. https://doi.org/10.3390/pharmaceutic

s13040546

Li, J., Wang, Y., Tang, M., et al. (2024). *New insights into nanotherapeutics for periodontitis: A triple concerto of antimicrobial activity, immunomodulation and periodontium regeneration*. *Journal of Nanobiotechnology*, *22*, 19. https://doi.org/10.1186/s12951-023-02261-y

Li, Y., Liu, Y., Li, R., & Lin, Y. (2021). Collagen-based biomaterials for bone tissue engineering. *Materials & Design, 210*, 110049. https://doi.org/10.1016/j.matdes.2-021.110049

Liang, H., Yin, J., Man, K., Yang, X. B., Calciolari, E., Donos, N., Russell, S. J., Wood, D. J., & Tronci, G. (2022). A long-lasting guided bone regeneration membrane from sequentially functionalised photoactive atelocollagen. *Acta Biomaterialia*, *140*, 190–205. https://doi.org/10.1016/j.actbio.2021.12.004

Liang, Y., Liang, Y., Zhang, H., & Guo, B. (2022). Antibacterial biomaterials for skin wound dressing. *Asian Journal of Pharmaceutical Sciences*, *17*(3), 353–384. https://doi.org/10.1016/j.ajps.2022.01.001

Lim, Y. S., Ok, Y. J., Hwang, S. Y., Kwak, J. Y., & Yoon, S. (2019). Marine collagen as a promising biomaterial for biomedical applications. *Marine Drugs*, *17*(8). https://doi.org/10.3390/md17080467

Liu, P., Li, Q., Yang, Q., Zhang, S., Lin, C., Zhang, G., & Tang, Z. (2020). Three-dimensional cell printing of gingival fibroblast/acellular dermal matrix/gelatin-sodium alginate scaffolds and their biocompatibility evaluation: *In vitro RSC Advances*, *10*(27), 15926–15935. https://doi.org/10.1039/d0ra02082f

Liu, X. et al. (2022). *Porous collagen–chitosan scaffolds as carriers for drug delivery and cell growth*. Carbohydrate Polymers, 278, 118974. https://doi.org/10.1016/j.carbpol .2021.118974

Liu, Y., Chen, H., He, J., Ye, D., Huang, Y., Zhao, Y., & Li, X. (2021). Integrated printed BDNF/collagen/chitosan scaffolds with low temperature extrusion 3D printer accelerated neural regeneration after spinal cord injury. *Regenerative Biomaterials*, *8*(6), rbab047. https://doi.org/10.1093/rb/rbab047

Löfmark, S., Edlund, C., & Nord, C. E. (2010). Metronidazole is still the drug of choice for treatment of anaerobic infections. *Clinical Infectious Diseases*, *50*(SUPP.1).

https://doi.org/10.1086/647939

Loh, Q. L., & Choong, C. (2013). Three-dimensional scaffolds for tissue engineering applications: Role of porosity and pore size. *Tissue Engineering - Part B: Reviews*, *19*(6), 485–502. https://doi.org/10.1089/ten.teb.2012.0437

Losi, P., Briganti, E., Errico, C., Lisella, A., Sanguinetti, E., Chiellini, F., & Soldani, G. (2013). Fibrin-based scaffold incorporating VEGF- and bFGF-loaded nanoparticles stimulates wound healing in diabetic mice. *Acta Biomaterialia*, *9*(8), 7814–7821. https://doi.org/10.1016/j.actbio.2013.04.019

Luo, C. J., Wightman, R., Meyerowitz, E., & Smoukov, S. K. (2015). A 3-dimensional fibre scaffold as an investigative tool for studying the morphogenesis of isolated plant cells. *BMC Plant Biology*, *15*(1), 1–15. https://doi.org/10.1186/s12870-015-0581-7

Lustriane, C., Dwivany, F. M., Suendo, V., & Reza, M. (2018). Effect of chitosan and chitosan-nanoparticles on post harvest quality of banana fruits. *Journal of Plant Biotechnology*, *45*(1), 36–44. https://doi.org/10.5010/JPB.2018.45.1.036

Lutzweiler, G., Halili, A. N., & Vrana, N. E. (2020). *The overview of porous, bioactive scaffolds as instructive biomaterials for tissue regeneration and their clinical translation*. *Pharmaceutics*, *12*(7), 602. https://doi.org/10.3390/pharmaceutics12070602

Ma, S., Adayi, A., Liu, Z., Li, M., Wu, M., Xiao, L., Sun, Y., Cai, Q., Yang, X., Zhang, X., & Gao, P. (2016). Asymmetric collagen/chitosan membrane containing minocycline- loaded chitosan nanoparticles for guided bone regeneration. *Scientific Reports*, *6*(July), 1–10. https://doi.org/10.1038/srep31822

Magliaro, C., Mattei, G., Iacoangeli, F., Corti, A., Piemonte, V., & Ahluwalia, A. (2019). Oxygen consumption characteristics in 3D constructs depend on cell density. *Frontiers in Bioengineering and Biotechnology*, *7*, 1–9. https://doi.org/10.3389/fbioe.2019.00251

Maitz, M. F. (2015). Applications of synthetic polymers in clinical medicine. *Biosurface and Biotribology*, *1*(3), 161–176. https://doi.org/10.1016/j.bsbt.2015.08.002

Malvern Panalytical. (n.d.). *Zeta potential - Overview*. Retrieved May 20, 2025, from https://www.malvernpanalytical.com/en/products/measurement-type/zeta-potential

Mamikutty, R., & Ng, C. W. (2022). Systemic antibiotics as an adjunct to subgingival debridement: A network meta-analysis. *Antibiotics*, 11(12), 1716. https://doi.org/1-0.3390/antibiotics11121716

Mao, J. S., Zhao, L. G., Yin, Y. J., & Yao, K. De. (2003). Structure and properties of bilayer chitosan-gelatin scaffolds. *Biomaterials*, *24*(6), https://doi.org/10.1067–1074.1016/S042-9612(02)00442-8

Marconi, G. D., Fonticoli, L., Rajan, T. S., Lanuti, P., Della Rocca, Y., Pierdomenico, S. D., Trubiani, O., Pizzicannella, J., & Diomede, F. (2021). Transforming growth factor-Beta1 and human gingival fibroblast-to-myofibroblast differentiation: Molecular and morphological modifications. *Frontiers in Physiology*, *12*, Article 676512. https://doi.org/10.3389/fphys.2021.676512

Marin, N., Moragón, A., Gil, D., García-García, F., & Bisbal, V. (2023). Acclimation and blood sampling: Effects on stress markers in C57BL/6J mice. *Animals, 13*(18), 2816. https://doi.org/10.3390/ani13182816

Martin, J. T., Milby, A. H., Ikuta, K., Poudel, S., Pfeifer, C. G., Elliott, D. M., ... & Mauck, R. L. (2015). A radiopaque electrospun scaffold for engineering fibrous musculoskeletal tissues: Scaffold characterization and *in vivo* applications. *Acta biomaterialia*, *26*, 97-104.

Martínez, A., Blanco, M. D., Davidenko, N., & Cameron, R. E. (2015). Tailoring chitosan/collagen scaffolds for tissue engineering: Effect of composition and different crosslinking agents on scaffold properties. *Carbohydrate Polymers*, *132*, 606–619. https://doi.org/10.1016/j.carbpol.2015.06.084

Masarudin, M. J., Cutts, S. M., Evison, B. J., Phillips, D. R., & Pigram, P. J. (2015). Factors determining the stability, size distribution, and cellular accumulation of small, monodisperse chitosan nanoparticles as candidate vectors for anticancer drug delivery: Application to the passive encapsulation of [14C]-doxorubicin. *Nanotechnology, Science and Applications,8,67–80*. https://doi.org/10/2147/NSA/S91785

Matawo, N., Adeleke, O. A., & Wesley-Smith, J. (2020). Optimal design, characterization and preliminary safety evaluation of an edible orodispersible formulation for pediatric tuberculosis pharmacotherapy. *International Journal of Molecular*

Sciences, *21*(16), 5714. https://doi.org/10.3390/ijms21165714

McGovern, J. A., Griffin, M., & Hutmacher, D. W. (2018). Animal models for bone tissue engineering and modelling disease. *DMM Disease Models and Mechanisms*, *11*(4). https://doi.org/10.1242/dmm.033084

Mehravani, M., Houshyar, E., Jamalnia, S. and Gharaaghaji, R. (2024). Effects of local and systemic metronidazole as adjunctive treatment in chronic periodontitis patients. *Clinical and Experimental Dental Research*, 10(6), e70050. https://doi.org/10.100-2/cre2.70050

Mei, L., Huang, X., Xie, Y., Chen, J., Huang, Y., Wang, B., Wang, H., Pan, X., & Wu, C. (2017). An injectable in situ gel with cubic and hexagonal nanostructures for local treatment of chronic periodontitis. *Drug Delivery*, *24*(1), 1148–1158. https://doi.org /10.1080/10717544.2017.1359703

Mikušová, V., & Mikuš, P. (2021). Advances in chitosan-based nanoparticles for drug delivery. *International Journal of Molecular Sciences*, *22*(17), 1–93. https://doi org/ 10.3390/ijms22179652

Ministry of Health Malaysia. *National Oral Health Survey of Adults (NOHSA) 2020*. Ministry of Health Malaysia, 2020

Mirzaeei, S., Mansurian, M., Asare-Addo, K., & Nokhodchi, A. (2021). Metronidazole- and amoxicillin-loaded PLGA and PCL nanofibers as potential drug delivery systems for the treatment of periodontitis: In vitro and *in vivo* evaluations. *Biomedicines*, *9*(8). https://doi.org/10.3390/biomedicines9080975

Mishra, A. K., Kumar, A., Mishra, A., & Mishra, H. V. (2014). Development of ultraviolet spectroscopic method for the estimation of metronidazole benzoate from pharmaceutical formulation. *Journal of Natural Science, Biology and Medicine*, *5*(2), 261–264. https://doi.org/10.4103/0976-9668.136154

Mndlovu, H., Kumar, P., du Toit, L. C., & Choonara, Y. E. (2024). A review of biomaterial degradation assessment approaches employed in the biomedical field. *NPJ Materials Degradation*, 8(1), 66. https://doi.org/10.1038/s41529-024-00487-1

Mo, X., Zhang, D., Liu, K., Zhao, X., Li, X., & Wang, W. (2023). Nano-hydroxyapatite composite scaffolds loaded with bioactive factors and drugs for bone tissue engineering. *International Journal of Molecular Sciences*, *24*(2). https://doi.org/10.

3390/ijms24021291

Mohammed, M. A., Syeda, J. T. M., Wasan, K. M., & Wasan, E. K. (2017). An overview of chitosan nanoparticles and its application in non-parenteral drug delivery. *Pharmaceutics*, *9*(4). https://doi.org/10.3390/pharmaceutics9040053

Mohan, S., Karunanithi, P., Raman Murali, M., Anwar Ayob, K., Megala, J., Genasan, K., Kamarul, T., & Balaji Raghavendran, H. R. (2022). Potential use of 3D CORAGRAF- loaded PDGF-BB in PLGA microsphere seeded mesenchymal stromal cells in enhancing the repair of calvaria critical-size bone defect in rat model. *Marine Drugs*, *20*(9), 1–11. https://doi.org/10.3390/md20090561

Mondal, N., Pal, T. K., & Ghosal, S. K. (2007). Development and validation of a spectrophotometric method for estimation of letrozole in bulk and pharmaceutical formulation. *Pharmazie*, *62*(8), 597–598. https://doi.org/10.1691/ph.2007.8.6305

Moody, C. M., Chua, B., & Weary, D. M. (2014). The effect of carbon dioxide flow rate on the euthanasia of laboratory mice. *Laboratory Animals*, *48*(4), 298–304. https://doi.org/10.1177/0023677214546509

Mugri, M. H. (2022). Efficacy of systemic amoxicillin–metronidazole in periodontitis patients with diabetes mellitus: A systematic review of randomised clinical trials. *Medicina*, 58(11), 1605. https://doi.org/10.3390/medicina58111605

Muhsin, M. D. A., George, G., Beagley, K., Ferro, V., Wang, H., & Islam, N. (2016). Effects of chemical conjugation of l -leucine to chitosan on dispersibility and controlled release of drug from a nanoparticulate dry powder inhaler formulation. *Molecular Pharmaceutics*, *13*(5), 1455–1466. https://doi.org/10.1021/as.molpharmaceut.5b00859

Mukherjee, P., Roy, S., Ghosh, D., & Nandi, S. K. (2022). Role of animal models in biomedical research: a review. *Laboratory Animal Research*, *38*(1), 1–17. https://doi.org/10.1186/s42826-022-00128-1

Munk, A., Philippi, V., Buchecker, V., Bankstahl, M., Glasenapp, A., Blutke, A., Michelakaki, E., Talbot, S. R., Huwyler, J., Jirkof, P., Kopaczka, M., Merhof, D., Palme, R., & Potschka, H. (2024). Refining pain management in mice by comparing multimodal analgesia and NSAID monotherapy for neurosurgical procedures. *Scientific Reports*, *14*,

Nair, S. C., & Anoop, K. R. (2012). Intraperiodontal pocket: An ideal route for local antimicrobial drug delivery. *Journal of Advanced Pharmaceutical Technology and Research*, *3*(1), 9–15. https://doi.org/10.4103/2231-4040.93558

Namazi, H., Hasani, M., & Yadollahi, M. (2019). Antibacterial oxidized starch/ZnO nanocomposite hydrogel: Synthesis and evaluation of its swelling behaviours in various pHs and salt solutions. *International Journal of Biological Macromolecules*, *126*, 578–584. https://doi.org/10.1016/j.ijbiomac.2018.12.242

Nastri, L., De Rosa, A., De Gregorio, V., Grassia, V., & Donnarumma, G. (2019). A New Controlled-Release Material Containing Metronidazole and Doxycycline for the Treatment of Periodontal and Peri-Implant Diseases: Formulation and *in Vitro* Testing. *International Journal of Dentistry*, *2019*.

Nature Communications. (2023). A review of biomaterial degradation assessment approaches. *Nature Communications*, 14, Article 487. https://www.nature.com/articles/s41529-024-00487-1

Nath, S., Kalmodia, S., & Basu, B. (2013). *In vitro* biocompatibility of novel biphasic calcium phosphate-mullite composites. Journal of Biomaterials Applications, 27(5), 497–509. https://doi.org/10.1177/0885328211412206

Needleman, I., Worthington, H. V, Giedrys-Leeper, E., & Tucker, R. (2006). Guided tissue regeneration for periodontal infra-bony defects. *Cochrane Database of Systematic Reviews*, *4*. https://doi.org/10.1002/14651858.cd001724.pub2

Negut, I., Dorcioman, G., & Grumezescu, V. (2020). Scaffolds for Wound Healing Applications. *Polymers*, *12*(9), 2010. https://doi.org/10.3390/polym12092010

Nicolaescu, O. E., Belu, I., Mocanu, A. G., Manda, V. C., Rău, G., Pîrvu, A. S., Ionescu, C., Ciulu-Costinescu, F., Popescu, M., & Ciocîlteu, M. V. (2025). Cyclodextrins: Enhancing drug delivery, solubility and bioavailability for modern therapeutics. *Pharmaceutics, 17*(3), 288. https://doi.org/10.3390/pharmaceutics17030288

Nikolova, M. P., & Chavali, M. S. (2019). Recent advances in biomaterials for 3D scaffolds: A review. *Bioactive Materials, 4*, 271–292. https://doi.org/10.1016/j.bioactmat.2019.10.005

Nokoorani, Y. D., Shamloo, A., Bahadoran, M., & Moravvej, H. (2021). Fabrication and characterization of scaffolds containing different amounts of allantoin for skin

tissue engineering. *Scientific Reports*, *11*(1), 1–33. https://doi.org/10.1038/s41598-021-95763-4

Nurilmala, M., Suryamarevita, H., Husein Hizbullah, H., Jacoeb, A. M., & Ochiai, Y. (2022). Fish skin as a biomaterial for halal collagen and gelatin. *Saudi Journal of Biological Sciences*, *29*(2), 1100–1110. https://doi.org/10.1016/j.sjbs.2021.09.056

Nyman, S. (1991). Bone regeneration using the principle of guided tissue regeneration. *Journal of Clinical Periodontology*, *18*(6), 494–498.https://doi.org/10.1111/j.1600-051X.1991.tb02322.x

O'Brien, F. J. (2011). Biomaterials & scaffolds for tissue engineering. *Materials Today*, *14*(3), 88–95. https://doi.org/10.1016/S1369-7021(11)70058-X

Oh, J. W., Chun, S. C., & Chandrasekaran, M. (2019). Preparation and *in vitro* characterization of chitosan nanoparticles and their broad-spectrum antifungal action compared to antibacterial activities against phytopathogens of tomato. *Agronomy*, *9*(1). https://doi.org/10.3390/agronomy9010021

Olaitan, A. O., Dureja, C., Youngblom, M. A., Topf, M. A., Gonzales-Luna, A. J., Deshpande, A., Hevener, K. E., Freeman, J., Wilcox, M. H., Palmer, K. L., Garey, K. W., Pepperell, C. S., & Hurdle, J. G. (2023). Decoding a cryptic mechanism of metronidazole resistance among globally disseminated fluoroquinolone-resistant *Clostridioides difficile*. *Nature Communications*, *14*, 4130. https://doi.org/10.1038/s41467-023-39429-x

Oliveira, A., Araújo, A., Rodrigues, L. C., Silva, C. S., Reis, R. L., Neves, N. M., Leão, P., & Martins, A. (2022). Metronidazole delivery nanosystem Able to reduce the pathogenicity of bacteria in colorectal infection. *Biomacromolecules*, *23*(6), 2415–2427. https://doi.org/10.1021/acs.biomac.2c00186

Oliveira, P. N., Montembault, A., Sudre, G., Alcouffe, P., Marcon, L., Lux, F., Albespy, K., Centis, V., Campos, D., Oliveira, P. N., Montembault, A., Sudre, G., Alcouffe, P., & Marcon, L. (2021). Self-crosslinked fibrous collagen / chitosan blends: Processing, properties evaluation and monitoring of degradation by bi-fluorescence imaging. *HAL Id: hal-02335447*.0–35.

Omar Zaki, S. S., Ibrahim, M. N., & Katas, H. (2015). Particle size affects concentration-dependent cytotoxicity of chitosan nanoparticles towards mouse hematopoietic

stem cells. *Journal of nanotechnology*, *2015*(1), 919658.

Ono, M., Sonoyama, W., Nema, K., Hara, E. S., Oida, Y., Pham, H. T., Yamamoto, K., Hirota, K., Sugama, K., Sebald, W., & Kuboki, T. (2014). Regeneration of calvarial defects with escherichia coli-derived rhBMP-2 adsorbed in PLGA Membrane. *Cells Tissues Organs*, *198*(5), 367–376. https://doi.org/10.1159/000356947

Öztürk, K., Kaplan, M., & Çalış, S. (2024). Effects of nanoparticle size, shape, and zeta potential on drug delivery. *International Journal of Pharmaceutics*, *124799*. https://doi.org/10.1016/j.ijpharm.2024.124799

Pacheco, F., Barrera, A., Ciro, Y., Polo-Cerón, D., Salamanca, C. H., & Oñate-Garzón, J. (2024). Synthesis, Characterization, and Biological Evaluation of Chitosan Nanoparticles Cross-Linked with Phytic Acid and Loaded with Colistin against Extensively Drug-Resistant Bacteria. *Pharmaceutics*, 16(9), 1115. https://doi.org/10.3390/pharmaceutics16091115

Pahuja, B. K. (2019). Implementing mass level strategies towards prevention of periodontal disease. In *Biomedical Journal of Scientific & Technical Research 20*(1). https://doi.org/10.26717/bjstr.2019.20.003386

Parenteau-Bareil, R., Gauvin, R., & Berthod, F. (2010). Collagen-based biomaterials for tissue engineering applications. *Materials*, *3*(3), 1863–1887. https://doi.org/10.3390/ma3031863

Park, J. H., Jiang, Y., Zhou, J., Gong, H., Mohapatra, A., Heo, J., Gao, W., Fang, R. H., & Zhang, L. (2021). Genetically engineered cell membrane-coated nanoparticles for targeted delivery of dexamethasone to inflamed lungs. *Science Advances, 7*(25), eabf7820. https://doi.org/10.1126/sciadv.abf7820

Patterson, J., Martino, M. M., & Hubbell, J. A. (2010). Biomimetic materials in tissue engineering. *Materials Today*, *13*(1–2), 14–22. https://doi.org/10.1016/S1369-7021(10)70013-4

Pawar, H. V., Narkhede, M. R., Jain, S. P., Patel, S., & Waghmare, S. (2023). Chitosan: A potential biopolymer in drug delivery and biomedical applications. *Pharmaceutics*, *15*(4), 1313. https://doi.org/10.3390/pharmaceutics15041313

Peerapattana, J., Ngamsupsiri, T., Cheucharoenvasuchai, N., & Saikaew, C. (2015). Optimization of metronidazole sustained-release films using D-optimal design.

International Journal of Pharmaceutics, *484*(1–2), 1–7. https://doi.org/10.1016/j.ijpharm.2015.02.019

Pérez-Pacheco, Y., Tylkowski, B., & García-Valls, R. (2025). Chitosan micro/nanocapsules in action: Linking design, production, and therapeutic application. *Molecules, 30*(2), 252. https://doi.org/10.3390/molecules30020252

Petersen, P. E., & Ogawa, H. (2005). Strengthening the Prevention of Periodontal Disease: The WHO Approach. *Journal of Periodontology*, *76*(12), 2187–2193. https://doi.org/10.1902/jop.2005.76.12.2187

Phaechamud, T. and Mahadlek, J. (2018). Preparation and evaluation of metronidazole-loaded pectin films for potentially targeting a microbial infection associated with periodontal disease. *Polymers*, 10(9), 1021. https://doi.org/10.3390polym10091021

Pham, D. T., Phewchan, P., Navesit, K., Chokamonsirikun, A., Khemwong, T., & Tiyaboonchai, W. (2021). Development of metronidazole-loaded in situ thermosensitive hydrogel for periodontitis treatment. *Turkish Journal of Pharmaceutical Sciences*, *18*(4), 510–516. https://doi.org/10.4274/tjps.galenos.2020.09623

Piszko, P. J., Piszko, A., Kiryk, S., et al. (2024). *Bone regeneration capabilities of scaffolds containing chitosan and nanometric hydroxyapatite—Systematic review based on in vivo examinations*. *Biomimetics*, *9*(8), 503. https://doi.org/10.3390/ biomimetics 9080503

Porgham Daryasari, M., Dusti Telgerd, M., Hossein Karami, M., Zandi-Karimi, A., Akbarijavar, H., Khoobi, M., Seyedjafari, E., Birhanu, G., Khosravian, P., & SadatMahdavi, F. (2019). Poly-l-lactic acid scaffold incorporated chitosan-coated mesoporous silica nanoparticles as pH-sensitive composite for enhanced osteogenic differentiation of human adipose tissue stem cells by dexamethasone delivery. *Artificial Cells, Nanomedicine and Biotechnology*, *47*(1), 4020–4029. https://doi.org/10.1080/21691401.2019.1658594

Potrč, T., Baumgartner, S., Roškar, R., Planinšek, O., Lavrič, Z., Kristl, J., & Kocbek, P. (2015). Electrospun polycaprolactone nanofibers as a potential oromucosal delivery system for poorly water-soluble drugs. *European Journal of Pharmaceutical Sciences*, *75*, 101–113. https://doi.org/10.1016/j.ejps.2015.04.004

Potschka, H. (2024). Refining pain management in mice by comparing multimodal analgesia and NSAID monotherapy for neurosurgical procedures. *Scientific Reports, 14*, 18691. https://doi.org/10.1038/s41598-024-69075-2

Preshaw, P. M., Alba, A. L., Herrera, D., Jepsen, S., Konstantinidis, A., Makrilakis, K., & Taylor, R. (2012). Periodontitis and diabetes: A two-way relationship. *Diabetologia*, *55*(1), 21–31. https://doi.org/10.1007/s00125-011-2342-y

Priya, G., Madhan, B., Narendrakumar, U., Suresh Kumar, R. V., & Manjubala, I. (2021). *In vitro* and *in vivo* Evaluation of Carboxymethyl Cellulose Scaffolds for Bone Tissue Engineering Applications. *ACS Omega*, *6*(2), 1246–1253. https://doi.org/10.1021/acsomega.0c04551

Przybylek, M., & Beldowski, P. (2023). Molecular dynamics simulations of the affinity of chitin and chitosan for collagen: The effect of pH and the presence of sodium and calcium cations. *arXiv preprint arXiv:2310.04143*. https://arxiv.org/abs/2310.04143

Przybyłek, M., Bełdowski, P., Wieland, F., Cysewski, P., & Sionkowska, A. (2023). Collagen type II–chitosan interactions as dependent on hydroxylation and acetylation: Insights from molecular dynamics simulations. *Molecules*, *28*(1), 154. https://doi.org/10.3390/molecules28010154

Qasim, S. B., Delaine-Smith, R. M., Fey, T., Rawlinson, A., & Rehman, I. U. (2015). Freeze gelated porous membranes for periodontal tissue regeneration. *Acta Biomaterialia*, *23*, 317–328. https://doi.org/10.1016/j.actbio.2015.05.001

Queiroz, M. F., Melo, K. R. T., Sabry, D. A., Sassaki, G. L., & Rocha, H. A. O. (2015). Does the use of chitosan contribute to oxalate kidney stone formation? *Marine Drugs*, *13*(1), 141–158. https://doi.org/10.3390/md13010141

Rabie, A. M. I., Ali, A. S. M., Al-Zeer, M. A., Barhoum, A., El-Hallouty, S., Shousha, W. G., Berg, J., Kurreck, J., & Khalil, A. S. G. (2022). Spontaneous formation of 3D breast cancer tissues on electrospun chitosan/poly(ethylene oxide) nanofibrous scaffolds. *ACS Omega*, 7(2), https://doi.org/2114–2126.10.1021/acsmega.1c05646

Rad, J., Quispe, C., Butnariu, M., Rotariu, L. S., Sytar, O., Sestito, S., Rapposelli, S., Akram, M., Iqbal, M., Krishna, A., Kumar, N. V. A., Braga, S. S., Cardoso, S. M., Jafernik, K., Ekiert, H., Cruz-Martins, N., Szopa, A., Villagran, M., Mardones,

L., & Calina, D. (2021). Chitosan nanoparticles as a promising tool in nanomedicine with particular emphasis on oncological treatment. *Cancer Cell International, 21*(1), 1–21. https://doi.org/10.1186/s12935-021-02025-4

Rahbari, M., Rahlfs, S., Jortzik, E., Bogeski, I., & Becker, K. (2017). H2O2 dynamics in the malaria parasite Plasmodium falciparum. *PLoS ONE*, *12*(4), 2–5. https://doi.org/10.1371/journal

Rajitha, K., Prasanna, N. L., Vasundhara, G., Kumar, R. N., & Kumar, A. A. (2014). UV spectrophotometric method development and validation for the simultaneous quantitative estimation of mebeverine hydrochloride and chlordiazepoxide in capsules. *International Journal of Pharmacy and Pharmaceutical Sciences, 6,* 345–349.

Rambhia, K. J., & Ma, P. X. (2015). Controlled drug release for tissue engineering. *Journal of Controlled Release, 219*, 119–128. https://doi.org/10.1016/j.jconrel.2015.08.049

Rams, T. E., Degener, J. E., & van Winkelhoff, A. J. (2020). Comparative in vitro resistance of human periodontal bacterial pathogens to tinidazole and four other antibiotics. *Antibiotics, 9*(2), 68. https://doi.org/10.3390/antibiotics9020068

Rams, T. E., Degener, J. E., & van Winkelhoff, A. J. (2023). Emergence of antibiotic-resistant *Porphyromonas gingivalis* in United States periodontitis patients. *Antibiotics, 12*(11), 1584. https://doi.org/10.3390/antibiotics12111584

Rangabhatla, A. S. L., Tantishaiyakul, V., Boonrat, O., Hirun, N., & Ouiyangkul, P. (2017). Novel in situ mucoadhesive gels based on Pluronic F127 and xyloglucan containing metronidazole for treatment of periodontal disease. *Iranian Polymer Journal (English Edition), 26*(11), 851–859. https://doi.org/10.1007/s13726-017-0569-2

Rao, S. K., Jaison, D., Sridhar, K., Kasthuri, N., Gopinath, V., Sivaperumal, P., & Patil, S. (2020). Melatonin delivery from PCL scaffold enhances glycosaminoglycans deposition in human chondrocytes – Bioactive scaffold model for cartilage regeneration. *Process Biochemistry*, *99*, 36–47. https://doi.org/10.1016/j.procbio.2020.08.015

Rasni, H., Ervina, I., & Ilyas, S. (2018). *In vitro* chitosan hydrogel based metronidazole cytotoxicity test on 3t3 fibroblast viability. *International Conference on Innovative Design and Manufacturing (IDSM), 44*. https://doi.org/10.2991/idsm-

17.2018.44

Reise, M., Wyrwa, R., Müller, U., Zylinski, M., Völpel, A., Schnabelrauch, M., Berg, A., Jandt, K. D., Watts, D. C., & Sigusch, B. W. (2012). Release of metronidazole from electrospun poly(l-lactide-co-d/l-lactide) fibers for local periodontitis treatment. *Dental Materials*, *28*(2), 179–188. https://doi.org/10.1016/j.dental.2011.12.006

Ren, T., Hu, M., Cheng, Y., Shek, T. L., Xiao, M., Ho, N. J., Zhang, C., Leung, S. S. Y., & Zuo, Z. (2019). Piperine-loaded nanoparticles with enhanced dissolution and oral bioavailability for epilepsy control. *European Journal of Pharmaceutical Sciences, 137*, 104988. https://doi.org/10.1016/j.ejps.2019.104988

Retzepi, M., & Donos, N. (2010). Guided Bone Regeneration: Biological principle and therapeutic applications. *Clinical Oral Implants Research*, *21*(6), 567–576. https://doi.org/10.1111/j.1600-0501.2010.01922.x

Rezwan, K., Chen, Q. Z., Blaker, J. J., & Boccaccini, A. R. (2006). Biodegradable and bioactive porous polymer/inorganic composite scaffolds for bone tissue engineering. *Biomaterials*, *27*(18), 3413–3431. https://doi.org/10.1016/j.biomaterials.2006.01.039

Ribeiro, E. F., de Barros-Alexandrino, T. T., Assis, O. B. G., Junior, A. C., Quiles, A., Hernando, I., & Nicoletti, V. R. (2020). Chitosan and crosslinked chitosan nanoparticles: Synthesis, characterization and their role as Pickering emulsifiers. *Carbohydrate Polymers, 250*, 116878. https://doi.org/10.1016/j.carbpol.2020.116878

Rinwa, P., Eriksson, M., Cotgreave, I., & Bäckberg, M. (2024). 3R-refinement principles: Elevating rodent well-being and research quality. *Laboratory Animal Research, 40*, 11. https://doi.org/10.1186/s42826-024-00198-3

Rivis, M., Simonca, A. G., Marin, M. M., Valeanu, A. N., Rau, I., Albu Kaya, M. G., Ianes, E., Chelaru, C., Pirvu, C. D., & Ghica, M. V. (2018). New treatment for dentistry regeneration based on metronidazole release from collagen/strontium sponges. *Materiale Plastice*, *55*(2), 243–246. https://doi.org/10.37358/MP.18.2.5006

Rodrigues, M., Cunha, D., Latorre, F., Maia, M., Iatecola, A., Massimino, C., Maria, A., Plepis, D. G., Navarro, D., Rocha, D., Mariano, E. D., Muniz, R., Eduarda, B., Oliveira, G. De, & Pelegrine, A. (2023). *In vivo* vvaluation of collagen and chitosan

scaffold, associated or not with stem cells in bone repair. *Journal of Biomedical Materials Research Part B: Applied Biomaterials*, *111*(1), 1–12. https://doi.org/10.1002/jbm.b.34874

Rodríguez-Vázquez, M., Vega-Ruiz, B., Ramos-Zúñiga, R., Saldaña-Koppel, D. A., & Quiñones-Olvera, L. F. (2015). Chitosan and its potential use as a scaffold for tissue engineering in regenerative medicine. *BioMed Research International*, *2015*. https://doi.org/10.1155/2015/821279

Ruchika, & Himanshi. (2019). Formulation and Evaluation of Metronidazole Loaded Chitosan Nanoparticles. *International Journal of Applied Pharmaceutics*, *11*(3), 49-52. https://doi.org/10.22159/ijap.2019v11i3.31932

Russell, W. M. S., & Burch, R. L. (1959). *The principles of humane experimental technique*. London: Methuen.

Saczko, J., Dominiak, M., Kulbacka, J., Chwiłkowska, A., & Krawczykowska, H. (2008). A simple and established method of tissue culture of human gingival fibroblasts for gingival augmentation. *Folia Histochemica et Cytobiologica*, *46*(1), 117–119. https://doi.org/10.2478/v10042-008-0017-4

Sahai, N., Ahmad, N., & Gogoi, M. (2018). Nanoparticles based drug delivery for tissue regeneration using biodegradable scaffolds: A review. *Current Pathobiology Reports*, *6*(4), 219–224. https://doi.org/10.1007/s40139-018-0184-8

Saini, R., Saini, S., & Saini, S. R. (2010). Periodontitis: A risk for delivery of premature labor and low-birth-weight infants. *Journal of Natural Science, Biology and Medicine*, *1*(1), 40–42. https://doi.org/10.4103/0976-9668.71672

Sakhi, M., Khan, A., Iqbal, Z., Khan, I., Raza, A., Ullah, A., Nasir, F., & Khan, S. A. (2022). Design and characterization of paclitaxel-loaded polymeric nanoparticles decorated with trastuzumab for the effective treatment of breast cancer. *Frontiers in Pharmacology*, *13*, 1–15. https://doi.org/10.3389/fphar.2022.855294

Salgado-Peralvo, A. O., Peña-Cardelles, J. F., Kewalramani, N., Mateos-Moreno, M. V., Jiménez-Guerra, Á., Velasco-Ortega, E., Uribarri, A., Moreno-Muñoz, J., Ortiz-García, I., Núñez-Márquez, E., & Monsalve-Guil, L. (2022). Preventive antibiotic therapy in the placement of immediate implants: A systematic review. *Antibiotics*, *11*(1). https://doi.org/10.3390/antibiotics11010005

Salis, A., et al. (2021). The MTT assay: Utility, limitations, pitfalls, and interpretation in bulk and single-cell analysis. *International Journal of Molecular Sciences*, *22*(23), 12827. https://doi.org/10.3390/ijms222312827

Salvi, G. E., Roccuzzo, A., Imber, J. C., Stähli, A., Klinge, B., & Lang, N. P. (2023). Clinical periodontal diagnosis. *Periodontology 2000*, *92*(1), 1–19. https://doi.org/10.1111/prd.12435

Sánchez-Carreño López, M. R., Gómez-López, V. M., Mercader-Ros, M. T., Lucas-Abellán, C., Silva-Cullishpuma, D. A., Velasquez, P., Salazar, K., & Maté Sánchez de Val, J. E. (2025). Antimicrobial properties of different multilayered scaffolds complexed with metronidazole and metronidazole-ozone. *Boletín de la Sociedad Española de Cerámica y Vidrio, 64*. https://doi.org/10.1016/j.bsecv.2025.03.002

Sánchez-Carreño López, M., Rodríguez-Alonso, L., Beltrán, A. M., & Osorio, R. (2025). Antimicrobial properties of multilayered scaffolds loaded with metronidazole and ozone for bone regeneration. *Boletín de la Sociedad Española de Cerámica y Vidrio*. https://www.elsevier.es/es-revista-boletin-sociedad-espanola-ceramica-vidrio-26-avance-resumen-antimicrobial-properties-different-multilayered-scaffolds-S0366317525000159

Sangnim, T., Dheer, D., Jangra, N., Huanbutta, K., Puri, V., & Sharma, A. (2023). Chitosan in oral drug delivery formulations: A review. *Pharmaceutics, 15*(9), 2361. https://doi.org/10.3390/pharmaceutics15092361

Sangsen, Y., Benjakul, S., & Oungbho, K. (2011). Fabrication of novel shark collagen-pectin scaffolds for tissue engineering. BMEiCON-2011 - 4th Biomedical Engineering International Conference, January 2011, 273–278. https://doi.org/10.1109/ BMEiCon.2012.6172069

Sanz, M., Marco del Castillo, A., Jepsen, S., Gonzalez-Juanatey, J. R., D'Aiuto, F., Bouchard, P., Chapple, I., Dietrich, T., Gotsman, I., Graziani, F., Herrera, D., Loos, B., Madianos, P., Michel, J. B., Perel, P., Pieske, B., Shapira, L., Shechter, M., Tonetti, M., … Wimmer, G. (2020). Periodontitis and cardiovascular diseases: Consensus report. *Journal of Clinical Periodontology*, *47*(3), 268–288. https://doi.org/10.1111/jcpe.13189

Sato, N., Handa, K., Venkataiah, V. S., Hasegawa, T., Njuguna, M. M., Yahata, Y., & Saito,

M. (2020). Comparison of the vertical bone defect healing abilities of carbonate apatite, β-tricalcium phosphate, hydroxyapatite and bovine-derived heterogeneous bone. *Dental Materials Journal*, *39*(2), 309–318. https://doi.org/10.4012/dmj.2019-084

Schmitz, J. P., & Hollinger, J. O. (1986). The critical size defect as an experimental model for craniomandibulofacial nonunions. *Clinical Orthopaedics and Related Research*, *205*, 299–308.

Schoeller, J., Itel, F., Wuertz-Kozak, K., Gaiser, S., Luisier, N., Hegemann, D., Ferguson, S. J., Fortunato, G., & Rossi, R. M. (2021). pH-responsive chitosan/alginate polyelectrolyte complexes on electrospun PLGA nanofibers for controlled drug release. *Nanomaterials*, *11*(7), 1–16. https://doi.org/10.3390/nano11071850

Schwerdt, G., Schulz, M. C., Kopf, M., Mildenberger, S., Reime, S., & Gekle, M. (2025). Physiological regulation of oral saliva ion composition and flow rate are not coupled in healthy humans—Partial revision of our current knowledge required. *Pflügers Archiv - European Journal of Physiology*, 477(1), 55–65. https://doi.org/10.1007/s00424-024-03025-9

Shrestha, A., & Kishen, A. (2021). Nanoparticle-mediated drug delivery systems in endodontics: A review. *Journal of Endodontics, 47*(1), 117–126. https://doi.org/10.1016/j.joen.2020.09.012

Shrestha, A., Zhu, Y., Tao, C., & Goh, C. (2023). Innovative biomaterials for the treatment of periodontal disease. *Frontiers in Dental Medicine, 4*, 1163562. https://doi.org/10.3389/fdmed.2023.1163562

Shrestha, S., Tripathi, S., Singh, B. N., Mallick, S. P., & Srivastava, P. (2021). Design and evaluation of ciprofloxacin-loaded collagen–chitosan oxygenating scaffold for infected wound healing. *Biomedical Materials, 16*(2), 025021. https://doi.org/10.1088/1748-605X/abd1b8

Sedghi, R., Jalali, M., & Kharaziha, M. (2021). Antimicrobial scaffolds for periodontal regeneration:From delivery mechanisms to clinical impact. *International Journal of Pharmaceutics, 599*, 120450. https://doi.org/10.1016/j.ijpharm.2021.120450

Šidlauskienė, I., Jankauskas, J., & Kučinskienė, I. (2024). Antibacterial photodynamic therapy for the treatment of chronic periodontitis: Clinical efficacy and challenges.

Stomatologija, 26(1), 19–26. https://doi.org/10.6001/stomatologija.v26i1.4707

Sigma-Aldrich. (n.d.). *Cell types & culture characteristics*. Retrieved from https://www.sigmaaldrich.com/US/en/technical-documents/technical-article/cell-culture-and-cell-culture-analysis/mammalian-cell-culture/cell-types-culture

Sethi, S., Medha, & Kaith, B. S. (2022). A review on chitosan-gelatin nanocomposites: Synthesis, characterization and biomedical applications. *Reactive and Functional Polymers*, *179*(October), 1–6.

Setterstrom, J. A., Ticet, T. R., & Myerst, W. E. (2000). Development of encapsulated antibiotics for topical administration to wounds. In J. M. Anderson (Ed.), *Recent advances in drug delivery systems* (Vol. 2, pp. 185–186). Plenum Press.

Sheehy, E. J., Diemling, C. Von, Ryan, E., Widaa, A., Donnell, P. O., Ryan, A., Chen, G., Brady, R. T., Adolfo, L., Zeiter, S., Moriarty, T. F., & Brien, F. J. O. (2025). Biomaterials antibiotic-eluting scaffolds with responsive dual-release kinetics facilitate bone healing and eliminate *S. aureus* infection. *Biomaterials*, *313*.122774. https://doi.org/10.1016/j.biomaterials.2024.122774

Shimauchi, H., Nemoto, E., Ishihata, H., & Shimomura, M. (2013). Possible functional scaffolds for periodontal regeneration. *Japanese Dental Science Review*, *49*(4), 118–130. https://doi.org/10.1016/j.jdsr.2013.05.001

Simpson, E., Sarwar, H., Jack, I., & Lowry, D. (2024). Evaluation of the potential of chitosan nanoparticles as a delivery vehicle for gentamicin for the treatment of osteomyelitis. *Antibiotics*, *13*(3), 208.

Singh, G., Faruk, A., & Bedi, P. M. S. (2018). Spectral analysis of drug loaded nanoparticles for drug-polymer interactions. *Journal of Drug Delivery and Therapeutics*, *8*(6), 111–118. https://doi.org/10.22270/jddt.v8i6.2030

Singh, S. K., Chouhan, H. S., Sahu, A. N., & Narayan, G. (2015). Assessment of *in vitro* antipsoriatic activity of selected Indian medicinal plants. *Pharmaceutical Biology*, *53*(9), 1295–1301. https://doi.org/10.3109/13880209.2014.976713

Smith, R. A., Walker, R. C., Levit, S. L., & Tang, C. (2019). Single-step self-assembly and physical crosslinking of PEGylated chitosan nanoparticles by tannic acid. *Polymers*, *11*(5), 1–10. https://doi.org/10.3390/polym11050749

Soares, G. M. S., Figueiredo, L. C., Faveri, M., Cortelli, S. C., Duarte, P. M., & Feres, M.

(2012). Mechanisms of action of systemic antibiotics used in periodontal treatment and mechanisms of bacterial resistance to these drugs. *Journal of Applied Oral Science*, *20*(3), 295–305. https://doi.org/10.1590/S1678-77572012000300002

Sousa, I., Mendes, A., Pereira, R. F., & Bártolo, P. J. (2014). Collagen surface modified poly(ε-caprolactone) scaffolds with improved hydrophilicity and cell adhesion properties.*Materials Letters*,*134*,263–267.

Sousa, T. L. de, Dourado, D., Rodrigues, J. S., Rebouças, J. de S., Resende, M. A. J., Silva, J. N. L. da, Oliveira, R. G. de M., Granjeiro, J. M., Souza, T. M. de, & Teles, F. H. B. (2024). Treatment of periodontal disease: Does drug delivery matter? *Frontiers in Bioengineering and Biotechnology*, *12*, 1427758. https://doi.org/10.3389/fbio-e.2024.1427758

Southard, G. L., & Godowski, K. C. (1998). Subgingival controlled release of antimicrobial agents in the treatment of periodontal disease. *International journal of antimicrobial agents*, *9*(4), 239-253.

Spicer, P. P., Kretlow, J. D., Young, S., Jansen, J. A., Kasper, F. K., & Mikos, A. G. (2012). Evaluation of bone regeneration using the rat critical size calvarial defect. *Nature Protocols*, *7*(10), 1918–1929. https://doi.org/10.1038/nprot.2012.113

Sreeharsha, N., Rajpoot, K., Tekade, M., Kalyane, D., Nair, A. B., Venugopala, K. N., & Tekade, R. K. (2020). Development of metronidazole loaded chitosan nanoparticles using QBD approach—a novel and potential antibacterial formulation. *Pharmaceutics*, *12*(10), 1–22. https://doi.org/10.3390/pharmaceutics12100920

Srinatha, A., Pandit, J., & Singh, S. (2008). Ionic cross-linked chitosan beads for extended release of ciprofloxacin: *In vitro* characterization. *Indian Journal of Pharmaceutical Sciences*, *70*(1), 16–21. https://doi.org/10.4103/0250-474X.40326

Suamte, L., Tirkey, A., Barman, J., & Jayasekhar Babu, P. (2023). Various manufacturing methods and ideal properties of scaffolds for tissue engineering applications. *Smart Materials in Manufacturing*, *1*(2022), 100011. https://doi.org/10.1016/j.smmf.2022.100011

Subramaniam, D., & Sekaran, S. (2024). In vitro biocompatibility assessment of a novel membrane containing magnesium-chitosan/carboxymethyl cellulose and alginate intended for bone tissue regeneration. *Cureus*, 16(2).

Sujathan, P., & Sharma, U. K. (2021). Development and characterization of metronidazole loaded microsponges for the management of diabetic foot. *International Journal of Research and Review*, *8*(10), 440–457. https://doi.org/10.52403/ijrr.20211059

Sukhbir, K., Chawla, V., Narang, R. K., & Aggarwal, G. (2017). Comparative mucopenetration ability of metronidazole loaded chitosan and pegylated chitosan nanoparticles. *Asian Journal of Pharmaceutical and Clinical Research*, *10*(6), 125–130. https://doi.org/10.22159/ajpcr.2017.v10i6.17643

Sukhbir, K., Chawla, V., Narang, R. K., Aggarwal, G., & Bhardwaj, T. R. (2017). Isolation and characterization of antibiotic/antitumor producing. *Research Journal of Pharmaceutical, Biological and Chemical Sciences*, *6*(1917), 1917–1929.

Sun, T., Liu, M., Yao, S., Ji, Y., Xiong, Z., Tang, K., Chen, K., Yang, H., & Guo, X. (2018). Biomimetic composite scaffold containing small intestinal submucosa and mesoporous bioactive glass exhibits high osteogenic and angiogenic capacity. *Tissue Engineering- Part A*,*24*(13–14),1044–1056. https://doi.org/10.1089/ten.tea.2017.0398

Sun, Y., Lu, R., Liu, J., Wang, X., Dong, H., & Chen, S. (2021). The early adhesion effects of human gingival fibroblasts on bovine serum albumin loaded hydrogenated titanium nanotube surface. *Molecules*, *26*(17).https://doi.org/10.3390/molecules26175229

Sundaram, G., Ramakrishnan, T., Parthasarathy, H., Raja, M., & Raj, S. (2018). *disease : A cross - link of sorts ! 26*, 113–118. https://doi.org/10.4103/jisp.jisp

Suvarnapathaki, S., Wu, X., Zhang, T., Nguyen, M. A., Goulopoulos, A. A., Wu, B., & Camci-Unal, G. (2022). Oxygen generating scaffolds regenerate critical size bone defects. *Bioactive Materials*, *13*, 64–81. https://doi.org/10.1016/j. bioactmat.2021.11.002

Szewczyk, A., Warmińska, D., Ruszkowski, J., Szymankiewicz, M., & Prokopowicz, M. U. (2024). Solubility enhancement of metronidazole using natural deep eutectic solvents: Physicochemical and thermodynamic studies. *Journal of Molecular Liquids, 410*, 125604. https://doi.org/10.1016/j.molliq.2024.125604

Szewczyk, P. K., Metwally, S., Karbowniczek, J. E., Marzec, M. M., Stodolak-Zych, E., Gruszczyński, A., Bernasik, A., & Stachewicz, U. (2019). Surface-potential-

controlled cell proliferation and collagen mineralization on electrospun polyvinylidene fluoride (PVDF) fiber scaffolds for bone regeneration. *ACS Biomaterials Science and Engineering*, *5*(2), 582–593. htpps://doi.org/10.1021/acs biomaterials.8b0 1108

Szymańska-Chargot, M., Chylińska, M., Pertile, G., Pieczywek, P. M., Cieślak, K. J., Zdunek, A., & Frąc, M. (2019). Influence of chitosan addition on the mechanical and antibacterial properties of carrot cellulose nanofibre film. *Cellulose*, *26*(18), 9613– 9629. https://doi.org/10.1007/s10570-019-02755-9

Tadich, T., & Tarazona, A. M. (2023). Replacement, Reduction and Refinement: Ethical Considerations in the Current Applications of the 3Rs. In R. de Miguel Beriain & I. Alfonso García (Eds.), *Handbook of Bioethical Decisions. Volume I: Decisions at the Bench* (pp. 667–683). Springer. https://doi.org/10.1007/978-3-031-32135-8_39

Takallu, S., Kakian, F., Bazargani, A., Khorshidi, H., & Mirzaei, E. (2024). Development of antibacterial collagen membranes with optimal silver nanoparticle content for periodontal regeneration. *Scientific Reports*, *14*, 7262. https://doi.org/10.1038/s415 98-024-57951-w

Thamilselvan, G., David, H., Sajeevan, A., Rajaramon, S., Solomon, A. P., Durai, R. D., & Narayanan, V. H. B. (2023). Polymer based dual drug delivery system for targeted treatment of fluoroquinolone resistant Staphylococcus aureus mediated infections. *Scientific Reports*, *13*(1), 1–19. https://doi.org/10.1038/s41598-023-38473-3

Thang, N. H., Chien, T. B., & Cuong, D. X. (2023). Polymer-based hydrogels applied in Drug Delivery: An Overview. *Gels*, *9*(7), 1–38.

Theodoridis, K., Arampatzis, A. S., Liasi, G., Tsalikis, L., Barmpalexis, P., Christofilos, D., & Assimopoulou, A. N. (2023). 3D-printed antibacterial scaffolds for the regeneration of alveolar bone in severe periodontitis. *International Journal of Molecular Sciences, 24*(23), 16754. https://doi.org/10.3390/ijms242316754

Tipa, C., Cidade, M. T., Borges, J. P., Costa, L. C., Silva, J. C., & Soares, P. I. P. (2022). Clay-Based Nanocomposite Hydrogels for Biomedical Applications: A Review. *Nanomaterials*, *12*(19). https://doi.org/10.3390/nano12193308

Togari, K., Miyazawa, K., Yagihashi, K., Tabuchi, M., Maeda, H., Kawai, T., & Goto, S. (2012). Bone regeneration by demineralized dentin matrix in skull defects of rats.

Journal of Hard Tissue Biology, *21*(1), 25–34. https://doi.org/10.2485/jhtb.21.25

Tonetti, M. S., & Van Dyke, T. E. (2013). Periodontitis and atherosclerotic cardiovascular disease: consensus report of the Joint EFP/AAPWorkshop on Periodontitis and Systemic Diseases. *Journal of Periodontology*, *84*(4S), 24–29. https://doi.org/10.19 .02/jop.2013.1340019

Toosi, S., Naderi-Meshkin, H., Esmailzadeh, Z., Behravan, G., Ramakrishna, S., & Behravan, J**.** (2022). Bioactive glass–collagen/poly(glycolic acid) scaffold nanoparticles exhibit improved biological properties and enhance osteogenic lineage differentiation of mesenchymal stem cells. *Frontiers in Bioengineering and Biotechnology, 10,* Article 963996. https://doi.org/10.3389/fbioe.2022.963996

Tripathi, S., Singh, B. N., Singh, D., kumar, G., & Srivastava, P. (2021). Optimization and evaluation of ciprofloxacin-loaded collagen/chitosan scaffolds for skin tissue engineering. *3 Biotech*, *11*(4), 1–17. https://doi.org/10.1007/s13205-020-02567-w

Trivedi, M. K., Patil, S., Shettigar, H., Bairwa, K., & Jana, S. (2015). Spectroscopic characterization of biofield treated metronidazole and tinidazole. *Medicinal Chemistry*, *5*(7), 340–344. https://doi.org/10.2174/2211732315666151109122452

Ullah, S., Zainol, I., & Idrus, R. H. (2017). Incorporation of zinc oxide nanoparticles into chitosan-collagen 3D porous scaffolds: Effect on morphology, mechanical properties and cytocompatibility of 3D porous scaffolds. *International Journal of Biological Macromolecules*, *104*, 1020–1029. https://doi.org/10.1016/j. ijbiomac.2 017.06.080

University of IOWA. (2020). Anesthesia (Guideline). *Vertebrate Animal Research Website*, 1. https://animal.research.uiowa.edu/iacuc-guidelines-anesthesia

University of Michigan's Unit for Laboratory Animal Medicine (ULAM). (2015). *Pain assessment in rats*. https://az.research.umich.edu/file/1255

Uribe, F., Vásquez, B., Alister, J. P., & Olate, S. (2022). Comparison of rhBMP-2 in combination with different biomaterials for regeneration in rat calvaria critical-size defects. *BioMed Research International, 2022*.https://doi.org/10. 1155/2022/62 81641

Vaezifar, S., Razavi, S., Golozar, M. A., Karbasi, S., Morshed, M., & Kamali, M. (2013). Effects of some parameters on particle size distribution of chitosan nanoparticles

prepared by ionic gelation method. *Journal of Cluster Science*, *24*(3), 891–903. https://doi.org/10.1007/s10876-013-0583-2

Valamvanos, T. F., Dereka, X., Katifelis, H., Gazouli, M., & Lagopati, N. (2024). Recent advances in scaffolds for guided bone regeneration. *Biomimetics*, *9*(3), 11–14. https://doi.org/10.3390/biomimetics9030153

Van Winkelhoff, A. J., Rams, T. E., & Slots, J. (1996). Systemic antibiotic therapy in periodontics. *Periodontology 2000*, *10*(1), 45–78. https://doi.org/10.1111/j.1600-0757.1996.tb00068.x

Vertanessian, A., Allen, A., & Mayo, M. J. (2003). Agglomerate formation during drying. *Journal of Materials Research*, *18*(2), 495–506. https://doi.org/10.1557/ JMR.2003.0063

Walker, C. B. (1996). Selected antimicrobial agents: Mechanisms of action, side effects and drug interactions. *Periodontology 2000*, *10*(1), 12–28. https://doi.org/10.111/j.1600-0757.1996.tb00066.x

Wang, D., Zhou, X., Cao, H., Zhang, H., Wang, D., Guo, J., & Wang, J. (2023). *Barrier Membranes for periodontal guided bone regeneration: A potential therapeutic strategy*. Frontiers in Materials, 10**,** 1220420. https://doi.org/10.3389/ fmats.2023. 1220420

Wang, K. C., Yang, L. Y., Lee, J. E., Wu, V., Chen, T. F., Hsieh, S. T., & Kuo, M. F. (2022). Combination of indirect revascularization and endothelial progenitor cell transplantation improved cerebral perfusion and ameliorated tauopathy in a rat model of bilateral ICA ligation. *Stem Cell Research and Therapy*, *13*(1), 1–14. https://doi.org/10.1186/s13287-022-03196-1

Wang, L., Hu, C., & Shao, L. (2017). The antimicrobial activity of nanoparticles: Present situation and future perspectives. *International Journal of Nanomedicine*, *12*, 1227–1249. https://doi.org/10.2147/IJN.S124254

Wang, S., Sun, C., Guan, S., Li, W., Xu, J., Ge, D., Zhuang, M., Liu, T., & Ma, X. (2017). Chitosan/gelatin porous scaffolds assembled with conductive poly(3,4-ethylenedioxythiophene) nanoparticles for neural tissue engineering. *Journal of Materials Chemistry B*, *5*(24), 4774–4788. https://doi.org/10.1039/c7tb00608j

Wang, Y., Li, J., Tang, M., Peng, C., Wang, G., Wang, J., Wang, X., Chang, X., Guo, J., &

Gui, S. (2021). Development of metronidazole-loaded in situ thermosensitive hydrogel for periodontitis treatment. *Turkish Journal of Pharmaceutical Sciences*, 18(2), 219–227. https://doi.org/10.4274/tjps.galenos.2020.09623

Wang, L., Zhang, G., Gao, Y., Dai, T., Yu, J., Liu, Y., Bao, H., She, J., Hou, Y., Kong, L., & Cai, B. (2024). Extracellular vesicles derived from neutrophils accelerate bone regeneration by promoting osteogenic differentiation of BMSCs. *ACS Biomaterials Science & Engineering*, *10*(6), 3868–3882. https://doi.org/10. 1021/acsbiomaterials .4c00106

Wei, J., Wang, Y., Jiang, J., Yan, Y., Fan, D., Yang, X., Zuo, Y., Li, Y., Gu, H., & Li, J. (2019). Development of an antibacterial bone graft by immobilization of levofloxacin hydrochloride-loaded mesoporous silica microspheres on a porous scaffold surface. *Journal of Biomedical Nanotechnology*, *15*(5), 1097–1105.https:// doi.org/10.1166/jbn.2019.2743

Werner, N., Reißmann, D. R., Hegewald, J., Schön, H., & Walter, M. (2025). A retrospective study

on the impact of different antibiotic regimens in non-surgical periodontal therapy on microbial loads and therapy outcomes. *Frontiers in Oral Health*, *6*, 1578484. https://doi.org/10.3389/forh.2025.1578484

Winkel, E. G., van Winkelhoff, A. J., Timmerman, M. F., & van der Velden, U. (2001). Metronidazole plus amoxicillin in the treatment of adult periodontitis patients. *Journal of Clinical Periodontology*, *28*(10), 833–839. https://doi.org/101034/j. 16. 00-051X.2001.281005.x

Winning, L., & Linden, G. J. (2017). Periodontitis and Systemic Disease: Association or Causality? *Current Oral Health Reports*, *4*(1), 1–7. https://doi.org/10.1007/s40496-017-0121-7

Woo, H. N., Cho, Y. J., Tarafder, S., & Lee, C. H. (2021). The recent advances in scaffolds for integrated periodontal regeneration. *Bioactive Materials*, *6*(10), 3328–3342. https://doi.org/10.1016/j.bioactmat.2021.03.012

Wood, W., & Martin, P. (2002). Structures in focus - Filopodia. *International Journal of Biochemistry and Cell Biology*, *34*(7), 726–730. https://doi.org/10.1016/S1357-2725(01)00172-8

Xia, H., Keane, C. T., Beattie, S., & O'Morain, C. A. (1994). Standardization of disk diffusion test and its clinical significance for susceptibility testing of metronidazole against Helicobacter pylori. *Antimicrobial Agents and Chemotherapy*, *38*(10), 2357– 2361. https://doi.org/10.1128/AAC.38.10.2357

Xu, C., Lu, W., Bian, S., Liang, J., Fan, Y., & Zhang, X. (2012). Porous collagen scaffold reinforced with surfaced activated PLLA nanoparticles. *The Scientific World Journal*, *2012*. https://doi.org/10.1100/2012/695137

Xue, J., He, M., Niu, Y., Huang, Y., Zhao, Y., & Fan, Y. (2014). Drug-loaded electrospun nanofibers for periodontal disease treatment. *Materials Science and Engineering: C*, *41*, 52–59. https://doi.org/10.1016/j.msec.2014.04.051

Xue, J., He, M., Niu, Y., Liu, H., Crawford, A., Coates, P., Chen, D., Shi, R., & Zhang, L. (2014). Preparation and *in* vivo efficient anti-infection property of GTR/GBR implant made by metronidazole loaded electrospun polycaprolactone nanofiber membrane. *International Journal of Pharmaceutics*, *475*(1), 566–577. https://doi.org/10.1016/j.ij pharm.2014.09.026

Yamada, S., Yamamoto, K., Ikeda, T., Yanagiguchi, K., & Hayashi, Y. (2014). Potency of fish collagen as a scaffold for regenerative medicine. *BioMed Research International*, *2014*(3). https://doi.org/10.1155/2014/302932

Yamamoto, K., Igawa, K., Sugimoto, K., Yoshizawa, Y., Yanagiguchi, K., Ikeda, T., Yamada, S., & Hayashi, Y. (2014). Biological safety of fish (tilapia) collagen. *BioMed Research International*, *2014*. https://doi.org/10.1155/2014/630757

Yan, L. P., Wang, Y. J., Ren, L., Wu, G., Caridade, S. G., Fan, J. B., Wang, L. Y., Ji, P. H., Oliveira, J. M., Oliveira, J. T., Mano, J. F., & Reis, R. L. (2010). Genipin-cross-linked collagen/chitosan biomimetic scaffolds for articular cartilage tissue engineering applications. *Journal of Biomedical Materials Research - Part A*, *95(*2), 465–475. https://doi.org/10.1002/jbm.a.32869

Yanat, M., & Schröen, K. (2021). Preparation methods and applications of chitosan nanoparticles; with an outlook toward reinforcement of biodegradable packaging. *Reactive and Functional Polymers, 161*, 104849. https://doi.org/10.1016/j.reactfunctpolym.2021.104849

Yang, B.-Y., Hu, C.-H., Huang, W.-C., Ho, C.-Y., Yao, C.-H., & Huang, C.-H. (2019).

Effects of bilayer nanofibrous scaffolds containing curcumin/lithospermi radix extract on wound healing in streptozotocin-induced diabetic rats. *Polymers*, *11*(11), 1745. https://doi.org/10.3390/polym11111745

Yang, W., Fu, J., Wang, T., & He, N. (2009). Chitosan/sodium tripolyphosphate nanoparticles: Preparation, characterization and application as drug carrier. *Journal of Biomedical Nanotechnology*, *5*(5), 591–595. https://doi.org/10.1166/jbn.2009.1067

Yang, Y., Yao, Z., Sun, Y., Nie, Y., Zhang, Y., Li, Z., Luo, Z., Zhang, W., Zhang, W., Qin, L., Sang, H., & Lai, Y. (2024). 3D-printed manganese dioxide incorporated scaffold promotes osteogenic-angiogenic coupling for refractory bone defect by remodeling osteo-regenerative microenvironment. *Bioactive Materials, 44*, 354–370. https://doi.org/10.1016/j.bioactmat.2024.10.019

Yildiz, H., Sen, E., Dalcik, H., & Meseli, S. E. (2023). Evaluation of cell morphology and adhesion capacity of human gingival fibroblasts on titanium discs with different roughened surfaces: an *in vitro* scanning electron microscope analysis and cell culture study. *Folia Morphologica (Poland)*, *82*(1),63–71. https://doi.org/10.5603/FM a2022.0072

Yousefi, M., Mohammadi, A., & Abbaspour, M. (2023). One factor at a time and factorial experimental design for formulation of L-carnitine microcapsules to improve its manufacturability. *Pharmaceuticals*, *16*(5), 429. https://www.ncbi.nlm.nih.gov/pmc/articles/PMC10851296/

Yusof, Z. Y. M., Jaafar, N., & Jamaluddin, R. (2024). *Economic burden of non-surgical periodontal treatment in specialist dental settings in Malaysia: A cost-of-illness study*. International Dental Journal. https://pubmed.ncbi.nlm.nih.gov/38500175/

Zain, N. M., & Hamdan, M. N. (2021). Tilapia fish collagen: Potential as halal biomaterial in tissue engineering applications. *Nusantara Halal Journal (Halal Awareness, Opinion, Research, and Initiative)*, *2*(1), 24–32. https://doi.org/10. 17977/um060. 2021v2p024-032

Zainol, I., Ullah, S., Jaafar, C. N. A., Rahim, N. A., & Daud, N. (2022). Effect of Dehydrothermal (Dht) Treatment on the Physicochemical Properties of 3D Porous Chitosan-Collagen-Glycerine Scaffold for Potential Skin Regenerating

Template Applications. In *Malaysian Journal of Microscopy 17*(2), 111–121

Zamani, F., Jahanmard, F., Ghasemkhah, F., Amjad-Iranagh, S., Bagherzadeh, R., Amani-Tehran, M., & Latifi, M. (2017). Nanofibrous and nanoparticle materials as drug-delivery systems. In *Nanostructures for Drug Delivery* (pp. 239–270). Elsevier.

Zare, Y., Rhee, K. Y., & Hui, D. (2017). Influences of nanoparticles aggregation/agglomeration on the interfacial/interphase and tensile properties of nanocomposites. *Composites Part B: Engineering*, *122*, 41–46. https://doi.org.10.16/j.compositesb.2017.04.008

Zayi, N. A. M., Halim, L., Ismail, A. Fahmi. H.I., & Mohamad, M. Y. (2023). Fabrication and Characterization of fish-derived collagen chitosan scaffold loaded with metronidazole nanoparticle for periodontal bone regeneration. *Malaysian Journal of Microscopy*, *19*(2), 141–152.

Zhang, H., Wu, F., Li, Y., Yang, X., Huang, J., Lv, T., Zhang, Y., Chen, J., Chen, H., Gao, Y., Liu, G., & Jia, L. (2016). Chitosan-based nanoparticles for improved anticancer efficacy and bioavailability of mifepristone. *Beilstein Journal of Nanotechnology*, *7*, 1861–1870. https://doi.org/10.3762/bjnano.7.178

Zhang, H. Y., Jiang, H. B., Ryu, J. H., Kang, H., Kim, K. M., & Kwon, J. S. (2019). Comparing properties of variable pore-sized 3D-printed PLA membrane with conventional PLA membrane for guided bone/tissue regeneration. *Materials*, *12*(10), 1–11. https://doi.org/10.3390/MA12101718

Zhang, J., Ma, S., Liu, Z., Geng, H., Lu, X., Zhang, X., Li, H., Gao, C., Zhang, X., & Gao, P. (2017). Guided bone regeneration with asymmetric collagen-chitosan membranes containing aspirin-loaded chitosan nanoparticles. *International Journal of Nanomedicine*, *12*, 8855–8866. https://doi.org/10.2147/IJN.S148179

Zhang, Z., Gan, Y., Guo, Y., Lu, X., & Li, X. (2021). Animal models of vertical bone augmentation. *Experimental and Therapeutic Medicine*, *22*(3), 919. https://doi.org/10.3892/etm.2021.10351

Zhang, S., Vijayavenkataraman, S., Lu, W. F., & Fuh, J. Y. H. (2019). A review on the use of computational methods to characterize, design, and optimize tissue engineering scaffolds, with a potential in 3D printing fabrication. *Journal of Biomedical MaterialsResearch - Part B Applied Biomaterials*, *107*(5), 1329–1351.

https://doi. org/10.1002/jbm.b.34226

Zhang, X., & Hartmann, P. (2023). How to calculate sample size in animal and human studies. *Frontiers in Medicine*, *10*. https://doi.org/10.3389/fmed.2023.1215927

Zhang, Y., Liu, X., & Chen, H. (2025). Functional supramolecular polymer carriers for reversible drug delivery systems**.** *Chemistry – A European Journal*. https://doi.org-/10.1002/chem.202404617

Zhang, Y., Wang, L., & Huang, Y. (2021). Recent advances in marine collagen-based biomaterials for biomedical applications. *Carbohydrate Polymers*, 266, 118134. https://doi.org/10.1016/j.carbpol.2021.118134

Zhao, R., Ma, Y., & Xu, H. (2023). Functional collagen scaffolds for regenerative medicine :Fabrication, characterisation, and applications. *Polymers*, 16(1), 3429. https://doi.org/10.3390/polym16023429

Zhou, K., Azaman, F. A., Cao, Z., Brennan Fournet, M., & Devine, D. M. (2023). Bone Tissue Engineering Scaffold Optimisation through Modification of Chitosan/Ceramic Composition. *Macromol*, *3*(2), 326–342. https://doi.org/10.3390/ macromol3020021

Zucchelli, G., Sforza, N. M., Clauser, C., Cesari, C., & Sanctis, M. De. (1999). Topical and systemic antimicrobial therapy in guided tissue regeneration. *Journal of Periodontology*, *70*(3), 239–247. https://doi.org/10.1902/jop.1999.70.3.239

APPENDIX I

ETHICAL APPROVAL

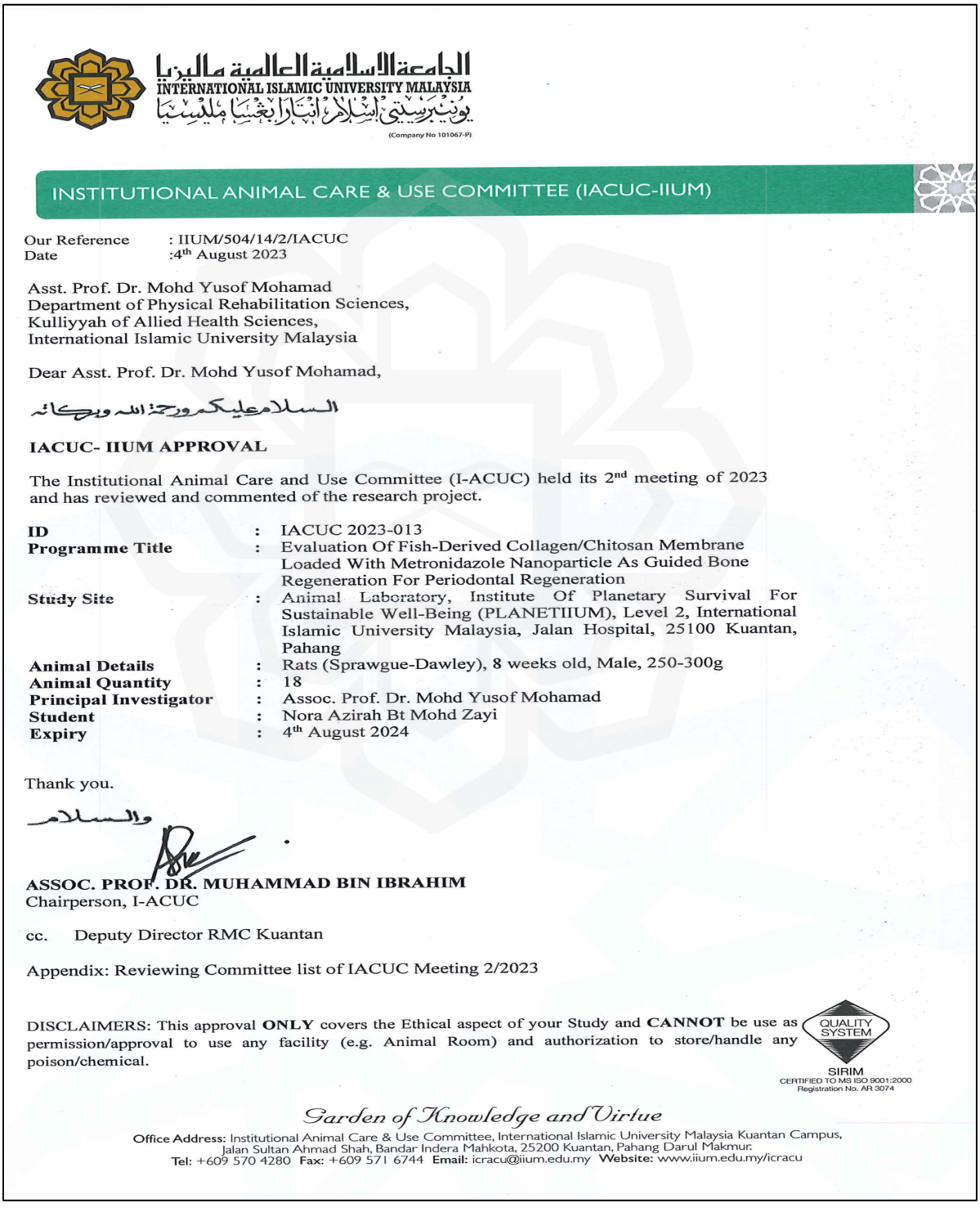

الجامعة الإسلامية العالمية ماليزيا
INTERNATIONAL ISLAMIC UNIVERSITY MALAYSIA
يونيفرسيتي إسلام انتارابغسا ملايسيا
(Company No 101067-P)

INSTITUTIONAL ANIMAL CARE & USE COMMITTEE (IACUC-IIUM)

Our Reference : IIUM/504/14/2/IACUC
Date :4th August 2023

Asst. Prof. Dr. Mohd Yusof Mohamad
Department of Physical Rehabilitation Sciences,
Kulliyyah of Allied Health Sciences,
International Islamic University Malaysia

Dear Asst. Prof. Dr. Mohd Yusof Mohamad,

السلام عليكم ورحمة الله وبركاته

IACUC- IIUM APPROVAL

The Institutional Animal Care and Use Committee (I-ACUC) held its 2nd meeting of 2023 and has reviewed and commented of the research project.

ID	:	IACUC 2023-013
Programme Title	:	Evaluation Of Fish-Derived Collagen/Chitosan Membrane Loaded With Metronidazole Nanoparticle As Guided Bone Regeneration For Periodontal Regeneration
Study Site	:	Animal Laboratory, Institute Of Planetary Survival For Sustainable Well-Being (PLANETIIUM), Level 2, International Islamic University Malaysia, Jalan Hospital, 25100 Kuantan, Pahang
Animal Details	:	Rats (Sprawgue-Dawley), 8 weeks old, Male, 250-300g
Animal Quantity	:	18
Principal Investigator	:	Assoc. Prof. Dr. Mohd Yusof Mohamad
Student	:	Nora Azirah Bt Mohd Zayi
Expiry	:	4th August 2024

Thank you.

والسلام

ASSOC. PROF. DR. MUHAMMAD BIN IBRAHIM
Chairperson, I-ACUC

cc. Deputy Director RMC Kuantan

Appendix: Reviewing Committee list of IACUC Meeting 2/2023

DISCLAIMERS: This approval **ONLY** covers the Ethical aspect of your Study and **CANNOT** be use as permission/approval to use any facility (e.g. Animal Room) and authorization to store/handle any poison/chemical.

QUALITY SYSTEM
SIRIM
CERTIFIED TO MS ISO 9001:2000
Registration No. AR 3074

Garden of Knowledge and Virtue

Office Address: Institutional Animal Care & Use Committee, International Islamic University Malaysia Kuantan Campus, Jalan Sultan Ahmad Shah, Bandar Indera Mahkota, 25200 Kuantan, Pahang Darul Makmur.
Tel: +609 570 4280 Fax: +609 571 6744 Email: icracu@iium.edu.my Website: www.iium.edu.my/icracu

APPENDIX II

FULL ARTICLES, CONFERENCE PROCEEDINGS, AND ABSTRACTS CONTRIBUTED TO THIS THESIS

Sustainable & Green Materials

In vitro Analysis of Collagen Chitosan Scaffold Loaded with Metronidazole Nanoparticle for Periodontal Disease Treatment

Journal:	*Sustainable & Green Materials*
Manuscript ID	TSGM-2024-0009
Manuscript Type:	Research Article
Date Submitted by the Author:	27-Aug-2024
Complete List of Authors:	Mohamad, MOHD Yusof; International Islamic University Malaysia - Kuantan Campus, Physical Rehabilitation Sciences, KAHS Mohd Zayi, Nora Azirah; International Islamic University Malaysia - Kuantan Campus, Physical Rehabilitation Sciences Mohamed Halim, Muhammad Lutfi; International Islamic University Malaysia - Kuantan Campus, Physical Rehabilitation Sciences, KAHS Harun, Ahmad Fahmi; International Islamic University Malaysia - Kuantan Campus, Physical Rehabilitation Sciences, KAHS
Keywords:	Periodontal disease, Collagen, Chitosan, Metronidazole, Nanoparticle.
Abstract:	Periodontal diseases pose significant challenges to oral health, often requiring advanced therapeutic interventions involving the utilization of three-dimensional (3D) scaffolds, However, this intervention could not prevent inflammatory reactions. Hence, recent years have seen a growing emphasis on developing new antibacterial scaffolds in dental tissue engineering. This study aimed to address these challenges by evaluating the antibacterial and biocompatibility properties of a novel collagen-chitosan scaffold loaded with metronidazole nanoparticles (CC-MT) for periodontal therapy. The antibacterial activity of CC-MT against Porphyromonas gingivalis and Fusobacterium nucleatum was assessed using the Disk Diffusion Test. Additionally, cytocompatibility was evaluated by examining cell viability and proliferation using Human Gingival Fibroblast cells (HGF-1), and cell attachment was characterized using Fourier scanning electron microscopy. Our findings revealed that CC-MT exhibited antibacterial effects against the pathogens, with CC-MT (30% metronidazole) showing a higher inhibitory effect, with no significant difference compared to the positive control (metronidazole disc) ($p<0.05$). In addition, in vitro cell culture studies revealed that the CC-MT (30% metronidazole) has no negative effect on cell morphology, viability, and proliferation and possesses good biocompatibility. Based on these results, CC-MT's demonstrated potential as drug carriers and could be promising candidates for the treatment of periodontal disease.

Nora Azirah Mohd Zayi et al. Malaysian Journal of Microscopy Vol. 19, No. 2 (2023), Page 141-152

FABRICATION AND CHARACTERIZATION OF FISH-DERIVED COLLAGEN SCAFFOLD LOADED WITH METRONIDAZOLE NANOPARTICLE FOR PERIODONTAL BONE REGENERATION

Nora Azirah Mohd Zayi[1], Lutfi Halim[1], Ahmad Fahmi Harun @ Ismail[1,2] and Mohd Yusof Mohamad[1,2,*]

[1]Department of Physical Rehabilitation Sciences, Kulliyyah of Allied Health Sciences, International University Islam Malaysia, 25200, Kuantan Pahang
[2]Cluster of Cancer Research Initiative IIUM (COCRII), International Islamic University Malaysia, Kuantan Campus, 25200, Kuantan, Pahang, Malaysia

*yusofkahs@iium.edu.my

Abstract. Periodontal disease poses a significant challenge to oral health, affecting the tissue and bone supporting the teeth. Tissue engineering emerges as a promising approach for restoring periodontal tissue and preventing bone loss using scaffolds. However, concern arises when using collagen sourced from mammals like porcine and bovine in scaffolds regarding halal status and disease transmission. Additionally, conventional treatment involves systemic antibiotics to control infection, leading to adverse side effects. This study aims to develop a scaffold using fish-derived collagen incorporated with metronidazole nanoparticles (MNP) and analyze scaffold properties while indirectly addressing safety and halal concerns. The scaffold was fabricated by physically cross-linking collagen derived from the tilapia fish (*Tilapia mossambica*) and chitosan, with metronidazole nanoparticles (MNP) incorporated into the blend. The scaffold underwent analysis of its physical characteristics, morphology, and pore size using a scanning electron microscope (SEM), swelling, and biodegradability in phosphate buffer solutions (pH 7.4, 37 °C). The fish-derived collagen-chitosan exhibited a consistent three-dimensional (3D) physical structure and optimal pore sizes (>100 µm). Scaffolds with MNP concentrations ranging from 0 to 40 w/t% displayed excellent swelling ability and biodegradability, exceeding 80%. As the concentration of MNP increased, the scaffold's biodegradation rate slowed, suggesting potential as a controlled drug release vehicle aligned with the rates of new bone formation *in vivo*. In conclusion, the 3D porous scaffold with metronidazole nanoparticles met important criteria for physical structure, pore size, swelling ability, and biodegradability. These halal-compliant scaffolds hold promising potential for applications in tissue engineering and drug delivery and are subject to further *in vivo* and *in vitro* studies.

Keywords: Periodontal disease, metronidazole, nanoparticle, scaffold, controlled release

Article Info

Received 11th October 2023
Accepted 15th December 2023
Published 20th December 2023

ISSN: 1823-7010, eISSN: 2600-7444

Malaysian Journal of Chemistry, 2023, Vol. 25(3), 354-367
(Special Issue: *3rd IKMPB Online Symposium 2023 - Innovation in Chemistry Towards Sustainable Development*)

Development of Ultraviolet Spectroscopic Method for the Estimation of Metronidazole Nanoparticles for Periodontal Disease Treatment

Nora Azirah Mohd Zayi[1], Muhammad Lutfi Mohamed Halim[1], Ahmad Fahmi Harun Ismail[1,2], Mohd Yusof Mohamad[1,2]

[1]Department of Physical Rehabilitation Science, Kulliyyah of Allied Health Sciences, International Islamic University Malaysia, Kuantan Campus, 25200 Kuantan, Pahang, Malaysia
[2]Cluster of Cancer Research Initiative IIUM (COCRII), International Islamic University Malaysia, Kuantan, 25000, Kuantan, Pahang, Malaysia
*Corresponding author (e-mail: yusofkahs@iium.edu.my)

In periodontitis treatment, metronidazole (MT) is applied topically to reduce systemic side effects and reach the target site. treatment of periodontitis via sustained MT release. The UV-spectrophotometer analysis was developed and validated to quantify the encapsulated MT according to ICH Q2 (R1) guidelines, which include parameters such as specificity, linearity, accuracy, precision (in the form of repeatability), the limit of detection (LOD) as well as the limit of quantification (LOQ), range, robustness, and ruggedness. Metronidazole nanoparticles (MT-NP) were fabricated at different concentrations (0.15–0.60 mg/mL) using ionic gelation. The encapsulated MT was examined using a UV spectrophotometer, a Nano Zetasizer, Fourier transform infrared spectroscopy (FTIR), and a field emission scanning electron microscope (FESEM). The maximum wavelength (max) was discovered to be 320 nm, and it obeyed Beer's law with a linear relationship ($R^2 = 0.999$) in the range of 2-12 µg/mL. The parameters analyzed met ICH Q2 (R1) standards. MT-NP had a spherical structure and absorption band similar to chitosan empty (CS), with a size of 308.0 ± 9.18 nm, a polydispersity index of 0.374 ± 0.37, 46.6 ± 0.23, and an encapsulation efficiency of 87.95 ± 0.07. These findings suggest that UV-visible can be a useful tool for the estimation of MT nanoparticles and MT-NP as promising local antibacterial agents to treat periodontitis.

Keywords: Metronidazole nanoparticle; UV/Vis spectroscopy; local drug delivery; eriodontal disease

Received: January 2023; Accepted: April 2023

Periodontal disease, also known as periodontitis, is a serious dental health problem where, according to the Global Burden Disease Study (2019), about 14.5% of the global population suffers from severe periodontal disorders. Periodontal disease causes redness, swelling, gingival pain, and bad breath, and if left untreated, the development of a periodontal pocket occurs, where the gum tissue pulls away from the tooth. Patients with low innate ability often experience slow regeneration of healthy periodontal tissue, which worsens the disease due to bacteria accumulation. These microorganisms can damage the periodontal gum, alveolar jaw, and other supporting tooth structures, which can lead to tooth loss [1]. Periodontal disease is caused by poor oral hygiene, stress, aging, alcohol, depression, smoking, and systemic conditions such as cardiovascular disease and diabetes [1, 2]. The data collected showed that periodontal disease is linked to the buildup of *Porphyromonas gingivalis*, *Treponema denticola*, *Fusobacterium nucleatum*, *Aggregatibacter actinomy-cetemcomitans*, *Prevotella intermedia*, and *Tannerella forsythia*. These species are present in subgingival plaque in patients suffering from chronic periodontitis [3]. The presence of *Porphyromonas gingivalis* and *Treponema denticola*, which have been demonstrated to exhibit synergistic virulence in animal models, was found to be significantly correlated with the development and severity of chronic periodontitis. Another study found that *Tannerella forsythia* is also one of the bacteria that inhabit the subgingival cavity and initiates connective tissue and alveolar bone degeneration [4]. Among them is *Porphyromonas gingivalis*, a gram-negative anaerobic bacterium prevalent in the oral cavity. It secretes hydrolytic, proteolytic, lipolytic, and toxic metabolites [5].

In the early stages of periodontal disease, non-surgical treatments, including scaling and root planing, as well as local or systemic antibiotics, are the most successful treatments. In chronic periodontitis, several systemic antibiotic therapies such as tetracyclines, penicillin, metronidazole, or clindamycin are early approaches to minimizing infections after dental surgery. Among the antibiotics used, metronidazole (MT) is a

†Paper presented at the 3rd IKMPB Online Symposium 2023 - Innovation in Chemistry Towards Sustainable Development

Revelation and Science
Vol. 13, No. 01 (1444H/2023) 26-38

A Current Review of Local Metronidazole Antibiotics for the Treatment of Periodontal Disease

Nora Azirah Mohd Zavi[1], Muhammad Lutfi Mohamed Halim[1], Mohd Yusof Mohamad[1,3]

[1]Department of Physical Rehabilitation Sciences, Kulliyyah of Allied Health Science, International Islamic University Malaysia, Kuantan Campus, 25200 Kuantan, Pahang, Malaysia.

[2]Department of Fundamental Dental and Medical Sciences, Kulliyyah of Dentistry, International Islamic University Malaysia, Kuantan Campus, 25200, Kuantan, Pahang, Malaysia.

[3]Cluster of Cancer Research Initiative IIUM (COCRII), International Islamic University Malaysia, Kuantan Campus, 25200, Kuantan, Pahang, Malaysia.

Abstract

Periodontal disease affects around 14.5% of the global adult population. It affects the tooth's supporting tissues, causing inflammation and tooth loss. Periodontitis treatment aims to prevent further disease progression by restoring the lost tissue and preventing bacterial infection. Nevertheless, periodontal breakdown may still occur post-treatment due to the periodontal pathogens. Antibiotics were utilized to control and prevent the infection. Local drug delivery system (LDD) is being developed to deliver the antibiotic due to its site-specific benefits. Metronidazole (MET) is widely used to treat periodontal infection following treatments due to its efficacy against obligate anaerobes and broad-spectrum characteristics. Despite its advantages, MET is attributed to systemic side effects. Therefore, this article aimed to review *in vitro*, *in vivo,* and clinical studies on the current local application of MET to treat periodontal diseases. 13 relevant research articles were analysed and provide valuable insights into the local application of metronidazole for periodontal treatment.

Keywords: metronidazole; local drug delivery; periodontitis, antibiotic

Abstrak

Penyakit periodontal menjejaskan sekitar 14.5% daripada populasi dewasa global. Ia menjejaskan tisu penyokong gigi, menyebabkan keradangan dan kehilangan gigi. Rawatan periodontitis bertujuan untuk mencegah perkembangan penyakit selanjutnya dengan memulihkan tisu yang hilang dan mencegah jangkitan kuman. Namun begitu, kerosakan periodontal mungkin masih berlaku selepas rawatan disebabkan oleh patogen periodontal. Antibiotik digunakan untuk mengawal dan mencegah jangkitan. Sistem penghantaran ubat tempatan (LDD) sedang dibangunkan untuk menyampaikan antibiotik kerana faedah khusus tapaknya. Metronidazole (MET) digunakan secara meluas untuk merawat jangkitan periodontal berikutan rawatan kerana keberkesanannya terhadap ciri anaerob obligat dan spektrum luas. Walaupun kelebihannya, MET dikaitkan dengan kesan sampingan sistemik. Oleh itu, artikel ini bertujuan untuk mengkaji secara in vitro, in vivo, dan kajian klinikal mengenai aplikasi tempatan semasa MET untuk merawat penyakit periodontal. 13 artikel penyelidikan yang berkaitan telah dianalisis dan memberikan pandangan yang berharga tentang aplikasi tempatan metronidazole untuk rawatan periodontal.

Kata Kunci: metronidazole; penghantaran ubat tempatan; periodontitis, antibiotik

**Corresponding author:*
Mohd Yusof Mohamad
Department of Physical Rehabilitation Sciences,
Kulliyyah of Allied Health Science,
International Islamic University Malaysia,
Email: yusofkahs@iium.edu.my

THE USE OF COLLAGEN BIOMATERIAL IN ORAL CANCER: A SYSTEMATIC REVIEW

Muhammad Lutfi Mohamed Halim[1], Nora Azirah Mohd Zayi[1], Mohd Yusof Mohamad[1]*, Mohd Hafiz Arzmi[2]

[1] Department of Physical Sciences, Kulliyyah of Allied Health Sciences, International Islamic University Malaysia, Jalan Sultan Ahmad Shah, Bandar Indera Mahkota, 25200 Kuantan, Pahang Darul Makmur, Malaysia
[2] Department of Fundamental Dental and Medical Sciences, Kulliyyah of Dentistry, International Islamic University Malaysia, Jalan Sultan Ahmad Shah, Bandar Indera Mahkota, 25200 Kuantan, Pahang Darul Makmur, Malaysia

*Corresponding author: yusofkahs@iium.edu.my

ABSTRACT

Introduction: Oral cancer is the sixth most common malignancy in the world. It is a major concern in Southeast Asia primarily due to betel quid chewing, smoking, and alcohol consumption. In Malaysia, oral cancer related cases accounts for 1.55% of the cause of deaths. Despite recent advances in cancer diagnoses and therapies, the survival rate of oral cancer patients only reached 50% in the last few decades. Tissue engineering (TE) principles may provide new technology platforms to study mechanisms of angiogenesis and tumour cell growth as well as potentially tumour cell spreading in cancer research. The use of biomaterial, appropriate cell source and proper signalling molecules are vital components of TE. Collagen biomaterial are widely used scaffold or membrane in oral application. Nevertheless, no review has been performed on the its usage for the study of oral cancer. This study aimed to systematically review the use of collagen scaffold in oral cancer application. **Methods:** Research articles were searched using Scopus, Pubmed and Web of Science (WOS) databases. The keywords were limited to "collagen membrane OR collagen scaffold" AND "oral cancer". **Results:** Initial search yielded 61 papers (Scopus:37, Pubmed: 12, WOS: 12). Further scrutinization of the papers based on the inclusion criteria resulted total of 3 papers. Two of the papers used collagen membrane for regeneration of oral mucosal defect and increment of alveolar ridge height post-surgery. The remaining paper utilize collagen biomaterial as scaffold for the culture of adenoid cystic carcinoma (ACC) cells. All papers reported significant role of collagen biomaterial in terms of tissue formation, healing scaffold and cellular proliferation. **Conclusion:** Collagen utilization as biomaterial offers potential use for regeneration of oral related structures as well providing useful model for therapeutics anti-cancer research.

IIUM Journal of Orofacial and Health Sciences 2022, Volume 3, Supplement 1

ABSTRACT ID: 135

DEVELOPMENT OF CHITOSAN LOADED METRONIDAZOLE NANOPARTICLE AS STABLE LOCAL DRUG DELIVERY FOR PERIODONTAL TREATMENT

Nora Azirah Mohd Zayi[1]*, Muhammad Lutfi Mohamed Halim[2], Mohd Yusof Mohamad[1,2], Ahmad Fahmi Harun[1,2], Mohd Hafiz Arzmi[2,3]

[1]Department of Physical Rehabilitation Sciences, Kulliyyah of Allied Health Science, International Islamic University Malaysia, Kuantan Campus, 25200 Kuantan, Pahang, Malaysia
[2]Cluster of Cancer Research Initiative IIUM (COCRII), International Islamic University Malaysia, Kuantan Campus, 25200, Kuantan, Pahang, Malaysia
[3]Department of Fundamental Dental and Medical Sciences, Kulliyyah of Dentistry, International Islamic University Malaysia, Kuantan Campus, 25200, Kuantan, Pahang, Malaysia

*Corresponding author email: nora.azirah@live.iium.edu.my

ABSTRACT

Metronidazole is one of the most effective antibiotics for treating bacterial infections in periodontal disease. However, antibiotic resistance has emerged as one of the biggest risks to public health worldwide. Consequently, new approaches are required to manage the drawback of conventional antibiotics and prevent the emergence of antibiotic resistant-. The drug entrapped, attached, or encapsulated in the nanomaterial matrix shown great potential in medical applications. The combination of nanotechnology and antibiotics would be the most promising strategy to overcome antibiotic-resistant bacteria and improving drug efficiency. Thus, this study aims to optimise the drug size, stability, and encapsulation efficiency within a nanocarrier before using it as a therapeutic agent in periodontal treatment. The concentrations of chitosan and metronidazole were chosen as optimising parameters at constant crosslinker sodium tripolyphosphate (STPP). Chitosan-loaded metronidazole nanoparticles (CS-MNPs) were fabricated by ionic gelation of chitosan with tripolyphosphate anions, and the prepared nanoparticles were evaluated for particle size, zeta potential, and drug entrapment efficiency. In this study, the smallest CS NPS of 303.86 ± 62.78 nm was successfully developed through ionic crosslinking with a stable NPs surface charge of 46.6 ± 0.231 mV at a CS: MN mass ratio of 3: 1. The entrapment efficiency of 88% was achieved when MN was loaded into CS the nanoparticles. The result showed that highly stable chitosan-loaded metronidazole nanoparticles were developed by the ionic crosslinking method. This nanoparticle has the potential to increase the efficacy of the drug while decreasing the antibiotic's effect. However, further studies are needed to evaluate the suitability of chitosan-loaded metronidazole nanoparticles for periodontal treatment.

Keywords:
local drug delivery, metronidazole, nanoparticle, periodontal disease

Acknowledgment:
The authors would like to thank the financial support provided by the FRGS19-146-0755 grant.

APPLICATION OF METRONIDAZOLE LOADED MEMBRANE FOR PERIODONTAL DISEASE: A BRIEF REVIEW

Nora Azirah Mohd Zayi, Muhammad Lutfi Mohamed Halim, Mohamad Yusof Mohamad*

Department of Physical Rehabilitation Sciences, Kulliyyah of Allied Health Science, International Islamic University Malaysia, Kuantan Campus, Pahang, Malaysia

*Corresponding author email: yusofkahs@iium.edu.my

ABSTRACT

Periodontitis is the inflammation of periodontal tissues that support the teeth. 86% of adults over the age of 70 suffer at least one case of moderate periodontitis leading to the 25% cases of teeth loss. Guided bone regeneration (GBR) is an effective technique used for periodontium reconstruction. This technique uses barrier membranes which prevent epithelial growth in the wound site and can be supplemented with antibiotics to protect the wound against opportunistic infections. Traditionally, the clinic therapy for anti-infection is to use antibiotics through injection or oral administration resulted in poor delivery of antibiotic to the defect site leading to cytotoxicity. Metronidazole (MNA), commonly used antibiotics, offer the benefits of a high degree of efficacy and with limited adverse side effects. This paper aimed to systematically review the current use of metronidazole loaded onto membranes in periodontitis treatment. SCOPUS and PubMed databases were used to search the articles systematically. The search strategy performed using the following keywords: "metronidazole", "membrane" and "periodontal disease". The inclusion criteria were all original studies published in English within five years. The exclusion criteria were any dissertations, unpublished documents, and review articles. Initial screening of papers yielded 15 papers (Scopus=9 and Pubmed=6), but only five articles met the inclusion criteria dealing with MNA antibiotics delivery. Many of the papers reported MNA in forms of mucoadhesive tablet or gel loaded onto different types of membranes (poly 3-hydroxybutyrate, collagen, and chitosan) as topical application of sustained release of antibiotic. The drug delivery employed were able to deliver the desired antibiotics dose to the infected site with an extended period while minimising cytotoxicity. However, a high amount of MNA delivered to the defect site leading to cytotoxicity. In conclusion, the use of MNA loaded membrane demonstrated promising results for periodontitis, but improvement is needed in terms of drug delivery mechanism.

Keywords: Metronidazole, Membrane, Periodontitis.

Acknowledgement: The authors are grateful to the financial support by International Islamic University Malaysia under the research grant FRGS19-146-0755.

APPENDIX III

LIST OF OTHER ARTICLES, PROCEEDINGS, AND ABSTRACTS

Mohd Zayi, Nora Azirah and Mohamed Halim, Muhammad Lutfi and Mohamad, Mohd Yusof and Harun Ismail, Ahmad Fahmi and Arzmi, Mohd Hafiz (2022) Development of chitosan loaded metronidazole nanoparticle as stable local drug delivery for periodontal treatment. IIUM Journal of Orofacial and Health Sciences, 3 (1). p. 25. E-ISSN 2735-0584 (In Press).

Mohamed Halim, Muhammad Lutfi and **Mohd Zayi, Nora Azirah** and Mohamad, Mohd Yusof and Harun @ Ismail, Ahmad Fahmi and Rostam, Muhamad Ashraf (2024) Fabrication of chitosan collagen glycerine scaffold for oral wound treatment. In: International Conference on Advanced Engineering Materials and Composites 2024, 20- 21 May 2024, Faculty of Engineering, UPM.

Mohd Zayi, Nora Azirah and Halim, Lutfi and Harun @ Ismail, Ahmad Fahmi and Mohamad, Mohd Yusof and Arzmi, Mohd Hafiz (2021) Fabrication of chitosan loaded metronidazole nanoparticle for periodontal disease treatment. In: The 4th International Conference on Oral Microbiology and Oral Immunology, International Islamic University Malaysia. (Unpublished).

Mohd Zayi, Nora Azirah and Mohamad, Mohd Yusof and Harun @ Ismail, Ahmad Fahmi and Mohamed Halim, Muhammad Lutfi and Arzmi, Mohd Hafiz (2020) Chitosan as a potential drug nanocarrier for oral disease treatment. In: 3rd International Conference on Oral Microbiology and Oral Immunology in conjunction with 13th Postgraduate e- Conference 2020, 8th-9th September 2020, Kuala Lumpur (Online via Google Meet). (Unpublished).

Mohd Zayi, Nora Azirah and Mohamed Halim, Muhammad Lutfi and Mohamad, Mohd Yusof (2020) Application of metronidazole loaded membrane for periodontal

disease: a brief review. In: IIUM Kuantan Research Day 2019, 23rd October 2019, Kuantan, Pahang. (In Press).

APPENDIX IV: AWARDS AND ACHIEVEMENT

THIRD YOUNG RESEARCH AWARD (ORAL PRESENTER) AT 9th ASIAN BIOMATERIAL CONGRESS, 2023

ENCOURAGEMENT AWARD AT THE 2022 TERMIS ASIAN PACIFIC VIRTUAL STUDENT PAPER CONTEST (ORAL PRESENTER)

IIUM 2024 THREE MINUTE THESIS (3MT) (UNIVERSITY LEVEL)

الجامعة الإسلامية العالمية ماليزيا
INTERNATIONAL ISLAMIC UNIVERSITY MALAYSIA
يونيفرسيتي إسلام انتارابغسا ملسيا

Certificate of Participation

This is to certify that

NORA AZIRAH BINTI MOHD ZAYI

has participated in the

IIUM 2024 Three Minute Thesis (3MT) Competition
(University Level)

on
16TH MAY 2024

Organized by
Centre for Postgraduate Studies (CPS)

PROF. DR. SHAHRUL NA'IM SIDEK
Dean
Centre for Postgraduate Studies

THIRD WINNER IN THE 2ND KAHS COLLOQUIIUM 2024 (POSTER PRESENTER)

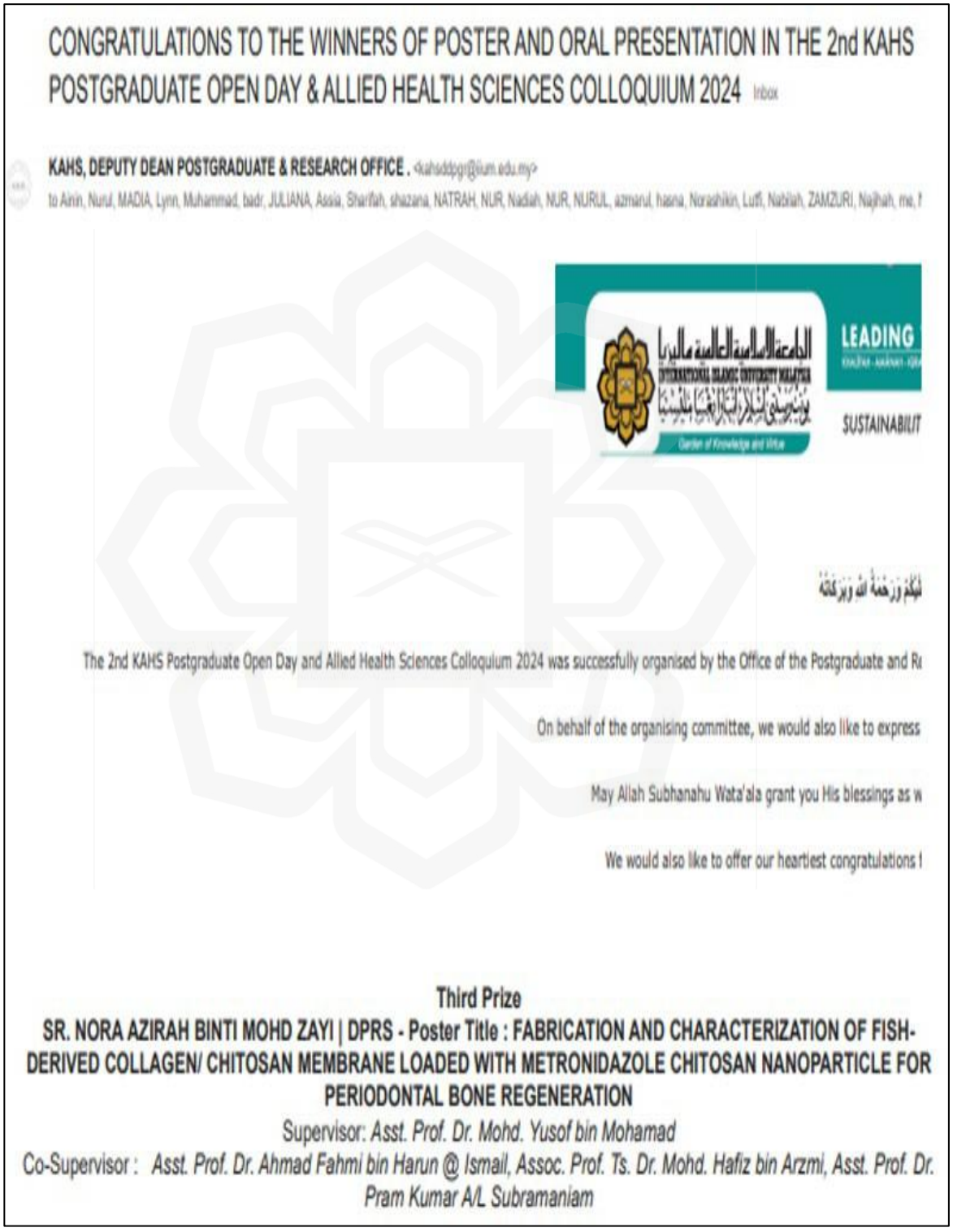

CONGRATULATIONS TO THE WINNERS OF POSTER AND ORAL PRESENTATION IN THE 2nd KAHS POSTGRADUATE OPEN DAY & ALLIED HEALTH SCIENCES COLLOQUIUM 2024 Inbox

KAHS, DEPUTY DEAN POSTGRADUATE & RESEARCH OFFICE . <kahsddpgr@iium.edu.my>

to Ainin, Nurul, MADIA, Lynn, Muhammad, badr, JULIANA, Assia, Sharifah, shazana, NATRAH, NUR, Nadiah, NUR, NURUL, azmarul, hasna, Norashikin, Lutfi, Nabilah, ZAMZURI, Najihah, me, f

LEADING

SUSTAINABILIT

وَبَرَكَاتُهُ

The 2nd KAHS Postgraduate Open Day and Allied Health Sciences Colloquium 2024 was successfully organised by the Office of the Postgraduate and R

On behalf of the organising committee, we would also like to express

May Allah Subhanahu Wata'ala grant you His blessings as w

We would also like to offer our heartiest congratulations t

Third Prize

SR. NORA AZIRAH BINTI MOHD ZAYI | DPRS - Poster Title : FABRICATION AND CHARACTERIZATION OF FISH-DERIVED COLLAGEN/ CHITOSAN MEMBRANE LOADED WITH METRONIDAZOLE CHITOSAN NANOPARTICLE FOR PERIODONTAL BONE REGENERATION

Supervisor: *Asst. Prof. Dr. Mohd. Yusof bin Mohamad*

Co-Supervisor : *Asst. Prof. Dr. Ahmad Fahmi bin Harun @ Ismail, Assoc. Prof. Ts. Dr. Mohd. Hafiz bin Arzmi, Asst. Prof. Dr. Pram Kumar A/L Subramaniam*

SILVER AWARD IN THE IIUM RESEARCH & INNOVATION DAY 2022

BRONZE AWARD IN THE KUANTAN RESEARCH DAY (2020) (POSTER PRESENTER

CONSOLATION AWARD AT ORAL MICROBIOLOGY AND ORAL IMMUNOLOGY CONFERENCE 2021 (ORAL PRESENTER)

GOLD AWARD AT THE IIUM RESEARCH DAY 2021 (POSTER PRESENTER)

CONGRATULATIONS TO POSTGRADUATE STUDENTS - AWARD WINNERS IN THE IIUM RESEARCH DAY 2021

1 message

KAHS, DEPUTY DEAN POSTGRADUATE & RESEARCH OFFICE . <kahsddpgr@iium.edu.my> Mon, Nov 29, 2021 at 11:47 AM

To: kahsgrp <kahsgrp@iium.edu.my>, nora azirah <noraazirah.mdzayi@gmail.com>, Najihah Amir <najihah9054@gmail.com>, "MOHD. YUSOF BIN MOHAMAD Mohamad" <yusofkahs@iium.edu.my>, SARAH BINTI RAHMAT <sarahrahmat@iium.edu.my>

السلام عليكم ورحمة الله وبركاته

Congratulations!

On behalf of the Kulliyyah of Allied Health Sciences, we would like to congratulate our postgraduate students for the award received at the ***IIUM Research Day 2021*** recently,

Sr. Nora Azirah Mohd Zayi

DEVELOPMENT OF CHITOSAN LOADED METRONIDAZOLE NANOPARTICLE AS STABLE LOCAL DRUG DELIVERY FOR PERIODONTAL TREATMENT

Gold Award Winner